



University of  
**Nottingham**

UK | CHINA | MALAYSIA

# Analytical approach to Electrical Distribution Systems for Aircraft

Cosimo Spagnolo

id: 14289919

Supervised by:

Professor Serhiy Bozhko

Doctor Sharmila Sumsurooah

Department of engineering

University of Nottingham

I hereby declare that this dissertation is all my own work, except as indicated in  
the text

Date 29/10 /2021

Signature

I hereby declare that I have all necessary rights and consents to publicly distribute this dissertation via the University of  
Nottingham's e-dissertation archive



This thesis work is dedicated to my family, which constantly helped me in this  
hard journey

A special thanks to my Supervisor Professor Serhiy Bozhko that guided me  
through this Ph.D. and made me discover the world of aircraft electrification  
giving me the opportunity to present my research results all over the world

A special thanks to my loved Daniela and Giuseppe for their patience in  
following me through this adventure



## Thesis outline

<b>Abstract.....</b>	<b>9</b>
<b>Introduction.....</b>	<b>11</b>
1.1 Motivation.....	11
1.1.1 More Electric Aircraft.....	11
1.1.2 Supervisory control for MEA EPS.....	13
1.2 Research aims and objectives.....	17
1.3 Contributions.....	17
1.4 Thesis structure.....	18
1.5 Published papers related to this study.....	20
<b>Chapter 2: Algorithms and tools for the supervisory controller design.....</b>	<b>21</b>
2.1 Introduction.....	21
2.2 Methods.....	22
2.2.1 Re-configuration strategy.....	22
2.2.2 Load Allocation Problem.....	23
2.3 Algorithms.....	24
2.3.1 Knowledge based method.....	24
2.3.2 Linear temporal logic.....	25
2.3.3 Dynamic programming.....	26
2.3.4 Algorithms employed for the SC design.....	27
2.4 Tools.....	28
2.4.1 C language.....	28
2.4.2 Tulip - Python.....	30
2.4.3 Finite state machine.....	30
2.4.4 Tools selection.....	33

2.5	Conclusion.....	34
<b>Chapter 3: MEA EPS Architecture.....</b>		<b>35</b>
3.1	Introduction.....	35
3.1.1	Constant frequency architecture (CF).....	37
3.1.2	Variable frequency architecture (VF).....	40
3.1.3	High voltage variable frequency plus High voltage DC $\pm 270$ V (HVAC) .....	42
3.1.4	High Voltage pure DC $\pm 270$ V (HVDC) .....	43
3.2	Recent MEA EPS architectures.....	45
3.3	EPSs under study.....	50
3.4	Scaled down model of the EPS under study for the experimental tests.....	53
3.5	Conclusion.....	56
<b>Chapter 4: EPS Re-configuration strategy.....</b>		<b>57</b>
4.1	Overview.....	57
4.2	Generator overload reduction by smart power management.....	58
4.2.1	Overview .....	58
4.2.2	The EPS under study .....	59
4.2.3	The Control strategy .....	60
4.2.4	Strategy to logic .....	63
4.2.5	EPS model components description .....	66
4.2.6	Simulation results .....	67
4.2.7	Conclusion for study case 1 .....	71
4.3	Smart controller design for safety operation of the MEA electrical distribution system .....	72
4.3.1	The control strategy .....	72
4.3.2	Simulations and results .....	77
4.3.3	Conclusion for case study 2 .....	86

4.4	Conclusion.....	89
<b>Chapter 5: Load allocation problem (LAP).....</b>		<b>90</b>
5.1	Overview.....	90
5.2	LAP of representative MEA EPS.....	91
5.3	Knapsack method for LAP of representative MEA EPS.....	93
5.4	Case scenario and simulation results.....	98
5.5	Additional considerations.....	101
5.6	Conclusion.....	103
<b>Chapter 6: A practical scenario: ASPIRE project.....</b>		<b>105</b>
6.1	Overview.....	105
6.2	ASPIRE electrical power system.....	106
6.3	Energy management concept of the ASPIRE system.....	108
6.3.1	Logic rules definition.....	109
6.4	Application of the logic rules.....	110
6.5	Simulation model.....	111
6.5.1	Normal operation.....	114
6.5.2	Generator overload.....	116
6.5.3	Increase in power demand on LV HP bus 1 .....	119
6.6	Additional considerations.....	121
6.7	Conclusion.....	122
<b>Chapter 7: Case study for experimental application.....</b>		<b>123</b>
7.1	Introduction.....	123
7.2	Test scenario.....	123
7.3	FSM description.....	129
7.4	Simulation results.....	136
7.5	Conclusion.....	144

<b>Chapter 8: Experimental rig and study case scenario.....</b>	<b>145</b>
8.1 Introduction.....	145
8.2 Description of the components.....	147
8.3 Sensors and additional devices.....	151
8.4 Experimental case scenario.....	155
8.4.1 FSM description for the EPS emulator.....	159
8.4.2 Experimental results .....	164
8.5 Conclusion.....	173
<b>Chapter 9: Conclusion.....</b>	<b>175</b>
9.1 Introduction.....	175
9.2 Research outcomes.....	176
9.2.1 Theoretical aspects .....	176
9.2.1 Experimental aspects.....	177
9.3 Future research.....	179
<b>Appendix A – List of Simulink® Models.....</b>	<b>180</b>
<b>List of References:.....</b>	<b>199</b>
References to Chapter 1.....	199
References to Chapter 2.....	200
References to Chapter 3.....	204
References to Chapter 4.....	206
References to Chapter 5.....	206
References to Chapter 6.....	206
References to Chapter 7.....	206



## **Abstract**

---

The More Electric Aircraft concept (MEA) is one of the most discussed topics of the recent decades inside the aircraft market. It aims to enable the migration towards more efficient aircraft while reducing the environmental impact by substituting the hydraulic, pneumatic and mechanical parts with their electrical counterparts. As the electrical systems became more complex, it is inevitable the need of a control unit that can manage the EPS under all the possible scenarios. For this reason, this thesis presents different study cases that a supervisor controller (SC) unit must address for guarantying the optimal EPS operations. In particular, the SC must be able to manage the network overloads, for preventing unwanted operations or oversized design of the on-board generators. Moreover, applying constant EPS monitoring, the SC must be able to solve critical scenarios by splitting the power flow on a different path. Apart from failure and critical tasks, the SC must be also employed in the EPS optimization using a mathematical algorithm that ensures the correct power spreading across each bus. After the introduction to the actual employed algorithms and used EPS, all the described cases are simulated inside Simulink® environment and a test bench is then configured to emulate a portion of a scaled EPS in the laboratory.



## **Introduction**

---

### **1.1 Motivation**

#### **1.1.1 More Electric Aircraft**

Over the last few decades, there have been intensive research work and rapid developments in the area of aircraft electrification. Flying being the fastest and one of the safest ways to travel over long distances has led to a sharp increase in air traffic. Since the first passenger flight in 1914, the passenger air traffic has continuously increased, and before the covid-19 pandemic that affected the entire planet, it exceeded 100 000 flights daily [1, 2]. With the increasing number of air vehicles, it is extremely important to address the key issues related to aviation, starting from the constant increment of the carbon dioxide emissions with its significant environmental impact [3, 4] and air traffic noise [5]. To cope with high air traffic demand, and improve the overall aircraft performances, the introduction of the aircraft electrification seems to be the viable option to move forward towards the next air transport generation. Aircraft electrification is taking two main routes which are the more electric aircraft (MEA) and the hybrid- or fully electric propulsion. The MEA assumes the replacement of many mechanical, hydraulic and pneumatic components of the aircraft with their electrical equivalents. The electric propulsion regards the replacement (or boosting in hybrid-electric aircraft) of the main jet engines with electrical counterparts. The introduction of electrification to aircraft propulsion can have huge advantages in terms of environmental impact mitigation, noise reduction, and lower fuel consumption [6, 7]. However, extensive and long-term research studies will be still necessary to address these aspects due to the high power density requirements for the electrical machines, and high energy densities of batteries which are still low compared to that of fuel [8]. This work focusses on the aircraft electrification through the route of MEA technology development. Moving to MEA means significant increase of onboard electric power budget since it need to replace hydraulic, pneumatic, and mechanically powered systems. Correspondingly, the size and complexity of electric power system (EPS) used to transfer/distribute electric power from the generators to the loads significantly increase with the increase of onboard electric power demand [6]. Fig.

1.1 shows the growth of electrical power usage in aircraft compared with the take-off thrust, that brought a remarkable and sudden evolution of the "electrification in the air".

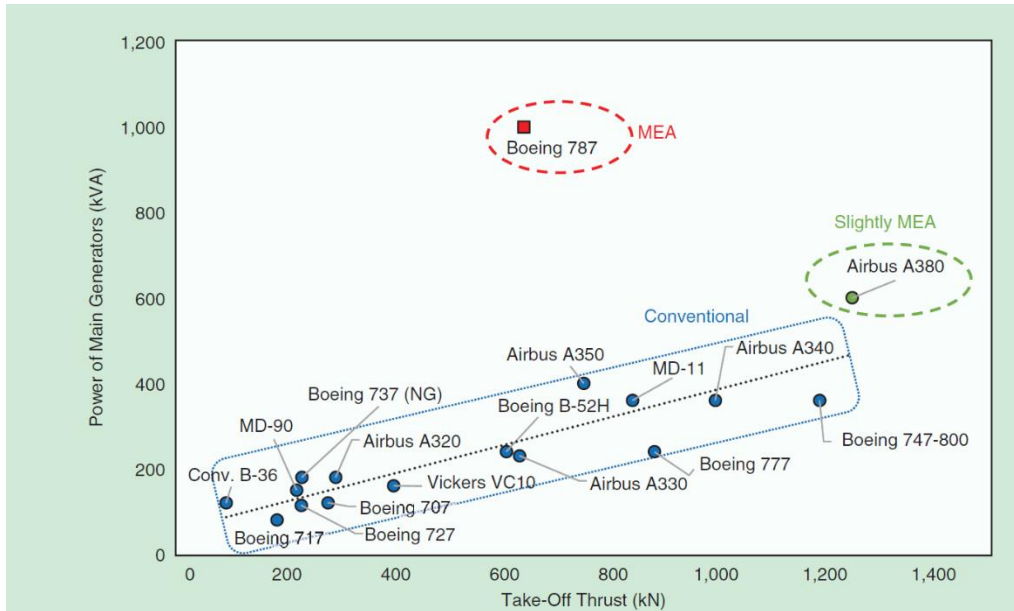


Fig. 1.1. Evolution of the electrical power need in kVA compared with the take-off thrust) [9]

As one can note, that in Fig. 1.1, the Boeing 787 Dreamliner, use a very high amount of electrical power which reaches nearly 1 MW for the Boeing 787. Aircraft electrification has many benefits. In a MEA, heavy, inefficient hydraulic or pneumatic systems, such as actuators, are replaced by a lighter, more efficient electrically driven systems [10, 11]. Furthermore, the electrification has been proven to be capable to bringing components that are higher reliable over the mechanical ones hence increasing the safety levels [12]. However, this electric expansion in the MEA introduces problems related to the design and management of the extensive EPS architecture, which inevitably becomes voluminous, weighty, and intricate due to the massive increment of the electric equipment onboard [13]. For this reason, one way to achieve EPS improvements it is to develop an Energy Management system (EMS). EMS is a system of computer-aided tools designed to achieve energy efficiency through logical or mathematical process optimization by monitoring the energy use by individual pieces of equipment [14]. Thus, for the successful and effective application of the MEA concepts, there is the need to find, and adopt power and energy management strategies, which consist of

tracking and optimizing the power and energy distributions across the EPS. This process involves the collection, and analysis of data (voltage, current, power) aimed to optimise the MEA EPS while ensuring safe operations. In order to do that, power and energy management strategies can be designed to control the behaviour of the aircraft EPS, managing power and energy from generation to loads. Moreover, the control strategies can be designed to have the capability of reconfiguring the EPS while optimising the energy profiles of the grid, allocating the right amount of power to each load onboard, and applying safety rules to avoid or solve critical fault scenarios. Thus, in order to adopt a power and energy management strategy, there is a need to introduce a supervisory controller (SC), which is an electronic system composed of inputs, outputs, and software. The SC has the task to control the power/energy distribution across the EPS by taking input variables, processing the data, and setting the status of the EPS through the outputs. The role of the SC is then to control the EPS at a high level, which means that every electrical appliance is controlled as a slave by the master (SC), thus, the task of the slave is to provide to the EPS the requested value from the Master. The employment of a SC is a key aspect of the MEA EPS design. For this reason, the main aspect of this thesis is to focus on the design of a SC.

### **1.1.2 Supervisory control for MEA EPS**

The MEA concept aims to enable the migration towards more efficient aircraft while reducing the environmental impact. However, as secondary result, it aims to extend and improve the EPS to achieve safe and reliable flight operations and maximize availability of electric power [15]. Thus, the main objectives are to guarantee a safer EPS with improved performances, in order to migrate to the MEA concept. Availability is defined as the probability that the system will operate properly when it is requested for use [16]. Thus, the EPS is not failed or undergoing a repair action when it needs to be used. Reliability is defined as the probability that a system will perform its intended function adequately for a specified period of time, or will operate in a defined environment without failure [17]. An EPS is considered safe when it can provide a high level of reliability, (i.e., having multiple parallel paths between the sources and the buses, and/or redundancy of the critical appliances). Moreover, the performances are maximised when the system can reduce or avoid overloads of the sources since it can be

translated into weight reduction due to the oversizing. Thus, avoiding the overrating of the sources will result in reduction of the entire EPS weight, and ensuring that all the loads are supplied with their requested power.

### 1.1.2.1 MEA EPS

For MEA EPSs, different architectures are being considered [18]. The EPS configuration can vary from AC systems to a total DC with different voltage levels, and in case of AC different frequencies. However, the topology of the EPS presents some common features through the different architectures. In a MEA EPS the electrical power is provided by the main generators, which are connected to the main engines, and through the uses of electrical buses, and power electronic converters (PECs) the loads are supplied with their needed power and voltage level [6, 10, 19]. For better understanding, consider a single-line diagram of a representative MEA EPS depicted in Fig. 1.2. Here, the energy sources G1, G2 supply the loads through the buses 1 to 4, and the power electronic converters PEC 1 and PEC 2. The PECs 1 and 2 are used to step-down the voltage level of the buses 3 and 4 or can be used to set the power level between the buses 1 and 2 with the buses 3 and 4, while the PECs 3 and 4 are used to set the voltage level. The batteries are used as back-up sources for secondary distributions, as well as can provide extra power during emergencies or scenarios; the switches C1 to C4 can be used to disconnect the loads; switches C5 and C6 can be used to tie the buses when required.

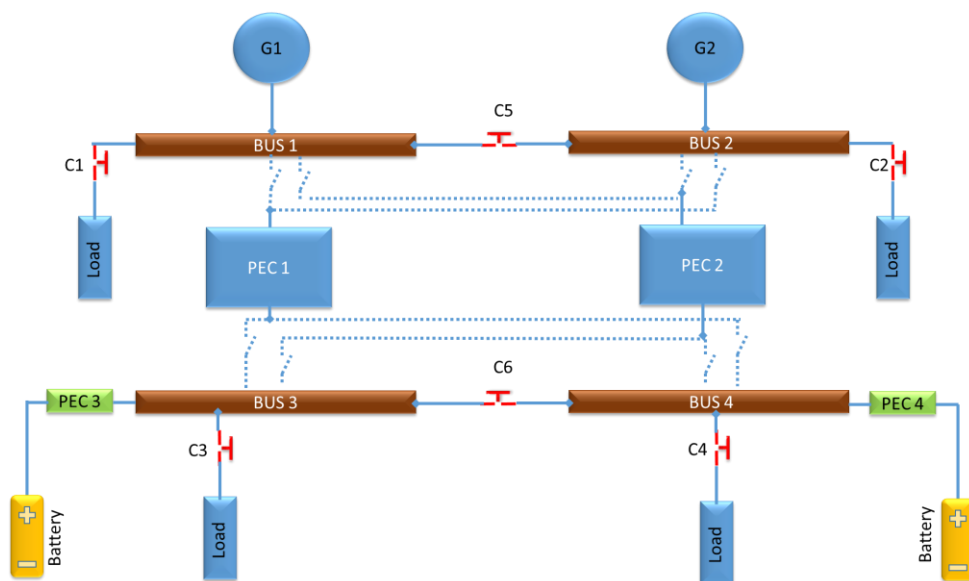


Fig. 1.2. Basic single-line diagram of a representative MEA EPS

The Fig. 1.2 gives a basic representation of a MEA EPS architecture. The main idea of this Thesis work is to investigate approaches for a SC design, with the aims to act on the EPS components and control the system setting (i.e., switches, batteries, converters) for improving the performances of a given typical MEA EPS topology. Thus, the main target is to obtain a safer, and reliable EPS, which is able to avoid overloads, and working under critical scenarios (i.e., critical component failure).

### **1.1.2.2 Supervisory controller (overview)**

The scope of this work is focused on the design methods for a SC, which aims to control the EPS, managing the power flows between its sources, loads, and other components. The SC will target the following two main functions:

- The reconfiguration of the EPS, which consists of modifying the power flow paths and/or activating energy sources (e.g., batteries) in order to guarantee an uninterrupted supply of the buses. This function is particularly required during critical scenarios (e.g., source or converter failure), where the SC can find an alternative path for supplying the loads.
- The allocation of the power, which means allocation of the power requested by the loads with the available power from the sources. The SC should ensure that the power required by the loads will not exceed the available power under all possible (abnormal) scenarios by acting on the switches (e.g., shedding non-essential loads) or batteries (e.g., demanding extra power to the EPS).

An example is given in the Fig. 1.3. The parameters of the EPS in Fig. 1.2 are given as input into the SC, processed, and the output values are used to modify the status of the EPS.

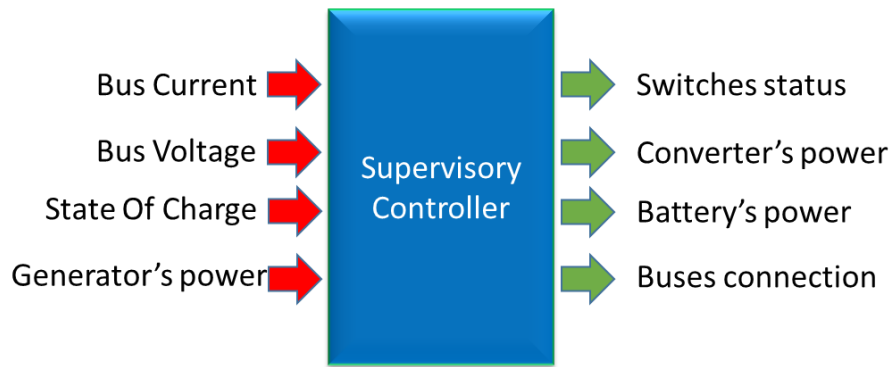


Fig. 1.3. Representative image of the SC with input and output variables

A general methodology is proposed and implemented, which aims to make the considered EPS safe, efficient and optimised by applying the '*re-configuration strategy method*' (RCS) and '*load allocation problem*' (LAP) in real-time. The implementation of the RCS and LAP is based on the application of different algorithms and tools which will be investigated as well.



## **1.2 Research aims and objectives**

As the electrification onboard becomes more extensive, the need to have safer, and optimised MEA EPSs becomes equally important.

The aim of this thesis is to propose and implement an approach to manage the power and energy of the entire MEA EPS such that the EPS works at its optimal and safety levels.

This will be achieved through the following research objectives:

- Develop a methodology to design a SC that is able to manage the entire MEA EPS
  - Moving to the enhanced performance and efficiency of the EPS, while respecting safety constraints
- Automatization of the EPS reconfiguration during occurring or critical scenarios, with automatic switch of the power on the vital loads
- Identify, implement and test practical and computationally inexpensive algorithms and tools for the design of the SC
- Validate the selected approach, algorithms and tools through different study cases in simulation and in laboratory experiment.

## **1.3 Contributions**

The research methods that have been implemented to meet the aforementioned objectives are presented in the main Chapters of this thesis and are outlined in the next Section. This effort has resulted in three main contributions.

- An approach has been developed for designing a SC that can be easily applied to the MEA EPS using one single development tool to make the EPS more efficient and safer
- A set of algorithms and tools have been identified, implemented and tested as computationally inexpensive and practically applicable to MEA EPS.
- The proposed design approach has been verified and validated using different case scenarios in simulation and in laboratory experiments.

## **1.4 Thesis structure**

The research findings are developed and presented in the CHAPTERSs of the Thesis, which is structured as follows:

**Chapter 1** provides the motivation behind the work in this Thesis, as well as states the main aim and objectives of this study. The first part is focused on the MEA solution for the impact reduction, while the second part introduces the thesis objectives deeper

**Chapter 2** deals with the literature review on the known main methods, algorithms, and tools used to create a SC. It describes the techniques used to control the EPS from easier to complex ones and wants to give an idea of the differences in using each method

**Chapter 3** gives an overview of the different architectures of the aircraft EPSs and the principal characteristic of each topology, for which the SC will be developed and tested. In particular, the last part is focused on the last theorized architectures for MEA EPSs

**Chapter 4** describes how the ‘re-configuration strategy method’ (RCS) is designed and implemented in a SC for an MEA EPS. It presents two simulation scenarios in which the EPS is subjected to a generator’s overload and multiple converter failures. In the two cases, the RCS method is used for addressing the critical condition

**Chapter 5** investigates the ‘load allocation problem’ (LAP). The mathematical formulation of the algorithm is first analysed, and the knapsack method [20] with its computational solution is then presented. This Chapter demonstrates how the ‘load allocation problem’ algorithm is integrated into the design of a SC for the MEA EPS. The design approach is verified through a case study where the ‘load allocation problem’ is used to optimise the power allocation to the MEA EPS buses.

**Chapter 6** applies and verifies the ‘re-configuration strategy method’ (RCS) on a practical MEA EPS demonstrator that is being developed under the Advanced Smart-Grid Power Distribution System (ASPIRE) project. The ASPIRE project aims at the implementation the Energy Management (EM) functionalities of the aircraft DC electrical power distribution system (EPDS), for achieving a substantial improvement in system efficiency, safety, power quality and eco-friendliness compared to existing solutions.

**Chapter 7** presents a study case that uses both the '*reconfiguration-strategy method*' (RCS) and the '*load allocation problem*' (LAP). These two methods gave the possibility to control the entire EPS, by monitoring the power across the network, and with a low expensive computational operation, it is possible to redistribute the power from the sources to the loads (RCS), and allocate the right power amount on each electrical bus (LAP).

**Chapter 8** presents the experimental rig for verification of the case study considered in Chapter 6 - 7, and its components used for performing the experimental tests. The hardware used to build the test rig is described as well as the control algorithm to implement the SC. After that, the experimental tests results for the case study described of Chapter 6 are presented. The Chapter demonstrates the capabilities of both the algorithms and the tools employed. The experimental results validate the design approach for the SC using the RCS and the LAP by successfully matching the experimental results to the simulation results.

**Chapter 9** discusses the significance as well as the implications of the findings presented in the thesis and provides suggestions for future works.

## **1.5 Published papers related to this study**

1. Spagnolo, C., Sumsurooah, S., Hill, C.I. and Bozhko, S., 2018. Finite state machine control for aircraft electrical distribution system. *The Journal of engineering*, 2018(13), pp.506-511.
2. Spagnolo, C., Sumsurooah, S., Hill, C.I. and Bozhko, S., 2018, October. Smart Controller Design for Safety Operation of the MEA Electrical Distribution System. In *IECON 2018-44th Annual Conference of the IEEE Industrial Electronics Society* (pp. 5778-5785). IEEE.
3. Spagnolo, C., Sumsurooah, S., Hill, C.I. and Bozhko, S., 2018, November. Generator overload reduction using smart power management. In *2018 IEEE International Conference on Electrical Systems for Aircraft, Railway, Ship Propulsion and Road Vehicles & International Transportation Electrification Conference (ESARS-ITEC)* (pp. 1-7). IEEE.
4. Spagnolo, C., Madonna, V., Sumsurooah, S., Hill, C.I. and Bozhko, S., 2019. Optimized LV loads allocation for MEA electrical power systems. In *AIAA Propulsion and Energy 2019 Forum* (p. 4489).
5. Spagnolo, C., Sumsurooah, S. and Bozhko, S., 2019, October. Advanced smart grid power distribution system for More Electric Aircraft application. In *2019 International Conference on Electrotechnical Complexes and Systems (ICOECS)* (pp. 1-6). IEEE.

## **Chapter 2: Algorithms and tools for the supervisory controller design**

---

### **2.1 Introduction**

This Chapter presents an overview of the methods, algorithms, and tools for the SC design. First, the most relevant are analysed and discussed with their advantages and disadvantages. Second, the algorithm and tool selected for the SC design is introduced.

In previous publications, different techniques have been investigated for the EPS controller design that aims to respect safety and performance constraints. The aircraft EPS respects safety constraints when it is able to ensure a high level of reliability, thus, operating without failures, or using redundancy or parallel paths between the sources, buses, and loads in order to guarantee the system operations. In this thesis work, the performances are assumed to be respected if the system is able to provide operation avoiding generator's overloads, hence saving weight and volume, costs, and reducing energy consumption.

There are two main methods, as already mentioned in the introduction, that are suitable for the EPS management, namely the 're-configuration strategy' (RCS) and the 'load allocation problem' (LAP). Furthermore, there are various algorithms used for the application of the RCS and the LAP including knowledge-based algorithms [21], dynamic programming (DP) [20, 22] and linear temporal logic [23, 24], while the tools that can be used to implement these algorithms are the finite state machine [25-27], Tulip, C language [28-29], and sliding control method [30, 31], as depicted in Fig. 2.1. The application of the methods, algorithms and tools for the design of the SC will be demonstrated in the various Chapters as illustrated in Fig. 2.1.

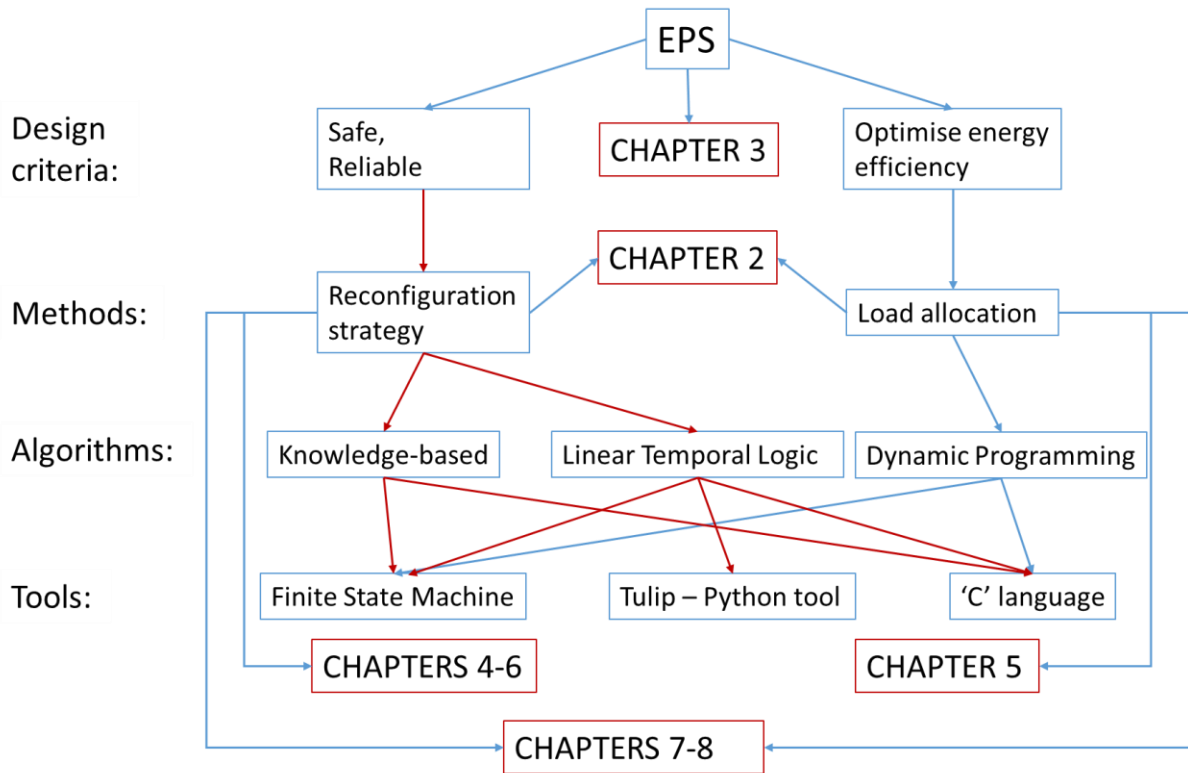


Fig. 2.1. Flowchart showing the methods, algorithms and tools used to design the SC for the aircraft EPS

The next subsection describes the methods and the choice of the algorithms and tools used for the SC design in this work with supporting evidence from the literature.

## 2.2 Methods

This section presents and discusses the methods considered for the design of SC (refer to Fig. 2.1).

### 2.2.1 Re-configuration strategy

The RCS (*re-configuration strategy method*) consists in defining alternate power paths within the EPS by the using a set of switches and PECs [32, 33]. By employing the RCS, different possible paths of power are made available from the various energy sources to the loads in the EPS. This is important for giving the EPS more degree of freedom, and as a mean of safety

improvement due to the higher number of EPS interconnections that leads to a higher number of parallel paths. In order to control the power paths, switches are used to select the routes power that can flow from the sources, through busbars, and to loads or busbars, and other busbars. Thus, the RCS is used to find the way to feed each load [21]:

- Avoiding unwanted overloads of the sources
- Avoiding critical conditions of the EPS in case of faults
- Guarantying redundancy under each possible scenario.

### **2.2.2 Load Allocation Problem**

The LAP (*load allocation problem*) consists of finding the best solution to accommodate a set of loads on each bus of the EPS. For example:

- Maximizing the number of loads utilising the currently available power without causing generator's overloading under variety of flight scenario
- Implementing a mathematical solution for supplying all the vital loads while having a limited amount of available power
- Smart disconnection of the non-vital loads in case of limited power, for example, matching the value of the available power from the main and secondary sources to the values of the power demand from onboard loads.

The critical loads are the set of loads characterised by a high level of priority; thus, they cannot be left unpowered to ensure flight safety and survivability of aircraft. The non-vital loads are the set of loads characterised by a lower priority level and they can be disconnected without compromising aircraft safety or causing problems to the EPS.

The use of LAP involves multi-objective optimization [34], which is used to implement the load shedding, power allocation, and power balance [35] as a way to allocate loads optimally. There is no constraint on the number of loads allocated to a busbar, and the number can be different from one busbar to another [36].

## **2.3 Algorithms**

This section presents and discusses the algorithms considered for the design of SC highlighting their advantages and disadvantages.

### **2.3.1 Knowledge based method**

The knowledge-based method, developed in the C Language Integrated Production System (CLIPS) environment [37], is a programming language used to implement rules and provide a reconfiguration solution according to scenarios associated with EPS component STATES. In [21] the authors proposed a method for the automatic reconfiguration of the EPS by applying the RCS under different scenarios. Aiming to improve the network performances, by regulating the power distribution, through the use of contactors/breakers, which is found by setting the optimal power path between sources and loads. The possible system configurations are captured based on the knowhow of the designers and implemented as rules of the EPS. The knowledge-based method uses a heuristic approach for the finding of the optimal path. The heuristic approach is used in computer science, artificial intelligence, and mathematical optimization, and is a technique designed for solving a problem more quickly, enabling faster solution for emergency scenarios, when classical methods are relatively slow (i.e., action between warning lights and human interaction), or for finding an approximate solution when classical methods fail to find any exact solution (i.e., mathematical solution is too approximate). The key idea of heuristic method is to adopt a quick solution obtaining a huge reduction of the computational time, sometimes at the cost of lower accuracy, especially in the case of several variables. Thus, this is achieved by trading optimality, completeness, accuracy, or precision for speed [38]. An example is given in the choice of what load must be supplied in each set, if a critical load is present in a given set, there is no needed to spend computational resources for calculating which loads need to be supplied, since a critical load has the priority, thus saving computational time.

However, this work aims to obtain an optimized EPS, thus, a heuristic method cannot be the best approach in all possible scenarios. But the heuristic approach can be embedded into the algorithm for helping the programmer in reducing coding time and help the system in reducing the running time due to reduced calculus operations. This is obtained



by monitoring the parameters of the system and depending on safety or optimization criteria. So, the possible scenarios of the EPS are grouped in a set of STATES of the system, in which each STATE represent a particular configuration of the EPS, it is possible to decide the setting of the STATE a priori, covering all the possible scenarios. In this work, the heuristic approach has been used to set the values of the variables known a priori (i.e., critical loads, non-critical loads), and thus define a known STATE (i.e., all the critical loads must be supplied, all the non-critical loads can be disconnected in case of needed). Further, it is important to note that in [21], the method is applied at the design phase of the EPS, while the work in this thesis is focused on the reconfiguration of a given EPS topology during real-time operations, thus the SC will apply a constant monitoring of the EPS's variables, and it will select the appropriate configuration accordingly with safety and optimisation constraints .

### **2.3.2 Linear temporal logic**

Linear temporal logic (LTL) is an extension of propositional logic [39, 40] that incorporates notions of temporal ordering to reason about correctness over sequence STATES. The use of temporal logic, to formally specify and verify behaviour, has been seen in various applications, including embedded systems, robotics, controls, and for the testing of the algorithm (model checking) [23]. The LTL method is developed in Python language through the use of the TULIP library, which is developed for the LTL algorithm integration in the Python language system. It is described in [28], while an example of its application is given in [29]. In [41] the authors propose a method for the design of cyber-physical systems by the use of mathematical and logic constraints over the heuristic approaches with the use of the contracts. A contract is a mathematical abstraction of component, which is used to define its characteristics in the computational environment, a more detailed definition is given in [42]. The LTL has been used to formalize the requirements in terms of contracts and, give a level of abstraction to the cyber-physical system (i.e., aircraft EPS), representing it with a set of Boolean variables. A rigorous design methodology for aircraft EPS that builds on a library of EPS model components and an initial set of design criteria has been proposed in [43], where, design specifications are expressed using LTL, signal temporal logic, arithmetic constraints on Boolean variables. It also uses Mixed Integer Linear Programming [44] to minimise the cost of the EPS topology, while

satisfying the design requirements. Moreover, in [24] the authors propose a method to improve the safety of the EPS using the LTL to satisfy the constraints of the system, calculating the number of the possible connections of each component of the grid and, taking into account the reliability level, irreversibly failures, unhealthy sources, and controller reaction time. Thus, the LTL, as explained in [45, 46], is very promising for the automata model checking of the reactive systems, and for the mission planning of mobile robots [47]. This is due to the characteristic of the method that allows to widely reduce the step length of the algorithm. However, the tool employed in the study [43] is complex and requires deep know-how in mathematics and computer science. In [41] a new method is presented for the EPS design, which aims to replace the heuristic methods with a mathematical one to improve the reliability and control specification of the EPS in the design phase. Nevertheless, the complexity of LTL, and its difficult integration with other design tools makes it unfeasible and impractical to fully implement LTL for the design of the SC in this work. Further, it is difficult to link the Python language, and consequently the TULIP library, with the developing kits, which allows the developers to place the code on the hardware. However, LTL has been partially integrated in this work to add temporal order to the code to design the SC and in this way take advantage of the benefits of LTL, as described earlier.

### **2.3.3 Dynamic programming**

In [36] the authors proposed the DP to optimize the number of loads allocated to each aircraft electrical busbar. DP has been used for addressing the LAP [22, 48]. It is both a mathematical optimization method and a computational method, which is essential for simplifying the developed algorithm, while seeking an optimized solution. The DP method is applicable when a problem can be divided into multiple simpler problems (subproblems), and there is a relation between the solution of the larger problem and the solution of the subproblems [49]. In [36] the problem comes from the high number of possible combinations that the EPS can have in allocating the loads. Thus, the algorithm, in this particular case, is developed to calculate the maximum weight reduction during EPS design phase. More specifically, the algorithm applied is the knapsack problem [20, 50], which is a mathematical problem solved with DP, and it aims to maximize the number of loads connected to a busbar without

exceeding the EPS available power. Knapsack is a well-known problem in combinatorial optimization [20, 50, 51]. When an optimization of a system with more than one variable is needed, (i.e., Status of the EPS contactors, Available power from the source, critical or non-critical load) the knapsack optimisation can be applied. However, the use of DP is not the best choice for the establishing the overall EPS management due to its complexity resulting in the too intricate code with unfeasible debugging. Yet, it can be added into selected scenarios, allowing the SC to allocate the load in case of a re-distribution of the power, as it will be implemented as such in this work.

#### **2.3.4 Algorithms employed for the SC design**

The algorithms presented in Sections above will be embedded into the SC proposed in this thesis work, taking the advantages given by the use of each of them. Moreover, the SC design will be created based on the requirements of the EPS under investigation. For example, the number of sources, number of critical and non-critical loads, available power paths, and redundant appliances. Thus, in the employed algorithm:

- The knowledge-based method will be used when there is the possibility to reduce the coding and running time. An example can be given as a request to activate a particular load when the drawn power is already known, hence there is no need to calculate it. Thus, the SC can send the command to the converter to supply the load with the predefined value of power.
- The DP will be used when a mathematical optimization is needed, and when the EPS need to be optimized by calculating the value of a variable subjected to one or more constraints, for example in the optimisation of the power distribution on multiple loads, thus, when a source need to be used for supplying a busbar, the power will be distributed across the critical loads first, and the remaining power will be used for the non-critical loads.
- The LTL will be used for the introduction of temporal ordering inside the code or for adding an instruction loop, saving the coding time, and reducing the code length. For example, if there is a set of sequential instructions such as a 'for' or 'if' cycle, the

temporal ordering will ensure that a portion of code is executed before the next instructions.

## **2.4 Tools**

To develop the algorithms described above, different tools can be used. In literature, the capabilities of these tools have been demonstrated in the control of power electronic devices for the EPS management for several applications. The tools used for the SC programming are overviewed in this section; these include C language, Tulip-Python tool, and Finite state machine.

### **2.4.1 C language**

In aerospace applications, majority of systems are programmed using 'C' language. The advantage lies in its simplicity, and easy availability. However, the use of C language is complex for intricate EPSs with multiple hardware to manage at the same time, and debugging is very difficult. For this reason, the 'C language' is used to program the behaviour of the single device, avoiding the management of multiple devices in the same code. The works [30, 52-54] illustrate a number of aircraft controller devices programmed in C language. In [52] the authors proposed an enhanced controller for a buck-boost converter for aerospace application, showing its capability in managing the power flow between the generator and the battery. Fig. 2.2 presents a block diagram of the system used for the simulations, which shows the PEC controlled by using a supervisor:

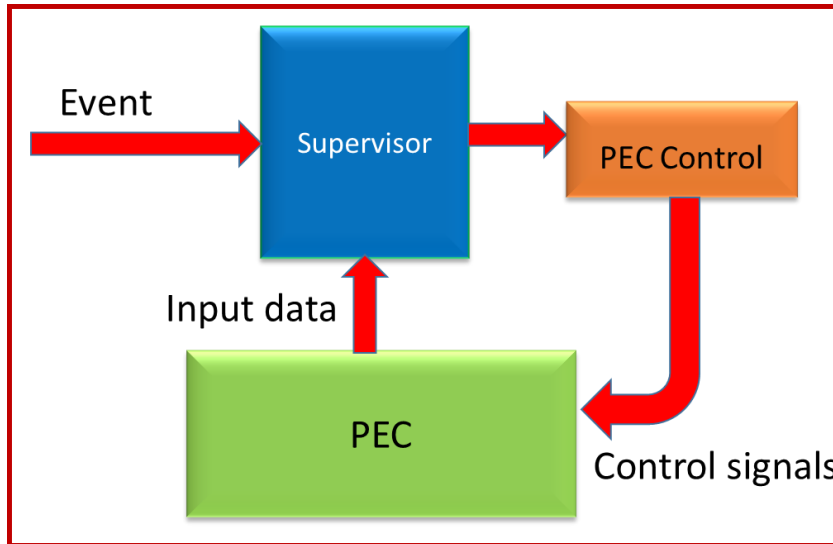


Fig. 2.2. Block diagram of a PEC managed by a SC designed through C language [30]

The control of the PEC have been performed using a sliding mode control in [31], where its mathematical model has been computed in 'C language' inside the Simulink® environment. Authors implemented a SC for the computing of the control equations used for performing the sliding control enabling a more efficient operations for bidirectional converters. In [53] the authors used 'C language' to compute the operations between the converter and battery, managing the EPS behaviour during power peak requests from the main generators, aiming to optimise the power transfer, and the reduction of the generator's size. In [54] the authors used a digital signal processor (DSP), programmed in 'C' language, to increase the bandwidth of the controller, thus giving more accuracy to the system operations (i.e. PECs control, computing of measured values). In [52-54] the authors presented a control strategy of an aircraft EPS based on the control of different devices (i.e., PECs, Batteries, switches) using MatLab environment and then translated in 'C' language, obtaining excellent performances, as described in the papers. However, the 'C language' has been used to manage a single unit of the aircraft electrical system in the aforementioned papers, while this thesis aims to manage the entire EPS, which implies the use, and coordination of multiple devices at the same time. For this reason, the 'C' language code is not the best candidate for this scope of work due to its basic algorithms, which could make the debugging much more difficult, and increase the coding time. However, it can be helpful in the design of part of the SC and will thus be used in the development of the mathematical optimization of the EPS.

### **2.4.2 Tulip - Python**

Python language has been widely used in recent years for programming a new low-cost hardware (i.e., Raspberry PI) due to its great accessibility. It is considered as an intuitive language, and very easy to use for most of programmers. The coding time including debugging time can be reduced as discussed in [55, 56], in which is performed a study on different programming languages showing the computational cost reduction in the using of Python language, and consequently the reduction of the debugging time. However, the Python language, together with the LTL instructions, is not the best candidate for programming the algorithm used to apply the control strategies. This is due to the fact that it cannot be easily integrated with the common controller design software used for the experimental platform. Thus, even if the authors in [24, 28, 43, 57, 58] used the Tulip library in Python language for the LTL coding, its integration with the simulation software (i.e., MatLab®, Simulink®) and the hardware deployed (i.e., control board) is either not possible or extremely difficult to implement. So, it is difficult to create an environment that gives the compatibility between the hardware and software in order to develop a SC, adapt it to an aircraft EPS.

### **2.4.3 Finite state machine**

Finite State Machine (FSM) is a tool where particular inputs cause particular changes in the state of a system, which means that for given inputs (i.e., available power, load current) a set of outputs (i.e., contactor opened/closed, battery on/off) are generated. FSM can be composed of one or more STATES, in which each STATE defines the output variables setting. The change from one STATE to another is called transition [59]. An example is given in Fig. 2.3, which illustrates STATES as a circle with all the instructions that define the system's behaviour and shows the arrows to denote possible transitions to other STATES together with the conditions for these transitions.

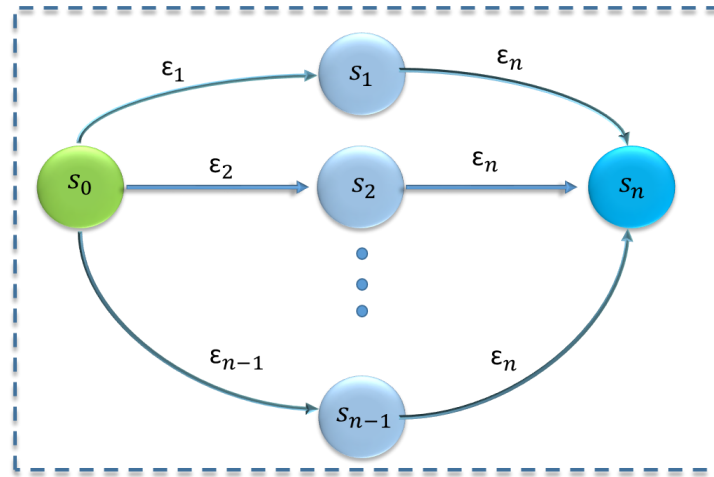


Fig. 2.3. Diagram of a FSM.  $S_0$  to  $S_n$  represent the STATES,  $\epsilon_1$  to  $\epsilon_n$  represent the transitions.

The FSM is widely used in the automated systems with the following advantages: [26]:

- Reduced dynamic memory allocation and simplicity of programming each system STATE separately
- Optimized use of the dynamic memory, which is an important aspect to consider when working with large complex systems.
- More STATES can be added simply by declaring new transition/s.
- Avoiding performing too many “if-else” statements. The system can reach the desired STATE with relatively less computational burden, which means the processor time is frozen for other tasks.

There is a lot of evidence of successful FSM applications. In the patent [60], the authors developed a sequencing control strategy for environmental system controllers, which improves the system operations by creating a series of steps to perform as the response to every variation of pre-set variables, i.e. ambient temperature or air conditioning system status. The aims are to enhance the performance of the EPS by regulating the load current and reduce operating costs by automatically switching off the conditioning system when the environmental parameters are satisfactory. While the patent [25] presents a method for improving the flight controls of unmanned and manned aircraft, where the use of FSM allowed to reduce the computational time and obtain an easier debugging. In [30] the authors proposed a method for PECs management using an FSM. The strategy consisted of using the PEC to regulate the power flow between the loads and the battery. This permit to reduce of

the generator's size, due to the battery, which can be used to cope with the overload request. Other advantages can be exploited from the point of view of the users [27] as given below:

- Given a set of inputs, and knowing the current STATE, the transition can be predicted, allowing for an easy testing.
- The FSMs are quick to design, implement and execute.
- FSMs are flexible. There are several ways to implement them, based on the system topology.
- Easy determination in the reachability of a STATE [61], which means that starting from the initial STATE of the system, it is possible to reach the final STATE, ensuring that unsafe/unexpected STATES are not reached.

Furthermore, the FSM is also well-known for its characteristic in managing reactive systems, i.e., systems which react to changes in its environment. An EPS is a perfect example of a reactive system, in fact it can change configurations as reactions to a variation of its STATE [62].

However, FSM also has some disadvantages as discussed in [59]:

- Some variables need to be specified more than once.
- With a high number of STATES, the code can become difficult to manage, this is due to the high number of STATES to consider together with the high number of behaviours that the system can assume, thus the number of errors can become untraceable.
- Its deterministic domain force the developer to predict in advance all the possible system STATES.

Hence, the FSM tool has many benefits as well as few disadvantages and for the purpose of this study it has been found to be conveniently applicable based on four main considerations:

- Possibility to develop the RCS and the LAP in a feasible and fast way, without having complex and intricate computational coding.
- Easy determination of each reachable STATE for an easy debugging.



- The tool easily to connected with the hardware; this allows for an easy deployment on the developing boards (i.e., FPGA, Microcontrollers) and communication with the sensors (i.e., current and voltage).
- The FSM is the best choice in the management of the reactive systems [63, 64]

Furthermore, the FSM is embedded into the Stateflow<sup>®</sup> of Simulink<sup>®</sup>. The Stateflow<sup>®</sup> provides a graphical language that includes state transition diagrams, flow charts, state transition tables, and truth tables [65]. It can be used to model the FSM, and also allows the additional numerical computations to be introduced inside the STATES. Moreover, owing to the graphical markers on each operating STATE in MatLab<sup>®</sup>, the debugging is easier compared with the earlier FSM development techniques [66]. As an example of its capability, in [30] the authors used the Stateflow<sup>®</sup> of MatLab<sup>®</sup> for generating the controller of an aircraft EPS, the aim was to reduce the generator's size mitigating the power peaks through the use of energy of the emergency battery.

#### **2.4.4 Tools selection**

There is a wide variety of tools that can be used for the design of the SC, the main ones have been presented in sections above. However, the selected candidate has to satisfy some conditions:

- Reduced complexity. It has to manage the entire EPS; thus, possible bugs must be easily identified.
- Easy to interconnect with multiple software. To process multiple data set, the tool must be adaptable to different software environments.
- Easy connections with the selected hardware. The communications between the tool and the selected hardware must guarantee on-line (analysing the code during the execution) and off-line (deploy the code on the hardware) operations.

For these reasons, the FSM is considered as the tool that respects the aims of this Thesis work and therefore it will be employed for the SC design in next Chapters.

## **2.5 Conclusion**

This Chapter has presented a literature review on the field of EPS SC.

First, the design criteria, divided in safeness, reliability, and optimised performances, have been chosen in order to define the objectives of the thesis work. Second, the RCS and LAP methods have been presented as capable to manage the EPS by reconfiguring its power flow paths. For the design of the SC, different types of algorithms and tools have been investigated. Based on the literature review, and taking into account the features presented in Section 2.3.4 and the desired characteristic of the tool reported in Section 2.4.4, it has been decided that a potential candidate tool to be used in this work will be FSM implemented in the MatLab® environment, this choice came from two important aspects:

- MatLab® environment integrates the Sym Power System library that can be used to simulate the design of the EPS
- The model designed in MatLab® environment can be exported on a control board, and used to emulate the SC behaviour on the experimental platform

The FSM tool, which is also integrated with the Simulink®/Stateflow® environment, allows the user to test the preliminary design of the SC coupled with the system architecture.

Next Chapter, based on findings reported above, will deal with the different EPS architectures. The aims are to present the various configuration of the EPS and show the model that will be used for the experimental test.

## Chapter 3: MEA EPS Architecture

### 3.1 Introduction

This Chapter gives an overview of the different EPS architectures that are generally considered for the MEA and introduces the EPS architecture that has been chosen for the further study in this work, including verifying and validating the developed high-level SC. The main challenge behind MEA technology is to increase the use of electric power onboard to replace non-electrically driven systems onboard aircraft, hence extending the electrical network to substitute pneumatic and hydraulic networks [1, 2]. This change in technology inevitably brings in significant changes in power generation, transmission, and distribution. The Fig. 3.1 depicts the concept of MEA, where the generator connected to the engine is used to supply the AC bus, while the rectifiers convert AC to DC power for the DC buses, and the transformer steps down the voltage level of the AC bus. The load scheme, divided by high power AC and DC, commercials and essential, are connected to the appropriate buses.

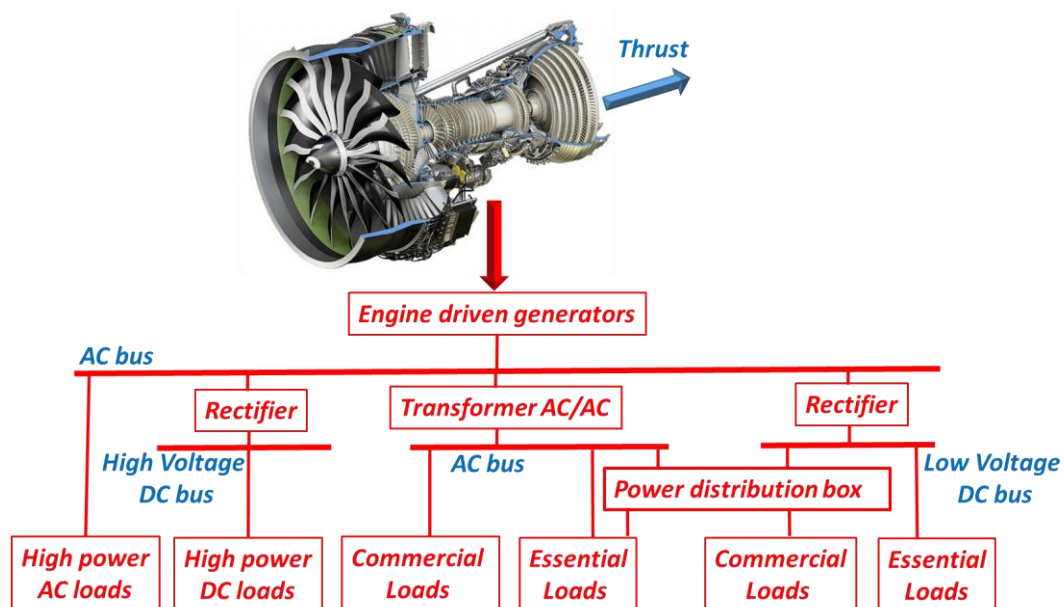


Fig. 3.1. Power source on MEA concept

The major changes between a conventional aircraft and an MEA are summarised in TABLE 3.1.

TABLE 3.1. Main changes between conventional aircraft and MEA [3]

Conventional Aircraft	MEA
Conventional engine is a source of hydraulic, pneumatic and electric power; pneumatic start-up	Bleedless engine, electric start-up
Conventional APU, generates hydraulic, pneumatic and electric power	Electrical APU, only generates electric power
A few power electronics converters	More power electronics converters
Hydraulic and pneumatic actuators	Electric actuators
Mechanical brakes	Electric brakes
AC circuit breakers and low voltage DC breakers	Solid state power contactors
Battery only used in emergency condition and for APU start-up	Used in all flight phases

Since one of the objectives of the MEA is to improve the energy efficiency of the aircraft, choosing the correct architecture as well as control systems is key in the MEA development. Thus, once the EPS architecture is defined, the control techniques, discussed in the previous Chapter, can be integrated into it with the aim to optimize its working operations. In order to transfer electric power effectively from the power sources to the power consuming equipment, a well-designed electrical distribution system in the aircraft is essential. In an aircraft, the generators are driven by the engine during the flight, and the auxiliary generator is driven by the auxiliary power unit (APU) when on-ground or in certain flight scenario. Power, produced from the main generators, is then converted and distributed to the loads in the aircraft [3, 4]. Based on the literature review [4, 5-9], four topologies have been the most popular in the EPS architectures, as listed below, where the 3 and 4 are resulted as dominating technologies:

1. Constant frequency (115 V<sub>AC</sub> 400 Hz)
2. Variable frequency (115 V<sub>AC</sub> 360 – 800 Hz) and 270 V<sub>DC</sub>
3. High Voltage variable frequency (230 V<sub>AC</sub> 360 – 800 Hz) and High Voltage DC ±270 V
4. High Voltage pure DC ±270 V

### 3.1.1 Constant frequency architecture (CF)

In CF aircraft EPS, the most popular generator is the three-stage wound field synchronous generator, and this is due to its safety capability, since the excitation can be instantaneously removed by deenergizing the machine through the direct control of the field [10]. In the Fig. 3.2 is shown a schematic of a three-stage wound field synchronous machine highlighting the three principal stages: 1) the PM generator; 2) the main exciter; 3) the main generator.

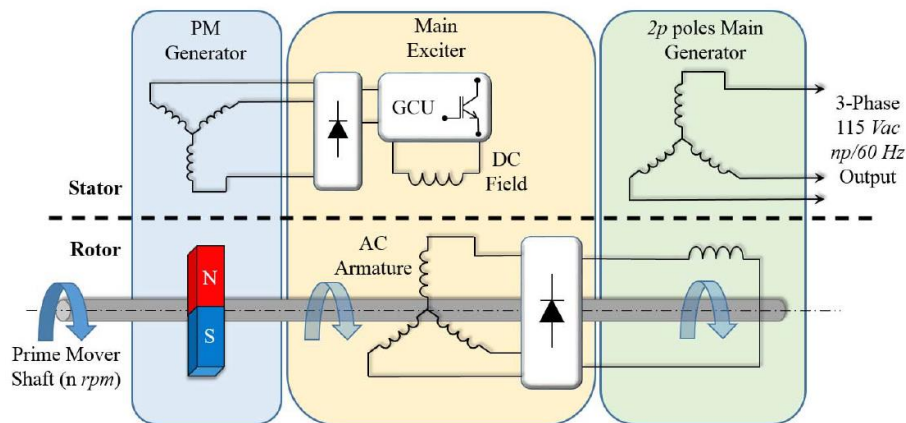


Fig. 3.2. Architecture of three-stage wound field synchronous generator [2]

In the first stage the generation system is powered by the PM generator, whose moving the PMs induce a three-phase voltage in the stationary armature. The ac voltage is then rectified and used for supplying the field circuit of the main exciter in the second stage. At this point, the generator control unit (GCU) acts to fulfil two essential tasks

- 1) Control the dc voltage amplitude, for regulating the excitation current of the main generator, which is in the third stage
- 2) Deenergises the dc circuit in case of faults or anomalous operations

The dc field induces a three-phase voltage in the moving armature of the main exciter, which is then converted into dc, for supplying the excitation field circuit of the main generator. The ac to dc conversion is performed by a rectifier, which rotates synchronously with the prime mover shaft, and the three-phase voltage is available at the output of the main generator armature. Since the frequency is dependant from the number of poles and the rotational speed, the prime move shaft plays an important role in the frequency setting. Thus, a variable-ratio gearbox, referred as CSD [11], is placed between the shaft and the generator in order to

provide constant rotational speed of the generator, at the cost of bulky, heavy and costly additional components, as shown in Fig. 3.3.

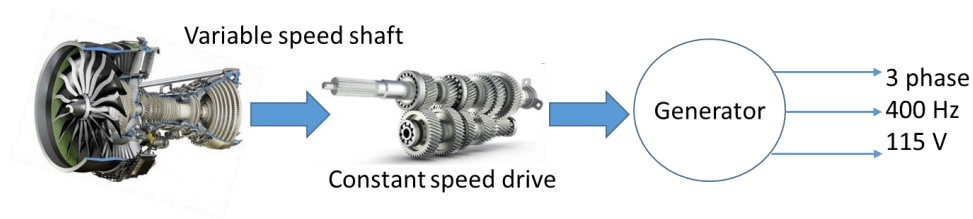


Fig. 3.3. CF generation through the use of CSD

For this reason, It is also possible to obtain a CF system without the adoption of a CSD, which helps to reduce the wight and size of the EPS, and also reduce the maintenance problems that comes to the CSD in order to remove the CSD a variable speed, two methods have been implemented. The first method consists in implementing a dc link between the ac generator and the ac loads, as shown in the Fig. 3.4.

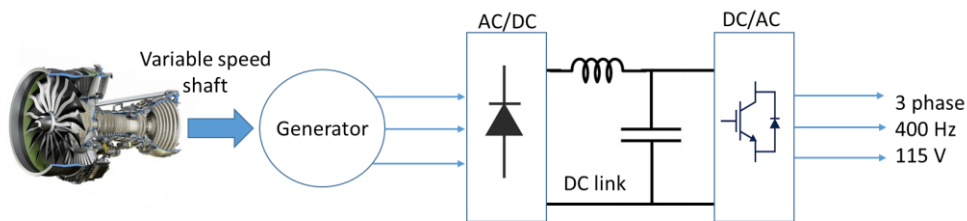


Fig. 3.4. CF generation system diagram using a rectifier and DC/AC converter

The second method consist in adding an ac/ac converter between the generator and the loads as shown in the Fig. 3.5.

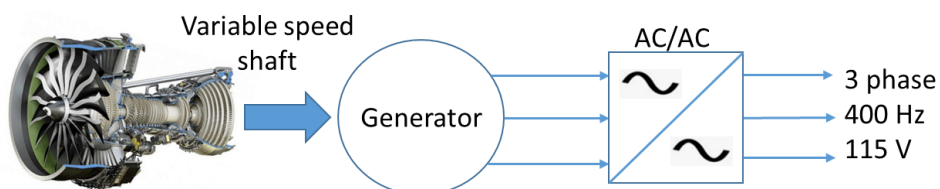


Fig. 3.5. CF generation system using an AC/AC converter

Fig. 3.6 shows the conventional CF aircraft EPS in which bus voltage is 115V at 400Hz AC and 28V DC.

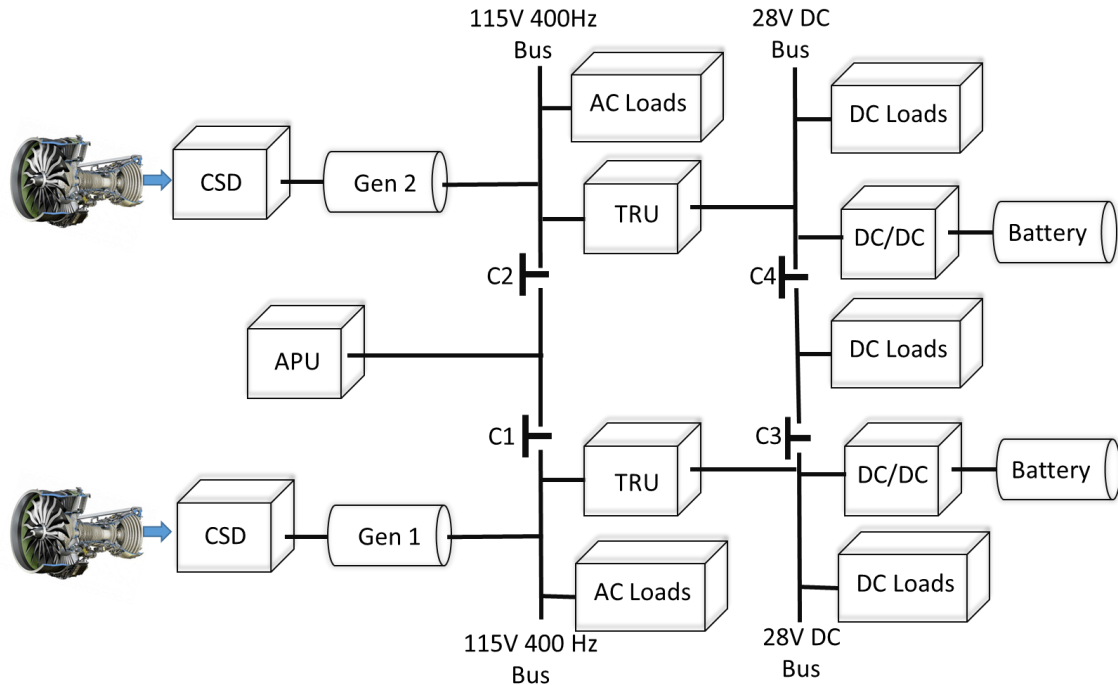


Fig. 3.6. Constant frequency aircraft EPS architecture

The constant rotating speed shaft is connected to the generator, which will then generate a CF power at 400Hz. As shown in Fig. 3.6, AC loads are directly powered by AC bus, while DC loads are supplied from the 28V DC bus. Transformer Rectifier Units (TRUs) are used to convert AC power into DC power. In CF aircraft EPS, AC/DC converter and TRU are the main power converters. Generally, batteries are used as the emergency power sources. An AC/DC inverter and bi-directional DC/DC converter connect the batteries with the AC bus and DC bus respectively. Although DC power can be obtained conventionally from a DC generator, this solution is not commonly implemented, mainly because the space around the aircraft main engine is extremely limited to install other AC or DC generators. For these reasons, TRUs are introduced to convert AC voltage to DC voltage. By installing the TRUs close to the DC bus, the weight and volume of EPS are minimised.

### 3.1.2 Variable frequency architecture (VF)

The trend of moving towards the MEA concept brought to the implementation of VF architectures, Using VF power system helps eliminate the bulky, heavy, inefficient constant speed drives from the aircraft and improve the performance of the aircraft EPSs. In VF aircraft EPS the frequency of the primary AC bus is 360Hz-800Hz with a voltage of 115V and the generator is connected to the engine shaft directly as shown in the Fig. 3.7.

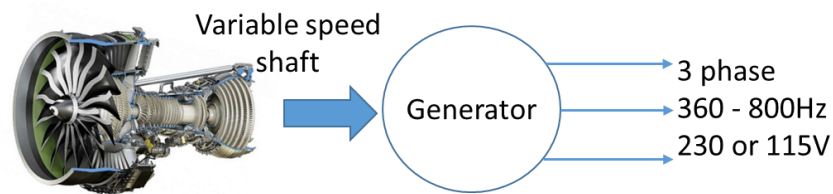


Fig. 3.7. VF aircraft generation system

The three-stage wound field synchronous generator are used as VF generators, where the frequency is proportional to the engine shaft speed [12]. Different types of converters are employed to convert VF voltage to multi voltage levels such as 115V AC and 270V DC. Since the primary AC bus has a variable frequency, a back-to-back converter [13] is needed to power CF loads. These converters must be designed carefully to meet the volume, weight, and harmonic requirements in line with aviation standards such as DO-160 or MIL-STD-704. Thus, according to the mission profiles the frequency varies during the take-off and landing, while it is almost unchanged for the cruise operations in the Fig. 3.8 is shown the architecture of typical VF EPS 115V.



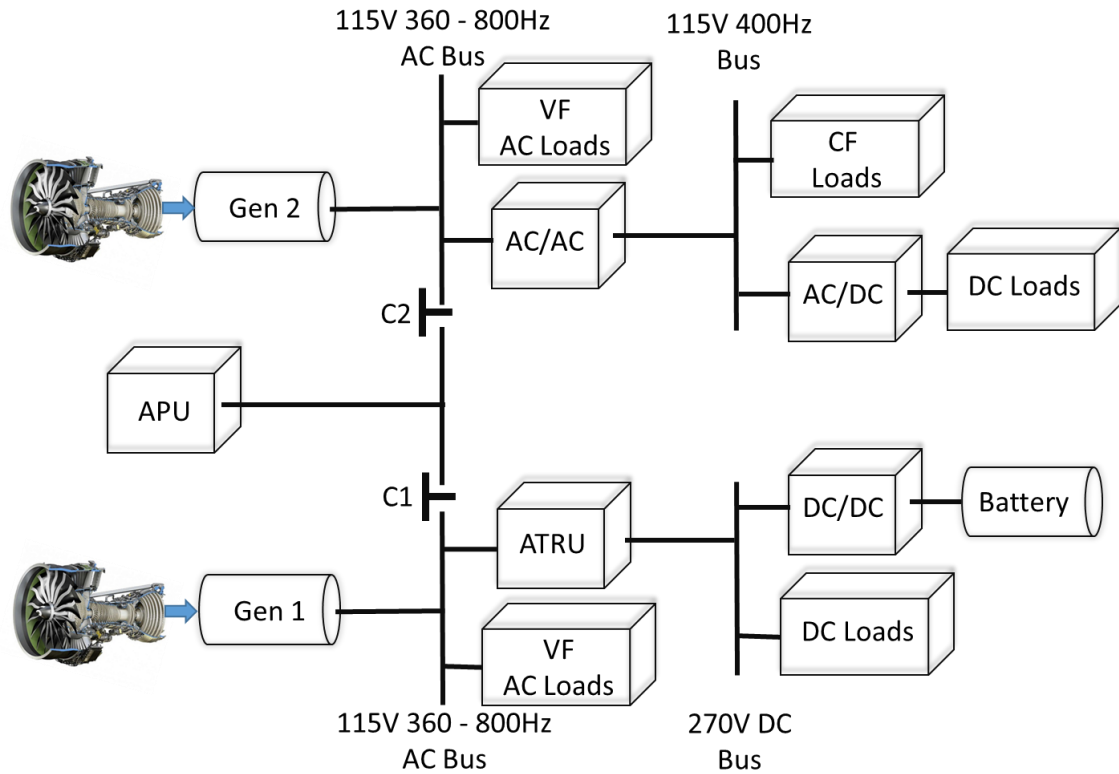


Fig. 3.8. Variable frequency aircraft EPS architecture

The VF EPS presents two VF buses that supplies VF AC loads, while through the use of the ATRU is powered the 270V DC bus. The AC/AC converter is connected between the VF and CF bus in order to supply constant frequency loads, while the 28V DC is obtained through the use of an AC/DC converter.

### 3.1.3 High voltage variable frequency plus High voltage DC $\pm 270$ V (HVAC)

A few new aircraft such as Boeing 787 have adopted High Voltage AC (HVAC) power system (230V at 360-800Hz). Compared to the conventional 115V EPS, power transmission loss and converter weight can be reduced by up to 50.7% and 42.5% respectively [14]. An example of HVAC EPS is depicted in Fig. 3. 9.

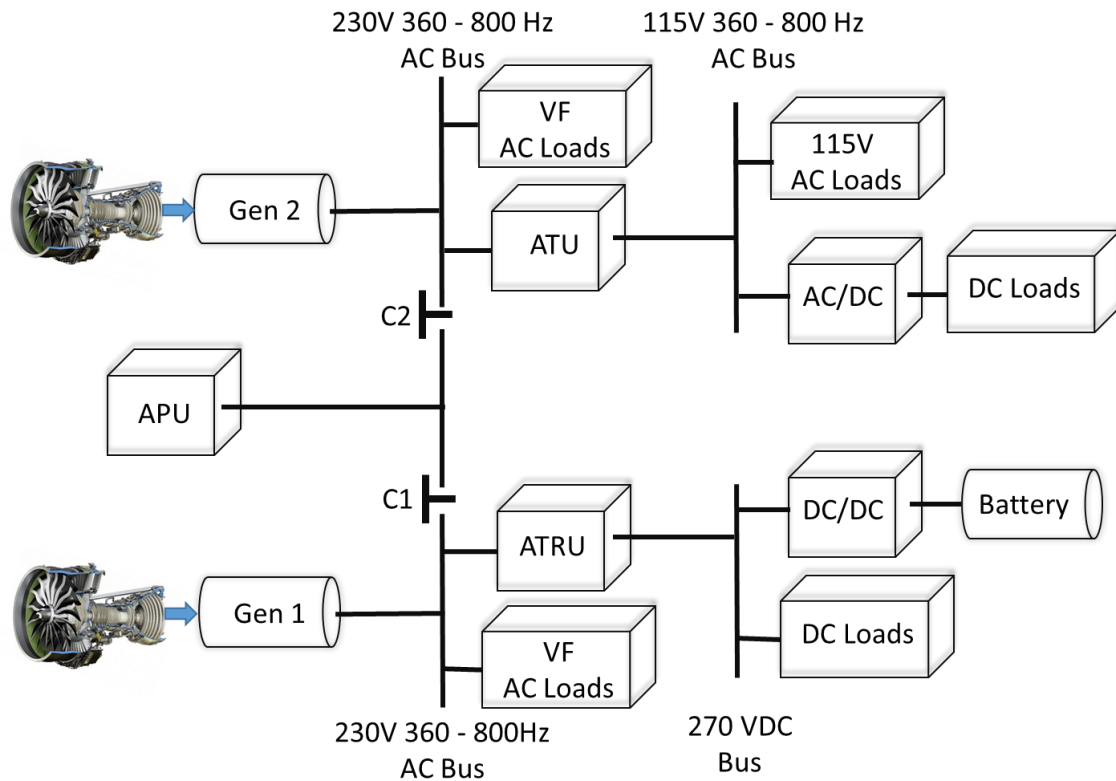


Fig. 3. 9. HVAC Aircraft EPS [4]

In this type of architecture, an auto transformer unit (ATU) is used to generate 115V variable frequency voltage. Buck Boost Converter Unit (BBCU), which consists of 2 DC-AC stages interfaced with a high frequency transformer, is used for the battery charger.

### **3.1.4 High Voltage pure DC $\pm 270$ V (HVDC)**

Future aircraft concepts aim to improve the overall EPS architectures. As reported in [15, 16] significant weight saving could be achieved by increasing the distribution voltage. Considering the same transmitted power, a higher voltage (for the distribution system) will result in smaller cable cross-sectional area. Furthermore, raising the voltage will allow greater line voltage drop [16]. In fact, the minimum allowed voltage is 108 Vac, for distribution system at 115 Vac, instead 250 Vdc are accepted on 270-Vdc systems (as per MIL-STD-704F) [17]. For these reasons, HVDC distribution systems at 270 and 540 Vdc are under investigation [16, 18]. Regarding the HVDC systems, the most obvious concerns are safety and the increased risk of electrical system failures, caused by the LP phenomenon, such as corona effects and insulation breakdown.

Several possible architectures of HVDC aircraft EPS are analysed in [14]:

- +/- 270V DC two phases with ground
- 270V DC one phase with ground
- +/-135V DC two phases with ground
- +/- 135V DC two phases without ground

In most cases, HVDC EPS can lead to weight savings from 4% (270V architecture with 230V AC supply) up to 28% (270V architecture with 115V AC supply). Fig. 3.10 illustrates an example of a 270V HVDC EPS. Generators are connected to the HV270V buses through an ATRU that provides 270V DC voltage. The 28V DC is obtained through a DC/DC converter.

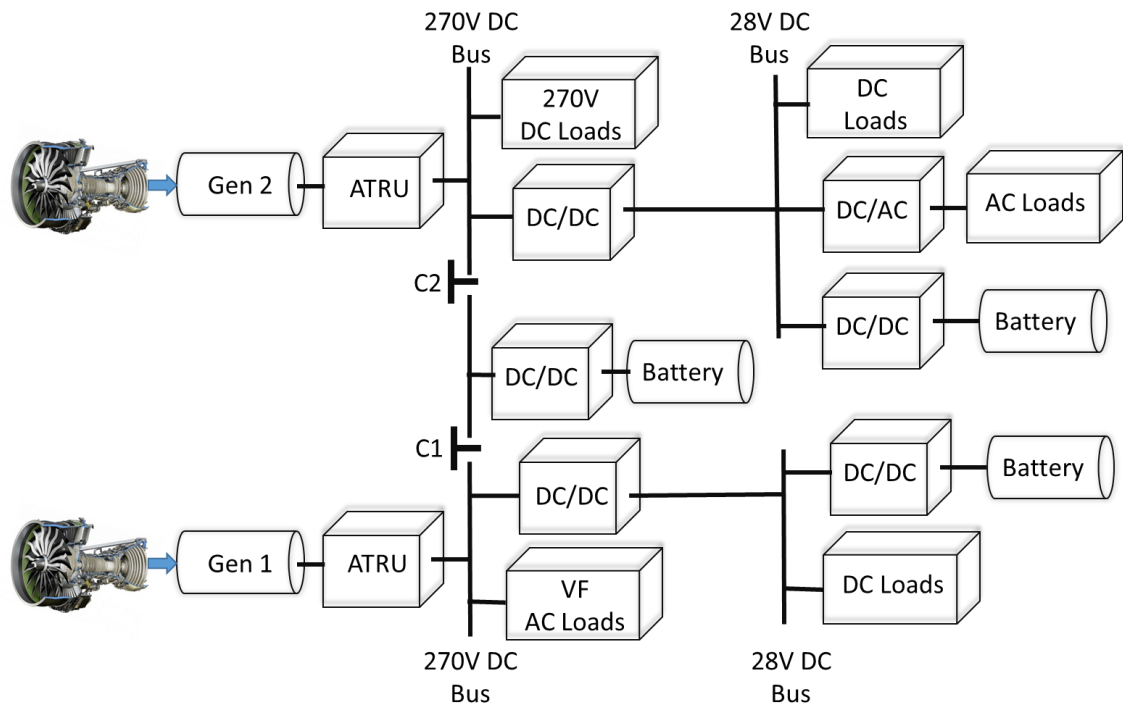


Fig. 3.10. 270 V HVDC Aircraft EPS

### 3.2 Recent MEA EPS architectures

The most recent studies in the MEA field brought to different solutions for the EPS architecture design. In Fig. 3. 11 is presented a MEA EPS architecture proposed in the More Open Electrical Technologies (MOET) project, [19, 20], and It is based on A380 power system [21].

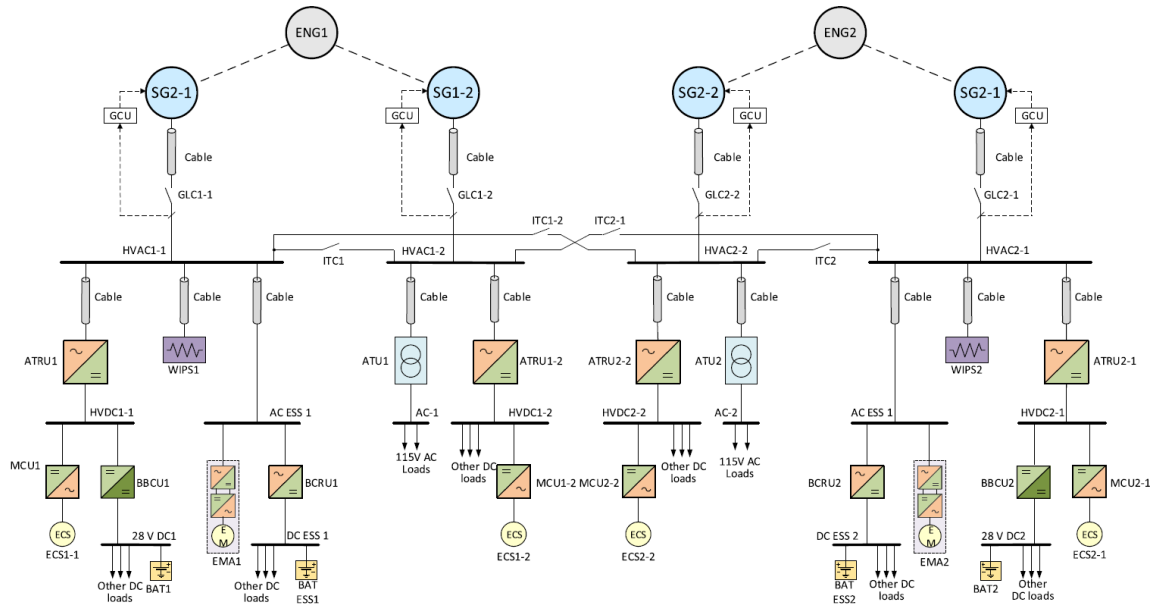


Fig. 3. 11. The MOET aircraft power system [22]

The primary source of MOET system consists of two gas turbine engines, ENG1 and ENG2. Each aircraft engine drives two starter/generator per channel (SG1 – SG4). The generators are controlled by their GCU for maintaining the voltage output at 230V RMS. Since the generator is directly driven by the engine, the power system is variable frequency (360 – 900Hz). The electrical power is distributed in AC through the four buses, (HVAC1 – 1, HVAC1 – 2, HVAC2 – 3, and HVAC2 – 4). In this system configuration, the power distribution is categorized in two kind of centres. The primary electrical power distribution centre (PEPDC), and the essential electrical power distribution centre (EEPDC). Thus, the PEPDC is used to supply the primary loads, such as the wing icing protection system (WIPS), the environmental conditioning system (ECS), back-up batteries and other AC loads. While, the EEPDC is used to supply the essential loads, which guarantee the flight control during emergency scenarios. As shown in Fig. 3. 11, the PEPDC1 is a multiple-bus power electrical system, which consists of a 230V AC

bus (HVAC1- 1), a 540V DC bus (HVDC1-1) and a 28V DC bus. The 540V DC bus is generated by converting the ac power to the dc form through the ATRU1. The buck-boost converter unit (BBCU) is connected to the 540V DC bus to feed a 28V DC bus. The similar power system architecture can be found in PEPDC2. In PEPDC3, the 230V AC bus (HVAC1-2, HVAC2-3) is converted to the 540V DC bus (HVDC1-2, HVDC2-3) by ATRU2 and ATRU3, respectively. The 115V AC bus (AC1, AC2) for supplying the legacy loads is fed by the HVAC1-2 and HVAC2-3 through the autotransformer unit (ATU1, ATU2). For the EEPDC1, it consists of a 230V AC essential bus (AC ESS1) and a 28V DC essential bus (DC ESS1) fed from a battery charge rectifier unit (BCRU1). The EMA1 is used to represent the AC-fed EMA fed by the AC essential bus. The EEPDC2 shares the same architecture as the EEPDC1. It can be easily seen that the MOET aircraft power system is symmetrical in terms of the arrangement of the on-board electrical loads. The SG1, SG2, PEPDC1, EEPDC1 and half of PEPDC3 are composed to be half of electrical aircraft power system. During the normal operation, SG1 supplies the power to PEPDC1, EEPDC1 and WIPS1. Similarity, SG4 feeds the PEPDC2, EEPDC2 and WIPS2. SG2 and SG3 supply the power to PEPDC3 in which the electrical loads are the ECS2, ECS3 and other 115 AC loads. Four batteries (BAT1, BAT ESS1, BAT2 and BAT ESS2) are charged during the normal operation conditions.

Since, MEA technologies relies on power electronics conversion, several EPS's architectures proposal aimed to optimise the use of PECs. In the Integrated Modular Power Electronic Concept (IMPEC) [23], the authors proposed a set of identical PECs used to supply different loads during different flight stages, with the reconnections established using matrix contactors. The number and rating of the PECs are calculated analytically, while the status of the contactors (ON/OFF) is decided in 2 different ways: 1) the current or torque control is realized by the closed control loop of each power module. 2) The voltage or speed control is realized by the SC. In Fig. 3.12 is shown an example of IMPEC architecture.

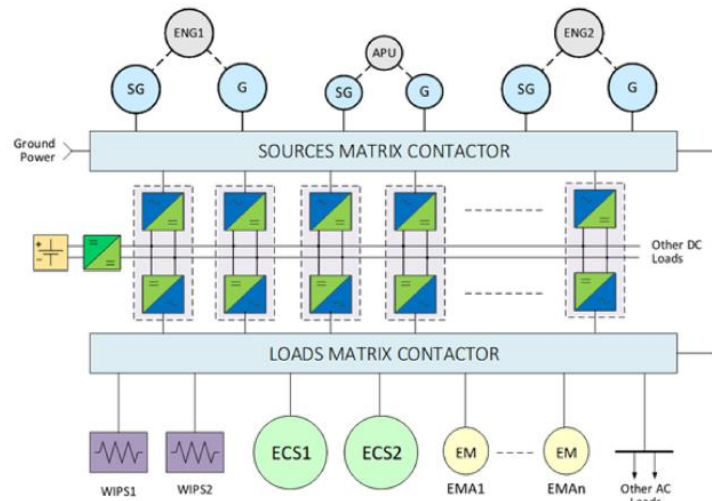


Fig. 3.12. The IMPEC concept architecture [22]

The idea of building MEA EPS using modular converters have also been investigated in [24], in which a small PEC that is a bi-directional converter called “cell” can connect any primary bus to a secondary. In this configuration the cells operate in parallel with the others, sharing the power request from the load, and avoiding power interruption. In Fig. 3.13 is shown the EPS architecture used in [24]:

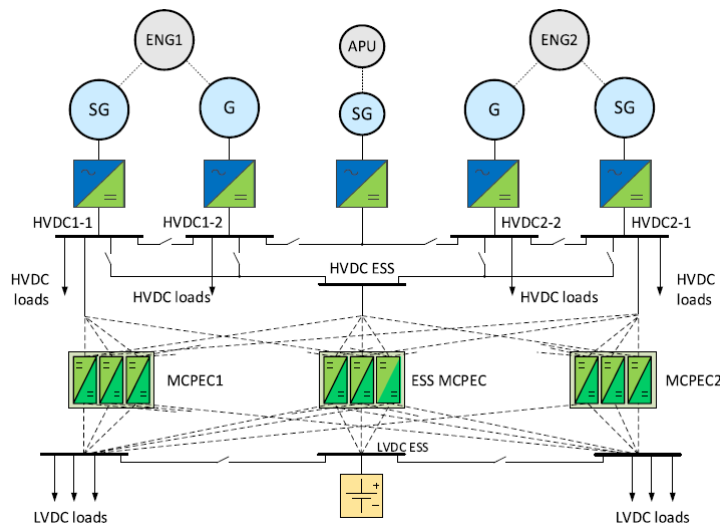


Fig. 3.13. Modular converter cells architecture [19]

In [25] has been presented an EPS topology for a potential electrical propulsion, where the architectures is shown in Fig. 3.14:

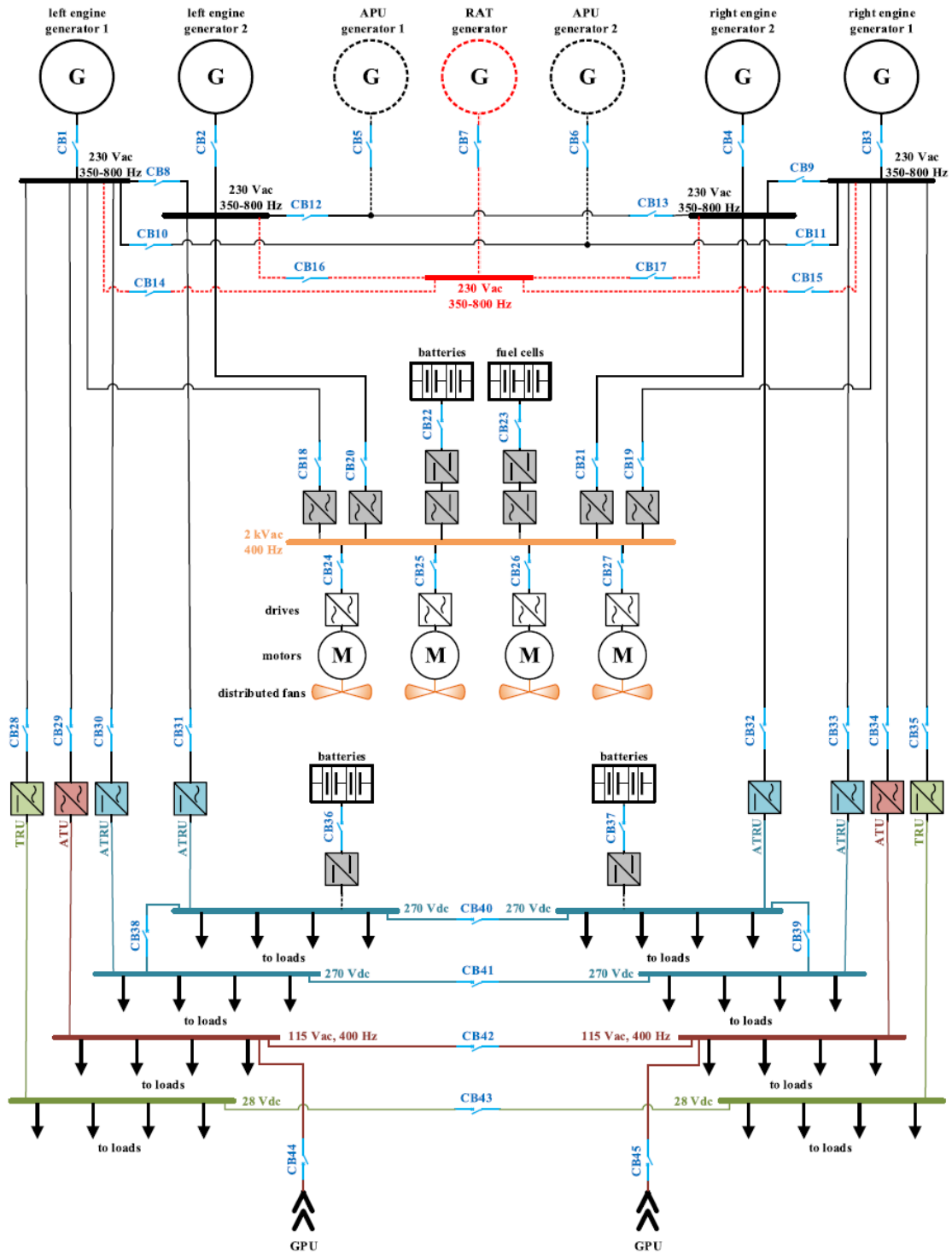


Fig. 3.14. representation of aircraft EPS with electric propulsion system [25]

In the system, each main engine is connected to two generators, the Ram Air Turbine (RAT), which is depicted as generator, is connected to the primary AC buses, and used in case of multiple failure. The considered electrical propulsion system, which is distributed (DPS), is directly supplied from the primary AC bus at 2kV AC. In addition, different buses are derived



### *Analytical approach to Electrical Distribution Systems for Aircraft*

from the primary buses using ATRU, TRU, and ATU. The different loads can be supplied by PECs or connected directly to the bus, based on their characteristic. While the circuit breakers (CBs) are used to distribute the power flow. The Ground Power Units (GPUs) are considered for ground maintenance.

Different EPS topologies can be applied for moving towards the MEA trend. Of course, the final choice relies on safety, reliability, and optimization needed.

### 3.3 EPSs under study

The previous section gave an overview of the different EPS architectures, and different methodologies for the MEA developing. Out of the four architectures presented in the earlier section, the high voltage 270V DC EPS coupled with the use of modular PECs has been selected to be used for designing and testing the high-level SC that is the focus of this thesis, as shown in Fig. 3.15.

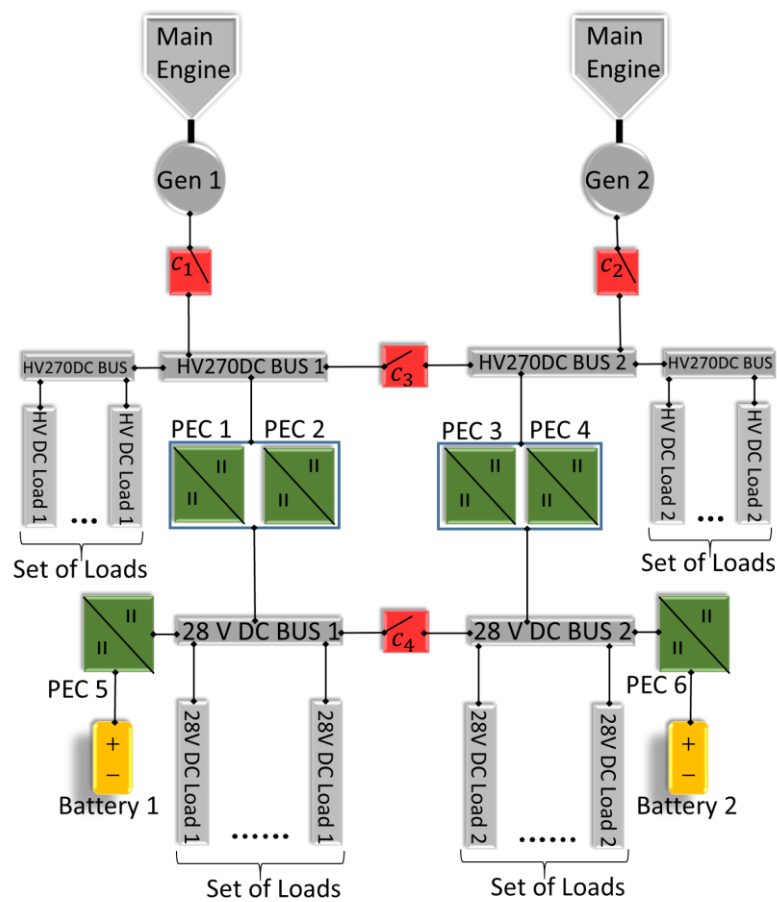


Fig. 3.15. Single-line diagram of the selected EPS

The HDVC architecture has been chosen for numerous advantages.

From the point of view of the control technique:

- DC systems are easier to control. There are no issues here with frequency synchronization, reactive power flows, and harmonics, which make paralleling of converters comparably easier respect to AC systems. In fact, the major task is the

regulation of the DC link voltage within the acceptable bounds during all operating conditions [26-28].

From the point of view of the architecture, the DC system can lead to better performances, while the use of bi-directional modular PECs, as seen above in the MOET and IMPEC project, increase the EPS safety and flexibility, thus:

- The weight of the EPS for the HVDC systems is around 35% less than AC systems [16, 29]
- The use of modular PECs makes the EPS more flexible, allowing the SC to have more degree of freedom
- The possibility to employ bi-directional PECs allows the power sharing from the battery to the HV buses, adding another level of safety in case of generator failure
- However, this system architecture as to deal with the problems related to a DC system fault (i.e. DC short circuit)

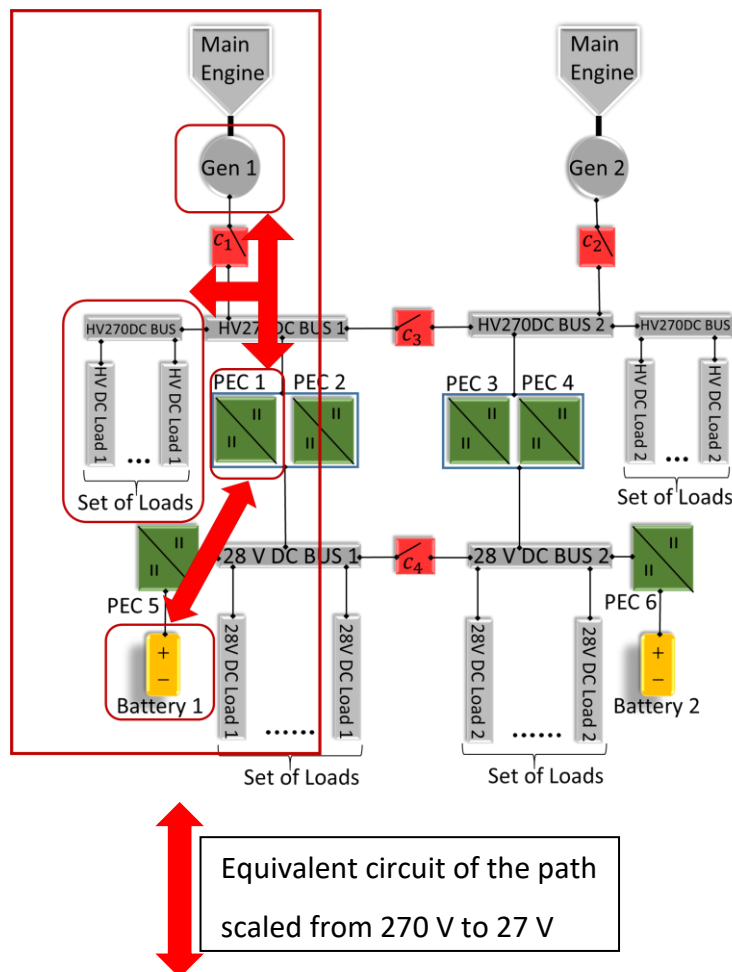
Fig. 3.15 shows the MEA EPS that has been chosen to test the SC for this work. Such EPS is composed of two main generators, Gen1 and Gen2, which are connected to the HV270DC main buses 1 and 2 through the contactors C1 and C2 respectively. The contactor C3 is kept open and used to feed the buses HV270DC BUS 1 or HV270DC BUS 2 in case of emergency, modifying the power flow distribution. In the event one of the generators fails, contactor C3 closes to enable the healthy generator to supply both 'sides' of the network. The generators supply power to two sets of high voltage loads (HV loads 1 and 2), and low voltage (LV loads 1 and 2) through four power electronics converter (PEC1, 2, 3 and 4) and through LV DC buses 1 and 2 as shown in Fig. 3.15. The four PECs are bi-directional converters, as discussed above in the modular converter "cell" architecture (IMPEC project) and are current controlled. This method helps to improve safety, reliability and flexibility of the EPS as they enable power flow in both directions, and guarantee redundancy to the faults, since the buses will be fed even in case of one or more "cell" fails, and enables more options for the SC in reconfiguring the EPS. The employment of modular PECs makes the EPS more flexible, since this method enables the power sharing through different tracks across the EPS. Through use of C4, the PECs can be used to enable power sharing through the low voltage buses, 28 V BUS 1 and 28 V BUS 2; The loads consist of a set low priority loads and vital loads, adding a level of priority

to the EPS. Moreover, the two batteries are designed to provide supplementary power to the EPS through DC/DC converters PEC5 and PEC6 respectively, and to the vital loads in particular, in case of faults in the electrical network. The PECs 5 and 6, as shown in Fig. 3.15, are voltage controlled, and used to maintain the voltage of the LV buses at 28 V. This design introduces redundancy in the power system and provides alternative paths to supply power to the loads in case one or more of the PECs fail. However, this will be reached at extra cost and weight for the entire EPS, so, the design phase must determine the correct balance between redundancy, cost, and weight. In particular, the SC can act on the EPS elements (i.e., PECs, Contactors, Batteries) to reconfigure the network in different scenarios:

- The failure of one generator
  - Covered by closing the contactor C3
  - Using one of the PECs to split the power on a different bus for providing additional power
- Failure of a converter
  - Covered by disconnecting non-essential loads, thus reducing the power request
  - Covered by using another available PEC coupled with the battery
- Optimization of the power flow
  - Use of the contactors for re-configuring the power paths
  - Use of the batteries for avoiding the overloads

### 3.4 Scaled down model of the EPS under study for the experimental tests

This section introduces the simulation model of the EPS which will be used in the experimental tests to support the analytical studies in this work. A reduced version is introduced for testing the capability of the designed SC in the laboratory. The proposed physical model (experimental set-up) is shown at the bottom part in Fig. 3.16 as a single-line diagram of the EPS that will be tested in experiment. It includes the main components and represents the key functionalities of the larger EPS in Fig. 3.15. The selected components which comprise generator 1, the set of loads connected to the HV bus 1 and battery 1 have been chosen in order to show the capability of the SC in managing power flow amongst them. The Gen 1 is used to supply the HV Loads through the HV Bus 1, while the PEC 1 and the Battery 1 are connected through the LV Bus 1 enabling the power sharing between the battery and the HV Bus 1. For clarity, the power path is highlighted in the Fig. 3.16.



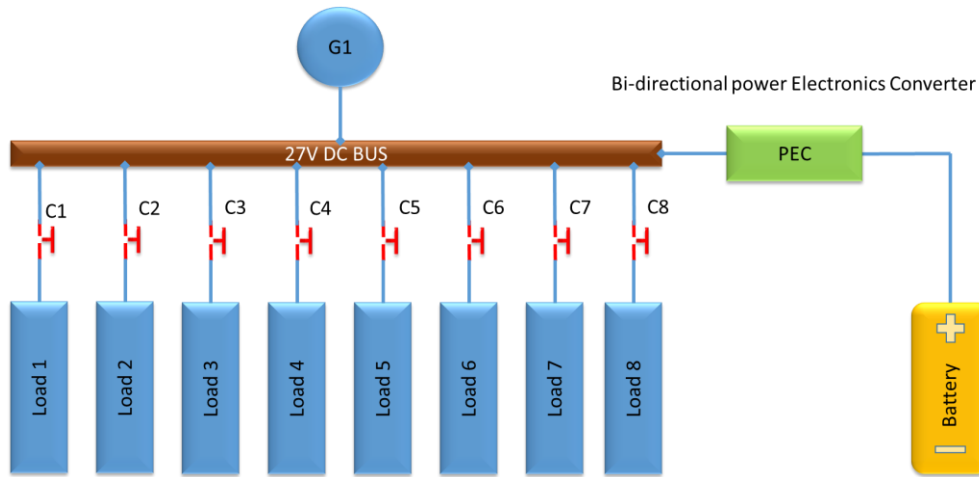


Fig. 3.16. Scaled single-line diagram of the EPS used for the experimental work at the bottom of the Figure compared with the full version of the EPS at the top of the Figure

Furthermore, the aforementioned reduced EPS in Fig. 3.16 will also be scaled down by 10 in voltage (from 270V DC to 27V DC) and power. The battery in the scaled down EPS is rated at 27V DC. It is to be noted that scaling down the voltage and power will not affect the experimental tests intended to test the logics of the SC. The scaled down version will also be safer to work with in the laboratory. The scaled down EPS model, as shown at the bottom of Fig. 3.16, is composed of a DC generators G1, which provides 27 V DC to the DC bus. The DC bus supplies 8 loads divided in 3 different levels of priority, 4 high priority loads (load 1 to load 4), 2 medium priority loads (Load 5 and Load 6), and 2 low priority loads (Load 7 and Load 8 ). Moreover, a set of contactors, C1 to C8, are used to connect/disconnect a load from the bus. A battery is connected in parallel to the generator through a bi-directional PEC, as shown in Fig. 3.16, to provide additional power to the loads. With the configuration presented in Fig. 3.16, the SC can be used to experimentally test the RCS and the LAP methods presented in Chapter 2, as will be presented in Chapter 8. However, the presence of one PEC will not allow the emulation of the converter failure that will be neglected in the experimental part. Fig. 3.17 represents the interface between the SC and the experimental EPS.

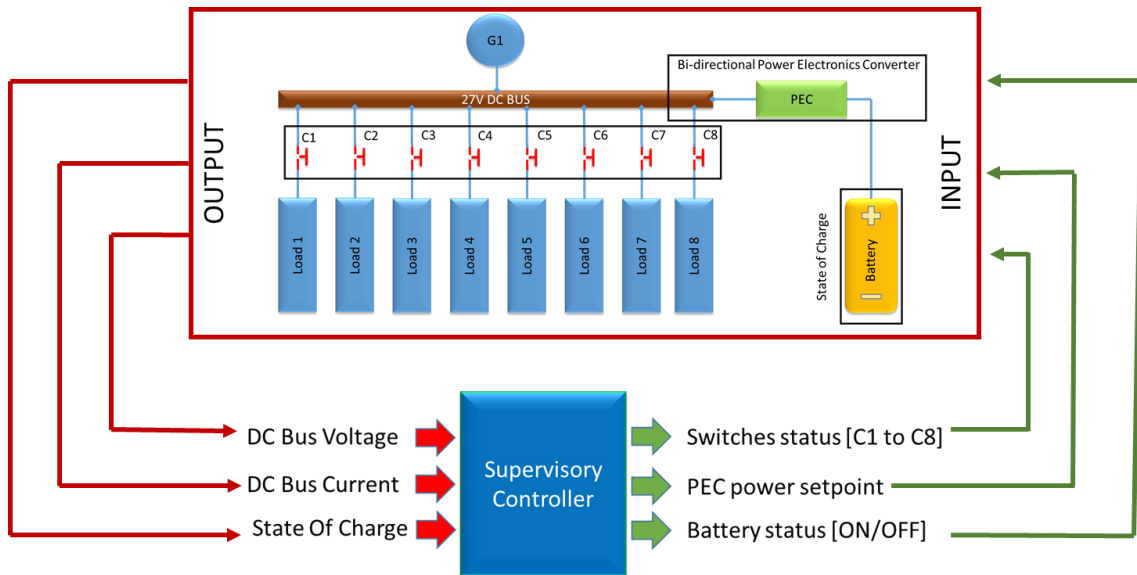


Fig. 3.17. Interface diagram of the SC with the EPS, in red are highlighted the inputs for the SC while in green are highlighted the outputs

As shown in Fig. 3.17, the SC receives as input the bus current, bus voltage, and the battery State of Charge from the EPS and transmits as outputs (arrows) to the EPS the switches status (open or closed), the power to be delivered from the PEC and the battery.

### **3.5 Conclusion**

This Chapter has provided a comprehensive description of the main different architectures for the MEA concept, and also explored different hybrid solutions for improving the EPS. Four different main types of architectures have been described, the CF, the VF, the HVAC, and the HVDC architecture. However, the most promising technologies for the MEA advancement seems to be given by the Hybrid EPSs, due to their safety, and reliability aspects coupled with the high flexibility. Thus, the simulations and experimental test will be performed on the HVDC architecture, which has been selected for its advantages, already discussed in the section 3.3, and coupled with the solution implemented in the MOET and IMPEC projects. The purpose of this work is to tests the SC capability in managing such EPS; from the design point of view, the HVDC architecture requires simpler control of its electrical components and has a reduced weight which is beneficial for the aerospace applications. Moreover, a simplified scaled version of the HVDC EPS has been proposed for the experimental tests of the SC capability with the objective of using a limited amount of hardware resources without affecting the final results analyses, verification and validation of the SC.

In the next Chapter will be presented the RCS method. It will be implemented in the SC and will be applied to the selected EPS shown in the Fig. 3.15. The simulations will be performed on two different case scenarios in order to test the capabilities of the SC in the application of the RCS.



## **Chapter 4: EPS Re-configuration strategy**

---

### **4.1 Overview**

The RCS method has been presented in Section 1.1.2. This Chapter reports two case studies to demonstrate the capability of the RCS approach for the high-level SC design, followed by the verification and validation of the method. In the first case study the RCS is employed to reconfigure the EPS to avoid the generator overload with the aim to reduce the generator sizing requirement, hence its weight and volume. In the second case study the aforementioned strategy is used to modify the power flow routes during one or multiple faults of the PECs with the objective to satisfy the specified EPS safety criteria. As already discussed in Chapter 1, RCS has been chosen for its intuitive algorithm and due to reduced coding complexity to ensure the correct power flow distribution across the EPS. The two case study scenarios are solved by considering the status of the entire EPS (under overload conditions or faulty elements), while adopting RCS and using the FSM tool for its features, already discussed in Chapter 2. This Chapter aims:

- To demonstrate that the application of the chosen reconfiguration strategy, algorithms and tools are practical and computationally inexpensive for the design of the SC, while reducing complex programming.
- To develop a methodology to design a high-level SC capable of improving EPS efficiency while respecting safety constraints by effectively managing the power of the entire MEA EPS.

## **4.2 Generator overload reduction by smart power management**

### **4.2.1 Overview**

In this section, a control strategy is designed to control the power flow of a representative MEA EPS with the aim to reduce overload of main generators while ensuring safety of the electrical network. This would allow to reduce overloading requirements for the generators design hence reduced generators weight and volume, with up to 15% reduction. The FSM, introduced in Chapter 2, is used to design the controller, and implement the control strategy. This section first describes the model of the EPS and the control strategy. The control logic is then implemented and ran within the simulation environment. Finally, the simulation results are presented and discussed.

### 4.2.2 The EPS under study

The control strategy developed in this case study is applied to the EPS shown in Fig. 4.1.

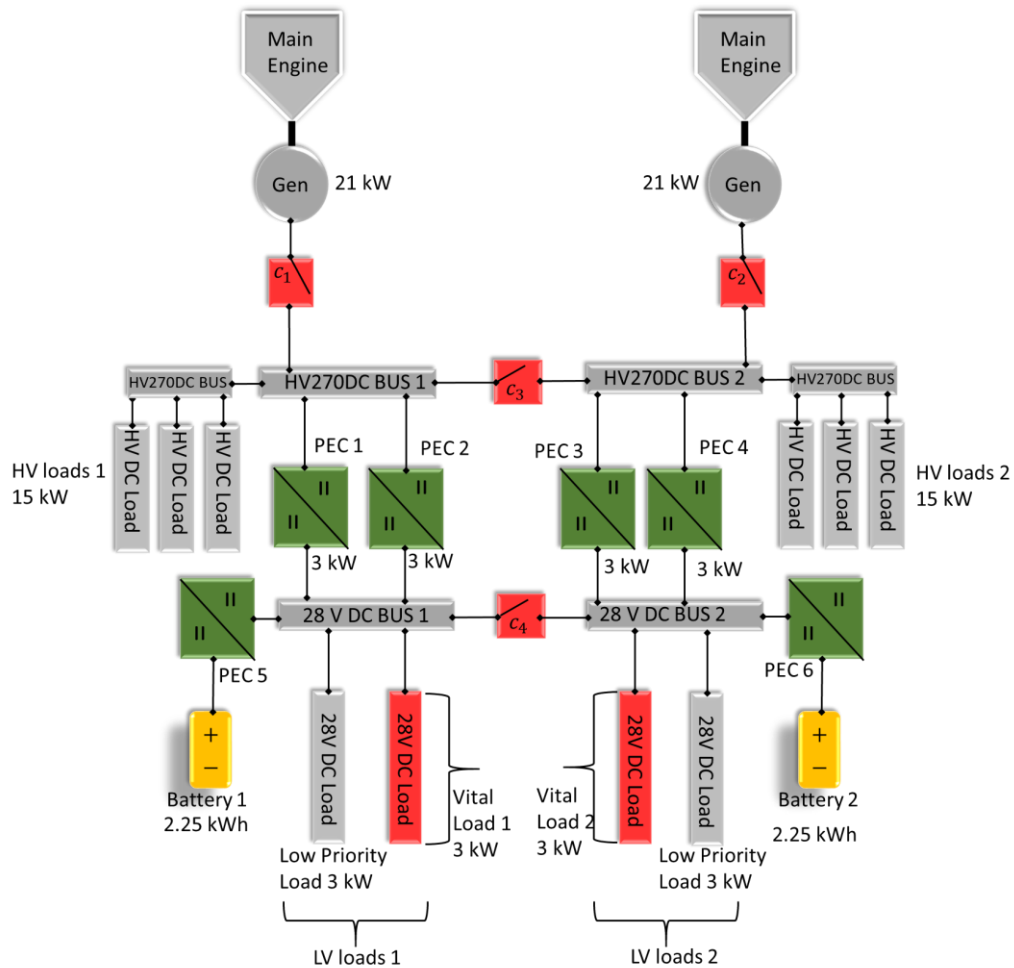


Fig. 4.1. Representative MEA EPS for the case study

The example MEA EPS, as shown in Fig. 4.1, is composed of two 21kW main generators, each connected to the 270V dc main buses 1 and 2 through the contactors  $C_1$  and  $C_2$  respectively. The contactor  $C_3$  is kept open during normal conditions of operation to avoid parallel connections of the two generators. Parallel operation of generators is not considered in this study. In the event one of the generators should fail, the contactors  $C_1$  or  $C_2$  are opened, and the contactor  $C_3$  is closed to enable the healthy generator to supply both 'sides' of the network as shown in Fig. 4.1. The generators supply power to two sets of high voltage loads

(HV loads 1 and 2) of 15kW each and low voltage (LV) buses 1 and 2 with their loads fed via four power electronics converters (PECs 1, 2, 3 and 4) as shown in Fig. 4.1. The HV loads comprise de-icing system, as will be explained later in this Chapter. The four PECs, rated 3kW each, are bidirectional converters to enable power flow in both directions. The four PECs are connected in pairs to LV buses 1 and 2; this design introduces redundancy in the system and enables power to be supplied to LV loads in case of one of the PECs fails. The LV loads consist of two low priority 3kW loads that can be shed if required and two vital loads 3 kW each for which power supply should be uninterrupted. Moreover, there are two batteries of 2.25kWh each to provide supplementary power to the EPS and to the vital loads in particular, in case of faults in the electrical network. The PECs 5 and 6, as shown in Fig. 4.1, are used to maintain the voltage of the LV buses at 28V. Since the focus of the case study is to demonstrate the control logic performance, all the components of the EPS will be modelled as ideal devices in the Simulink® environment.

### **4.2.3 The Control strategy**

The control strategy in this case study is developed with the aim to reduce the overloading of the EPS generators while ensuring the following safety requirements:

- Uninterrupted power to the vital loads,
- Avoiding parallel connections of electrical sources
- Avoiding discharging the batteries below a pre-set limit by monitoring the SOC.

The HV loads 1 and HV loads 2 shown in Fig. 4.1 represent de-icing system. The de-icing system is used in the aircraft to remove ice formations on the critical parts of the aircraft structure such as airfoils leading edges and require around 20-30% of the total power of the EPS.

During normal operations, the HV loads 1 and 2 consume 15kW of power each, as denoted as operation mode (OM) 1 in TABLE 4.1. The total power of the EPS is 42kW in OM1 as shown in TABLE 4.1. During de-icing conditions, each of the HV loads 1 and 2 require an additional 6kW of power (i.e., a total of 21kW each) for the de-icing system to function, as described in TABLE 4.1 under OM2. The total power required by the EPS increases from 42kW to 54kW during

de-icing conditions. In this case, these short-term loads can be supplied by using the energy stored in the batteries, which are sized to cope the power demand of the de-icing system for 12 minutes. A control strategy is to be devised to supply the surplus power to the de-icing system without oversizing the generators, which are rated at 21kW each. It is to be noted that depending on the generators design, these machines can be permitted to operate in overload modes for short period of times. However, such a design means an increase in weight of the generators. Since ice-protection and other overload requests are short-term loads, these pikes of load demands can be managed by batteries and therefore they may not count into the generator sizing task.

In this work, the control strategy is to be devised such that the generators do not need to go in overload, and hence do not need to be sized for short overload operations. This can be achieved by first shedding half of the low priority loads on buses 1 and 2, decreasing the total power supplied to them from 6kW to 3kW, as shown in TABLE 4.1 under OM2. This action will lower the total power requirement of the EPS in OM2 from 54kW to 51kW as shown in TABLE 4.1.

TABLE 4.1 Load power requested during OM1 and OM2

	Operation mode 1	Operation mode 2
<b><i>HV<sub>bus 1</sub></i></b>	15kW	<b>21kW</b>
<b><i>HV<sub>bus 2</sub></i></b>	15kW	<b>21kW</b>
<b><i>LV<sub>bus 1</sub> Vital load</i></b>	3kW	3kW
<b><i>LV<sub>bus 1</sub> Low priority load</i></b>	3kW	<b>1.5kW</b>
<b><i>LV<sub>bus 2</sub> Vital load</i></b>	3kW	3kW
<b><i>LV<sub>bus 2</sub> Low priority load</i></b>	3kW	<b>1.5kW</b>
<b>Total power</b>	42kW	51kW

Secondly, the additional 9kW required for the OM2 to further reduce the total power from 51kW to 42kW are to be supplied by the batteries. The two batteries supply 6kW to the de-icing system through two PECs operating in boost mode controlling the power flow from the battery to the loads (PECs 1 and 4 are selected in this study), and 3 kW to half of the active non-essential loads. It is to be ensured that the LV vital loads 1 and 2 have uninterrupted power. In this case study, it is assumed that the state of charge (SOC<sub>batt</sub>) of the batteries are kept at 90% during normal operating conditions. In addition, the minimum SOC (SOC<sub>min</sub>) of the batteries should be 50%; this reserve energy is to supply the vital loads in case of

emergency. Hence, 40% of the total energy ( $E_{tot}$ ) of the two batteries can be used to supply additional power required during the de-icing phase ( $P_{add}$ ) of 9kW for a total duration ( $t$ ) of 12 minutes as determined by eq. 4.1. Of note is that in the worst-case scenario, the de-icing system is required to operate for 5 minutes, which is within the time of 6 minutes each battery can supply additional power to the EPS [1-3].

$$t = \frac{E_{tot} * (SOC_{batt} - SOC_{min})}{P_{add}} = \frac{4.5kWh * 0.4}{9kW} \times 60 = 12 \text{ minutes} \quad 4.1$$

In Fig. 4.2 is shown the EPS load values during the two OMs:

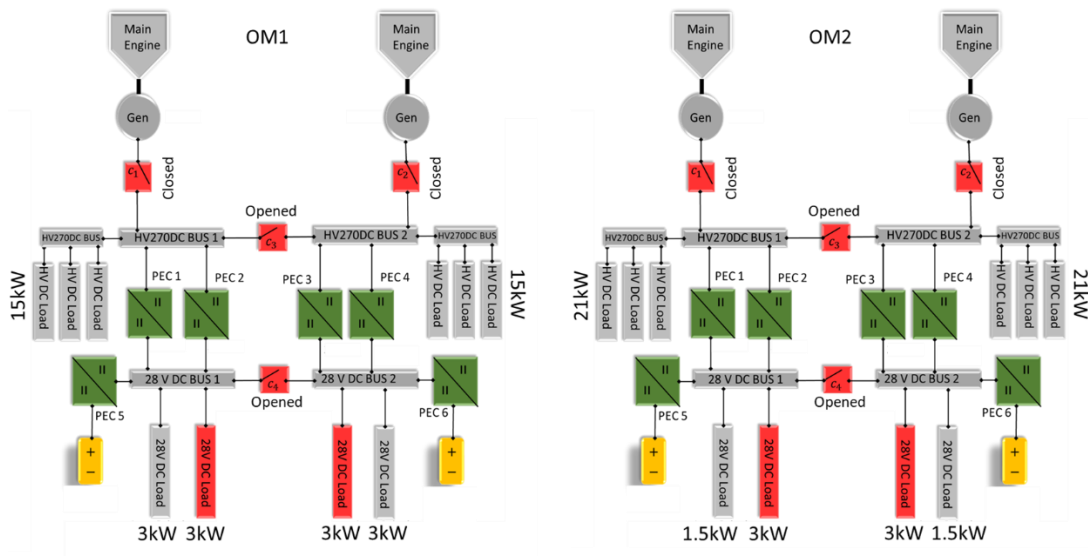


Fig. 4.2. EPS load configuration during the two OMs

The proposed strategy allows the SC to modify the power flow of the EPS based on the two different OMs. When the de-icing is not active the generators will supply the total EPS loads, while in case of de-icing activation the SC will modify the power paths to use the batteries to cover the power pikes.

### 4.2.4 Strategy to logic

Once the control strategy has been defined, it must be translated into a form that the SC can read and act upon. This work is based on the Finite state machine (FSM) and the control rules are written in state transition tables. The control strategy, which has been defined in the earlier subsection for this case study, describes the required behaviour of the system under different OM1 and 2. The control strategy is first converted into a state transition table, which the controller can read and then take required actions. The state table for this case study is shown in TABLE 4.2, where the variables are the state of charge of batteries 1 and 2 referred to as SOC 1 and SOC 2 respectively. When the power system has a power demand for the de-icing system, depending on the values of SOC 1 and SOC2, the system will transition to STATES (ST) 1, 2, 3 or 4 as shown in TABLE 4.2, and as described below

TABLE 4.2. State table used to define the SC behaviour during this case scenario

SOC	Battery 1: 50%<SOC<90%	Battery 1: SOC=50%
Battery 2: 50%<SOC<90%	<p>STATE 1: De-icing ON</p> <ul style="list-style-type: none"> <li>- C4 closed</li> <li>- Batteries 1, 2 connected</li> <li>- Load shedding on low priority loads</li> <li>- DC/DC PEC 1 and PEC 4 operated in boost mode and batteries 1/2 supply surge power</li> <li>- If SOC Battery 1 = 50% go to STATE 2</li> <li>- If SOC Battery 2 = 50% go to STATE 3</li> <li>- After power surge, go to STATE 4</li> </ul>	<p>STATE 2: Battery 1 OFF</p> <ul style="list-style-type: none"> <li>- C4 opened</li> <li>- Battery 1 disconnected; Battery 2 connected</li> <li>- Load shedding on low priority loads</li> <li>- DC/DC PEC 1 and PEC 4 operated in boost mode and battery 2 supplies surge power</li> <li>- If SOC Battery 2 = 50% go to STATE 3</li> <li>- After power surge, go to STATE 4</li> </ul>
Battery 2: SOC=50%	<p>STATE 3: Battery 2 OFF</p> <ul style="list-style-type: none"> <li>- C4 open</li> <li>- Battery 2 disconnected; Battery 1 connected</li> <li>- Load shedding on low priority loads</li> <li>- DC/DC PEC 1 and PEC 4 operated in boost mode and the battery 1 supplies surge power</li> <li>- If SOC Battery 1 = 50% go to STATE 2</li> <li>- After power surge, go to STATE 4</li> </ul>	<p>STATE 4: De-icing OFF</p> <p>If the Generator is not in overload</p> <ul style="list-style-type: none"> <li>- Charge batteries until 90% SOC (battery with lowest SOC charged first)</li> <li>- If SOC 1 exceeds 90%, disconnect battery 1, go to sub-state 4.1, charging only battery 2</li> <li>- If SOC 2 exceeds 90%, disconnect battery 1, go to sub-state 4.1, charging only battery 1</li> </ul> <p>If the Generator is not in overload</p> <ul style="list-style-type: none"> <li>- No action to reduce the Generator overload</li> </ul>

ST1 – De-icing ON: If SOC 1 and SOC 2 are between 50% and 90%, (normally 90% at the start), both batteries supply power to the de-icing system with the PECs 1 and 4 in boost mode, and half of the non-essential loads that are not shed (2 times 1.5kW). The system is maintained in this STATE until SOC1 and/or SOC2 falls to 50%. In the figure below (Fig. 4.3) the power flow from the battery to the HV loads when the de-icing is active is shown.

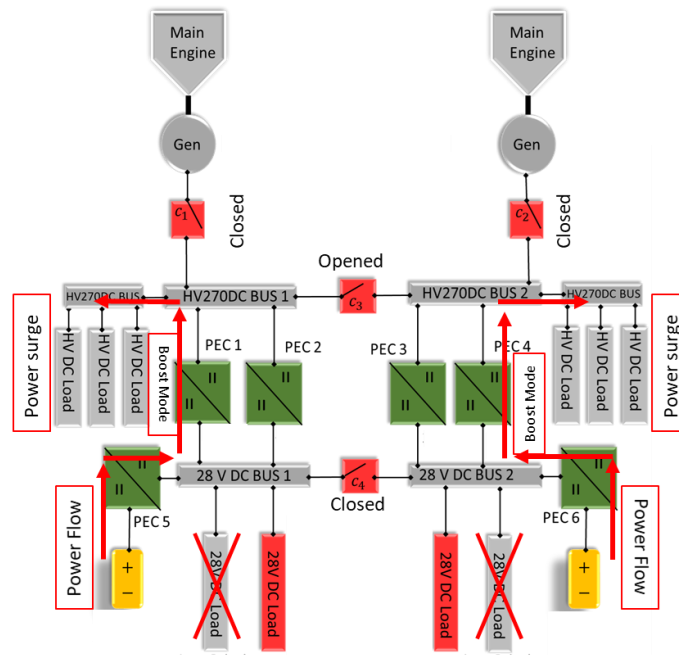


Fig. 4.3. Battery to HV Loads power flow during the De-icing ON scenario

**ST2 – Battery 1 OFF:** If SOC 1 reaches 50%, battery 1 is disconnected to preserve energy for the vital load in case of emergency. Only battery 2 is used to supply the de-icing system and half of the low priority loads that are not shed.

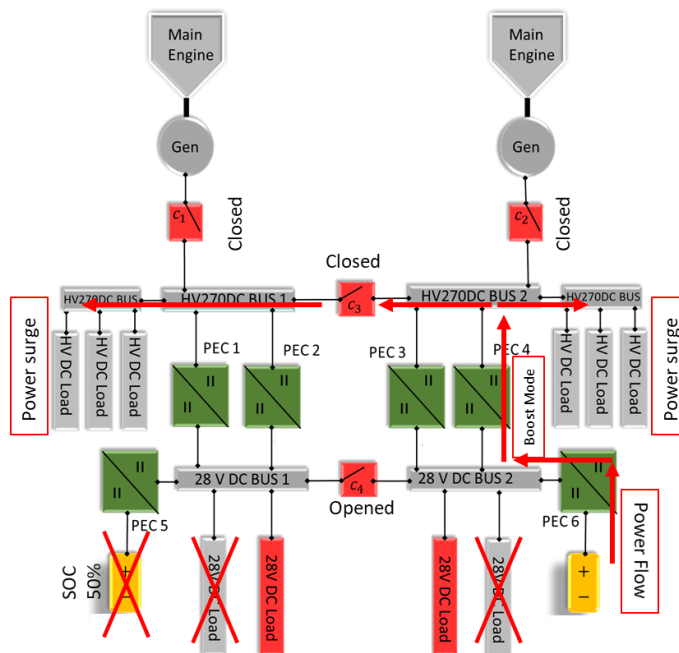


Fig. 4.4. Battery to HV Loads power flow during Battery 1 OFF scenario



ST3 – Battery 2 OFF: STATE 3 is similar to STATE 2. However, battery 1 instead of battery 2 supplies the additional requested power. Considering the symmetry of the EPS the probability to have different level of the SOC for the battery 1 and 2 is low. However, this scenario must be considered, in order to allow the SC to be able to manage all the possible scenarios.

ST4 – De-icing OFF: When SOC1 and SOC 2 both reach 50%, the system is in ST4. Thus, the system is no longer in de-icing power surge request. The SC enables the batteries charging until 90% of the SOC disconnecting the non-essential loads. Once the charge is completed the EPS gets back to normal operations.

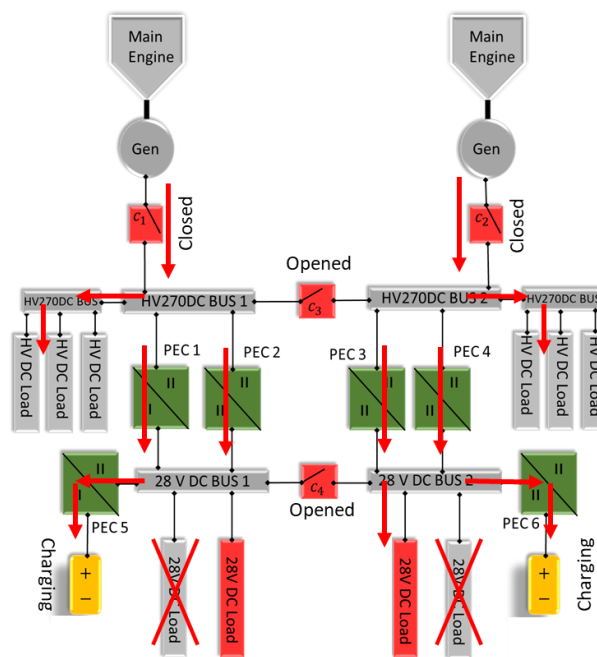


Fig. 4.5. Power flow during the De-icing OFF scenario

Assuming that the SOC of the batteries are always at 90% during normal operation i.e., OM1, and that the worst-case scenario of de-icing conditions i.e., OM2 require energy from the batteries for a maximum duration of 6 minutes on HV loads 1 and 2 respectively, then STATE 4 is used to charge the batteries back to 90%.

#### 4.2.5 EPS model components description

The EPS components are created in Simulink® environment, using the Sim Power system library, as highlighted in the figure below.

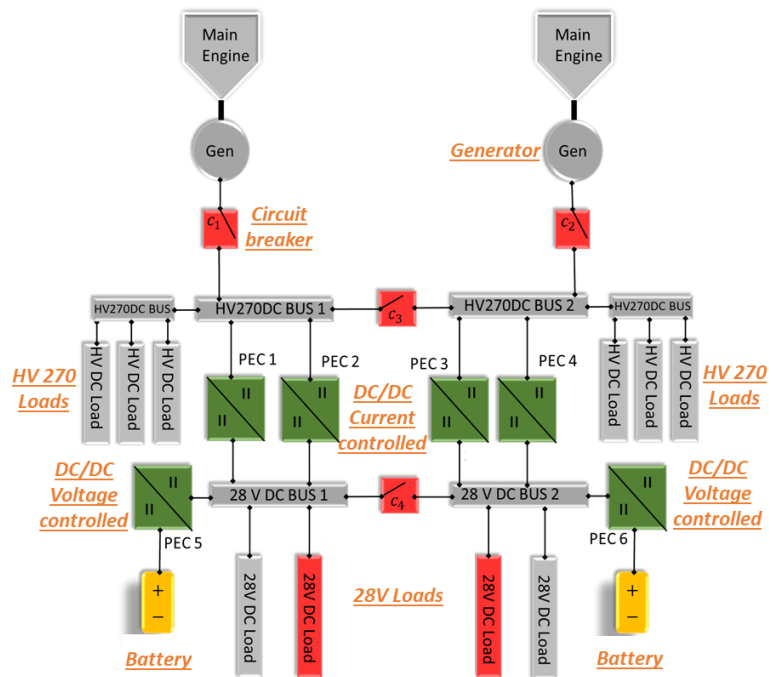


Fig. 4.6. List of the components modelled in Simulink® environment

Since the EPS is an HV 270V dc, an ideal dc generator has been used as a generator model. The 2 generators (G) supply the HV buses connected through a circuit breaker (C). The HV 270V Loads are modelled as resistive loads and are activated or de-activated through circuit breakers. The PECs, from the HV 270V buses to 28V buses, are bi-directional dc/dc current-controlled and working in a range of -3kW to 3kW so that the SC can be used to inject the calculated current value into the loads or reverse the power flow. The PECs, from the 28V buses to the batteries, are dc/dc voltage-controlled so that they can be used to maintain the voltage of the bus to 28V and supply the loads under emergency scenarios. While the battery is modelled with the predefined Simulink® battery tool without taking into account the thermal management since it was out of the scope of this work.

#### 4.2.6 Simulation results

In this section will be presented the simulations performed on the EPS model created on Simulink® environment. The scope is to test the SC capabilities in managing the power surge requests of the system. The simulation scenario assumes that the system is initially operating in normal conditions (OM1 as defined in TABLE 4.1). Assuming intense ice formation, which is considered as the worse-case scenario for the EPS, (OM2 as defined in TABLE 4.1), the EPS must supply the de-icing system with an additional  $2 \times 6\text{kW} = 12\text{kW}$  power for a duration of 6 minutes as considered in this case study. Fig. 4.7 shows the power request from the de-icing system of the HV load 1 rising from 15kW to 21kW at time 12s, which is similar for HV load 2. At time 12s, SOC1 is 70% and SOC 2 is 85%, as shown in Fig. 4.8; hence the system is in ST1 at time 12s as shown in Fig. 4.13.

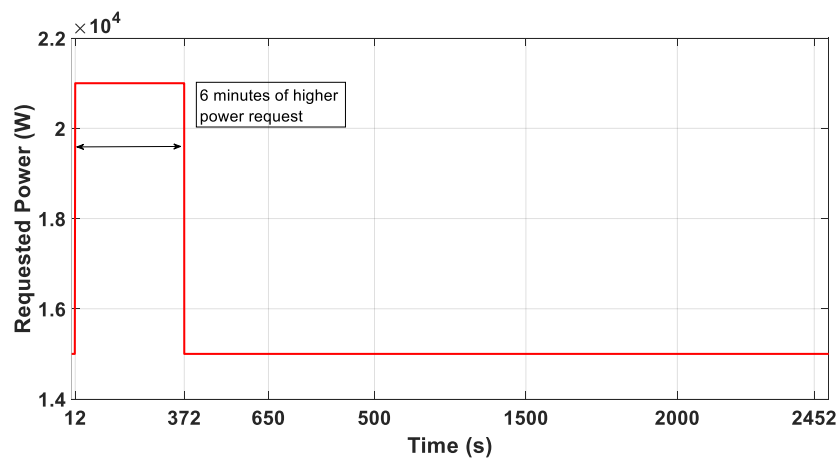


Fig. 4.7. Request of total of 12kW power for de-icing system with (i) 6kW to HV load 1 and (ii) 6kW to HV load 2, respectively

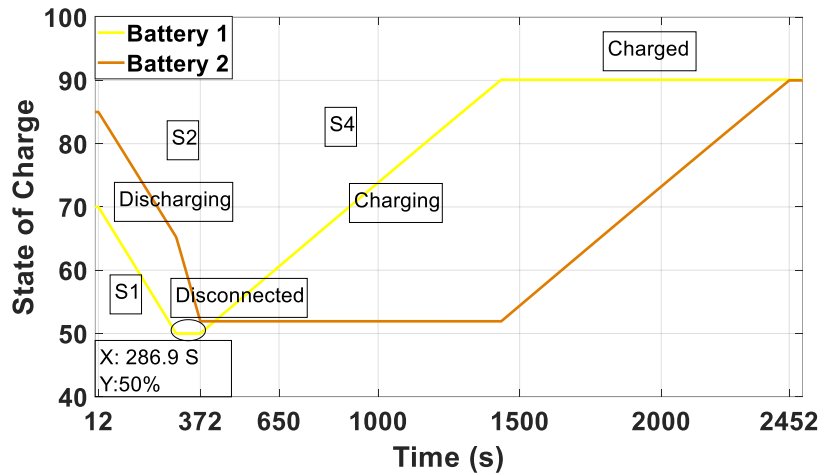


Fig. 4.8. State of charge of batteries 1 and 2 as the system changes STATE

The EPS remains in ST1 from time 12s to 286.9s. At time 286.9s, when SOC1 drops to 50% with SOC2 being still above 50%, the controller changes the system configuration from ST1 to ST2, in accordance with TABLE 4.2. The system is in ST2 until time  $t = 372$ s, as shown in Fig. 4.13. At time 372s, i.e., 6 mins after activation of OM2, the de-icing operation terminates, and the system is moved to ST4 as per TABLE 4.2, and as depicted in Fig. 4.13. In system ST4, the battery 1 is charged first until its SOC reaches 90% at time 1438s. Thereafter, battery 2 starts charging from time 1438s to time 2452s. It is to be noted that when the system is in ST1 and 2 from time 12s to 372s, PEC 1 and 4 are in boost mode, each transferring 3kW of power from the LV bus to the HV bus, as shown in Fig. 4.10. Fig. 4.9 shows the characteristic of one of the generators. The spike in Fig. 4.9 at time 12s is due to a power request. When a power surge comes the generator is subjected to a power request. However, the SC can see the generator's overload and activates the batteries mitigating the surplus power on the generator in a short period.

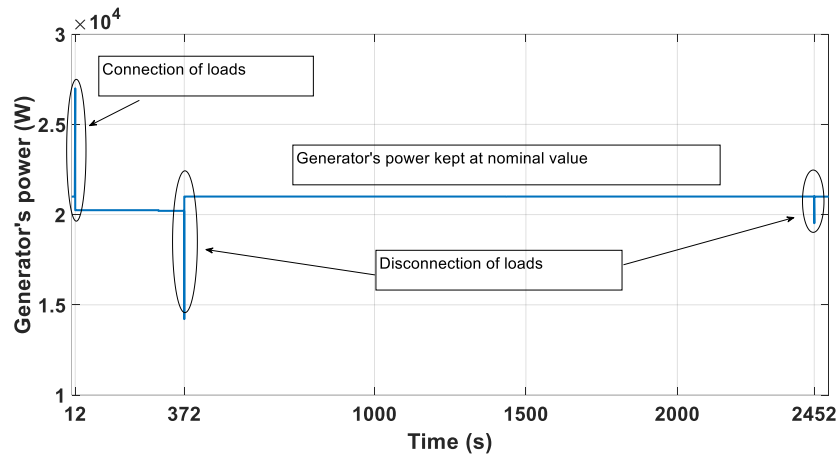


Fig. 4.9. Power characteristic of one generator, which shows that the generator does not go into overload

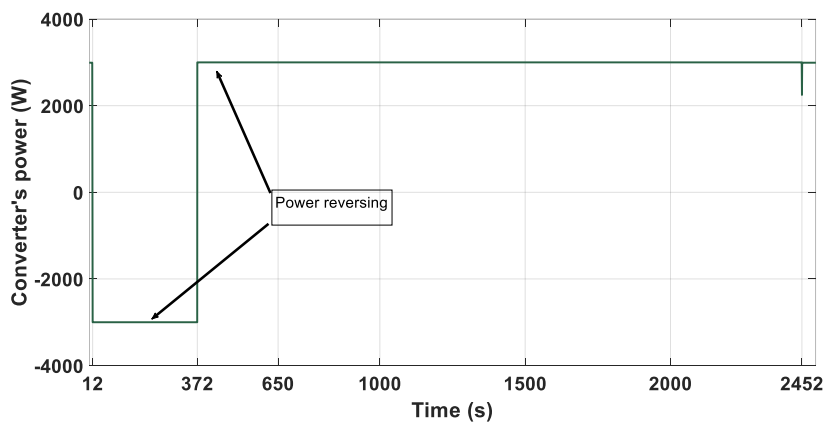


Fig. 4.10. Power characteristic of power electronic converter 1 which shows power flow reversal at  $t=372s$

The controller has also activated load shedding from time 12s to 2452s, to first supplement power for the de-icing system in STs 1 and 2 and then to recharge the batteries in ST4, as can be seen from Fig. 4.11. In addition, the PECs 5 and 6 have ensured that the voltage of the LV buses is maintained at 28V during the state transitions as can be seen in Fig. 4.12.

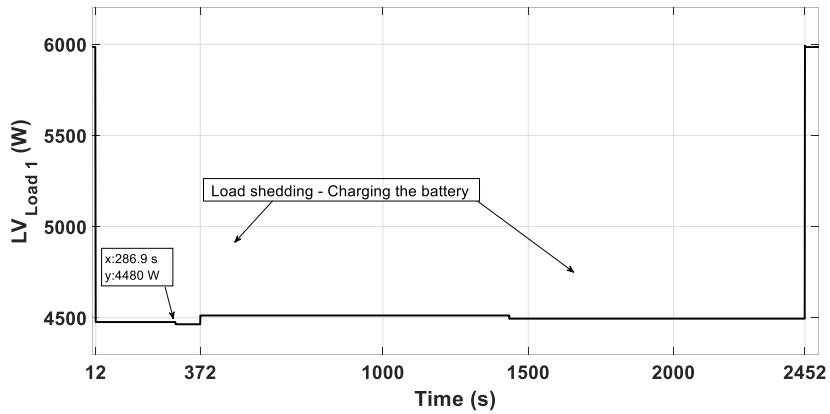


Fig. 4.11. Power characteristic of the LV bus1. At time  $t=12s$  to  $2452s$  power drops from  $6kW$  to  $4.5kW$  due to load shedding to supply de-icing systems in STs 1, and 2 and then to charge batteries in ST4

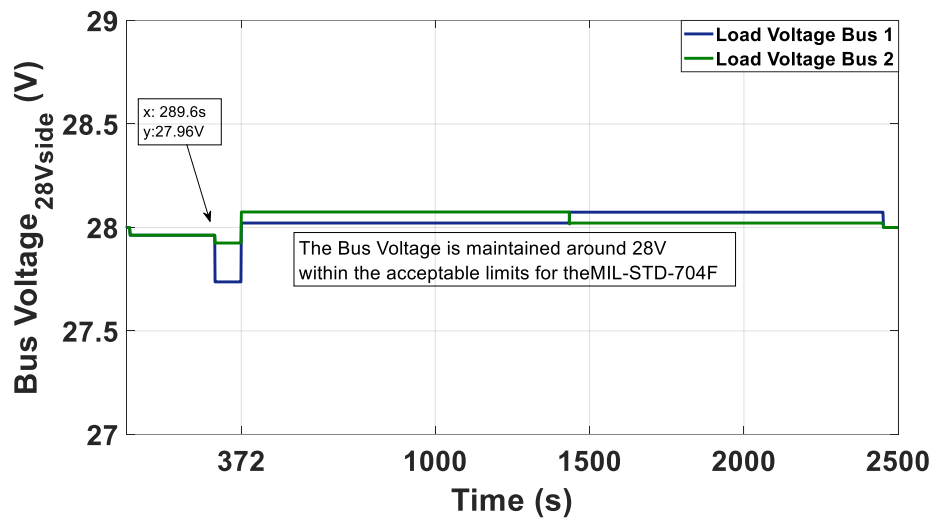


Fig. 4.12. Voltage on low voltage buses 1 and 2 maintained at 28V

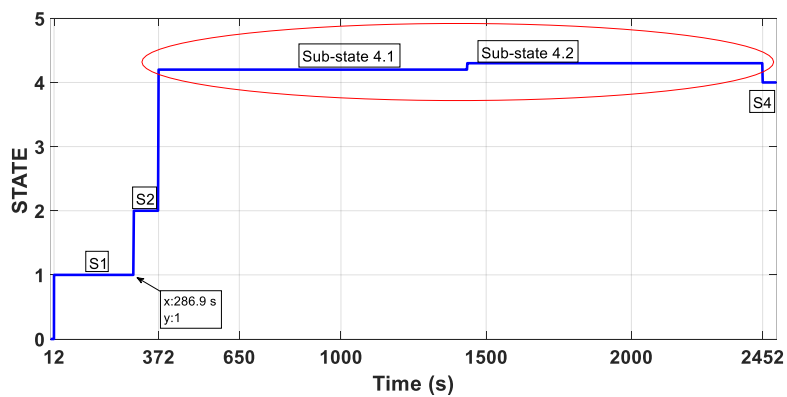


Fig. 4.13. System STs for the case study. System is in (i) ST1 from  $t=12s$  to  $t=287s$  (ii) ST2 from  $t=286.9s$  to  $t=372s$  (iii) ST4 from  $t=1438s$  to  $2500s$

#### **4.2.7 Conclusion for study case 1**

This section has exploited the re-configurability feature of a representative MEA EPS and has devised a control strategy aimed at reducing the overload on its two generators. Through simulations, it has been shown how an overload can be avoided on the generators by the application of a power management strategy implemented into the SC, which will allow the use of batteries enabling different power paths for the overload mitigation. This implies that smaller on-board generators can be used for the electrical network with consequent reduction of aircraft weight and fuel consumption.

### 4.3 Smart controller design for safety operation of the MEA electrical distribution system

This section demonstrates how the reconfiguration strategy can be used for safety operation of the EPS of a future aircraft as shown in Fig. 4.1 by ensuring uninterrupted power to its vital loads under fault conditions.

#### 4.3.1 The control strategy

For this case study the SC is designed to ensure the safe operation of the EPS by providing uninterrupted power to the two vital 6kW LV loads under a number of fault scenarios consisting of failures of one up to four of the 3kW DC/DC converters (PEC1, PEC2, PEC3, PEC4). The SC is designed such that it triggers certain specific set of actions for each of the abovementioned fault conditions; these are also dependent on the system variables, which are the states of charge of the batteries 1 and 2 (SOC 1 and SOC 2) respectively in the case study. The actions can be represented as 16 different STs, as given in TABLE 4.3 to TABLE 4.6.

##### 4.3.1.1 No fault scenario

During this scenario the EPS is working under normal operations, which means that there are not overload requests or faults. However, the SC monitors the EPS status checking the presence of faults, overloads or the SOC's status. Thus, under normal operations, depending on the values of SOC1 and SOC2, the system goes in STs 1 to 4 as shown in TABLE 4.3

TABLE 4.3. State table of the SC for the No fault scenario

No failure		
SOC	Battery 1: SOC 1=90%	Battery 1: 50%<SOC 1<90%
Battery 2: SOC 2=90%	STATE 1: - C4 open - Batteries 1, 2 connected - No load shedding - Batteries 1,2 disconnected	STATE 2: - C4 opened - Load shedding - Battery 2 disconnected - Battery 1 charged until 90% SOC, go to STATE 1
Battery 2: 50%<SOC 2<90%	STATE 3: - C4 opened - Load shedding - Battery 1 disconnected - Battery 2 charged until 90% SOC, go to STATE 1	STATE 4: - C4 closed - Load shedding on non-essential LV loads - Battery 1 charged until 90% SOC (Battery 2<90%), go to STATE 3 - Battery 2 charged until 90% SOC (Battery 1<90%), go to STATE 2



The aim of the controller in this no-fault condition is to ensure that the SOC of both batteries is kept at 90% so that they have enough energy to cater for any possible fault conditions should they occur. The batteries are considered charged and kept at 90% of their SOC in order to leave a margin in case there is a possibility to store extra energy and avoiding overcharge operations. In ST1 as shown in TABLE 4.3, when both batteries have a state of charge above 90%, the SC disconnects both batteries. If SOC2 falls below 90% with SOC1 still at 90%, the controller triggers an action which causes the system state to change from ST1 to ST3. Similarly, when SOC 1 falls below 90% with SOC2 still at 90%, the system transitions to ST2. In STs 2 and 3, when one of the two batteries have a SOC lower than 90%, that battery is charged until the SOC reaches 90%, at which point the system moves back to ST1. When both SOC1 and SOC2 reduce below 90%, that system transitions to ST4. In ST4, the controller sheds part the non-essential 28V loads in order to have enough energy to charge both batteries to 90%. The minimum SOC to be maintained for both batteries is 50% when the EPS is healthy.

4.3.1.2 Failure of one power electronic converter

In the event that one of the four 3kW PECs (1- 4) fails more STs must be added, thus the SC is required to transition the system to STs 5 to 8. The SC goes ST5 when there is a failure of a PEC and the batteries are charged. This ensure that all the non-essential loads can be supplied for a limited period of time under this critical scenario. The ST6 and ST7 enabling the disconnection of the batteries in case the SOC's level are low. While the ST8 enables the batteries disconnection in case of low SOC level, and the disconnection of the non-essential loads in order to use a small amount of power for charging the batteries until the 50% of the SOC. This allows the EPS to have extra energy stored for any other critical scenario that could occurs. In TABLE 4.4 are resumed the discussed STs.

TABLE 4.4. State table of the SC for one converter failure scenario

Failure of 1 DC/DC converter		
SOC	Battery 1: 20%<SOC 1<90%	Battery 1: SOC 1=20%
Battery 2: 20%<SOC 2<90%	STATE 5: - C4 closed - Batteries 1, 2 connected - If Battery 1 SOC=20%, go to STATE 6 - If Battery 2 SOC=20%, go to STATE 7 - If Battery 1/2 SOC=20%, go to STATE 8	STATE 6: - C4 closed - Battery 1 disconnected - Battery 2 connected – discharging faster - If Battery 2 SOC=20%, go to STATE 8
Battery 2: SOC 2=20%	STATE 7: - C4 closed - Battery 1 connected – discharging faster - Battery 2 disconnected - If Battery 1 SOC=20%, go to STATE 8	STATE 8: - C4 closed - Low priority LV loads disconnected - Fast charge of the batteries - Battery 1 charged until 50% SOC - Battery 2 – 50%<SOC<90%, go to STATE 5 - Battery 2 charged until 50% SOC - Battery 1 – 50%<SOC<90%, go to STATE 5 - Battery 1/2 SOC=50%, go to STATE 5

If the system is in ST5, the contactor C4 is closed, and both batteries are employed to supply the vital loads until their SOC's decrease to below 20%. The system then goes to ST6 if SOC1 reaches 20% first, or to ST7 if SOC2 reaches 20% first, or ST8 if both SOC1 and SOC2 reach 20%. In ST6, only battery 2 supplies power to the vital load, while in ST7, only battery 1 supplies power to the vital load. In ST8, the 6kW non-essential LV loads are shed so that there is enough power, which is transferred from the HV side through the remaining 3 numbers PECs, to supply both the vital loads and to charge the two batteries up to 50% of their SOC's.

4.3.1.3 Failure of two power electronic converters

The STs from 9 to 12 are created in the event that two out of four PECs fail. The ST9 enables the batteries to supply the non-essential loads and closes the beaker C<sub>4</sub> for allowing the power sharing between the LV buses. The STs 10 and 11 are used to disconnect one of the batteries in case of low SOC level. While in the ST12 the battery and the non-essential loads are disconnected and only the vital loads are supplied. The TABLE 4.5 depicts the four STs (9 to 12) of the EPS.

TABLE 4.5. State table of the SC for two converters failure scenario

Failure of 2 DC/DC converters		
SOC	Battery 1: 20%<SOC 1<90%	Battery 1: SOC 1=20%
Battery 2: 20%<SOC 2<90%	STATE 9: - C4 closed - Batteries 1, 2 connected - If Battery 1 SOC=20%, go to STATE 11 - If Battery 2 SOC=20%, go to STATE 10 - If Battery 1/2 SOC=20%, go to STATE 12	STATE 10: - C4 closed - Load shedding - Battery 1 disconnected - Battery 2 connected – discharging faster
Battery 2: SOC 2=20%	STATE 11: - C4 closed - Load shedding - Battery 1 connected – discharging faster - Battery 2 disconnected	STATE 12: - C4 closed - Low priority LV loads disconnected - Both batteries disconnected - High priority LV loads are supplied

The STs and the set of actions that have to be performed by the SC are similar to the earlier case when only of one of the four PECs fails and are described in TABLE 4.5. Note that there is ST12, when SOC1 and SOC2 are at 20%, both batteries and the non-essential LV loads are disconnected, and the vital LV loads are supplied directly from the HV bus through the two remaining healthy PECs.

4.3.1.4 Failure of three to four power electronic converters

In the unlikely event that 3 or 4 of the PECs fail, the SC performs a similar set of actions as for the abovementioned cases where one or two of the PECs are faulty; The STs (13 to 16) and set of actions in this case scenario are described in TABLE 4.6

TABLE 4.6. State table of the SC for three converters failure scenario

Failure of 3 DC/DC converters		
SOC	Battery 1: 20%<SOC 1<90%	Battery 1: SOC 1=20%
Battery 2: 20%<SOC 2<90%	STATE 13: - C4 closed - Batteries 1, 2 connected - If Battery 1 SOC=20%, go to STATE 15 - If Battery 2 SOC=20%, go to STATE 14 - If Battery 1/2 SOC=20%, go to STATE 16	STATE 14: - C4 closed - Battery 1 disconnected - Battery 2 connected – discharging faster - If Battery 2 SOC=20%, go to STATE 16
Battery 2: SOC 2=20%	STATE 15: - C4 closed - Battery 1 connected – discharging faster - Battery 2 disconnected - If Battery 1 SOC=20%, go to STATE 16	STATE 16: - C4 closed - Shedding of non-essential LV loads - Both batteries are disconnected - Low voltage buses disconnected, action in case the fourth converter fails

It is to be noted that in ST16, the non-essential LV loads and the discharged batteries are disconnected; if 3 PECs are faulty, then half of the vital LV loads are supplied by the single healthy PEC, and when all four PECs are faulty, then there is no power supplied to the vital loads. The probability of simultaneous failure of more than two PECs is assumed to be low.

The next section verifies the aforementioned control strategy by applying it to the representative MEA EPS model, already presented in section 4.4.2, in the Simulink® environment

### 4.3.2 Simulations and results

This section applies the control strategy outlined in section 4.3.1 to the EPS depicted in Fig. 4.1 by using the FSM. The simulations are performed in the Simulink® environment to show the SC action for the four cases described in the earlier section, namely the cases of no-fault operation, failure of one PEC, failure of two PECs and failure of three PECs, respectively.

#### 4.3.2.1 No fault scenario

During normal condition, the state of charge of the batteries are maintained at 90%, as described in the state space TABLE 4.3, and showed in Fig. 4.14.

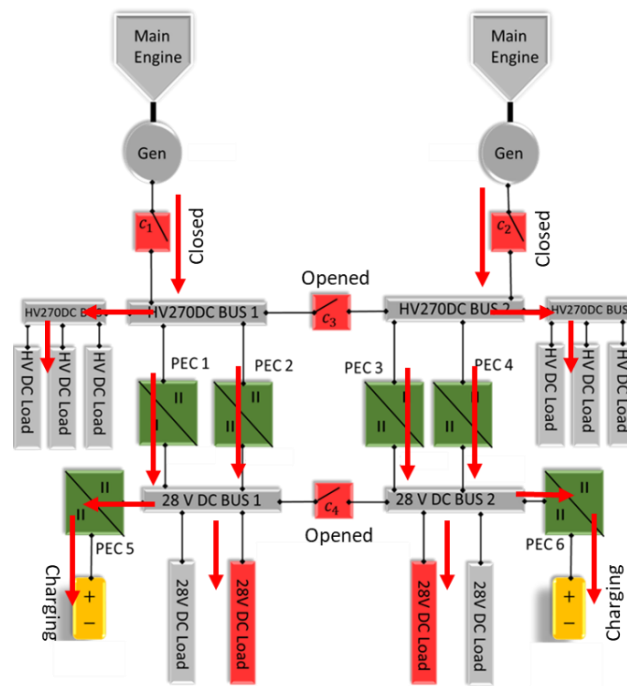


Fig. 4.14. EPS power flow during no PECs failure

Fig. 4.15 to Fig. 4.17 depict the simulation results under the no-fault scenario, and assuming the batteries with a SOC lower than 90% and not at the same level. This scenario will test the behaviour of the SC in charging operations with different SOC level. From Fig. 4.15, it can be seen that the SOC of battery 1 (SOC1) and battery 2 (SOC2) are below 90% at the beginning

of the simulation  $t=0s$  to  $t=263s$ ; the system is in ST4. Between  $263s$  and  $317s$ , the SOC1 is 90% while SOC2 is below 90%; the system changes from ST4 to ST3. When the system is in STs 4 and 3, the controller sheds the low priority loads even if the de-icing is OFF, which consist of 1.5kW on LV bus2 (from 6kW to 4.5kW), as is depicted in Fig. 4.16, and another 1.5kW on LV bus1. The power made available from load shedding is used to charge the batteries. The system goes to ST1 after time  $t=317s$  when the batteries are charged to 90%.

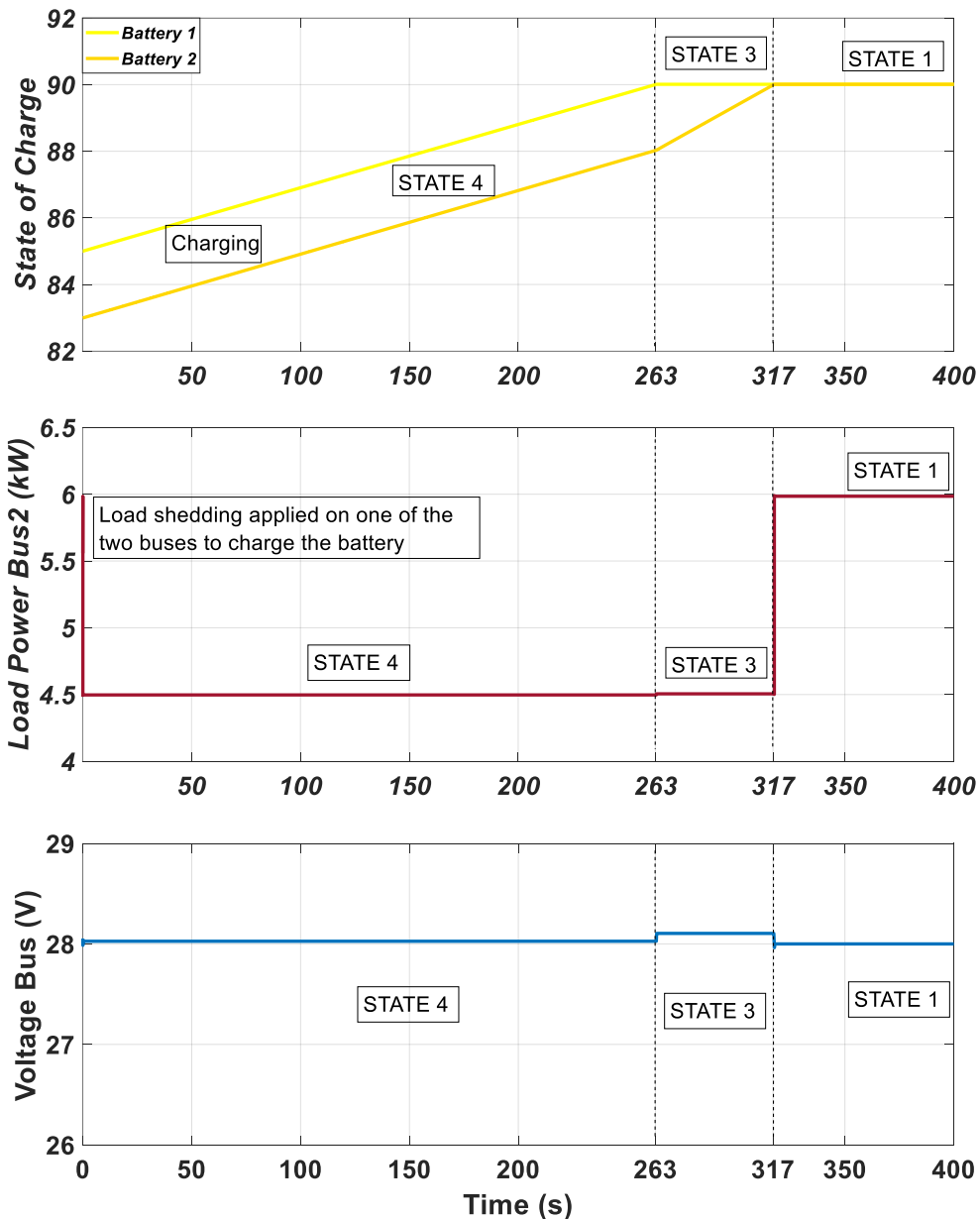


Fig. 4.15. No-fault scenario: states of charge of battery 1 and battery 2

Fig. 4.16. Load shedding of 1.5kW from LV bus 2 from  $t=0s$  to  $t=317s$  (and 1.5kW from LV bus 1 which is not shown in Fig. 4.10)

Fig. 4.17. Voltage maintained within the MIL-STD-704F on LV bus 2

The voltage on the buses is maintained within the voltage limits ( $\pm 10\%$ ) as per specified in the MIL-STD-704F, as shown in Fig. 4.17.

*4.3.2.2 Failure of one power electronic converter*

In this scenario, it is assumed that one of PECs (namely, PEC1) fails and the system uses the remaining three to feed the loads, as shown in Fig. 4.18.

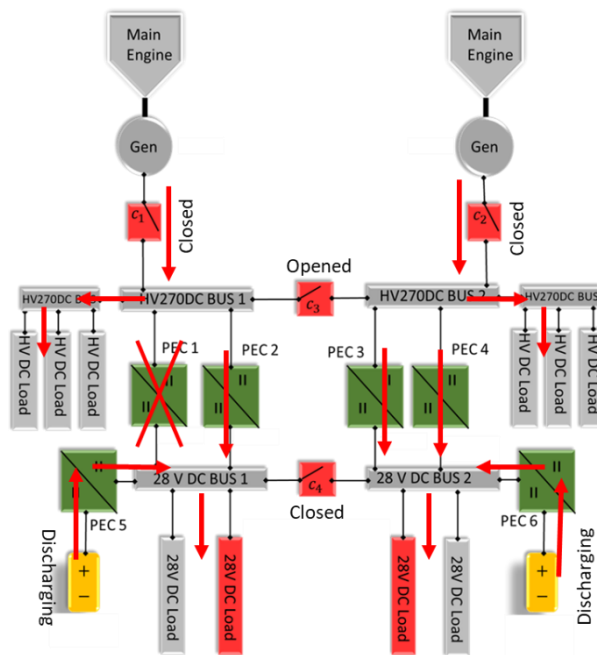


Fig. 4.18. EPS power flow during the failure of one PECs

The 3KW power that can no longer be supplied from the HV bus through the faulty PEC1, is now provided by the batteries. The batteries are used to supply all the LV loads until the SOC is below the minimum value of 20%. When the SOC drops to 20%, shedding is applied to the non-essential LV loads, and the surplus power is used to recharge the batteries up to 50% (ST4) as detailed in TABLE 4.4

The Fig. 4.19 to Fig. 4.22 show the behaviour of the system after the fault in PEC1. The failure of one converter is shown in Fig. 4.19 at time 2s. When the fault occurs, the system starts using the batteries in order to supply the LV loads; the system thus transitions to ST5 as shown in Fig. 4.20.

After battery 1 is discharged at time 2336s, the controller disconnects it, and the system moves from ST5 to ST7 where only the battery 2 is used to supply the LV load, as depicted in Fig. 4.20. The system drains current from the batteries until both SOC 1 and SOC 2 reach 20%. For 3530s, the batteries are used to supply the LV loads, including the vital loads. Once the SOC's reach the minimum of 20%, the controller moves the system from ST7 to ST8, as shown in Fig. 4.20. disconnects the non-essential loads and start to charge the battery until SOC of the batteries are 50%. It is to be noted that the EPS charges one battery at a time. Once the system charges both batteries up to 50%, the non-essential loads can be supplied again from the batteries as shown in Fig. 4.21 from time ( $t=5090s$ ), at which point the system moves to ST5. Fig. 4.21 shows the load power profiles for the LV bus 1 and LV bus 2. From time 2s to 3530s, the total power on LV buses 1 and 2 are 6kW each. At time 3530s, the non-essential loads on both LV buses are shed; at that point the total power on LV bus 1 is reduced to 4.5kW to supply only the vital loads on that bus and the total power on bus 2 is 1.5kW which is required by the vital loads on bus 2. Note that the vital loads are always supplied during the operation. The bus voltage is maintained within the MIL-STD-704F, as the system STs change, as can be seen in Fig. 4.22.



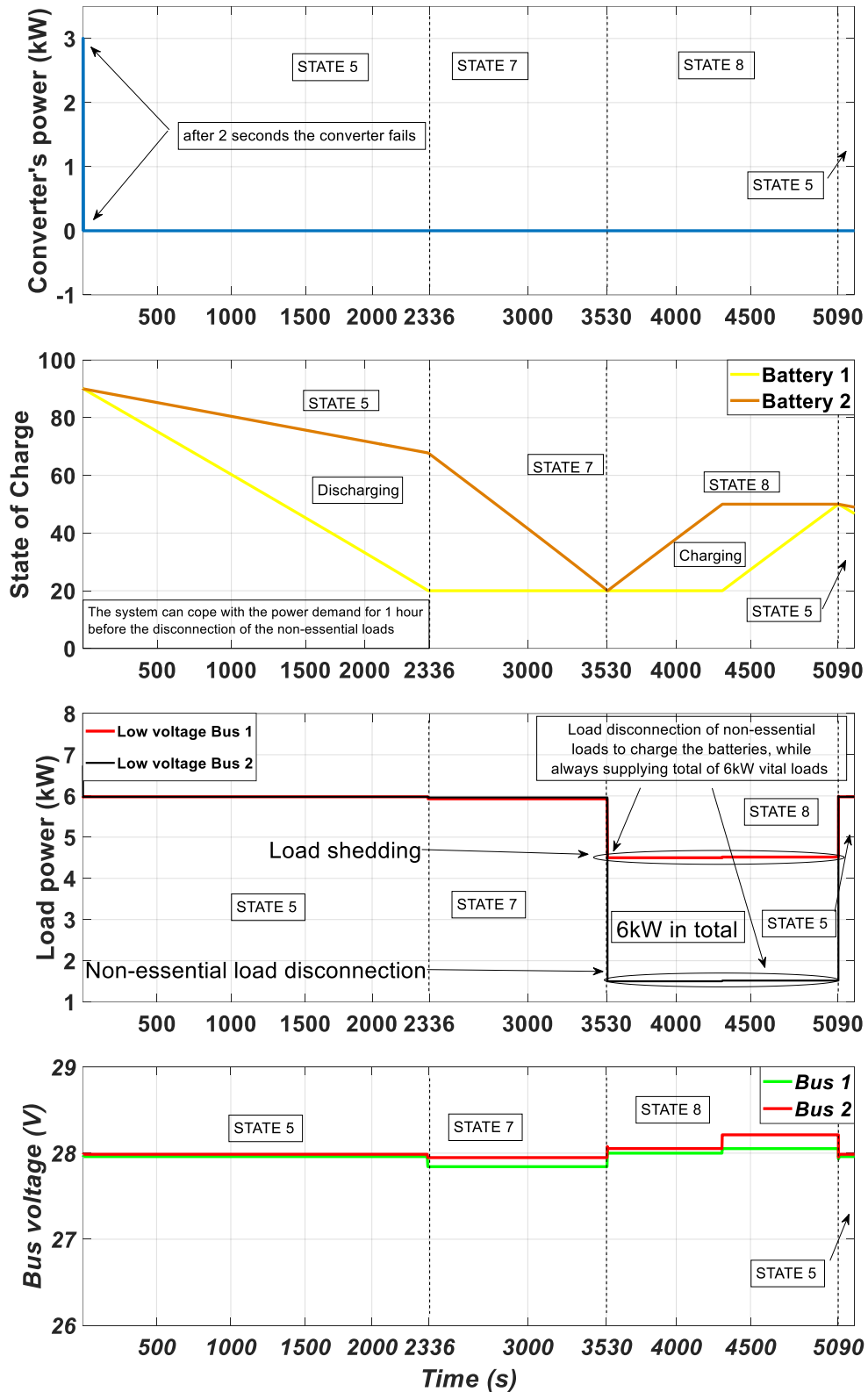


Fig. 4.19. Failure of one PEC: Power of PEC1 drops from 3kW to 0kW

Fig. 4.20. SOC of batteries 1 and 2

Fig. 4.21. Load shedding of 1.5kW on bus 1 and 4.5kW on bus 2, with uninterrupted power to the vital load of 4.5kW on bus 1 and 1.5kW on bus 2 from t= 3530s to 5200s

Fig. 4.22. Voltage on 28V bus

4.3.2.3 Failure of two power electronic converters

In the event of 2 PECs failure the system transfers power from the HV buses to the LV buses through the remaining two healthy PECs and uses the batteries to provide the additional power required to supply all the LV loads, as shown Fig. 4.23.

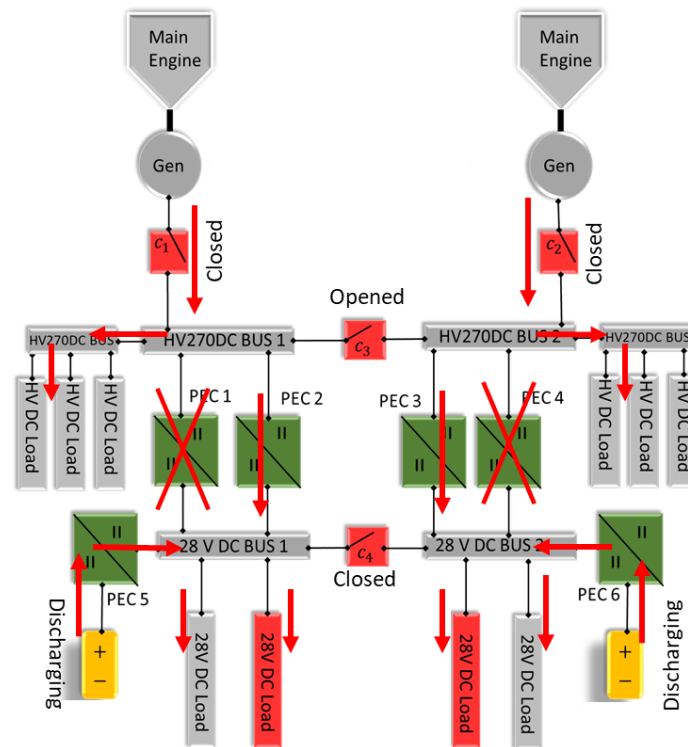


Fig. 4.23. EPS power flow during the failure of two PECs

This action is managed by the SC independently from what is the failed PEC; the system is in ST9 (refer to TABLE 4.5). The behavior of the system under this failure of the two PECs is shown in Fig. 4.24 to Fig. 4.26. The SOC of both batteries is 90% (normal operation, ST1) when the fault occurs; the system is in ST9. The contactor C4 is closed, enabling the power sharing between the LV buses 1 and 2. Both batteries supply the non-essential loads, which can no longer be supplied through the two faulty PECs. When the SOC of both batteries reach 20% at time  $t=1730s$  ( $\approx 28$  mins), the batteries are not able to cope with the power demand and therefore the controller need to shed the non-essential loads. According with the STs TABLE 4.5 the system changes from ST9 to ST12 once the SOC's are at 20%; the system disconnects

the non-essential loads (1.5kW on bus1 and 4.5kW on bus2) and the two converters are used to transfer power from the HV buses to the vital loads on the low voltage side (total of 6kW). The voltage is maintained within the MIL-STD-704F during the transitions between STs as shown in Fig. 4.26.

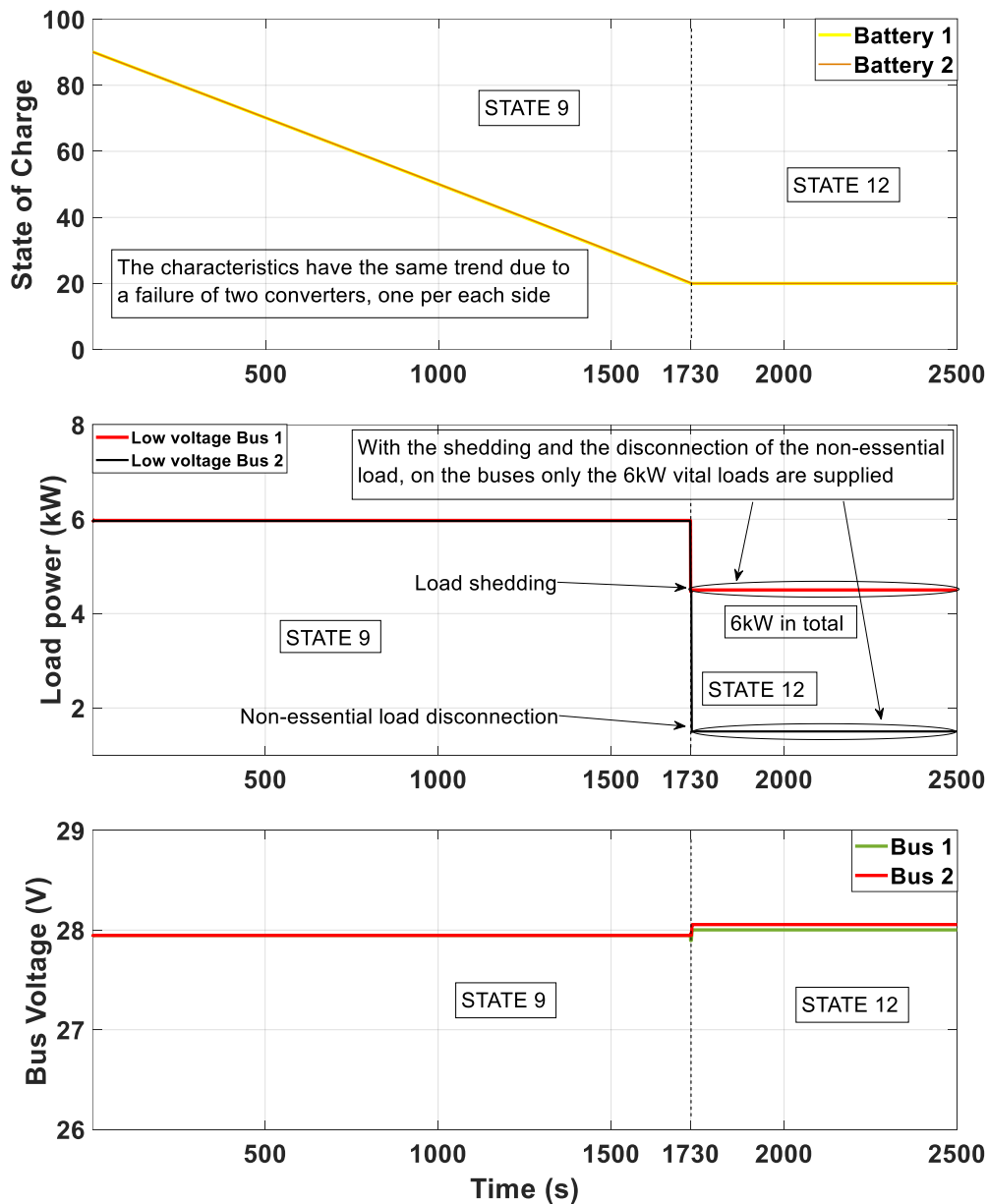


Fig. 4.24. SOC of batteries 1 and 2, in which the batteries are used until their SOC its 20% (ST9), then they are both disconnected (ST12)

Fig. 4.25. After 1680s the system disconnects the non-essential load of 1.5kW on bus 1 and 4.5kW loads on bus 2. All power through healthy PECs supply the total vital loads of 6kW

Fig. 4.26. Voltage of the 28V buses during all the operations

4.3.2.4 Failure of three to four power electronic converters

The system STs during the fault scenario are detailed in TABLE 4.6. With the failure of three out of four PECs (1 to 4), the controller uses the maximum power capability of the remaining healthy converter and the batteries to feed the low voltage high priority loads, as can be seen in the Fig. 4.27 that shows the EPS power flow.

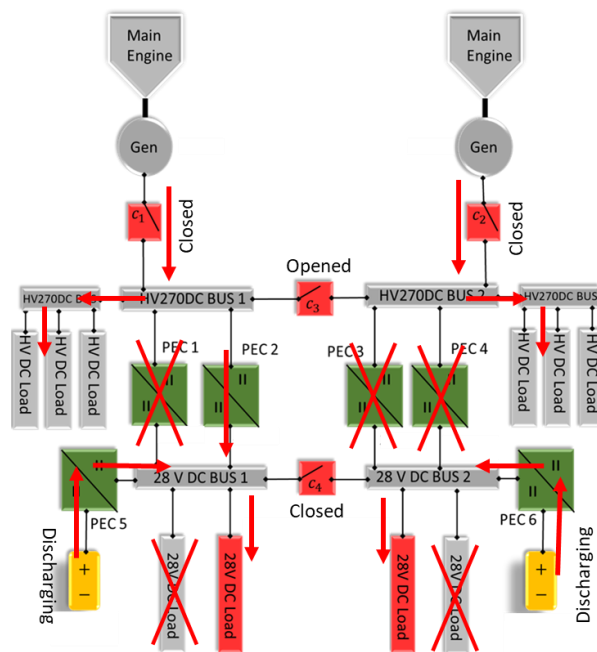


Fig. 4.27. EPS power flow during the failure of three PECs

The contactor C4 is closed, allowing the power sharing between the two LV buses. Shedding is applied to all the non-essential LV loads. As shown in Fig. 4.28, the total vital loads on LV side can be supplied for 1730s (28 minutes) before the SOC of the batteries drop to 20%; after this point, the healthy 3kW PEC is used to supply only the 1.5kW vital load.

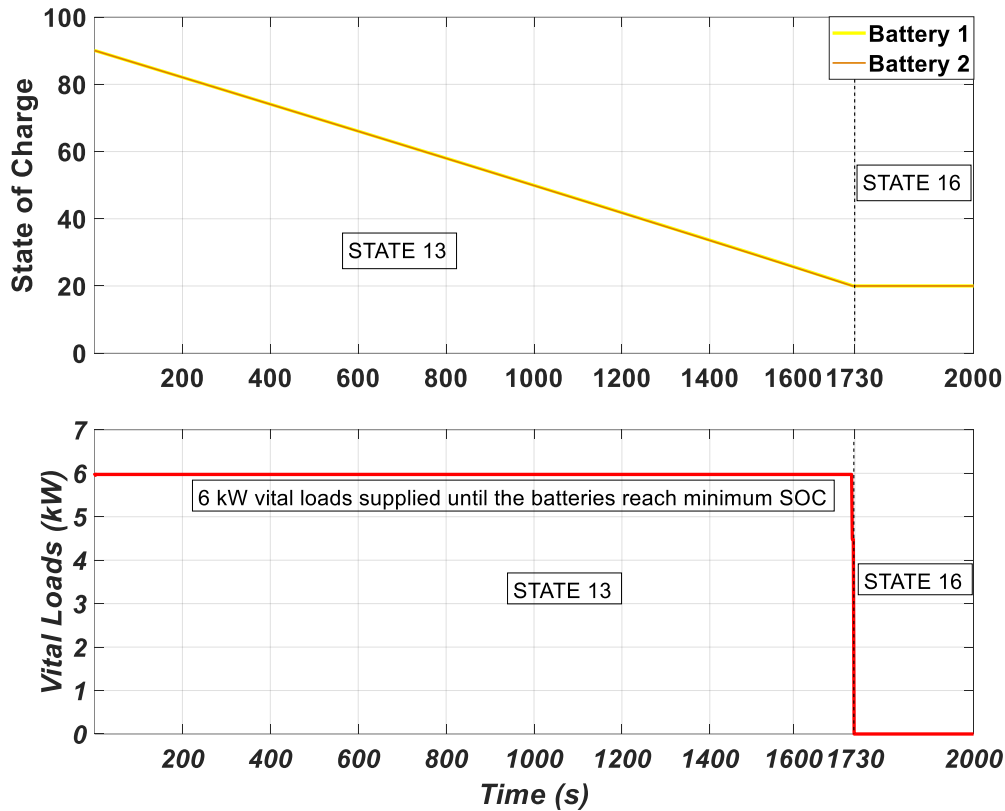


Fig. 4.28. SOC of the battery 1 and battery 2

Fig. 4.29. The total vital loads on LV side can be supplied for 1730s before the SOC of the batteries drop to 20% (ST13), after that the batteries are disconnected (ST16)

It is to be noted that if all four PECs fail, the batteries can supply the vital loads until their SOC drops to 20% at time 1730s (28 minutes), after which point, neither the 1.5kW nor the 4.5kW vital loads can be supplied as shown in Fig. 4.29. In actual systems, the fault scenarios of three or four PECs failure are less likely to happen. If such extreme fault scenario is to be accounted for, other emergency actions can be included in the design in a similar way.

### **4.3.3 Conclusion for case study 2**

The strategy for the SC has been devised with the aim to provide uninterrupted power to vital LV loads using FSM. The control strategy has been implemented in Simulink® Stateflow® and verified by considering faults scenarios involving the failure of one to four HV/LV DC/DC PECs. The simulation results have confirmed that the controller activates the correct STs such that the vital loads are always supplied for faults in up to two converters, as can be also noted in the state transition plot of each scenario showed in the Fig. 4.30 to Fig. 4. 33.

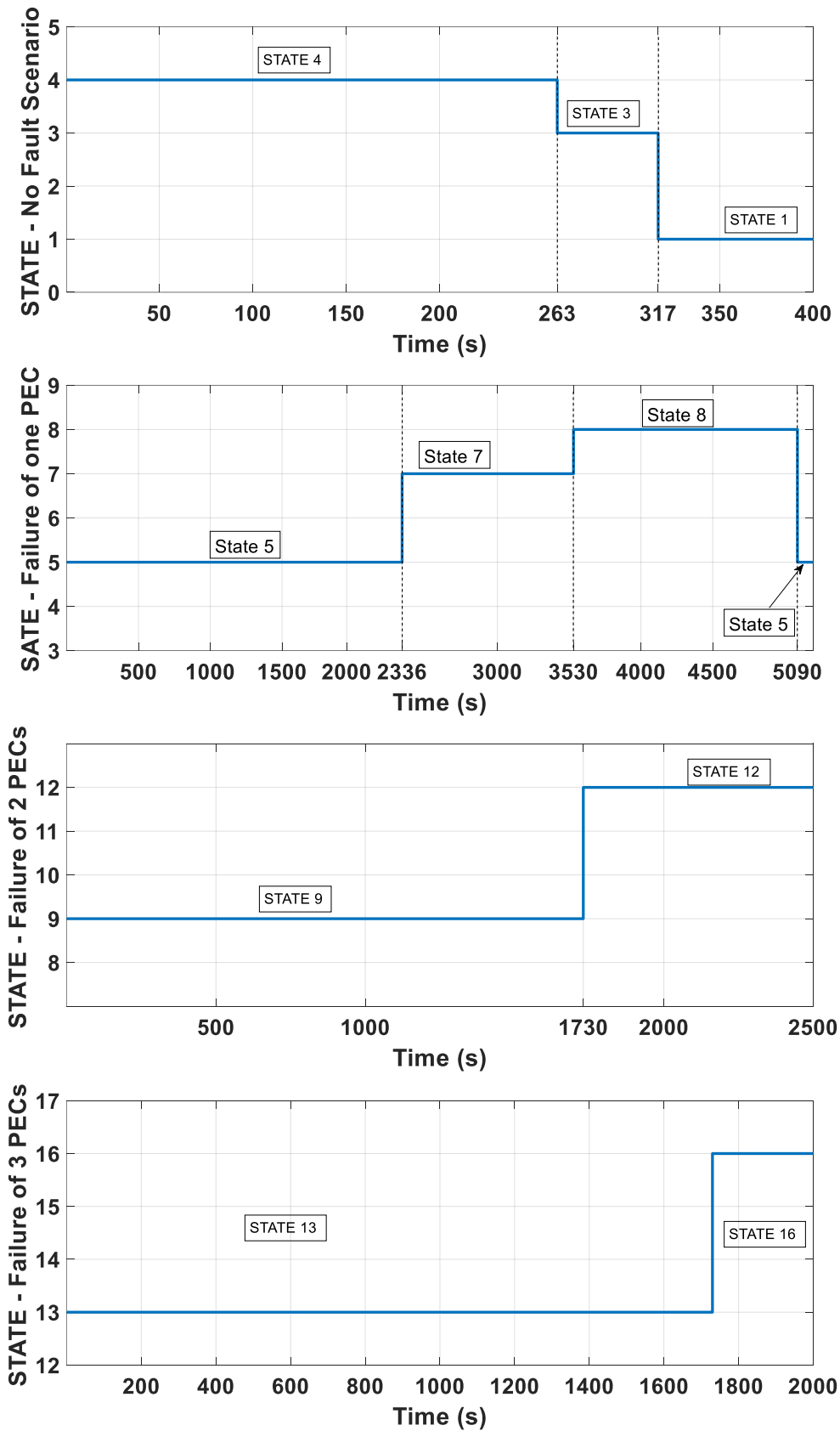


Fig. 4.30. State transition plot of scenario 1 (No-fault)  
 Fig. 4.31. State transition plot of scenario 2 (Failure of one PECs)  
 Fig. 4.32. State transition plot of scenario 3 (Failure of two PECs)  
 Fig. 4.33. State transition plot of scenario 4 (Failure of 3 PECs)

### *Analytical approach to Electrical Distribution Systems for Aircraft*

For the unlikely event of three or four power converters failing, the vital loads can be kept supplied for a limited amount of time. Supplementary emergency actions such as different power paths, management of additional storage devices, or generator's overloads, can be taken into account if required by the design. In fact, having a SC able to manage the entire EPS give high flexibility in the choice of the strategy.



## **4.4 Conclusion**

This Chapter, using MatLab® Simulink® time-domain simulations, has investigated and validated the application of the RCS method described in Chapter 2 with application to MEA EPS. In the first case study, the generator overloading problem is solved by re-configuring the EPS, allowing the batteries to provide additional power. In the second case study, the SC manages the EPS in emergency conditions, ensuring the EPS operation during multiple PECs faults, finding an alternative power path across the EPS, and maintaining the vital loads active until it is possible. From the obtained results it is clearly seen that the applied method is capable to redistribute the power across the EPS, solving different scenarios, which could be an overload due to a power surge request from the loads, or maintaining the EPS safe, in case of component's fault, without the need to reduce the power demands. This Chapter contributions include:

- Validation of the RCS method for the management of the MEA EPS, leading to the enhanced performance and efficiency of the EPS, while respecting safety constraints.
- Testing the RCS method that can be applied to the MEA EPS. RCS has shown to be a non complex method to make the EPS more flexible and safer.
- Analysing the SC feedback in the management of the entire EPS and test the FSM behaviour inside a simulation environment that includes multiple mathematical models

Moreover, it has to be remarked the aim of the test. The main focus is the control of an entire EPS by using a single central unit, SC, which has the task to monitor in real-time and provide feedback that moves the EPS configuration from one STATE to another. The novelty of these simulations consists in investigating the EPS behavior, as well as, the SC capabilities together with a non-complex programming tool, which can be graphically built (easier debugging) and with the freedom to add more STATES in case of need, due to its modularity. In the next Chapter another method re-distributing the power will be implemented based on mathematical operations and will be added to the one presented in this section.

## **Chapter 5: Load allocation problem (LAP)**

---

### **5.1 Overview**

This Chapter considers a case of study related to the LAP introduced in Chapter 2, Section 2.2.2 for the design of a high-level SC. This case study aims to demonstrate how the introduction of the LAP can be applied to the EPS for the power optimization on the buses. This technique relies on the use of dynamic programming (as discussed in Chapter 2), which adopt a mathematical optimization on the EPS's buses. It is a tool that the SC uses to manage the available power from the sources to feed the loads or to disconnect the non-essential loads in case of limitations on power availability. The use of dynamic programming, over the other methods such as heuristic approach, as has been discussed in earlier Chapter 2, has the advantage of providing a purely mathematical optimization for the EPS. The dynamic programming algorithm used for this work is the knapsack problem, which aims to maximize the available power on the buses, without causing the overload of the sources, and avoiding the disconnection of the vital loads. The LAP embedded into the SC together with the RS can manage the entire MEA EPS, leading to the enhanced performance and efficiency of the EPS, while respecting safety constraints. Thus, the LAP allows the SC to accomplish the following objectives:

- Lead to the enhanced performance and efficiency of the EPS, while respecting safety constraints.
- Automatization of the reconfiguration of the EPS based on the occurring scenario.

## 5.2 LAP of representative MEA EPS

The Fig. 5.1 shows a single line diagram of an EPS for MEA system, selected for the study that has been detailed in Chapter 3. Since the aim of the work in this Chapter is to demonstrate the capabilities of the SC and to validate the algorithm, the loads in the MEA EPS in Fig. 5.1 are depicted as generic loads that require a certain amount of power without focusing on the types of loads (i.e., motors, actuators, lights, emergency systems).

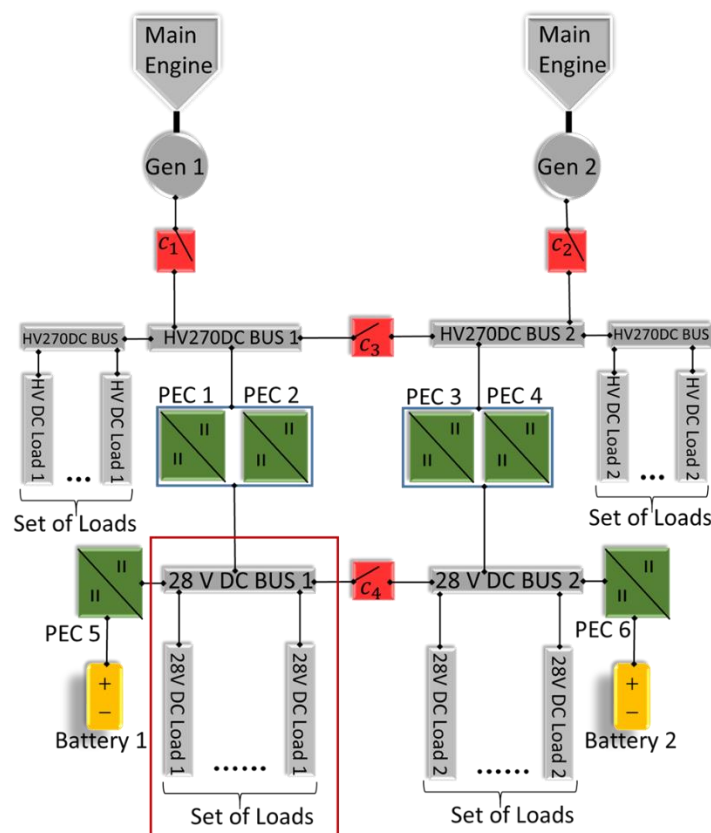


Fig. 5.1. Theoretical model of MEA EPS concept; LAP is applied to the part of the EPS highlighted in the rectangular box

In order to illustrate the LAP method and how it works in optimising the power on a bus, it has been applied to one part of the EPS, as highlighted in rectangular box in red in Fig. 5.1 and expanded in Fig. 5.2.

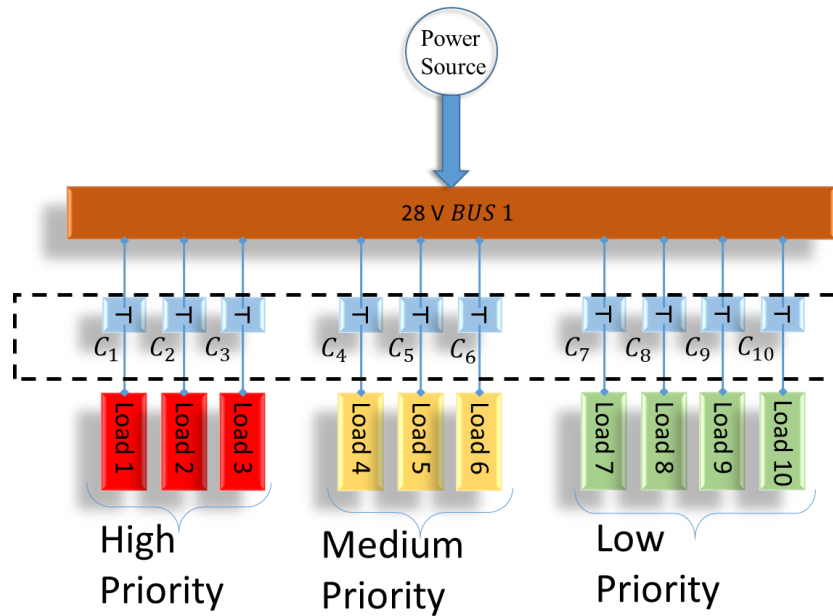


Fig. 5.2. The electrical power system subsystem model used for simulation

As shown in Fig. 5.2, the loads connected to the 28 V bus 1 are assigned with different priority levels (high, medium, and low). The power source represents the power that can be taken from the HV270DC bus 1 through power converters PEC 1 and PEC 2, while the Battery 1, for the purpose of this case study, it is assumed to be disconnected since the LAP depends only on the available power on the bus. As mentioned in the previous section, the aim of this case study is to solve the LAP, i.e., allocation of each load to the bus with respect to the level of priority assigned while respecting the available power of the EPS. The level of priority of a load can indicate if that load can be disconnected (low level of priority) or must be supplied without interruption under fault scenarios (high level of priority). The priority levels can be assigned different values for different flight phases as required. As an example, electro-mechanical actuators (EMAs) may be considered as a high priority loads. In this case study, ten individual loads are depicted in Fig. 5.2. Loads 1 to 3 are assumed to be high priority loads. Loads 4 to 6 are medium priority loads. Loads 7 to 10 are low priority loads. The knapsack algorithm will be devised to automatically supply power to each of the aforementioned ten loads depending on their levels of priority and power availability on the LV bus, as will be described in the following sections.

### **5.3 Knapsack method for LAP of representative MEA EPS**

The knapsack method will be used to solve the LAP. In this case study, the knapsack algorithm will be embedded in a SC and applied to the MEA EPS model. This section introduces the mathematical theory of the knapsack problem. In Chapter 2 several techniques ranging from the heuristic approaches, meta-heuristic to mathematical formulations have been presented and discussed in order to determine the best solution for allocating power on the EPS. The proposed knapsack method, which has been chosen in this work for reasons explained in the literature review in Chapter 2, use pure mathematical formulations for optimizing the power usage by the various MEA EPS loads with different priority levels.

The knapsack problem is an example of a mathematical combinatorial optimization problem [1-2]. This is a problem that has been studied for more than a century, when, there is a need to find a finite and optimized solution, where an exhaustive search is not possible. It is used in various fields such as applied mathematics, complexity theory, cryptography, combinatorial and computer science. In the knapsack problem, the given items have two attributes at minimum which can affect the solution: (i) an item's value, which affects its importance and (ii) an item's weight or volume, which is its limitation aspect. Based on the Knapsack problem, given a set of items, each with a weight and a value, the number of each item included in a collection must be determined so that the total weight is less than or equal to a given limit and the total value is as large as possible, and this is called optimal solution, as it uses the entire capacity of the knapsack and the maximum number of items to be taken. Fig. 5.3 represents a synthesis of the proposed problem, with a pre-defined capacity knapsack in which objects with weights and values are to be fitted into the knapsack without exceeding its capacity, while maximizing the value.



Fig. 5.3. Example of a knapsack problem

The following equations are used to describe the knapsack problem mathematically. Given two n-tuples of positive numbers “ $v_i$ ” as given in 5.1 which are representing the value of each item, “ $w_i$ ” as given in 5.2 which are representing the weight of each items, and the total capacity of the knapsack as defined by the equation 5.3,

$$\langle v_1, v_2, \dots, v_n \rangle \quad 5.1$$

$$\langle w_1, w_2, \dots, w_n \rangle \quad 5.2$$

$$W > 0 \quad 5.3$$

the task is to determine the subset

$T \subseteq \{1, 2, \dots, n\}$  that

$$\begin{aligned} & \text{maximizes } \sum_{i \in T} v_i \\ & \text{subject to } \sum_{i \in T} w_i < W \end{aligned}$$

It is possible to find a solution to the knapsack problem by using the dynamic programming, a computer programming method that consists in breaking a complex problem into a smaller one by obtaining a smaller set of simple problems, by following the steps below [3-5]:

- Decomposing the problem into smaller problems → from Fig. 5.3 a table is created, dividing the problem in column on index 'i' and rows 'w'
- Finding a relationship between the structure of the optimal solution of the original problem, and the solution of the smaller problems → scrolling each row a sub-solution is found that will be compared with other ones.
- Recursively defining the value of an optimal solution → by comparing the solutions of each rows with each other
- Bottom-up computation → compute the value of the optimal solution in a bottom-up fashion by using a table structure.
- Construction of the optimal solution from the computed information.

A numerical exercise is also proposed in [6], where a problem is numerically solved step-by-step for a better understanding the computational processes.


TABLE 5.1 shows how the first part of the code, in Fig. 5.4, fill-up the table (Bottom-up computing).

The values are stored into a matrix, represented by the table.

TABLE 5.1. Table representing the operation of dynamic programming approach

$V[i,w]$	w=0	1	2	3	...	...	W
i=0	0	0	0	0	...	...	0
1	→						
2	→						
⋮	→						
n	→						

bottom



up

The source code used to fill the TABLE 5.1 is shown in Fig. 5.4:

```
Knapsack(v, w, n, W)
{
  for(w=0 to W) V[0,w]=0; // Set the first row to 0
  for(i=1 to n)
    for(w=0 to W)
      if(w[i]<=w) // Scroll the elements of the table
        V[i,w]=max{V[i-1,w], v[i] + V[i-1,w-w[i]]};
      else // Set the value of
        V[i,w]=V[i-1,w]; // the element V[i,w]
  return V[n,W]; // at the maximum value
}
```

Fig. 5.4. Knapsack source code

However, the method does not give the optimal solution, but it only defines what the sub-sets are. The final part of the code, displayed in Fig. 5.5, give back the value of the sub-set T that contains the solution:

```
K=W;
for(i=n downto 1) // Scroll the elements backwards
  if(keep[i,K]==1) // if keep[i,k]==1 n belongs to T
  { // if keep[i,k]==0 n doesn't belong to T
    output i;
    k = k-w[i];
  }
```

Fig. 5.5. Source code used to extract the solution from the TABLE 5.1

Using the source code above, it is possible to scroll each element backward and find the solution that solves the problem. Referring to the Knapsack problem, it is possible to relate the optimization with the problem of the LAP.



### *Analytical approach to Electrical Distribution Systems for Aircraft*

In the case under study, it is possible to adopt the knapsack method to optimize the power supply to 'n' loads in the MEA EPS by using the following relationships:

$\langle v_1, v_2, \dots, v_n \rangle \quad \rightarrow \text{Level of priority for each of the 'n' loads}$

$\langle w_1, w_2, \dots, w_n \rangle \quad \rightarrow \text{Power of each of the 'n' loads in Watt}$

$W > 0 \quad \rightarrow \text{Available power}$

Thus, by solving the Knapsack problem with the variables above, it is possible to obtain a vector of solution that can be used to connect or disconnect the various loads in the system based on available power and priority levels of the loads. The next section will apply the knapsack method to develop a SC, which will be used to solve the LAP in the representative EMA EPS for three case scenarios.

### 5.4 Case scenario and simulation results

Three case scenarios are considered in this section to optimize the power allocation given the priority level ( $v_i$ ) for each load and the power ( $w_i$ ) required by each load as shown in TABLE 5.2. It is to be noted that the total power required by all the ten loads is 20kW.

TABLE 5.2. Priority level and power required by each load

	Loads									
	1	2	3	4	5	6	7	8	9	10
<b>Priority (<math>v_i</math>)</b>	1000	900	800	70	60	50	4	3	2	1
<b>Power (<math>w_i</math>)</b>	3kW	3kW	2kW	2kW	2kW	2kW	2kW	2kW	1kW	1kW

In case 1 at the start of the simulation the system has to supply 20kW loads with 20kW of available power ( $W=20kW$ ). In case 2, which occurs after 10s the available power is reduced to 17 kW ( $W=17kW$ ), and therefore, the control system has to recalculate a new solution. After a further 10s the available power is reduced from 17kW to 13kW ( $W=13kW$ ) forcing the system to change configuration again.

It is to be noted that in order to guarantee that the loads with the highest priority will not be disconnected before the ones with medium and low priority, eq. 5.4 is introduced. The eq.  $\sum_{i=1}^n HP_{load_i} > \sum_{j=1}^m MP_{load_j} > \sum_{k=1}^z LP_{load_k}$  imposes that the sum of the power of the high priority (HP) loads must be greater than the sum of the medium priority (MP) loads, and the sum of the medium priority loads must be greater than the sum of the low priority (LP) loads.

$$\sum_{i=1}^n HP_{load_i} > \sum_{j=1}^m MP_{load_j} > \sum_{k=1}^z LP_{load_k} \quad 5.4$$

The state models were run for the three cases and the resulting vector of solutions that configure the status of the switches (C1 to C10 as shown in Fig. 5.2) are given in TABLE 5.2. The contactor status is “1” when the contactor is closed and “0” when the contactor is open.

As shown in TABLE 5.2 for case 1, which occurs from time 0 to time 10s, all the contactors are closed. For case 2 where the power available is reduced to 17kW, contactors 8 and 10 are switched off. For case 3, the contactors 6, 7, 8 and 10 are open.

TABLE 5.3. Configuration of the switches for each case (1='closed', 0='opened')

Case	Available power (W)	State of switches									
		C <sub>1</sub>	C <sub>2</sub>	C <sub>3</sub>	C <sub>4</sub>	C <sub>5</sub>	C <sub>6</sub>	C <sub>7</sub>	C <sub>8</sub>	C <sub>9</sub>	C <sub>10</sub>
1	20 kW	1	1	1	1	1	1	1	1	1	1
2	17 kW	1	1	1	1	1	1	1	0	1	0
3	13 kW	1	1	1	1	1	0	0	0	1	0

The states of the contactors for each of the three cases, as shown in TABLE 5.3, are shown in the Fig. 5.6(a) to (c), respectively, for clarity. In Fig. 5.6(a) all the switches are closed since the 20kW provided from the power source are enough to supply all the loads. In the Fig. 5.6(b) the power source is only able to provide 17kW, thus, the switches C<sub>8</sub> and C<sub>10</sub> are opened disconnecting the loads with the lowest priority. In the Fig. 5.6 (c), the available power from the power source is 13kW, thus, the algorithm opened the switches C<sub>6</sub>, C<sub>7</sub>, C<sub>8</sub>, and C<sub>10</sub> using all the available power to supply only the load with the highest priority.

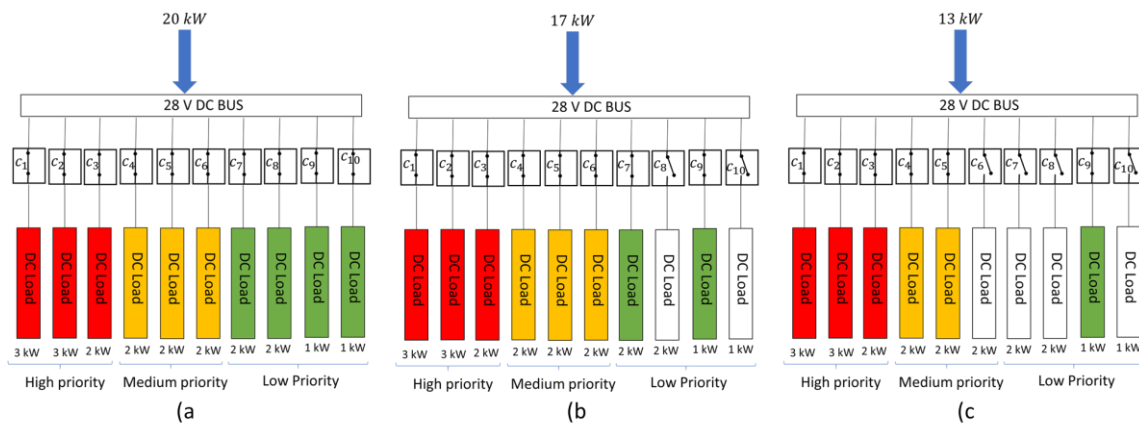


Fig. 5.6. a) Load distribution based on 20kW of available power, all the switches are closed (b) Load distribution based on 17kW of available power, the switches C<sub>8</sub> and C<sub>10</sub> are opened (c) Load distribution based on 13kW of available power, the switches C<sub>6</sub>, C<sub>7</sub>, C<sub>8</sub>, and C<sub>10</sub> are opened.

Fig. 5.7 shows the measured power on the LV bus at different times of the simulation. It can be noted that from time 0s to 10 s, the power allocated on the bus is 20kW, which matches

the available power. From time 10s to 20s, the power allocated on the bus is 17kW, and finally from time 20s to 40s, the power on the LV bus is 13kW.

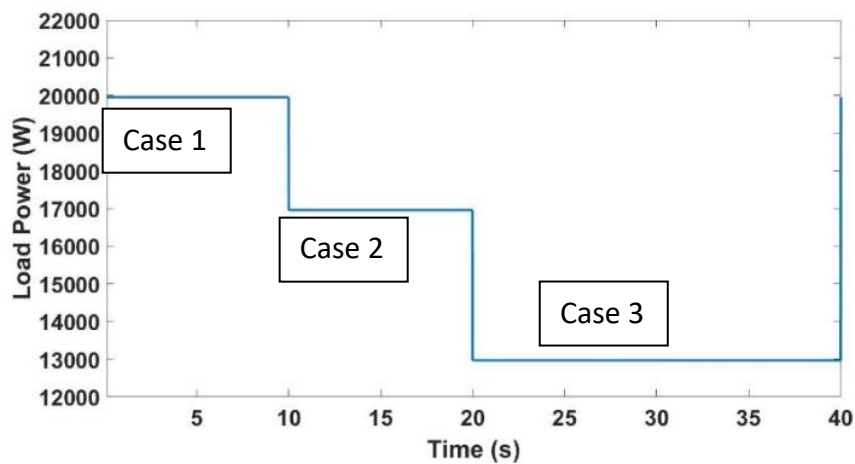


Fig. 5.7. The measure power on the LV buses match the available power for cases 1, 2 and 3

As seen in the simulation results, the SC with the knapsack algorithm, changes the status of the switches automatically, hence optimizing usage of the bus power based on available power and priority levels. From the simulation results, it can be seen that the power supplied to the loads in all three cases match the available power on the LV bus. These simulation results validate the knapsack algorithm applied for the load allocation problem.

### 5.5 Additional considerations

To clarify the work methodology of the knapsack method, which for the solution presented above is hidden by the Simulink® script, this section presents a numerical example that shows how Bottom-up computing is used to solve a simple knapsack problem.

Let  $W$  be the knapsack capacity equal to 10.

TABLE 5.4 are presented the elements with their value

TABLE 5.4. Numerical example used for solving the Knapsack problem with the Bottom-up computing

i	1	2	3	4
$v_i$	10	40	30	50
$w_i$	5	4	6	3

Applying the first part of the algorithm presented in the Fig. 5.4, the following solution shown in TABLE 5.5 is obtained:

TABLE 5.5. Table filled with the values found in the first algorithm execution

$V [i, w]$	0	1	2	3	4	5	6	7	8	9	10
$i=0$	0	0	0	0	0	0	0	0	0	0	0
1	0	0	0	0	0	10	10	10	10	10	10
2	0	0	0	0	40	40	40	40	40	50	50
3	0	0	0	0	40	40	40	40	40	50	70
4	0	0	0	50	50	50	50	90	90	90	90

The solution is then given by the value  $V [10, w]$ , which is not the best solution. Thus, the second part of the code shown in Fig. 5.5 is used to scroll the TABLE 5.5. backward and find the optimal solution by using the Boolean array  $keep [i, k]$ . the  $keep$  function in this case is used to memorize of the previous values. The solution results is given by selecting the item {2, 4}.

There would be also the possibility to have some scenarios in which a load has the same level of priority and value as another one. In that case, a conflict could be created into the algorithm execution, thus this problem must be solved into the SC design phase by setting and checking the correctness of each rule.

Thus, the applied Knapsack method for optimizing the EPS has successfully demonstrated that a mathematical methodology can be used to allow the SC to take an automatic decision for distributing the power on the buses, and in an optimized way in a fast computational time. In fact, optimizing the power spreading allows the system to work more efficiently since the energy-wasting is reduced, and the energy sources are made working at their rating conditions (maximum efficiency) for most of the time. Moreover, the developed algorithm is integrated into the same development tool used for applying the RCS method, thus the combination of RCS and LAP can easily embed into the FSM.

## **5.6 Conclusion**

In this Chapter, the LAP has been applied to a typical MEA electrical power subsystem. Based on the defined characteristics of the SC presented in Chapter 2, the LAP has been implemented for the management and optimization of the power on the EPS bus. This study case applied the mathematical method, based on the Knapsack problem, through the use of dynamic programming, introduced in section 2.2.4, to optimize the power allocation on the busbar while taking into account the available power, and the level of priority of each load. First, the mathematical theory beyond the knapsack method has been introduced. Second, the method has been embedded into the SC. It has been demonstrated how the proposed algorithm successfully allocates a fixed amount of available power to a set of loads that have varying levels of priorities and power requirements. This Chapter has developed a methodology to design a high-level SC based on LAP, which lead to the enhanced performance and efficiency of the EPS, while respecting safety constraints already discussed in Chapter 1. It has been applied to manage the power of a MEA electrical power subsystem in this work and can be expanded for the power management and optimisation of an entire MEA EPS. Moreover, this Chapter contributed to:

- Validation of the LAP method for the management of the MEA EPS buses, leading to the enhanced performance and efficiency of the EPS.
- Testing the LAP embedded into the selected SC that can be easily applied to the MEA EPS using one single development tool, as already discussed in Chapter 2. This has shown a noncomplex method to make the EPS more efficient





## **Chapter 6: A practical scenario: ASPIRE project**

---

### **6.1 Overview**

This Chapter aims to demonstrate the capability of the RCS method presented in section 1.1.2 to verify this by applying it for the design of the high-level SC considering the Electrical Power Distribution System (EDPS) of a prototype for a real airplane. The proposed case study is based on the Advanced Smart-Grid Power Distribution System (ASPIRE) project, investigated in collaboration with the University of Nottingham [2]. The ASPIRE project aims for the development of Cellular DC/DC converter cells for facilitating the implementation of Energy Management (EM) functionalities to the aircraft DC electrical power distribution system (EPDS) and to achieve substantial improvement in system efficiency, safety, power quality and eco-friendliness compare to existing solutions [1]. The project also looks at the development of novel DC/DC converter topologies and advanced EM and control approaches for achieving smart DC grid concept. The main objectives of ASPIRE include but are not limited to [1]:

- The development of novel regulation techniques for the DC/DC converter to provide the most efficient operation in both buck and boost modes, allowing on-fly mode inversion and employing innovative modulation principles
- The development of an innovative energy management strategy to reduce overloading capability requirements for main power sources (generators) thus reducing the overall EPS weight and volume
- The development of protection and fault management strategies to enable uninterruptable power delivery in the case of cell(s) or communication failures

One project objective is to identify suitable approaches for the ASPIRE EPS SC design. The selected approach will then be employed for the implementation of the smart grid concept and the enhanced electrical energy management functionalities. The RCS method is used to reconfigure the EPS for the reduction of the generator overloads with the aim to reduce the generator design weight. The proposed method solves the case scenario considering the

status of the entire EPS, while adopting an intuitive algorithm, RCS, for having reduced coding complexity and applying FSM tool.

This Chapter aims:

- To demonstrate that the application of the chosen reconfiguration strategy, algorithms and tools are practical and computationally inexpensive for the design of the SC, while reducing complex programming.
- To develop a methodology to design a high-level SC that is capable of making the EPS more efficient while respecting safety constraints by effectively managing the power of the entire MEA EPS.
- To demonstrate that the RCS method is an effective method for the SC design of practical EPDS by applying it to the ASPIRE based EPDS.

## 6.2 ASPIRE electrical power system

The ASPIRE EPDS model is depicted in Fig. 6.1.

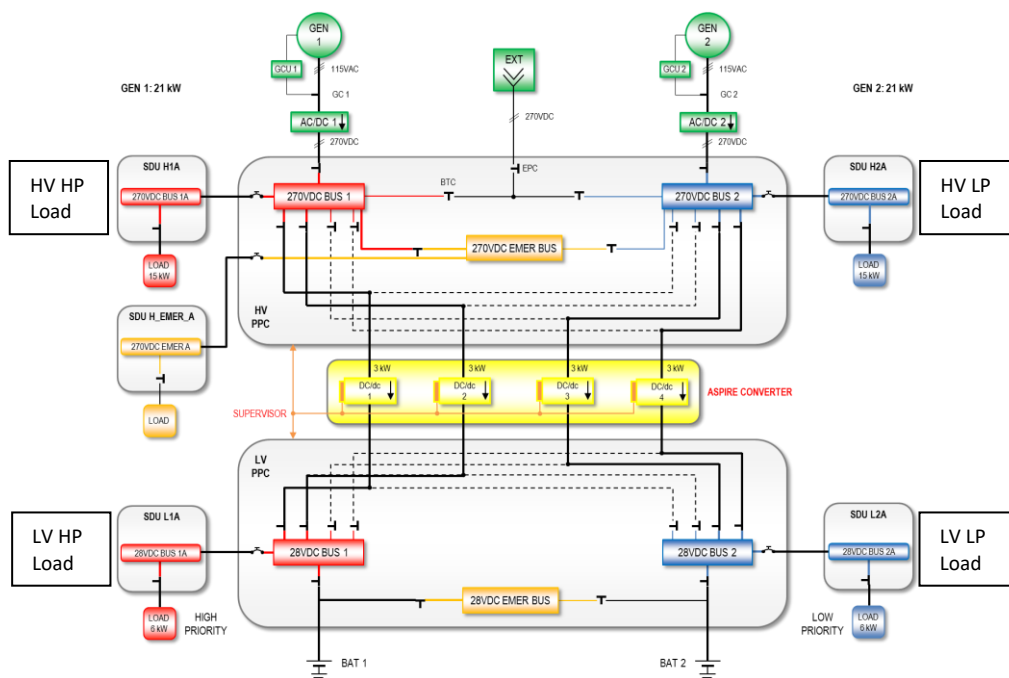


Fig. 6.1. Single-line circuit diagram of the EDPS topology for the ASPIRE project [1]

The EPDS presented in Fig. 6.1 is composed of two main generators of 21 kW each where the voltage is rectified through AC/DC converters to feed HVDC buses. The EPDS is DC, divided in high voltage side (HV 270 V) and Low Voltage side (LV 28 V). The HV side is composed of two main buses (270V buses 1 & 2), and another essential bus (270V Emer bus) used to supply some critical loads. The LV side is composed by two main buses (28V buses 1&2) and an essential bus (28V Emer Bus). Two batteries (BAT 1 and BAT 2) are connected to the LV side. The HV and LV buses are connected through four DC/DC converter cells which are 3 kW bi-directional converters. As discussed in Chapter 3, in this configuration the cells operate in parallel with the others, sharing the power request from the load, and avoiding power interruption, thus giving redundancy to the EPDS. The DC/DC converters can be connected to the HV buses through a set of four channels and to the LV buses through another set of four channels as shown by the blue dotted lines in Fig. 6.2. The DC/DC converters have the capability to switch from one channel to another depending on the requirements of the system. Moreover, this particular architecture gives an additional degree of freedom to the system. Since all the buses can be connected to each other through the bus switches, all the loads can be reached from different power paths, allowing the batteries to be used to supply HV or LV loads under each scenario.

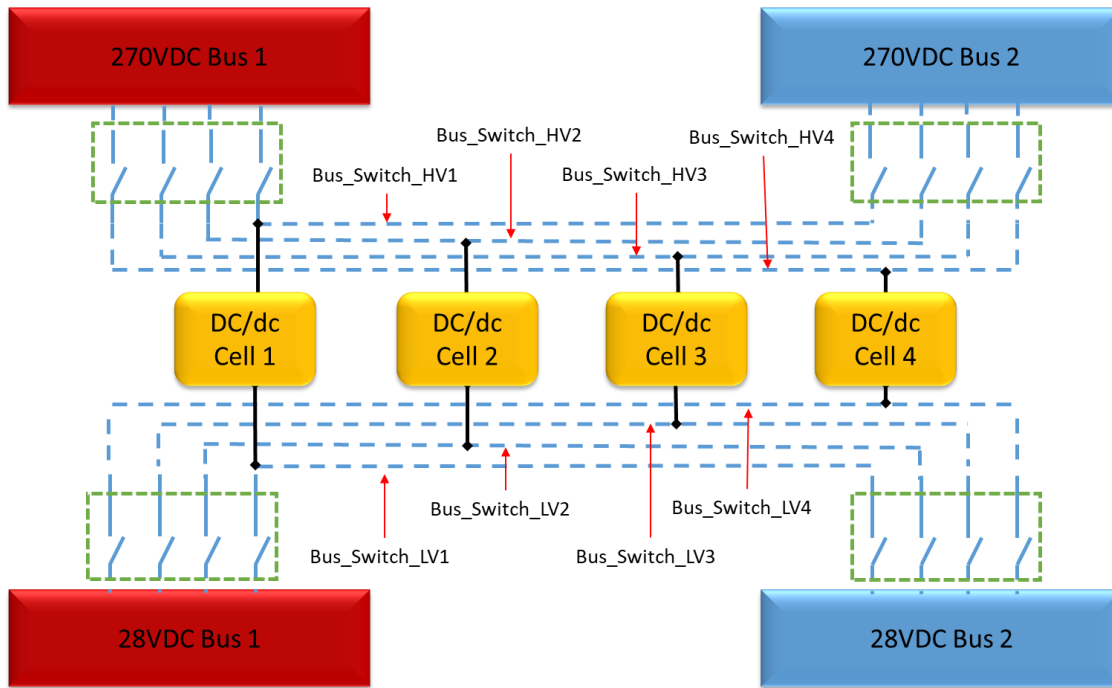


Fig. 6.2. An example of possible connections between the four DC/DC power electronic converters and the HV and LV buses 1 and 2

The loads in the system in Fig. 6.1 are assigned with different levels of priority. The buses highlighted in red represent high priority loads (HP), and they need to be kept powered at all times. The buses and loads in Fig. 6.1 highlighted in blue are low priority (LP) and can be subjected to power shedding for a limited period of time in case of an emergency. A detailed description of the management rules will be discussed in the next section.

### 6.3 Energy management concept of the ASPIRE system

The EM system of the ASPIRE aims to optimize the performance of the EPDS of the aircraft through the use of a smart controller. A list of predefined rules is set up in the ASPIRE project to enable the reconfiguration of the smart network in accordance with particular sets of events as given below. For instance, in case of a fault in the system, the EM system has the task to reconfigure the power paths of the network in order to re-distribute the available power while considering the level of priority of each load or avoiding generators to overload.

### 6.3.1 Logic rules definition

Knowing the ASPIRE EPDS model, based on the operating scenario of the aircraft, a set of rules need to be defined in order to impose and prioritize important behaviours of the system.

The set of rules that have been defined for the ASPIRE project are given hereunder, TABLE 6.1.

TABLE 6.1

<b>Definition of the logic rules that will be used for programming the FSM</b>	
1	High priority Buses must be fed at 100% of their power demand
2	The Buses with the same priority are fed by sharing the available power. The available power is calculated as the difference between rated and instantaneous power.
3	The battery connected to the high priority bus should not be discharged first
4	The battery connected to the lower priority bus must be used in power reversal mode
5	Reversal mode is only allowed in case of generator's overload
6	If the number of the active cells is less than needed, they have to be removed from the Low Priority buses and fed the High Priority buses
7	The change of network configuration is made in case of: <ul style="list-style-type: none"> <li>a. Changing number of active cells</li> <li>b. Generator overload conditions</li> <li>c. Grid faults (i.e., generator fault)</li> </ul>

The aforementioned set of rules form the basis of the logics for the SC.

## 6.4 Application of the logic rules

FSM is used to implement the logic rules given in the previous section as depicted in the three states and three sets of conditions given in Fig. 6.3.

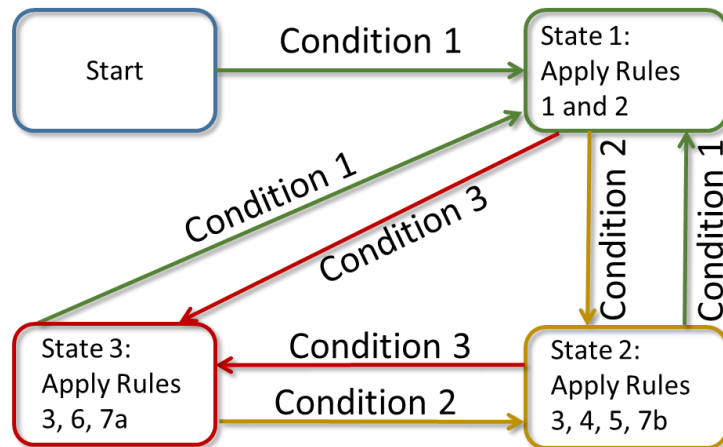


Fig. 6.3. Description of the condition for each transition

Condition 1: applies when the system is operating in normal conditions, all the loads are supplied, the generators are not overloaded and there is enough power on the high priority buses. It activates STATE1.

Condition 2: applies in case there is a generator overload. It activates STATE2.

Condition 3: applies when the system identifies a higher power request on the HP LV bus. It activates STATE3.

The FSM is set to the STATE1 when the EPDS is working at its rated conditions. In this case, rules 1 and 2 are applied. In this STATE, the SC will constantly check the value of the power flow across the buses of the EPDS. Once a variation of the nominal values identifies the SC will take action for addressing the power flow distribution.

Once the SC detects an overload condition the FSM goes in STATE2, where the rules 3, 4, 5, 7 are applied (TABLE 6.1). In this scenario, the SC will allow the EPDS to use the battery for avoiding the overload of the generator, but at the same time, as states in rule 3, the battery placed on the HP bus will not be discharged first.

The FSM will move to STATE 3, in which rules 3, 6, 7 will be applied (TABLE 6.1) when the SC detects a higher power request from the HV load bus. In this scenario the converter will be allowed to work in power reversal mode, disconnecting the LV loads in order to cover the overload request.

Thus, STATE 1 is activated subject to the condition 1. If the event condition 2 is valid, the system changes from STATE 1 or STATE 3 to STATE 2. Finally, STATE 3 is activated from STATE 1 or STATE 2 when condition 3 occurs.

In the next section the FSM design in Fig. 6.3 is used to apply the ASPIRE rules on the EPDS in Fig. 6.1.

## **6.5 Simulation model**

The EPDS in Fig. 6.1 has been modelled in the Simulink® environment. The FSM supervisor controller, which is based on the FSM shown in Fig. 6.3, has then been built by using the Stateflow® chart in Simulink®. The FSM acts on the EPDS system by controlling its converters and the contactors while the key parameters of the system are constantly monitored through real-time driven logic. TABLE 6.2 describes the input and output variables that are computed by the FSM, and Fig. 6.4 shows the simulation model of the FSM. These variables are required for allowing the FSM to compute a solution for the ongoing scenario. The SC computes the action to be performed by constantly monitoring the load power request, the battery SOC, and power delivered from the generators. As result, the SC uses this information to generate the outputs that re-configure the EPDS. After the solution is computed, the output is used to set the power delivered from the PECs, the connection of the buses, the power delivered from the batteries, and the eventual disconnection of non-critical loads.

TABLE 6.2. Description of the system variables

Variable	Value	Description
<b>P<sub>max</sub></b>	3000 [W]	Maximum power rating of DC/DC converter
<b>P1</b>	Range: -3000 to +3000 [W]	Actual power of converter cell 1
<b>P2</b>	Range: -3000 to +3000 [W]	Actual power of converter cell 2
<b>P3</b>	Range: -3000 to +3000 [W]	Actual power of converter cell 3
<b>P4</b>	Range: -3000 to +3000 [W]	Actual power of converter cell 4
<b>Batt1</b>	'1' when is in operation, '0' when is disconnected	Battery status on the HP side
<b>Batt2</b>	'1' when is in operation, '0' when is disconnected	Battery status on the LP side
<b>SOC1</b>	Range: 0 to 100%	State of charge of battery 1 (HP side)
<b>SOC2</b>	Range: 0 to 100%	State of charge of battery 2 (LP side)
<b>HP_Batt_Power</b>	Range: -6000 to +6000 [W]	Delivered power to Batt1
<b>Batt_Power</b>	Range: -6000 to +6000 [W]	Delivered power to Batt2
<b>Shed</b>	'0' when there is no Load shedding, '1' when the Load shedding is active	Load shedding on LV Bus 2 (LP side)
<b>P<sub>inst</sub></b>	Range: 0 to maximum power rating	Total actual power of the generators 1&2
<b>P<sub>highP</sub></b>	30000 [W]	Total power of HP loads
<b>P<sub>avl</sub></b>	$P_{inst} - P_{highP}$	Available power after deducting power to HP loads from total power from the generators
<b>P<sub>HP_Bus</sub></b>	Range: -15000 to +18000 [W]	Power request on Bus 1 on HP side
<b>Bus_Switch_HV1</b>	'1' to connect the converter cell 1 with the HV bus 1 and '0' to connect the converter cell 1 with the HV bus 2	Setting the connection of the cell 1 with the HV buses
<b>Bus_Switch_LV1</b>	'1' to connect the converter cell 1 with the LV bus 1 and '0' to connect the converter cell 1 with the LV bus 2	Setting the connection of the cell 1 with the LV buses
<b>Bus_Switch_HV2</b>	'1' to connect the converter cell 2 with the HV bus 1 and '0' to connect the converter cell 2 with the HV bus 2	Setting the connection of the cell 2 with the HV buses
<b>Bus_Switch_LV2</b>	'1' to connect the converter cell 2 with the LV bus 1 and '0' to connect the converter cell 2 with the LV bus 2	Setting the connection of the cell 2 with the LV buses
<b>Bus_Switch_HV3</b>	'1' to connect the converter cell 3 with the HV bus 1 and '0' to connect the converter cell 3 with the HV bus 2	Setting the connection of the cell 3 with the HV buses
<b>Bus_Switch_LV3</b>	'1' to connect the converter cell 3 with the LV bus 1 and '0' to connect the converter cell 3 with the LV bus 2	Setting the connection of the cell 3 with the LV buses
<b>Bus_Switch_HV4</b>	'1' to connect the converter cell 4 with the HV bus 1 and '0' to connect the converter cell 4 with the HV bus 2	Setting the connection of the cell 4 with the HV buses
<b>Bus_Switch_LV4</b>	'1' to connect the converter cell 4 with the LV bus 1 and '0' to connect the converter cell 4 with the LV bus 2	Setting the connection of the cell 4 with the LV buses



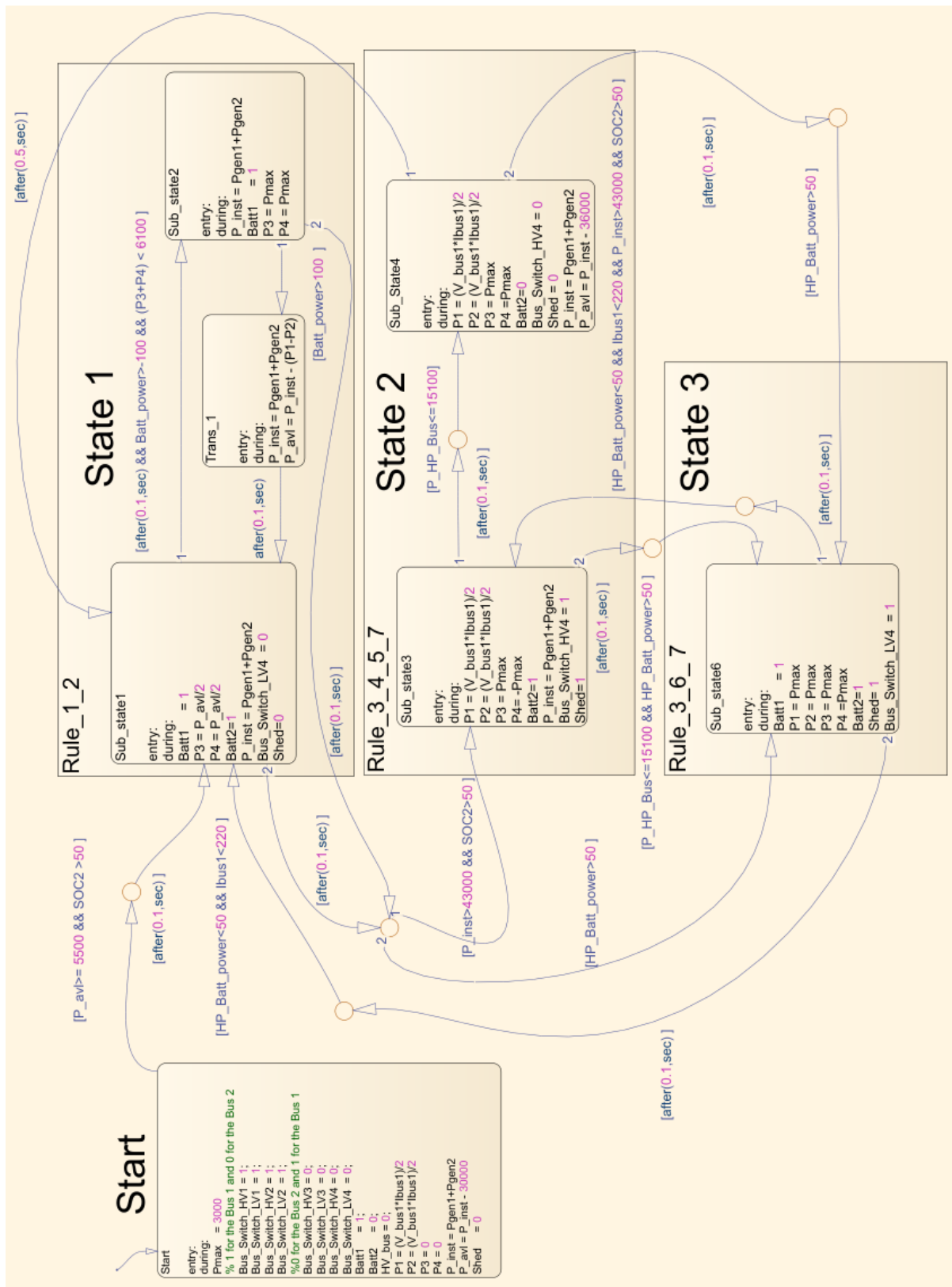


Fig. 6.4. Model of the FSM used to program the logic of the supervisor controller

Fig. 6.4 shows the STATES 1, 2, 3 of the system with the condition for each transition defined by the arrows. The conditions are applied, and the relevant STATES activated depending on the behaviour of the system such as the generator's operating conditions, the state of charge of the batteries and the level of priority.

Three case studies are presented in the subsequent subsections to demonstrate and validate the operation of the FSM in Fig. 6.4.

### **6.5.1 Normal operation**

For the normal operation scenario a 5s operation has been simulated, for showing the power setting when the EPDS is under the condition 1. At the start of the simulation, the system is initialized by defining the main parameters, such as the connection between the DC/DC converter cells and the buses, and computing the requested power from the HP loads, as shown in Fig. 6.4. Initially, the generators supply the HV loads, which require 30 kW in total, then the DC/DC converter cells 1 and 2 are supplied with 3kW each. After that, the system moves to STATE 1 (normal operation, condition 1, Fig. 6.3), and with the remaining available power  $P_{avl}$ , the generator 2 supplies the DC/DC converter cells 3 and 4. Fig. 6.5 shows the generator 2 power, which goes from 15kW to 21kW after 0.1s (actually the power goes over 21kW for a short period due to switches opening and closing operations) with the activation of the DC/DC converter cells 3 and 4.

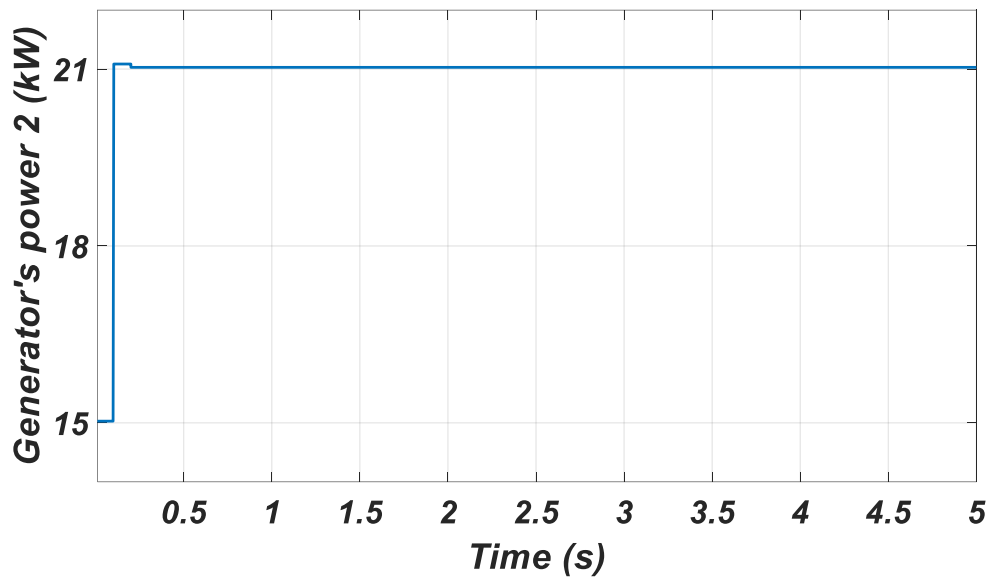


Fig. 6.5. Generator's power before and after the activation of converter 3 and 4 at 0.1s in a simulation scenario of 5s

Fig. 6. 6 and Fig. 6.7 show the power values of the DC/DC converter cells before and after the activation.

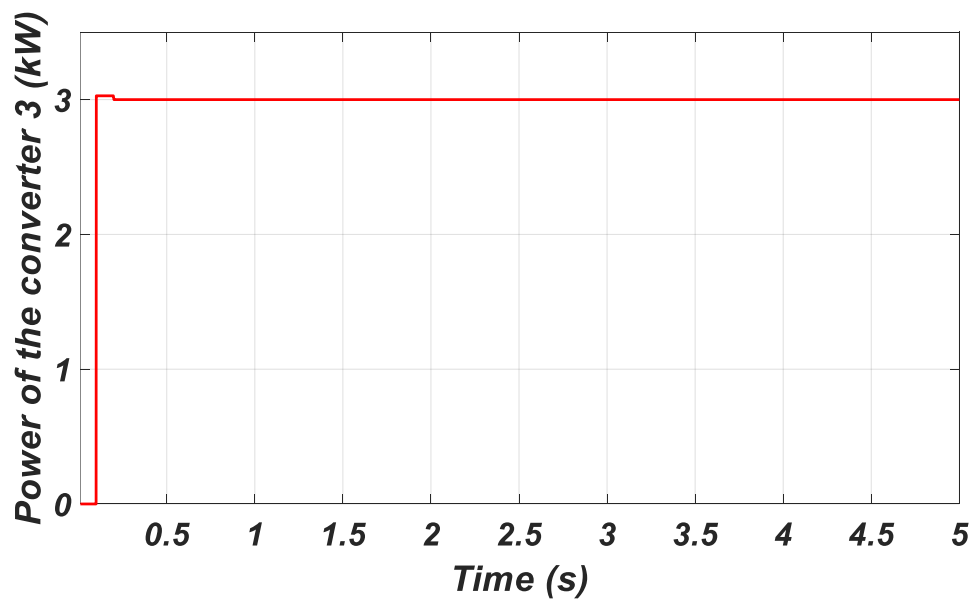


Fig. 6. 6. DC/DC converter cell 3 switched on after 0.1s, once the  $P_{avl}$  has been calculated

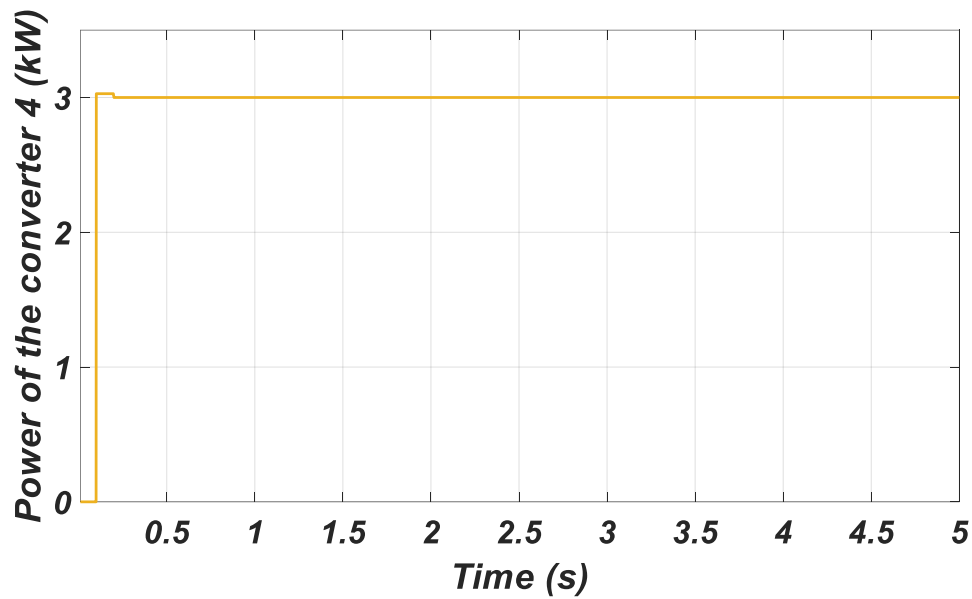


Fig. 6.7. DC/DC converter cell 4 switched on after 0.1s, once the  $P_{avl}$  has been calculated

During the normal operation, the rules 1 and 2 have been applied, with constant computing of the  $P_{avl}$ , and all the HP loads supplied.

### 6.5.2 Generator overload

In this case scenario, the power demand on the HV HP load increases from 15kW to 18kW, as shown in Fig. 6.8, which causes the generator 1 to go in overload from 21kW to 24kW.

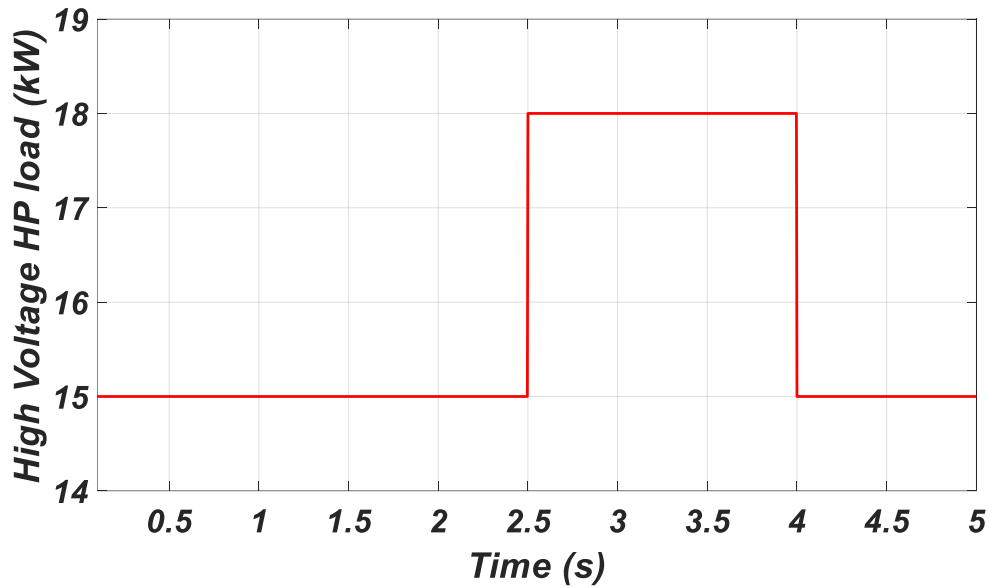


Fig. 6.8. power on the HP HV bus

The SC has the task to avoid generator overloads by applying a power reduction from the shedding of the LV LP load and the use the LP battery (batt2). In order to avoid generators' overloads, the rules 3, 4, 5, and 7b are applied. Referring to TABLE 6.1, the SC will allow the battery to be used for covering the overload, and since the overload is coming from the HV bus, the converter can work in power reversal mode enabling the power sharing from the LV bus to the HV bus. The Fig. 6.4 shows the logic of the system during a generator overload. After the overload occurs, the system passes into the STATE 2 (overload operation, condition 2, Fig. 6.3 ). In STATE 2, the converter 4 is made to work in power reversal mode as shown in Fig. 6.9. The power in converter 4 reverses from 3kW to -3kW at 2.5s as shown in Fig. 6.9. Of note is that since there is an overload on HV HP load, the converter 4 is disconnected from HV bus 2 through the Bus\_Switch\_HV 4 and connected to HV bus1.

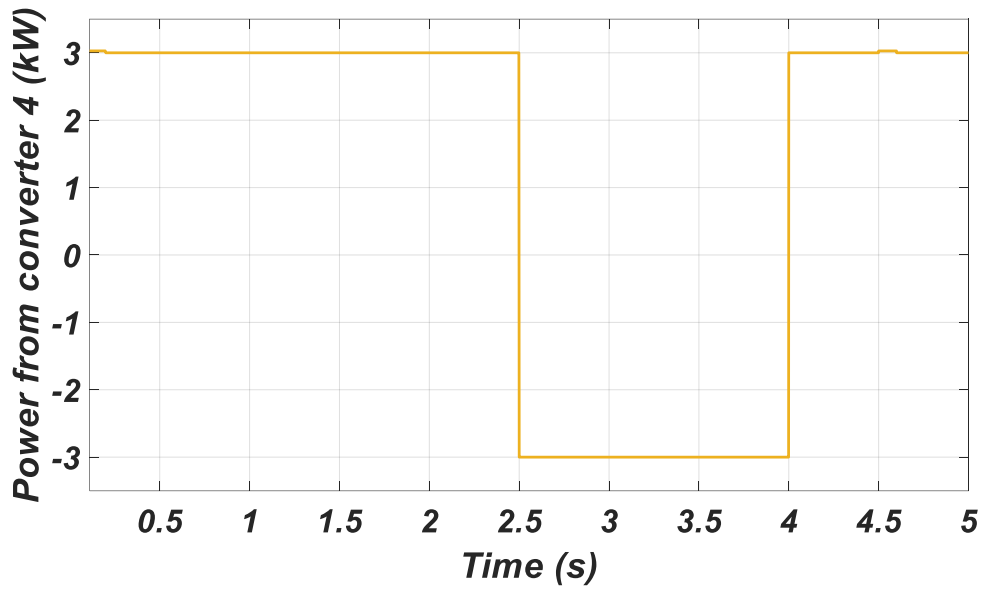


Fig. 6.9. Power on the converter 4. At 2.5 s the converter goes in power reversal mode

Further, the LP LV load is shed from 6kW to 3kW as shown in Fig. 6. 10. By shedding the LP LV load, the power from battery 2 (3kW) supplies the HV HP load through the converter 4. In order to avoid current loop on the LV bus2, the converter 3 is switched off.

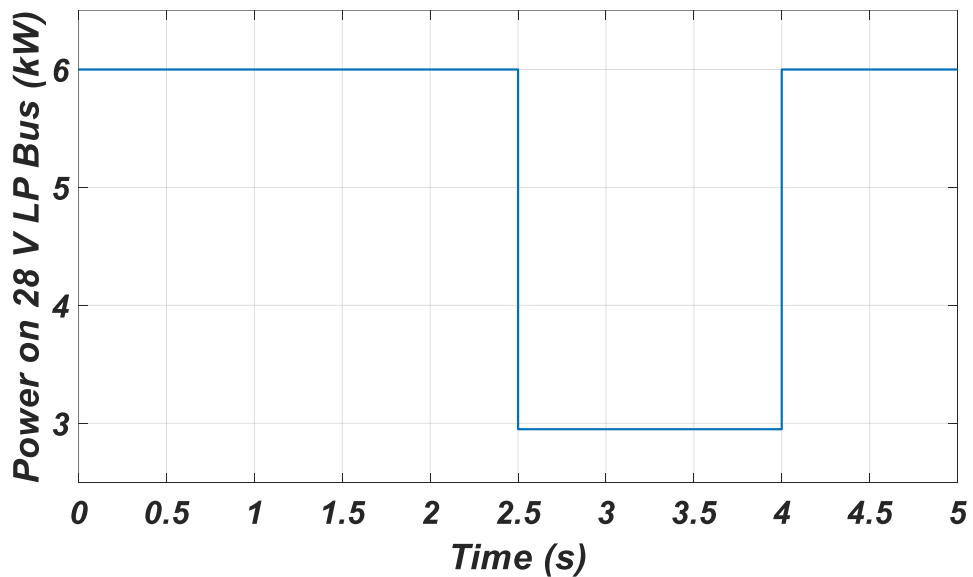


Fig. 6. 10. LV LP load shedding from 6kW to 3 kW at 2.5s

### 6.5.3 Increase in power demand on LV HP bus 1

In this case study, there is an increased power demand on the LV HP bus from 6kW to 9kW at 1.5s as shown in Fig. 6.11. The system transitions to STATE 3 as explained in section 6.4.

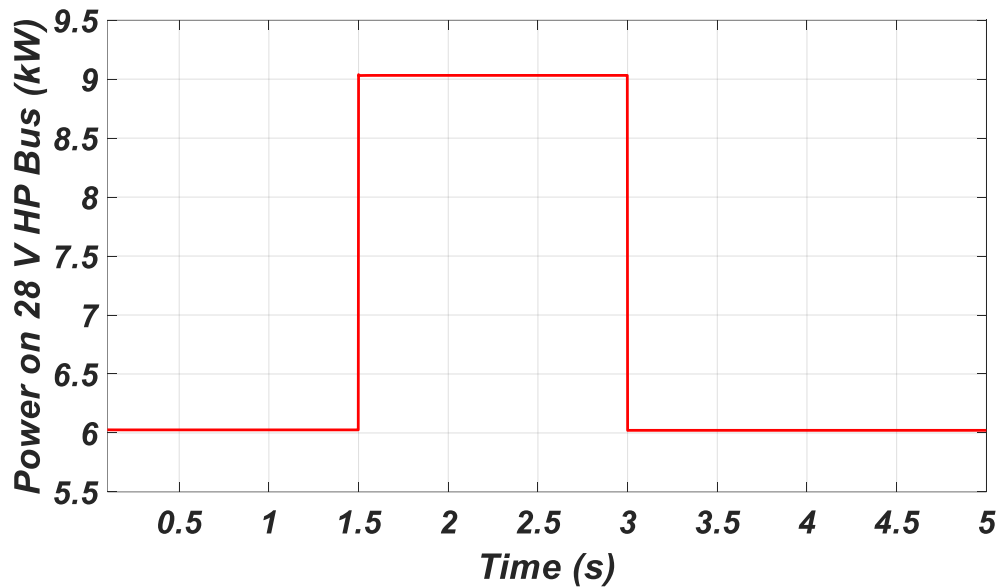


Fig. 6.11. Power demand on LV HP bus increases from 6kW to 9kW from 1.5s to 3s

With reference to Fig. 6.1, it can be seen that the two active DC/DC power converter cells are not sufficient to supply the LV HP load during this overload. Hence, the power converter 4 is disconnected from LV LP bus 2 and connected to LV HP bus 1, as required by rule 6 and 7a, which states that the converter cell can work in reversal mode (TABLE 6.1). As one power converter 4 has been removed from LV LP bus 2, only power converter 3 is supplying the LV LP load, which thus has to be shed from 6kW to 3kW, as shown in Fig. 6.12.

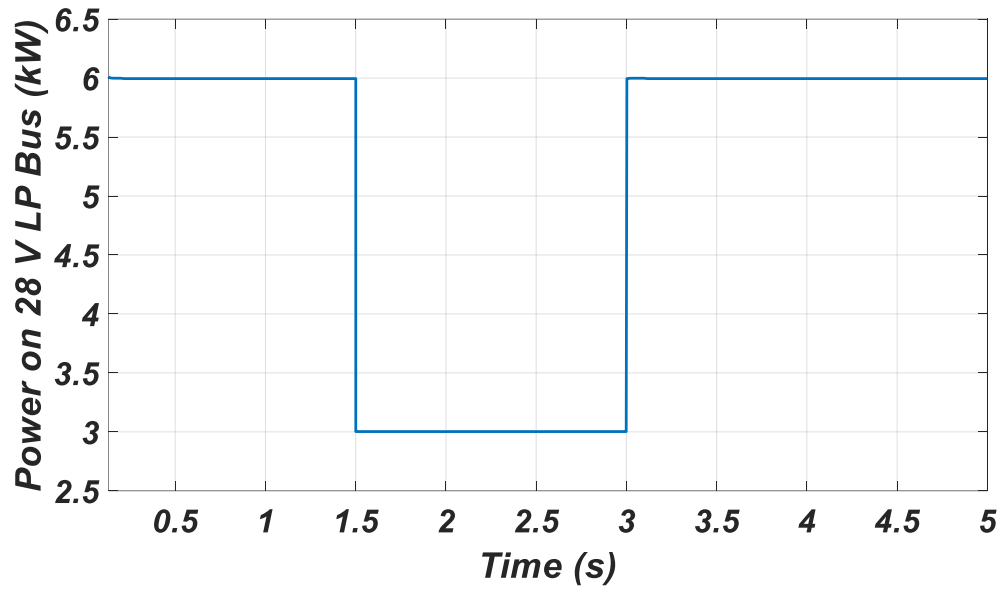


Fig. 6.12. Load shedding on LV LP load from 6kW to 3kW at 1.5s

By performing the power converter reconfiguration, the HP battery 1 has not been used as required by rule 3.



## **6.6 Additional considerations**

In the study case presented above, the simulation model has been used to test the capability of the SC controller on a potential EPDS candidate to be used in a commercial aircraft. The considered simulation scenarios showed the EPDS in its normal scenario, the overload operations, and a critical overload issue. However, as showed in Chapter 4, the capability of the SC can be expanded in solving emergency scenarios, which can consider multiple converters failure and very low SOC levels of the batteries. The EPDS presented in this Chapter is derived from the model presented in Chapter 3, section 3.2, which is composed by multiple converter 'cells'. The use of this architecture adds to the EPDS more degree of freedom, thus the FSM code presented in Chapter 4 regarding the safety operations, for addressing the emergency scenarios, can be easily applied to the ASPIRE model.

Thus, the set of rules presented in TABLE 6.1 can be expanded, adding more STATES that cover the emergency scenarios.

Chapter 5 has presented the knapsack problem to solve the LAP. The same concept can be easily transferred to ASPIRE EPDS giving an additional optimization of the power flow in case of multiple loads connected on the bus.

Moreover, this aspect will be considered in the Chapter 8 that will introduce the experimental test.

## **6.7 Conclusion**

This Chapter has validated the RCS method described in Chapter 2 by solving a real case scenario as defined by the ASPIRE project. The simulations have demonstrated how the RCS method can manage EPS overloads on both sides of the network, high voltage, and low voltage, and also respect the level of priorities while providing the requested power of the loads. The FSM tool has been used to apply a set of energy management and safety logic rules to a representative EPDS of an aircraft of the ASPIRE project based on real-time computational model. Depending on the events that can occur in the power system and that are captured through predefined sets of conditions, a particular system STATE is activated such that a set of agreed rules pertaining to the power system are respected. Moreover, the results showed in this Chapter satisfied the following tasks:

- Validate the RCS method for the management of the smart-grid EPS using example of ASPIRE project, considering a real scenario, leading to the enhanced performance and efficiency of the EPS, while respecting safety constraints
- Validate a methodology to design of a high-level SC that is able to manage the entire MEA EPS, leading to the enhanced performance and efficiency of the EPS, while respecting safety constraints.
- The used approach has been developed for designing a SC that can be easily applied to the MEA EPS using one single development tool to make the EPS more efficient and safer.

## Chapter 7: Case study for experimental application

### 7.1 Introduction

This Chapter presents a case study to be tested in the laboratory to validate experimentally the RCS method and the LAP operations that have been presented in earlier Chapters. For the selected case study, the SC will use optimisation technique to reduce or avoid the generator's overloads with the aim to reduce the generator's size and consequently the overall weight of the system. The presented case scenario will first be created and simulated in the Simulink® environment. Then the simulation model will be scaled in terms of voltage and power to be eventually assembled in the laboratory for experimental validation which will be presented in the next Chapter.

### 7.2 Test scenario

The EPS topology used for this case study is presented in Fig. 7.1.

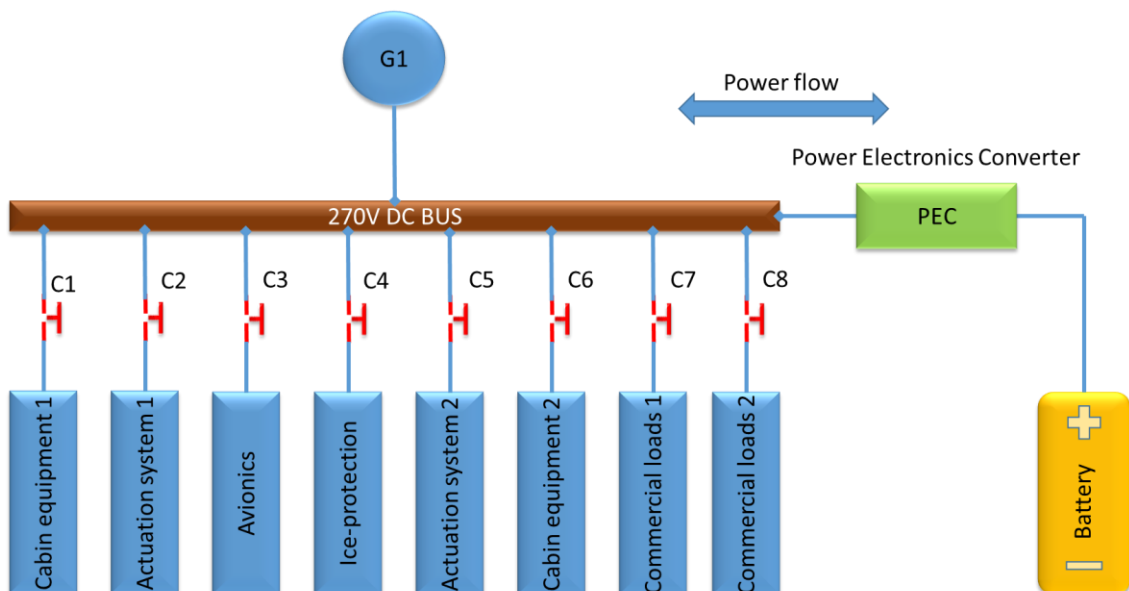


Fig. 7.1. Single-line diagram of the EPS configuration used for the test scenario

A generator (G1) is designed to supply a total load of 21kW (rated conditions), which includes the ice protection system, as resumed in TABLE 7.1. During peak icing conditions an additional 3kW power is required; this can be available either from the battery and/or by other loads shedding employing the knapsack method that has been presented in Chapter 5. An energy management strategy will be developed and implemented so that the generator’s power can be kept at rated 21kW instead of going to overload (24kW) during this peak icing conditions. The electrical power system (EPS) will be controlled by acting on two main variables, the requested power of the loads (PL) and the state of charge (SOC) of the battery. TABLE 7.1 details the EPS loads for the studied scenario. The loads are characterised by level of priority and the absorbed power, in case of extra EPS power demand (as peak icing case) their power demands can be reduced.

TABLE 7.1. EPS loads considered for the presented EPS

<b>Loads power during cruise flight stage in normal and peak conditions</b>					
	<b>Loads (represented by Resistive loads in experiment)</b>	<b>Normal Condition(kW)</b>	<b>Peak Conditions (kW)</b>	<b>Sheddable loads (kW)</b>	<b>Priority Level</b>
1	Commercial load1 / Commercial load 2 – Lights, entertainment systems	2	1	0.75	Low / Low
2	Ice Protection System - Nominal	5	5	0	High
3	Ice Protection Add. System - Peak	<b>0</b>	<b>3</b>	0	High (on request)
4	Avionics – Electronics systems and navigation	3	3	0	High
5	Cabin Equipment1 – Pressurization system	4	6	0	High
6	Cabin Equipment2 – Environmental control	2	2	1.25	Medium
7	Actuation system 1 - Flaps	3	3	0	High
8	Actuation system 2 – Flaps	2	3	0	Medium
	Total Load (PL)	21	<b>26</b>	<b>2</b>	
	Total power provided from the generator	21	<b>24</b>		

Fig. 7.2 is described the flow-chart of the STATES with the transition conditions. The FSM is initialized through the STATE 'start', which is used to define the main variables and the first configuration of the EPS. After that, the FSM will move to the STATE 3 in which all the components of the system work at their rated condition and assuming the battery charged and no overload requests. From STATE 3 the FSM can move to other STATES depending on the transition conditions defined beside the arrows (see Fig. 7.2). In the case of a low level of the SOC, and no overload requests the system will move into the STATE 1 or STATE 2 (depending on the SOC levels). If the FSM will detect an overload request with the battery charged (high SOC level), then it will go into the STATE 5 or STATE 6 (depending on the SOC level). While, if the FSM will detect an overload request with a low level of the SOC, then it will move into STATE 4.

TABLE 7.2 shows the STATES and transition conditions of the EPS. They are based on the battery SOC (high, medium, low), and the PL (< 21kW or > 21kW).

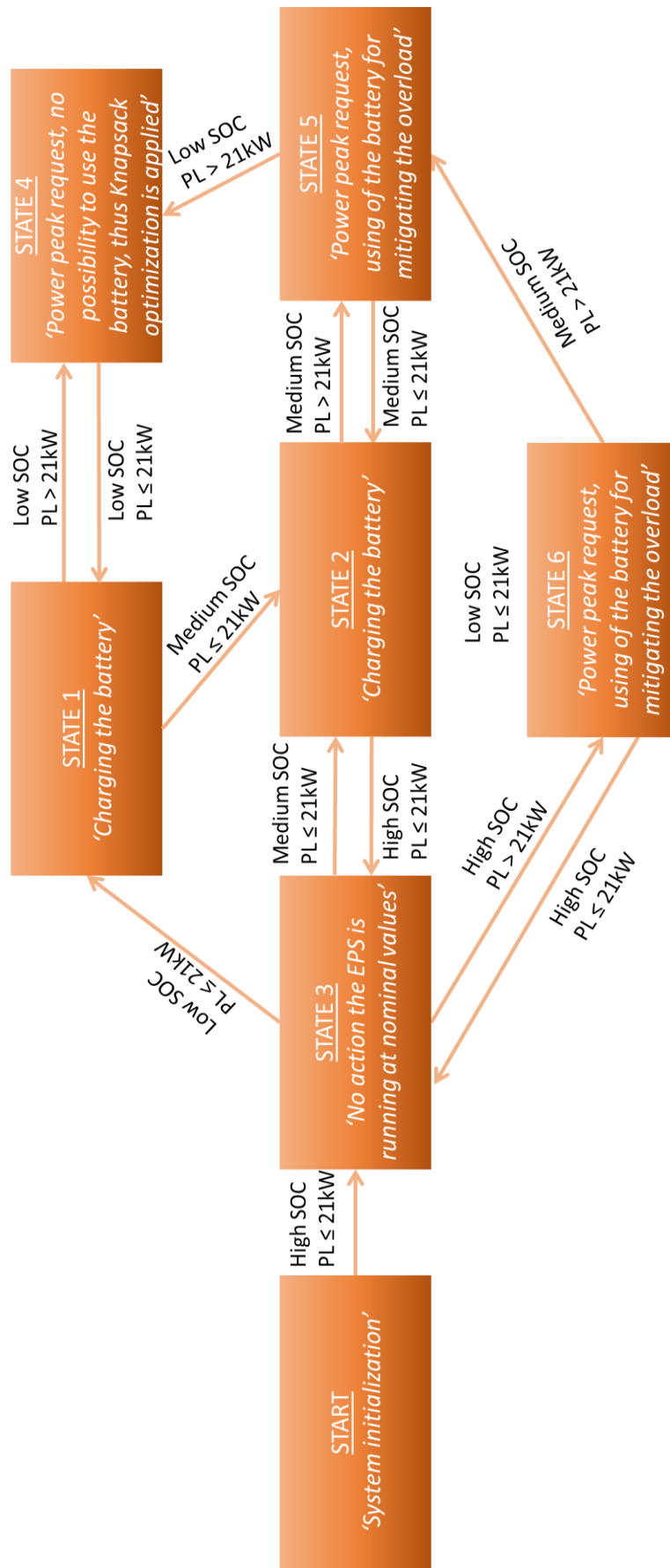


Fig. 7.2. Flowchart of the FSM available STATES for the EPS operations

TABLE 7.2 represents the 6 STATES, which are made to set-up the system during peak conditions (overloads) by applying the RCS and LAP strategy. The variable  $P_{batt}$  defines the amount and direction of the power flowing through the battery. In each STATE, the value of  $P_{batt}$  is calculated considering the requested power of the load  $P_L$  and the delivered power from the generator  $P_{gen}$ . If the power request is higher than the battery capacity of 3kW as in the case in STATES 5 and 6, the controller will apply the knapsack optimisation discussed in the Chapter 5 to provide the surplus power required through load shedding.

TABLE 7.2. State table used to define the SC behaviour

SOC/PL	PL ≤ 21kW	PL > 21kW
<b>SOC &lt; 30% (Low)</b>	<p>STATE 1: Battery discharged</p> <ul style="list-style-type: none"> <li>- Charging battery  <math>P_{batt} = P_{gen} - PL \rightarrow P_{bat}</math> positive, charging operation:  <u>Disconnect the load with the lowest priority level in order to do not overload the generator during the charging scenario</u></li> <li>- If SOC &gt; 30 %, goto STATE 2</li> <li>- If PL &gt; 21kW, goto STATE 4</li> </ul>	<p>STATE 4: Battery discharge + Overload Overload with low level of SOC</p> <ul style="list-style-type: none"> <li>- Apply <b>knapsack method</b> to shed load:  <u>In order to avoid generator's overload, when the battery is discharged the Knapsack method needs to be applied, disconnecting the loads with the lowest priority (see TABLE 7.1)</u></li> <li>- If PL ≤ 21kW, goto STATE 1</li> </ul>
<b>30% ≤ SOC ≤ 90% (Medium)</b>	<p>STATE 2: Battery with medium charge</p> <ul style="list-style-type: none"> <li>- Charging battery with  <math>P_{batt} = P_{gen} - PL \rightarrow P_{batt}</math> positive, charging operation:  <u>Disconnect the load with the lowest priority level in order to do not overload the generator during the charging scenario</u></li> <li>- If SOC &gt; 90% goto STATE 3</li> <li>- If PL &gt; 21kW, goto STATE 5</li> </ul>	<p>STATE 5: Battery with medium charge + overload Peak condition with acceptable level of the SOC</p> <ul style="list-style-type: none"> <li>- <math>P_{batt} = P_{gen} - PL \rightarrow P_{batt}</math> negative, discharging operation:  <u>The battery is providing power</u></li> <li>- If <math>P_{batt} \leq 3kW</math>  <u>Battery supplies power within its acceptable rating</u>  <math>P_{batt} = P_{gen} - PL</math></li> <li>- If <math>P_{batt} &gt; 3kW</math>  <u>The battery delivered power is fixed to 3kW (i) (Battery discharge rating power)</u>  <u>The Knapsack method is applied to avoid generator's overloads (ii)</u>                      (i) <math>P_{batt} = 3kW</math>                      (ii) and apply <b>knapsack method</b> to identify and shed load by (PL - 3kW)</li> <li>- If SOC &lt; 30% goto STATE 4</li> <li>- If PL ≤ 21kW goto STATE 2</li> </ul>
<b>SOC &gt; 90% (High)</b>	<p>STATE 3: Normal conditions</p> <ul style="list-style-type: none"> <li>- No action:  <u>The generator is able satisfy the power request</u></li> <li>- If PL &gt; 21kW, goto STATE 6</li> </ul>	<p>STATE 6: Battery fully charged + overload Peak condition, battery fully charged</p> <ul style="list-style-type: none"> <li>- <math>P_{batt} = P_{gen} - PL \rightarrow P_{batt}</math> negative, discharging operation:  <u>The battery is providing power</u></li> <li>- If <math>P_{batt} \leq 3kW</math>  <u>Battery supplies power within its acceptable rating</u>  <math>P_{batt} = P_{gen} - PL</math></li> <li>- If <math>P_{batt} &gt; 3kW</math>  <u>The battery delivered power is fixed to 3kW (i) (Battery discharge rating power)</u>  <u>The Knapsack method is applied to avoid generator's overloads (ii)</u>                      (i) <math>P_{batt} = 3kW</math>                      (ii) and apply <b>knapsack method</b> to identify and shed load by (PL - 3kW)</li> <li>- If SOC ≤ 90% goto STATE 5</li> <li>- If PL ≤ 21kW goto STATE 3</li> </ul>



### 7.3 FSM description

The FSM model is used to develop the algorithm presented in Fig. 7.2 and TABLE 7.2. In order to control the power flow within the EPS, the FSM will receive the SOC,  $P_{gen}$ , and PL as input variables and will give the status of the switches,  $C_1$  to  $C_8$ , and the value of  $P_{batt}$  as outputs. Fig. 7.3 shows the FSM block with the inputs (on the left) and outputs (on the right):

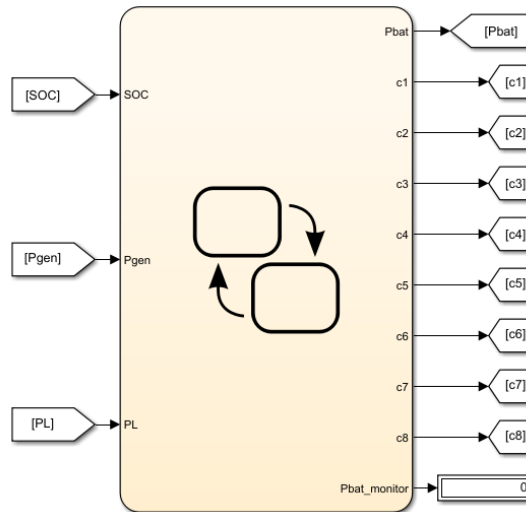


Fig. 7.3. Input and output variables of the FSM

The initialization of the system is showed in Fig. 7.4 as the 'Start' STATE, referring to Fig. 7.2 it is possible to see that is used to initialize the FSM configuration, and importing all the variables needed for the computation.

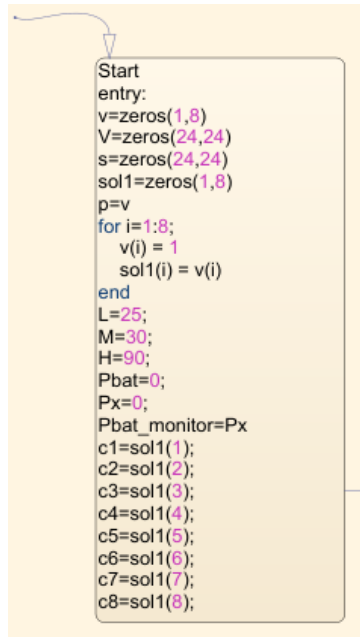


Fig. 7.4. Initialization STATE of the system

The matrices  $v$ ,  $V$ , and  $s$  are initialized to zero here, and will be used to calculate the solution for the knapsack problem. As already explained in Chapter 5, the knapsack method consists of using the available power for supplying as much load as possible respecting the priority levels, the algorithm used for finding the solution consist in storing the value inside a matrix of 'i' rows and 'j' columns and find the best solution by scrolling each value and match it with the previous one. In  $v$  are stored the value of the priority level of each considered load,  $V$  is used to store the value of the requested power of a selected load that has to be compared with the previous one, while  $s$  is used to keep record of the stored value from the selected load and compare it with the others in the table. The variable  $sol1$  is used to store the knapsack solution that will act on the eight switches and is set to '1' (switches closed/all the loads active) in the 'Start' STATE. The variables  $L$ ,  $M$ ,  $H$  refer to the SOC of the battery (low, medium, high).  $P_{bat}$  is used to store the value of the calculated power delivered to or absorbed by the battery.  $P_x$  and  $P_{bat\_monitor}$  is used to check the value of  $P_{bat}$ . The variables  $C_1$  to  $C_8$  are used to set the status of the switches. Once all the system variables are initialized, the system can pass into the operation STATES.

Initially, the SOC is set at high level (battery charged) and a rated power request of 21kW (nominal conditions) is made. The EPS system will operate in STATE 3 as per Table 7.2, and is shown in Fig. 7.5:

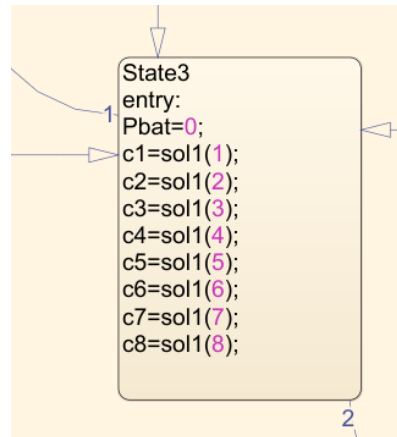


Fig. 7.5. STATE 3 of the system

In the STATE 3, the battery is disconnected, and all loads are working at their rated condition, so the total EPS load power is 21kW. Considering the aircraft in cruise operation and neglecting faulty scenarios, the system could go in the following STATES (referring to the TABLE 7.1 and 7.2):

- Overload due to the activation of the de-icing system (additional power request of 3kW)
- Overload due to power peak request of other loads (TABLE 7.1)
- Overload due to the combination of the activation of the de-icing system and other loads power peak request (TABLE 7.2)

Moreover, the controller must consider the SOC status during the abovementioned scenarios. From TABLE 7.2 it is possible to see 6 STATES, but the behaviour of the system can be resumed in 4 STATES, since the STATE 1 and STATE2 are similar as well as the STATE 5 and the STATE 6, in which the only difference is a lower level of the SOC in STATES 1 and 5 respectively, as it is possible to see in TABLE 7.3 below.

TABLE 7.3. Battery operations during the different STATES

<b>SOC/PL</b>	<b>PL ≤ 21kW</b>	<b>PL &gt; 21kW</b>
<b>SOC = Low</b>	STATE 1: <u>Charging battery</u>	STATE 4: Knapsack optimization
<b>SOC = Medium</b>	STATE 2: <u>Charging battery</u>	STATE 5: <u>Discharging battery</u>
<b>SOC = High</b>	STATE 3: No action	STATE 6: <u>Discharging battery</u>

Fig. 7.6 depicts the FSM code implemented in Simulink® for STATE 6 during the overload scenario when the SOC is high. In STATE 6.1 the system starts to use the battery by providing the required power, which is calculated as the rated power of the generator (21kW) minus the power requested from the load. The function ‘during’ enables the FSM to perform a continuous check (real time) on the delivered power during the STATE 6.1. In this STATE, all the loads are supplied since the system has enough power to cover the overload. In the eventuality of additional power, the FSM will go in the STATE K.6 that applies the knapsack optimization by disconnecting the loads with the lowest priority and using the maximum available power. Once the knapsack optimization has been applied the system will go in the STATE 6.2, which fixes the value of the drained power of the battery to its nominal (3kW) and disconnects the loads as calculated in the STATE K.6. When the overloads are extinguished the FSM can go back in the STATE 6.1

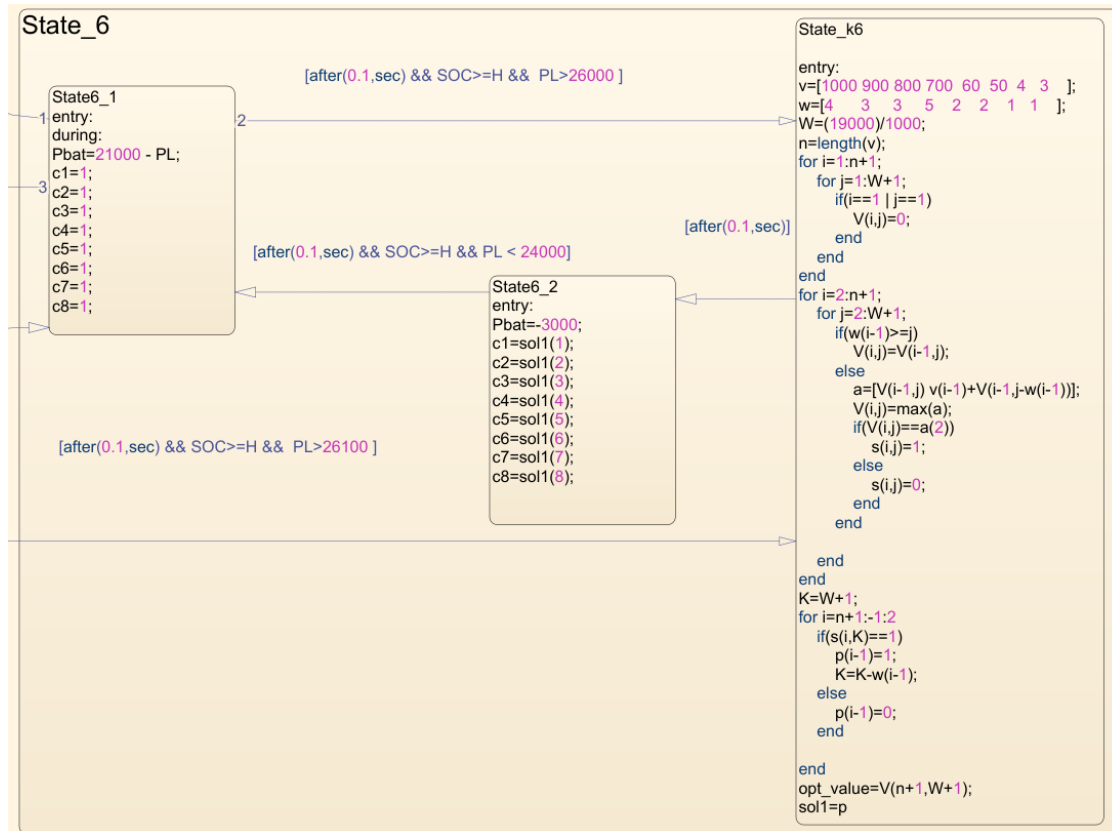


Fig. 7.6. STATE 6 the system reduces the generator’s overload using the battery or the knapsack optimisation

In the STATE 6.1 the power requested by the load 3 (Ice protection add. system) is within a range of 3kW, so the battery can help the generator; the power that should be delivered from the battery is calculated and stored in the variable  $P_{bat}$ . Moreover, if the power request is greater than 3kW the SC will go to the STATE k\_6, where the knapsack optimisation algorithm will be applied giving back a solution that allow the EPS to don’t overload the generator. After that, the SC will go into the STATE 6.2, where the battery will be set to provide 3kW (the maximum discharge rating allowed). Applying the presented algorithm, the system can maintain the generator’s power at 21kW.

Fig. 7.7 and Fig. 7.8 present the FSM code during rated conditions of the load (21kW) with a low level of the SOC (STATE 1) and peak conditions of the de-icing system and/or the peak condition of the other loads with a low level of the SOC (STATE 4) respectively, as resumed in TABLE 7.3.

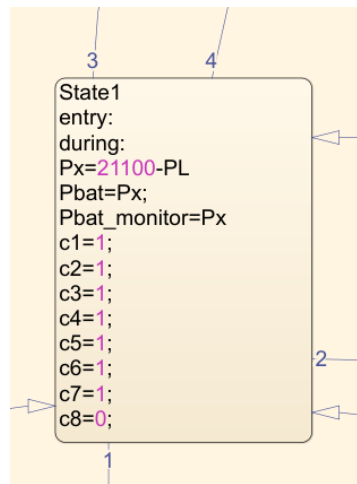


Fig. 7.7. STATE 1, battery charging operations

In STATE 1 the battery is in charging operation, disconnecting the load 8 (refer to Fig. 7.1), which is the one with the lowest priority level.

It is to be noted that in Fig. 7.7 the Generator's power is set to 21100W instead of 21000W in order to take into account small power variations. These variations are given by the combination of the current transient and the sampling period of the FSM in reading the values. These variations are very small. However, the desired value will never be exactly 21kW but in a small range around it, thus this behaviour must be taken into account during the coding stage, otherwise, it could destabilize the FSM.

In Fig. 7.8 the code used to cover the scenario in which a load power peak arrives during charging operations (STATE 4) is shown.

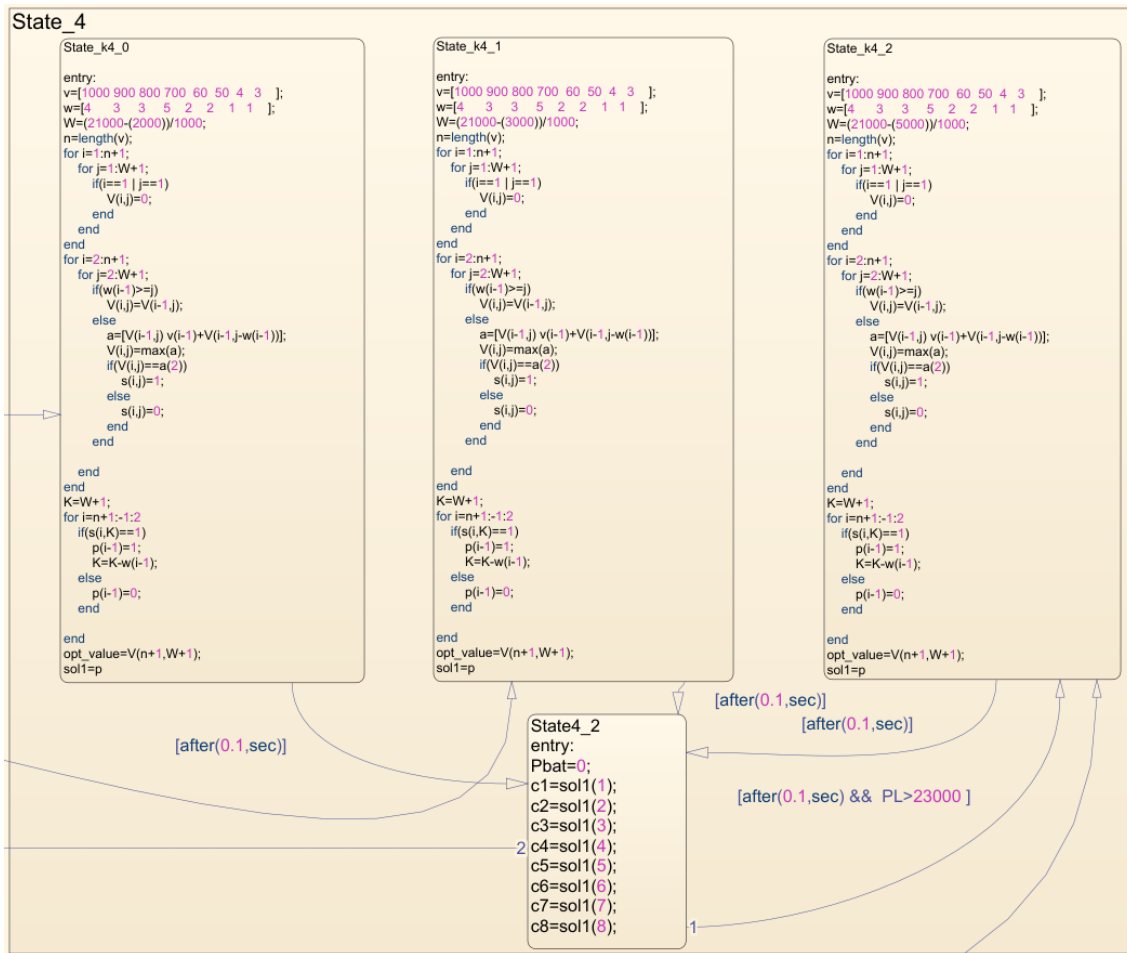


Fig. 7.8. STATE 4: overload scenario during low level of the SOC

From the code it is seen that the knapsack optimization can be applied under 3 different cases. In the STATE K4.0, the knapsack optimization is applied to an overload of 2kW, in the STATE K4.1 is considered an overload of 3kW, and in the STATE K4.2 is considered the maximum overload of 5kW. In this case, the code has been divided into three different calculations to obtain faster feedback when the knapsack method needs to be applied. Once the knapsack optimization has been calculated the SC will go into the STATE 4.2 where the knapsack is applied to arrange the contactor's configuration. Thus, if an overload occurs and the battery is discharged, the system goes into the STATE 4 where the charging operation is stopped, and the knapsack optimization is applied to avoid the generator's overload and keep the de-icing system active. In the next section presented FSM will be tested through simulations.

## 7.4 Simulation results

This section reports the simulation results for the above-described case study. It is divided in two different scenarios in order to show the operation with low and with a high battery SOC. In the first scenario the system initially is working at rated conditions with high SOC level. After 10 seconds the ice-protection is activated with a consequent increase of the requested power (according to [1] the worst-case scenario with peak demand of ice-protection is assumed to take 6 minutes). In addition, a peak power request from the other loads will be assumed during the ice-protection peak request as well, in order test the controller operation during multiple events.

### Scenario 1:

In Fig. 7.9 the behaviour of the load power during the first scenario is shown. For the first 10 seconds the system is working at rated conditions (21kW), when the de-icing system starts to request the peak power hence increasing the total load power demand from 21kW to 24kW. At the  $t=130s$  the system receives another peak request from other load (Cabin equipment 1 – Pressurization system, for this case); thus, the knapsack method is applied to reduce the power request from 26kW to 24kW.

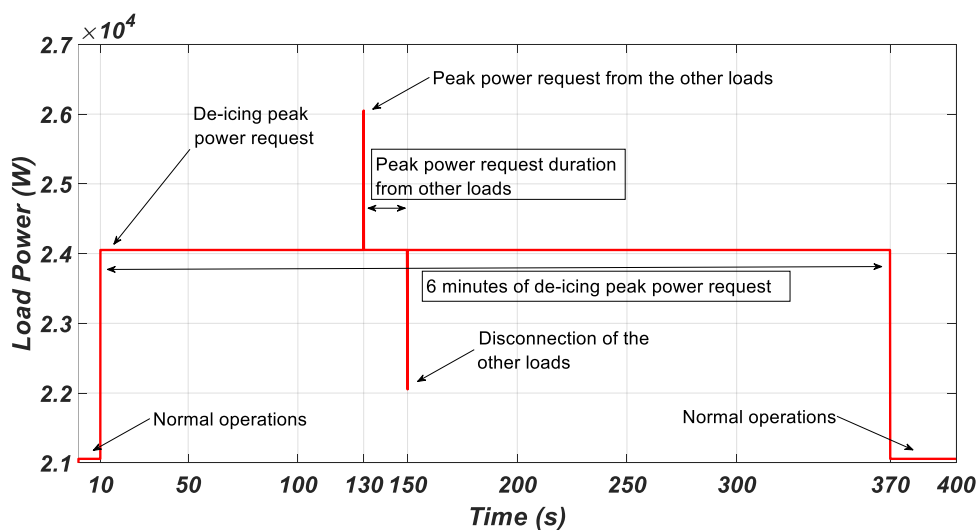


Fig. 7.9. Behaviour of the load power during different overload operations (scenario 1)



From Fig. 7.10 it's possible to see that at 10s the system starts to use the battery power in order to cope with the overload request. The drained power from the battery is calculated by the controller and it's around 3kW, which is the maximum value that the battery can provide. As explained in section 7.3 the power delivered from the battery is calculated from the controller, as the difference of the generator's power and the requested power, thus the value is not exactly 3kW but presents an oscillation around it due to the current transients.

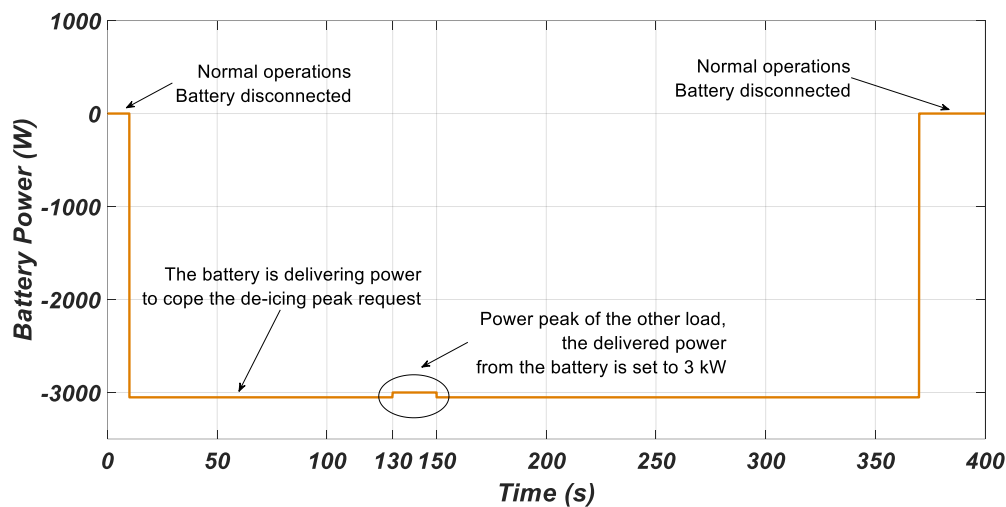


Fig. 7.10. Behaviour of the battery power during different overload operation (scenario 1)

From  $t = 130$ s to  $t = 150$ s, the EPS receives another overload request, 2kW, from the other load (Cabin equipment 1 – Pressurization system), although the battery is not able to provide more than 3kW; therefore, the battery's delivered power is set to 3kW and the knapsack optimization is applied in order to shed additional 2kW of loads. In the Fig. 7.11 the behaviour of the generator power is shown it can be remarked how the control system keeps the delivered power at the rated level of 21kW.

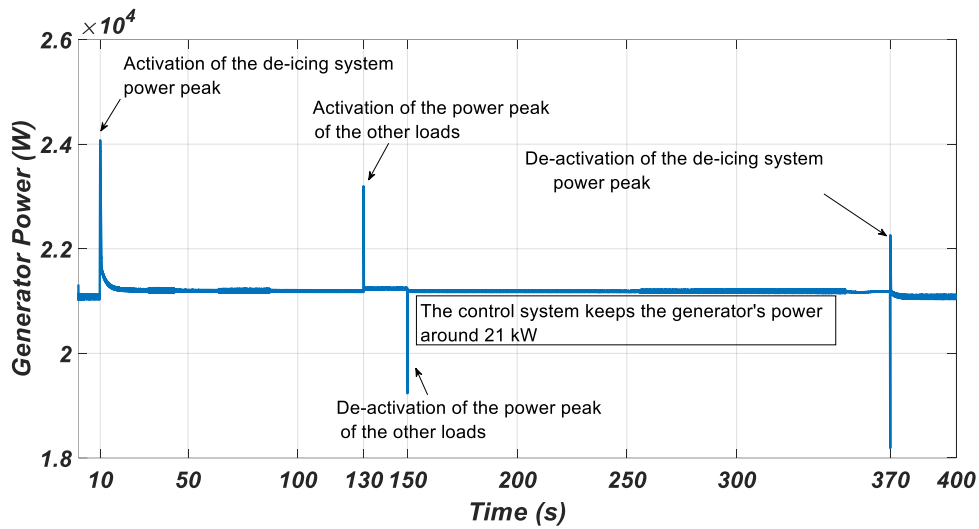


Fig. 7.11. Behaviour of the generator power during different loading conditions

The SOC of the battery is shown in Fig. 7.12. From the eq. 7.1 it's possible to calculate the amount of energy used to supply the loads for 6 minutes:

$$E_{\text{tot}} \cdot (\text{SOC}_{\text{initial}} - \text{SOC}_{\text{final}}) = P_{\text{de-icing}} \cdot t \quad (7.1)$$

where  $E_{\text{tot}}$  is the total battery energy in Wh,  $\text{SOC}_{\text{initial}}$  is the initial state of charge,  $\text{SOC}_{\text{final}}$  is the SOC value after the use of the battery,  $P_{\text{de-icing}}$  is the required power from the system in W, and  $t$  is the duration time of the discharge operation. For completion. Fig. 7.13 shows the system STATES during the scenario. This is used to track the moves of the controller during the variations of the system.

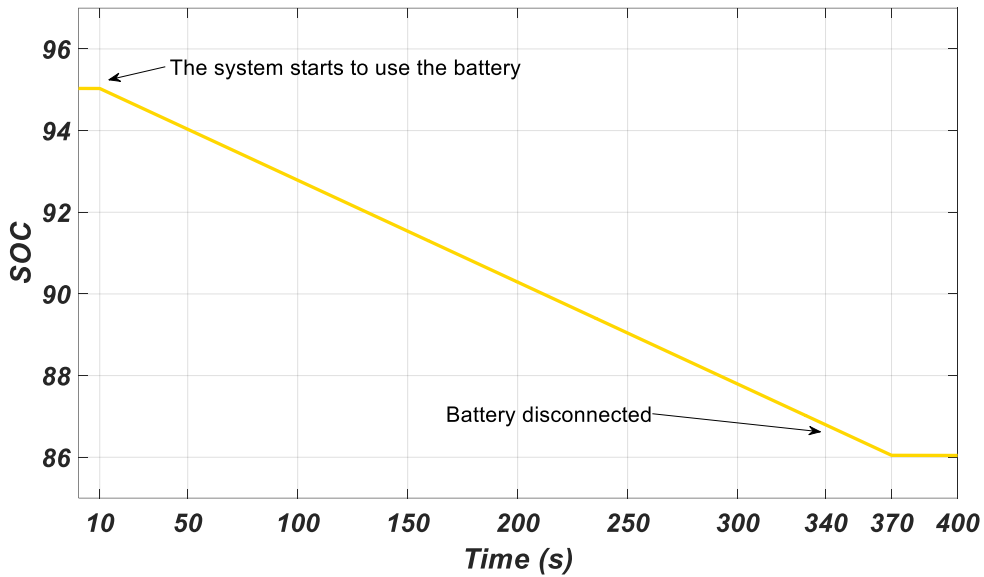


Fig. 7.12. Behaviour of the SOC during the scenario 1

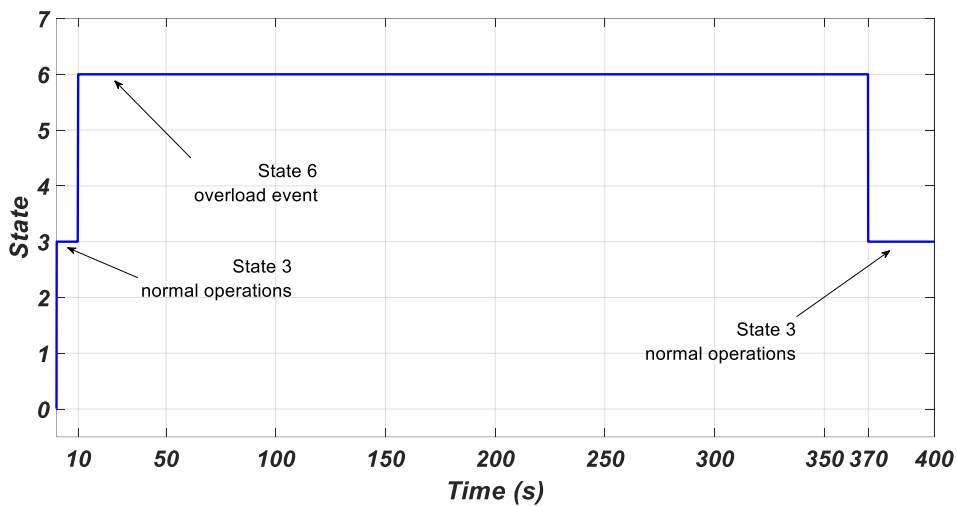


Fig. 7.13. STATE position of the system during the scenario 1

In Fig. 7.12 it is possible to see that the system started with 95% of the SOC, thus once an overload request arrived the system moved from the STATE 3 to the STATE 6 (Fig. 7.13), in accordance with Fig. 7.2, and TABLE 7.2.

In the scenario 1, the FSM was able to respect the rules provided in the TABLE 7.2 solving the overload request without pushing the generator behind its power rating. Moreover, the transitions between the STATES have been performed in a fast computational time (no transients are present in the plots), showing the capability of the FSM to manage the EPS.

Scenario 2:

In the scenario 2, the system will receive the same overload request as in the scenario 1, but the level of the SOC is low, thus the controller has the task to manage the variation of the loads without having help from the battery and try to charge the battery when the overloads are not present. Fig. 7.14 depicts the requested load power; initially the system is working at the rated condition, but the level of the SOC is low, thus the controller sheds 1kW of load in order to start charging the battery. At t=10s the system receives an overload request from the de-icing system (peak mode), the controller must stop the charging operation and apply the knapsack optimisation in order to avoid the overload of the generator.

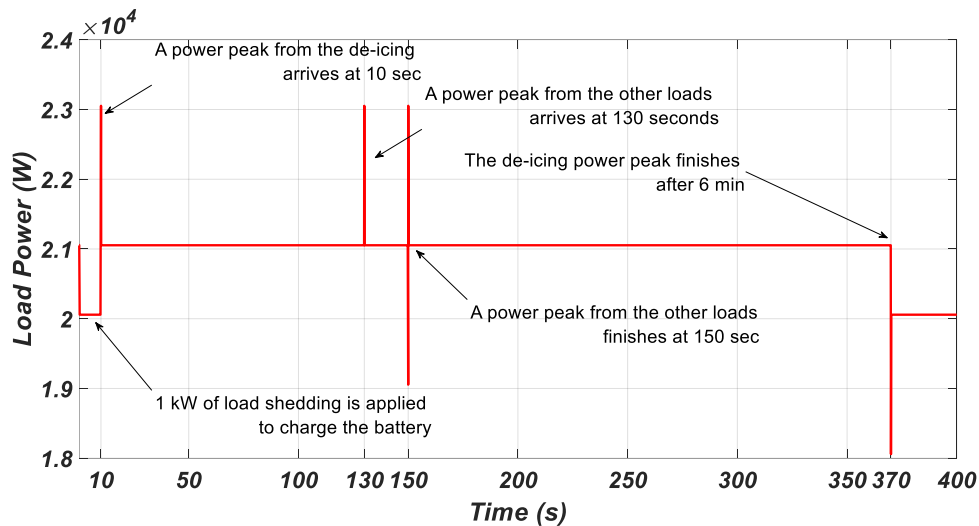


Fig. 7.14. Behaviour of the load power during the scenario 2

Referring to Fig. 7.14, a second overload request arrives at t=130s, in this case, the controller must apply the optimisation algorithm again aiming to shed more loads. In Fig. 7.15 the battery power characteristic is shown before the overload occurs, the battery is in charging operation at 1kW, and disconnected during the peak mode of the de-icing (6 mins).

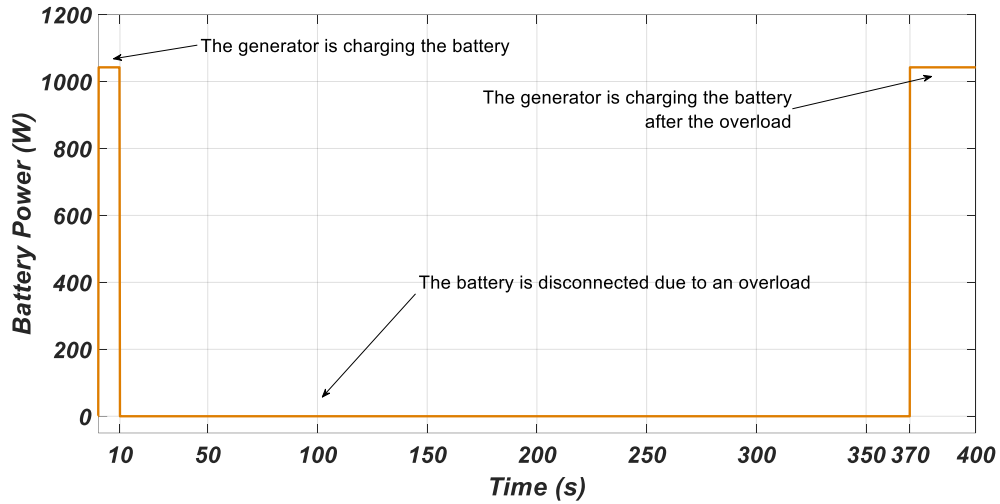


Fig. 7.15. Characteristic of the battery power

Fig. 7.16 shows the generator power during the scenario 2. As in case of the scenario 1, the controller is able to keep the power within a range of 21kW in much more complex scenario 2.

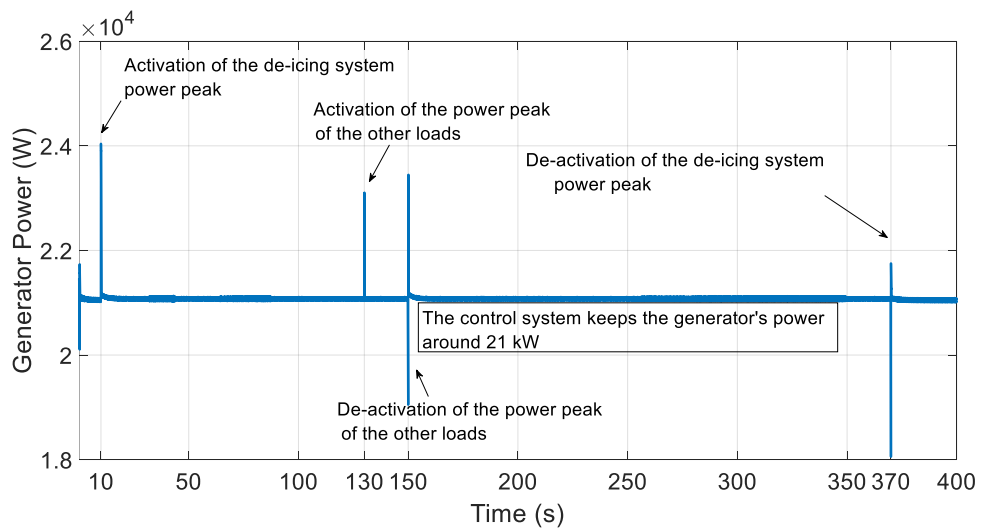


Fig. 7.16. Behaviour of the generator power during the scenario 2

According with the battery power characteristic, it's possible to see the SOC level during the simulation time in Fig. 7.17.

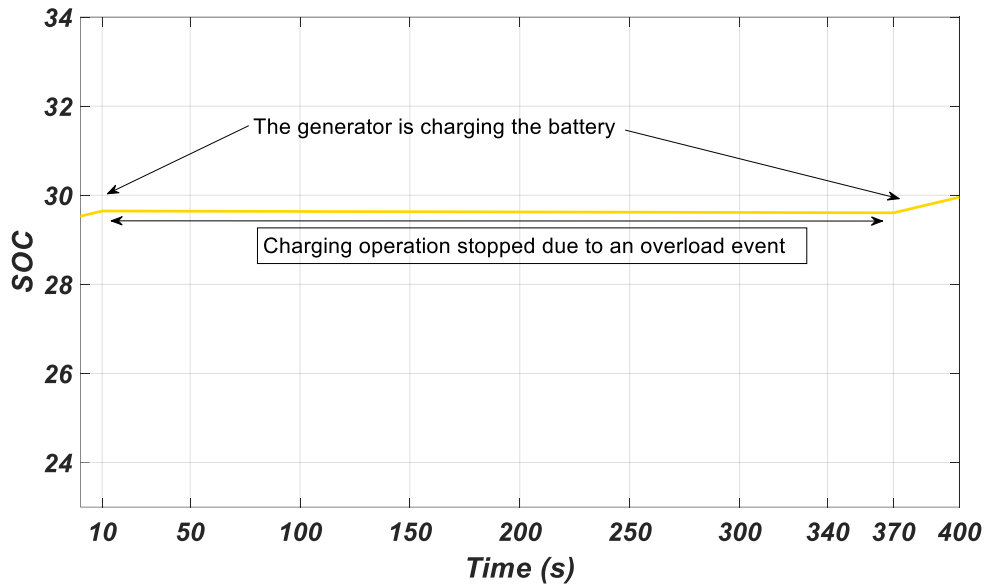


Fig. 7.17. SOC level during the charging and overload operations

In addition, Fig. 7.18 shows the operating state during all the simulation time, of note that at  $t=150s$  the system must apply the knapsack to recalculate the distribution of the power during the second overload passing from the STATE 1. As it is possible to see from the plot, it takes 0.2s for the re-calculation.

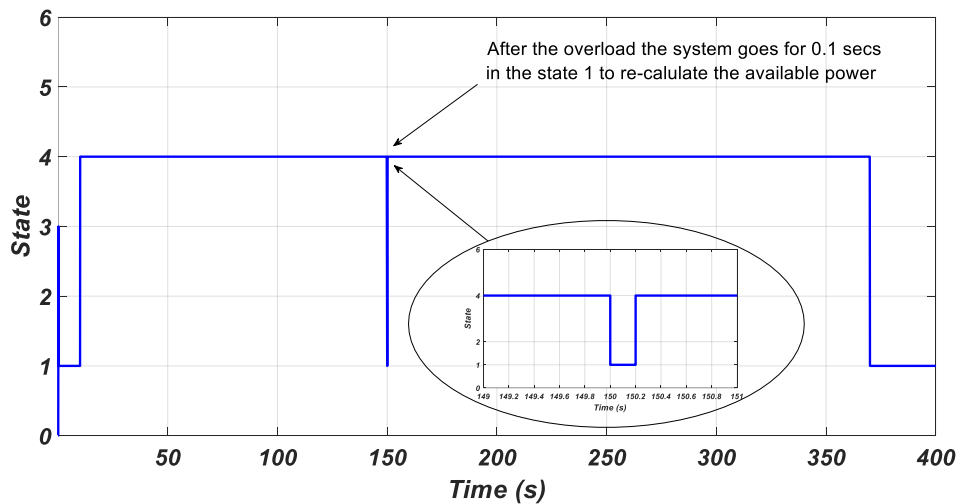


Fig. 7.18. STATE position of the system during the scenario 2

In the scenario 2, the FSM was able to respect the rules provided in the TABLE 7.2 solving the overload request, and with a low SOC level without pushing the generator behind its power rating. The scenario 2 is more critical due to the fact that the FSM cannot use the battery for covering the overload request. Thus, the knapsack optimization needs to be applied, forcing the FSM to solve a complex computing for re-distributing the power. Also, in this case, the transitions between the STATEs have been performed in a fast computational time (no transient are present in the plots), showing the capability of the FSM to manage the EPS under a critical scenario.

## **7.5 Conclusion**

This Chapter has reported case study scenarios that will be used for the experimental test in the laboratory. These simulations aim to demonstrate how the controller can apply the RCS method and the LAP for managing the different scenarios that could affect the EPS. The simulations have been divided into two parts. First, studying the behaviour of the SC and the EPS with a high level of the SOC. Second, the same scenario is proposed simulating a low level of the SOC. The simulation results demonstrated that the developed algorithm is in line with the thesis objectives, thus:

- The SC can manage the entire MEA EPS.
- Total automatization of the reconfiguration of the EPS based on the occurring scenario.
- The implemented algorithm is computationally inexpensive.
- Fast computational time even in case of complex computational operations

The key aim of the Chapter is to create a simulation model that matches the experimental results that will be performed in the next Chapter. As shown in the previous Chapters, the SC is able to correctly manage even more complex EPS, related to the one presented here, thus no problems were expected from the simulation side. However, this step has been necessary to create a model that can be imported into the experimental setup, in order to address the preliminary aspects of the EPS to be built, such as:

- Predicting and correct possible bugs that could affect the experimental scenario
- Analysing the behaviour of the system in the laboratory
- Defining the correct rules for the FSM that need to be transferred on the test bench

All the solutions have been realized in a short computational time. For the considered case, it has been used a small EPS in order to make it replicable in the laboratory. In the next Chapter will be presented the experimental bench that will be used to test the SC behaviour.



## **Chapter 8: Experimental rig and study case scenario**

---

### **8.1 Introduction**

This Chapter presents the experimental rig created for testing the proposed SC, and the FSM. A case study scenario used for performing the experimental tests is also presented. The platform aims to demonstrate the capability of the SC in applying the RCS and the LAP. The EPS considered for the test is shown in Fig. 8.1, it is scaled to 27V in order to operate at reduced power level verifying the developed control logic: since the test targets the SC operations, this approach can be adopted without affecting the final results. A simplified EPS topology has been chosen. The power to the rig is provided by a DC supply source, which feeds a DC Bus with 27V (1). The EPS loads are represented by a set of power resistors; they are conditionally divided into the levels of priority, from the highest to the lowest (1 to 8). The switches (3) are placed on a relay board and are used to interrupt the power to the loads. The bus is also connected to a 3-phase converter (4), which is used as bi-directional back-boost DC/DC converter (by using only one leg), to allow the power sharing between the Generator, representative loads, and the Battery. In order to emulate the behaviour of the battery, a Bi-directional DC power supply (5) has been used. A dSpace board RS1104 (6) is employed to deploy the designed FSM code, as well as manage communication between the converter, the switches, and the sensors.

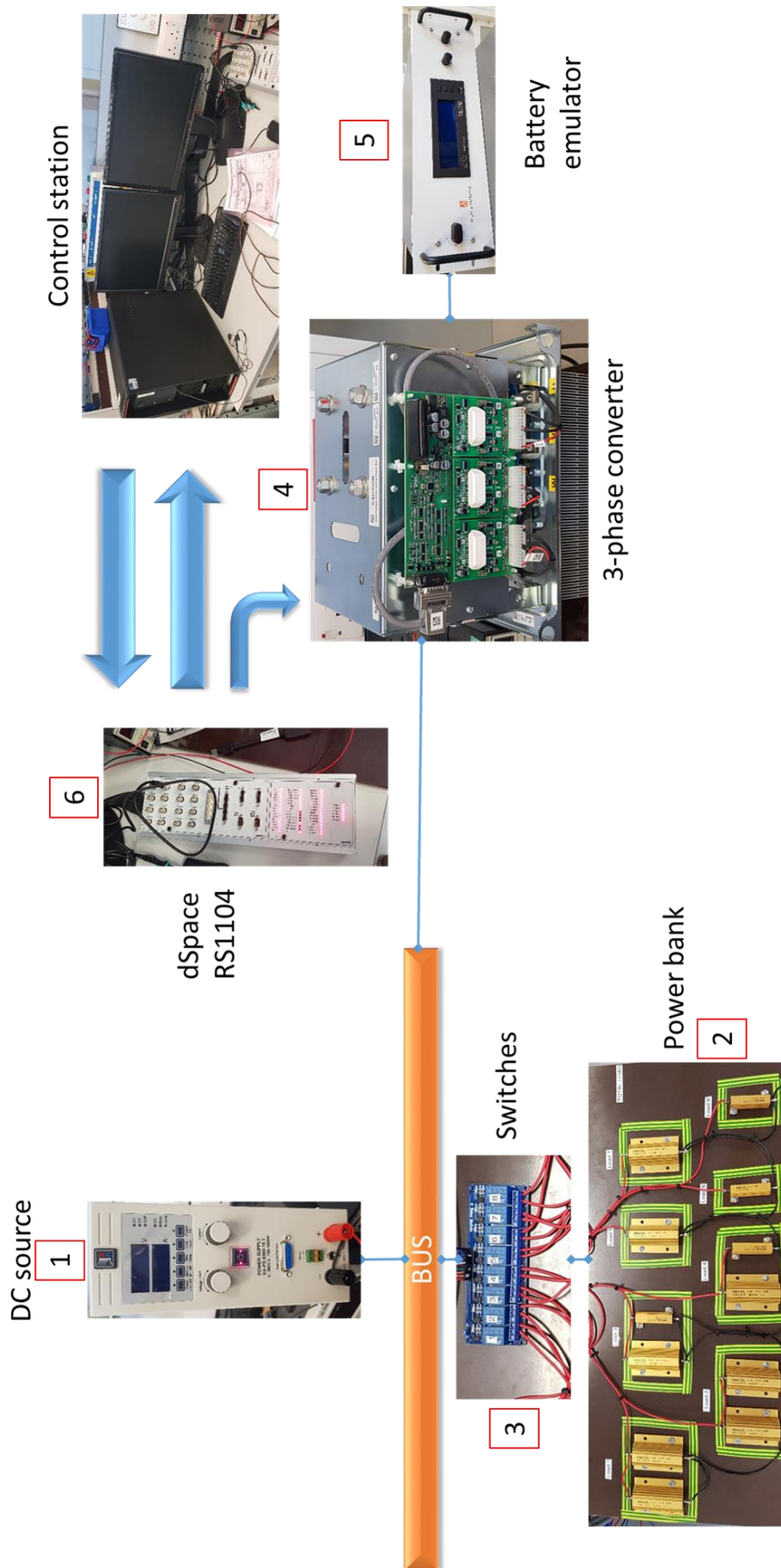


Fig. 8.1. scheme of the EPS used for the experimental test

## **8.2 Description of the components**

In this section all the components used for assembling the rig are presented in detail.

### *1 - DC power supply*

A DC power supply, in Fig. 8.2, has been used to emulate the DC power source. As the experiments will deal with the scaled EPS, the source provides 27V DC to the Bus and is set to deliver maximum 180W (without considering the losses). In the experimental test the DC power supply unit is set as constant voltage source.



Fig. 8.2. DC power supply used to obtain a constant DC voltage on the Bus

### *2 - DC load sets*

A set of power resistors has been assembled in order to emulate the loads on the DC Bus, each load is divided based on priority levels and the required power. Fig. 8.3 shows the set of power resistors used in the test rig. The circuit diagram will be presented in the section 8.4.

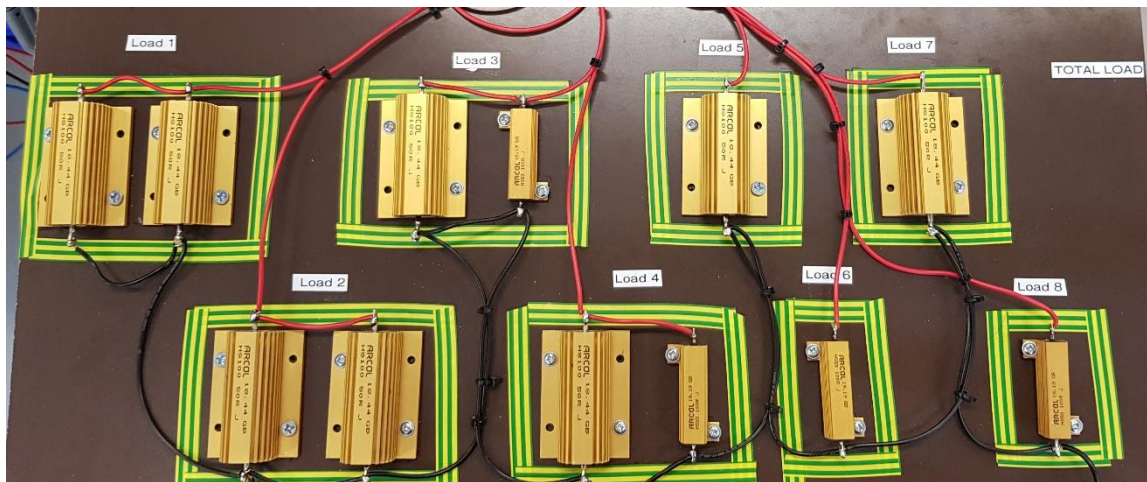


Fig. 8.3. DC loads created with a power resistors. The loads are labelled in order of priority from load 1 (highest) to load 8 (lowest)

### 3 - DC load switches

Fig. 8.4 shows the switches module board used to connect or disconnect the EPS emulator loads. The control logic will operate on the switches states in order to re-distribute the power.



Fig. 8.4. Switches module board used to connect or disconnect a load from the DC Bus

The switches are controlled through the digital input/output of the dSpace.

*4 - Power electronics converter*

In Fig. 8.5 the model of the power converter, Semikrone – Semikube, which has been used to control the power flow between the battery and the DC Bus is shown.

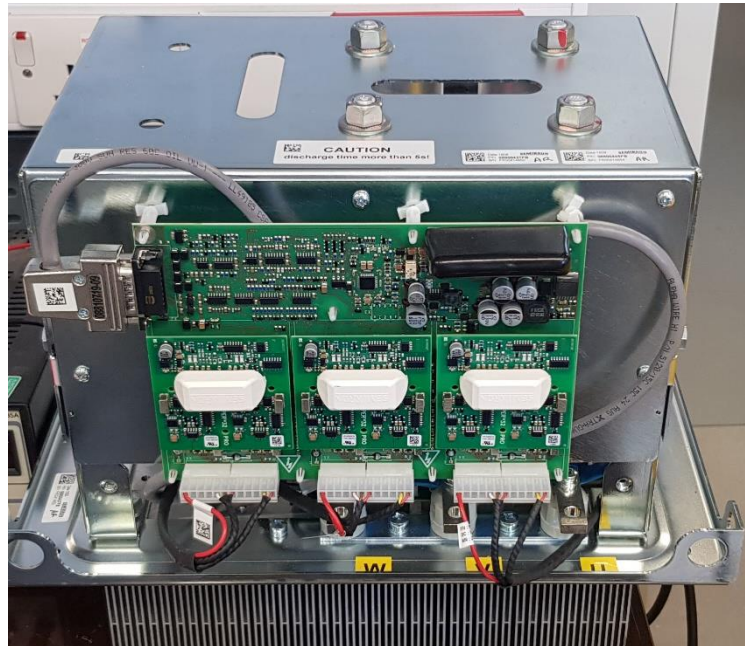


Fig. 8.5. 3-phase inverter used as back-boost DC\DC converter

The Semikube® is a three-phase, 3kW inverter and it will be used in buck-boost mode. In order to allow buck-boost operations for DC circuits, only one leg is used and controlled by PWM, which is generated from the dSpace.

*5 - Bi-directional supplier*

A bi-directional DC supply unit shown in Fig. 8.6 has been used to emulate the battery operations, input and output power, while the battery SOC is emulated inside the Simulink® environment. The unit is connected to the converter. The source is set to 16.5V/1Ah of capacity.



Fig. 8.6. DC\DC bi-directional supplier used to emulate the battery behaviour

### 6 - dSpace control board

The dSpace control Board Fig. 8.7A and the dSpace connection board RS1104 in Fig. 8.7b has been used to control the EPS emulation platform.



(a)



(b)

Fig. 8.7(a-b). dSpace control board (a) and RS1104 board (b) used to control EPS.

The control board implements the control algorithm developed in Simulink®, while the connection board sends the control signal to the inverter and switches, and receives the information from the sensors.

The components presented above are used to assemble the platform, and a scheme of the system is shown in Fig. 8.1.

### **8.3 Sensors and additional devices**

In this section will be explained the additional devices used to complete the rig

#### *Current and voltage sensors*

Current and voltage sensors have been built and calibrated in order to acquire data from the EPS emulator. The sensor boards are shown in Fig. 8.8 and Fig. 8.9.

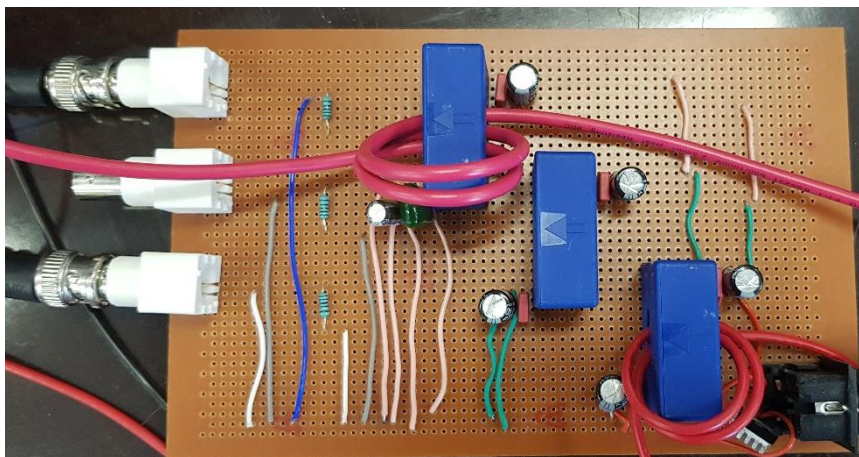


Fig. 8.8. Current sensor used to measure the battery and the BUS current

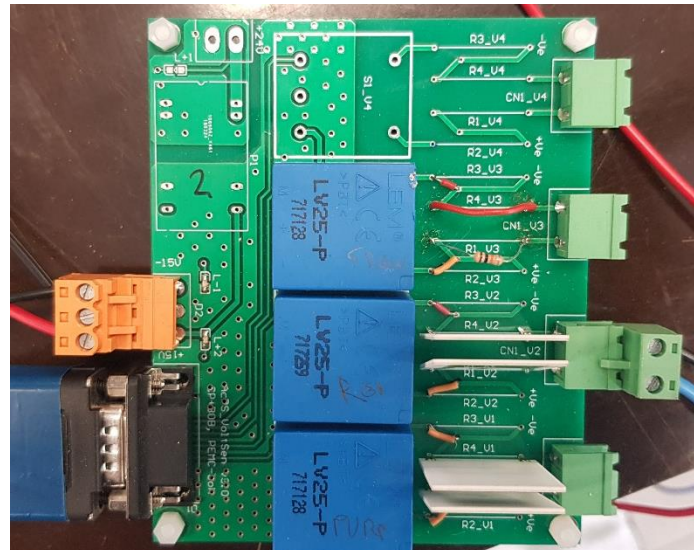


Fig. 8.9. Voltage sensor used to measure the battery voltage

For the measurement the selected components are:

- LEM LA 55-P current sensor



Fig. 8.10. Voltage sensor used to measure the battery voltage

- LEM LV25-P voltage sensor



Fig. 8.11. Voltage sensor used to measure the battery voltage



*Electro-optical converter*

In order to implement electrical insulation between the control board and the Inverter, the optical fibre communications are used. The PWM control signal is converted in optical signal by the use of the customised board in Fig. 8.12.

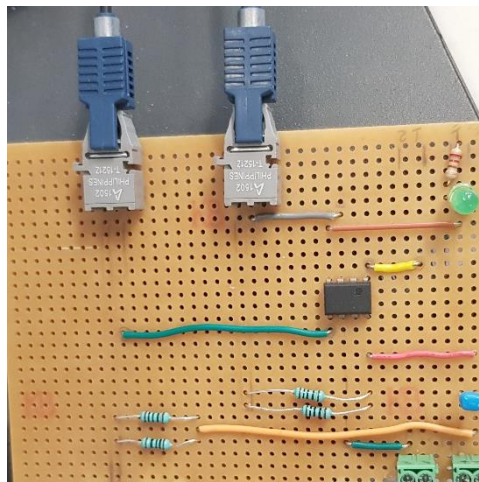


Fig. 8.12. Electro-optical converter used to send PWM to the converter

The electro-optical converter has been made using of the following main components:

- Broadcom AFBR-1624Z, 50MBd Fibre Optic Transmitter 685Nm



Fig. 8.13. Electro-optical converter used to send PWM to the converter

- Circuit driver IC SN75451BP

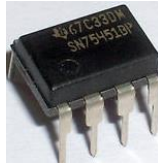


Fig. 8.14. Electro-optical converter circuit driver used to send PWM to the converter

### 8.4 Experimental case scenario

In this section, the experimental test on the assembled EPS platform will be presented. First, a single line diagram of the EPS will be given. Second, the study case of Chapter 7 will be emulated for demonstrating the FSM capability in the application of the RCS and the LAP.

As explained in the previous sections, the platform has been scaled in power and voltage compared with the model simulated in Chapter 7. However, this will not affect the method and behaviour of the SC, as well as the development of the algorithms. In Fig. 8.15 the single-line diagram of the regarding EPS is shown, while TABLE 8.1 presents the value of each component used for the experimental test.

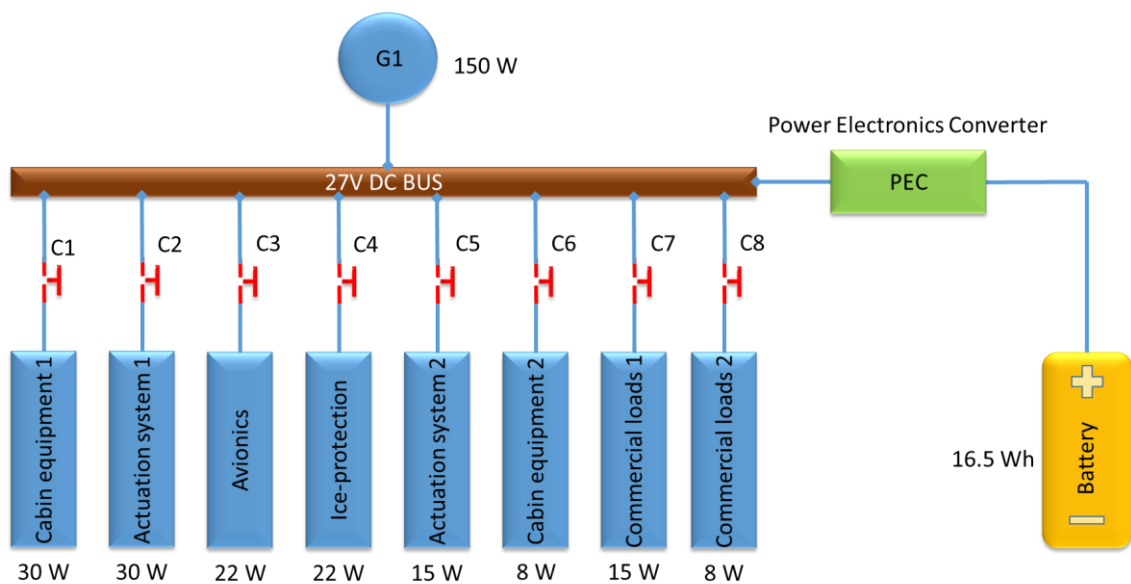


Fig. 8.15. Single-line diagram of the applied EPS for the experimental study case

TABLE 8.1. EPS loads considered for the presented EPS

Loads power during cruise flight stage in normal and peak icing conditions					
	Loads (experimental platform)	Normal Condition(W)	Peak Conditions (W)	Sheddable - through the Knapsack method	Priority Level
1	Commercial load1 / Commercial load 2	23	5	8	Low / Low
2	Ice Protection System - Nominal	22	0	0	High
3	Ice Protection Add. System - Peak	<b>0</b>	<b>15</b>	0	High (on request)
4	Avionics	22	0	0	High
5	Cabin Equipment1	30	5	0	High
6	Cabin Equipment2	8	0	8	Medium
7	Actuation system 1	30	0	0	High
8	Actuation system 2	15	5	0	Medium
Total Load (PL)		150	<b>180</b>	<b>30</b>	

A scaled generator (G1) is capable to supply a total load of 150W (rated conditions), which includes the de-icing system during the more prevalent normal icing conditions. During peak icing conditions an additional 15W of power to the Ice-protection system is required, as well as additional 5W required from the commercial loads, cabin equipment 1, and the actuation system 2. These can be provided by the battery in combination with load shedding decisions made by using the knapsack method developed in Chapter 5. Implementing the presented energy management strategy, the generator’s rated power can be kept to 150W instead of 180W. The EPS will be controlled by acting on two main variables, the requested power of the loads (PL) and the state of charge (SOC) of the battery. In Fig. 8.16 is presented the flow-chart of the STATES with the conditions for the transition, while TABLE 8.2 presents the EPS STATES and the conditions for the transitions. These are based on the battery SOC (high, medium, low), and the PL (< 150W or > 150W).

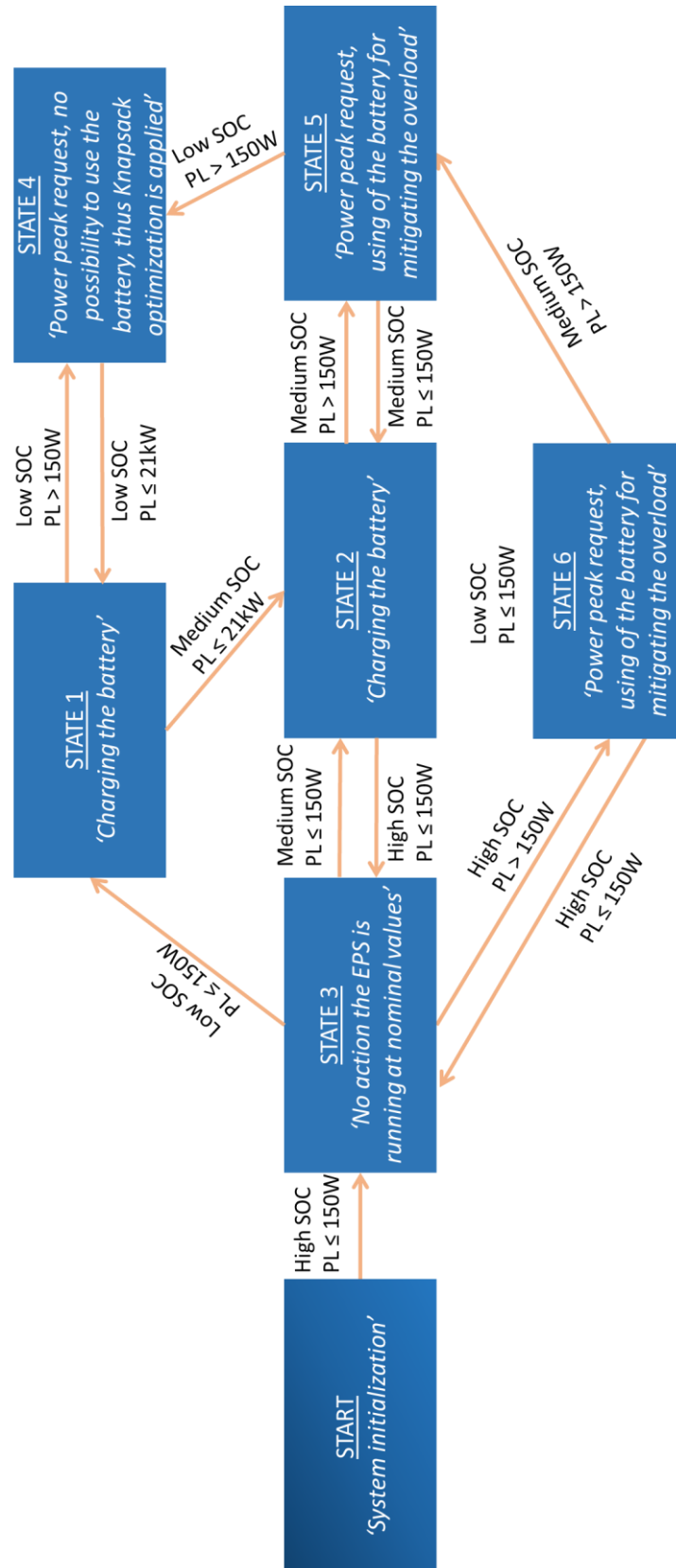


Fig. 8.16. Flowchart of the FSM available STATES for the experimental scenario

TABLE 8.2. State table used to define the SC behaviour

SOC/PL	PL ≤ 150W	PL > 150W
<b>SOC &lt; 30%</b>	<p>STATE 1: Battery discharged</p> <ul style="list-style-type: none"> <li>- Charging battery  <math>P_{batt} = P_{gen} - PL \rightarrow P_{bat}</math> positive, charging operation  <u>Disconnect the load with the lowest priority level in order to do not overload the generator during the charging scenario</u></li> <li>- If SOC &gt; 30 %, goto STATE 2</li> <li>- If PL &gt; 150W, goto STATE 4</li> </ul>	<p>STATE 4: Battery discharge + Overload                      Overload with low level of SOC</p> <ul style="list-style-type: none"> <li>- Overload with low level of SOC                      Apply <b>knapsack method</b> to shed load:  <u>In order to avoid generator's overload, when the battery is discharged the Knapsack method needs to be applied, disconnecting the loads with the lowest priority (see TABLE 7.1)</u></li> <li>- If PL ≤ 150W, goto STATE 1</li> </ul>
<b>30% ≤ SOC ≤ 90%</b>	<p>STATE2: Battery with medium charge</p> <ul style="list-style-type: none"> <li>- Charging battery with  <math>P_{batt} = P_{gen} - PL \rightarrow P_{batt}</math> positive, charging operation  <u>Disconnect the load with the lowest priority level in order to do not overload the generator during the charging scenario</u></li> <li>- If SOC &gt; 90% goto STATE 3</li> <li>- If PL &gt; 150W, goto STATE 5</li> </ul>	<p>STATE 5: Battery with medium charge + overload                      Peak condition with acceptable level of the SOC</p> <ul style="list-style-type: none"> <li>- Peak condition with acceptable level of the SOC</li> <li>- <math>P_{batt} = P_{gen} - PL \rightarrow P_{batt}</math> negative, discharging operation:  <u>The battery is providing power</u></li> <li>- If <math>P_{batt} \leq 15W</math>  <u>Battery supplies power within its acceptable rating</u>  <math>P_{batt} = P_{gen} - PL</math></li> <li>- If <math>P_{batt} &gt; 16W</math>  <u>The battery delivered power is fixed to 16W (i) (Battery discharge rating power)</u>  <u>The Knapsack method is applied to avoid generator's overloads (ii)</u>                      (i) <math>P_{batt} = 16W</math>                      (ii) and apply <b>knapsack method</b> to identify and shed load by (PL - 16W)</li> <li>- If SOC &lt; 30% goto STATE 4</li> <li>- If PL ≤ 150W goto STATE 2</li> </ul>
<b>SOC &gt; 90%</b>	<p>STATE 3: Normal conditions</p> <p>No action:  <u>The generator is able satisfy the power request</u></p> <ul style="list-style-type: none"> <li>- If PL &gt; 150W, goto STATE 6</li> </ul>	<p>STATE 6: Battery fully charged + overload                      Peak condition, battery fully charged                      Peak condition, battery fully charged</p> <ul style="list-style-type: none"> <li>- <math>P_{batt} = P_{gen} - PL \rightarrow P_{batt}</math> negative, discharging operation:  <u>The battery is providing power</u></li> <li>- If <math>P_{batt} \leq 15W</math>  <u>Battery supplies power within its acceptable rating</u>  <math>P_{batt} = P_{gen} - PL</math></li> <li>- If <math>P_{batt} &gt; 16W</math>  <u>The battery delivered power is fixed to 16W (i) (Battery discharge rating power)</u>  <u>The Knapsack method is applied to avoid generator's overloads (ii)</u>                      (i) <math>P_{batt} = 16W</math>                      (ii) and apply <b>knapsack method</b> to identify and shed load by (PL - 16W)</li> <li>- If SOC ≤ 90% goto STATE 5</li> <li>- If PL ≤ 150 W goto STATE 3</li> </ul>

TABLE 8.2 includes 6 STATES, which are made to set-up the system during peak conditions (overloads) by applying reconfiguration and load allocation strategy. The variable  $P_{batt}$  defines the amount and direction of the power flowing through the battery. In each STATE, the value of  $P_{batt}$  is calculated considering the requested power of the load  $P_L$  and the delivered power from the generator  $P_{gen}$ . If the power request is higher than the battery capacity, the system will apply the knapsack optimisation discussed in Chapter 5.

### 8.4.1 FSM description for the EPS emulator

The FSM model is used to develop the algorithm presented in TABLE 8.14. In order to control of the system, the FSM will compute the SOC,  $P_{gen}$ , and  $P_L$  as input variables and will give as outputs the status of the switches,  $C_1$  to  $C_8$ , and the value of  $P_{batt}$ . In Fig. 8.17 is shown the FSM block:

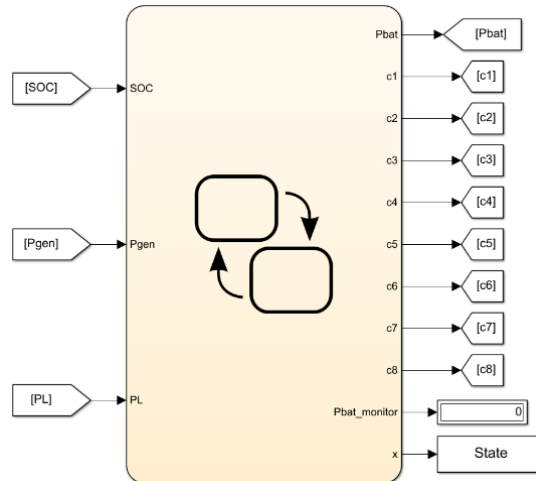


Fig. 8.17. Input and output variables of the FSM

The initialization of the system and the rating operations of the EPS, already presented in Chapter 7, are shown in Fig. 8.18, the 'Start' STATE and the STATE 3.

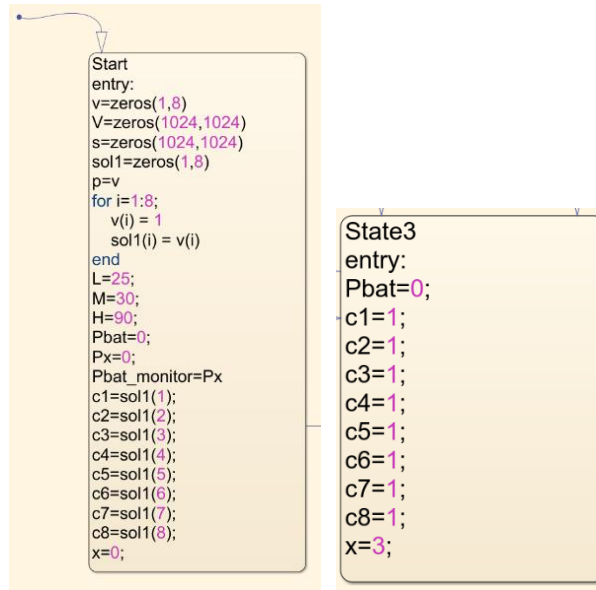


Fig. 8.18. Initialization STATE of the system and STATE 3 (normal conditions of the EPS)

the 'Start' STATE is used to set the system variables, the matrix  $v$ ,  $V$ , and  $s$  are used to calculate the solution for the knapsack problem and are set to zero (as already explained in the Chapter 7), while the variable  $x$ , which is present in all the STATES is used to take a record of the operating STATE. The variable  $sol1$  is used to store the knapsack solution that will act on the switches, it is set to '1' (switches closed/all the loads active) in the 'Start' STATE. The variables  $L$ ,  $M$ ,  $H$  refer to the SOC of the battery (low, medium, high).  $P_{bat}$  is used to store the value of the calculated power delivered or absorbed to the battery,  $P_x$  and  $P_{bat\_monitor}$  is used to check the value of  $P_{bat}$ . The variables  $C_1$  to  $C_8$  are used to set the status of the switches and the variable  $x$  is used to take record of the system status. Once all the system variables are initialized the system goes into the STATE 3. The following is considered as scenario' initial conditions: the SOC at high level (battery charged), the rated power request (150 W nominal conditions) and the battery disconnected. Assuming the aircraft is in cruise operation and neglecting faulty scenarios, the system could go in the following STATES (referring to TABLE 8.1 and 8.2):

- Overload due to the activation of the de-icing system
- Overload due to peak conditions of the loads



- Overload due to the combination of the activation of the de-icing system and load peak conditions

In addition, the SC must consider the SOC status during the mentioned scenarios above. From TABLE 8.2 it is possible to see 6 states, but the behaviour of the system can be condensed in 4 STATES, since the STATE 6 and the STATE 5 are similar, as well as the STATE 1 and STATE 2, in which the only difference is a lower level of the SOC. Thus, in the experiment 2 main scenarios are considered: a peak request of the de-icing system and/or a peak request from the other loads with a high level of the SOC and with the low level of the SOC. In Fig. 8.19 the FSM code during the overload scenario when the SOC is high is depicted.

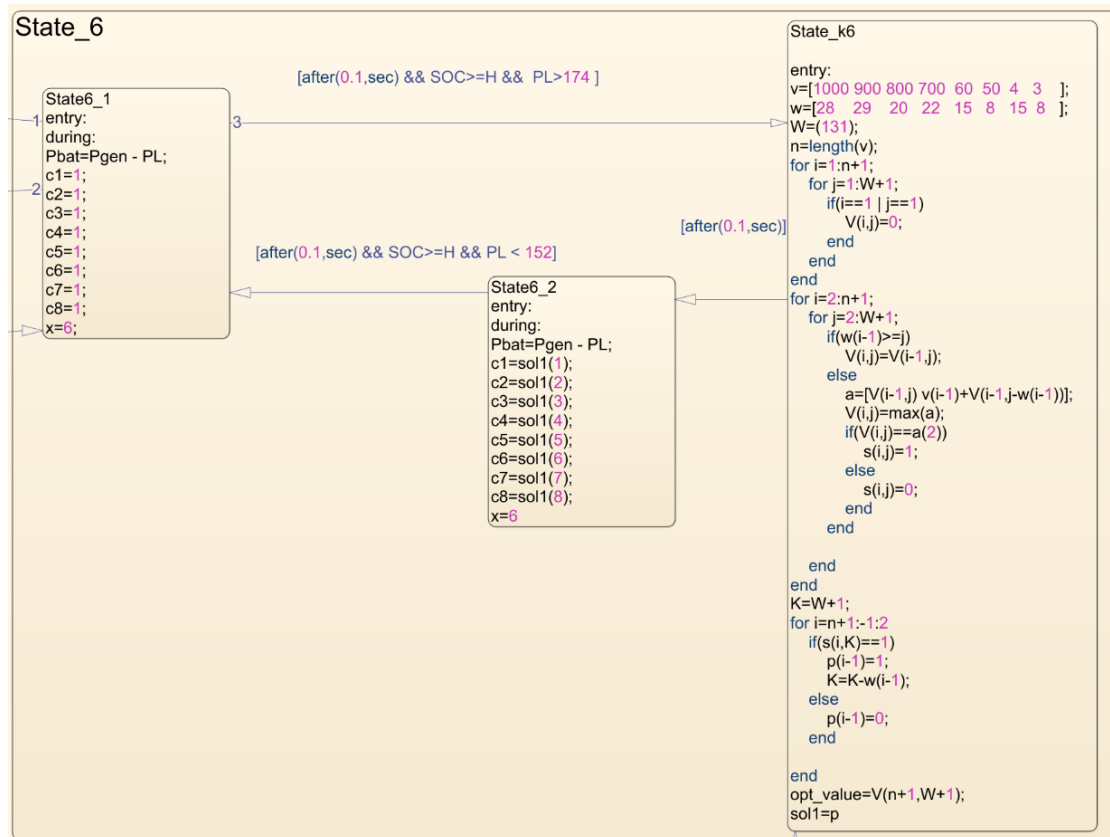


Fig. 8.19. STATE 6 of the system, it reduces the generator's overload using the battery or the knapsack optimisation

In the STATE 6.1 the extra power requested from the loads is within a range of 15W, so the battery can help the generator: the power that is to be delivered by the battery is calculated and stored in the variable  $P_{bat}$ . If the power request is greater than 15W the battery power

will be re-calculated, while the additional power request will be mitigated using the knapsack optimisation algorithm (in the STATE k6) and passing into the state 6.2. Applying the presented algorithm, the system can maintain the generator's power within 150W. Fig. 8.20 and Fig. 8.21 present the FSM code during rated conditions of the load (150W) with a low level of the SOC (STATE 1) and peak conditions of the de-icing system and/or the peak condition of the other loads with a low level of the SOC (STATE 4).

```
State1
entry:
during:
Px=Pgen - PL;
Pbat=Px;
Pbat_monitor=Px
c1=1;
c2=1;
c3=1;
c4=1;
c5=1;
c6=1;
c7=1;
c8=0;
x=1;
```

Fig. 8.20. STATE 1, battery charging operations

In the STATE 1 the battery is in charging operation, disconnecting the load 8 (refer to Fig. 8.20), which is the one with the lowest priority level. Fig. 8.21 shows the code used to cover the scenario in which a load power peak arrives during charging operations (STATE 4).

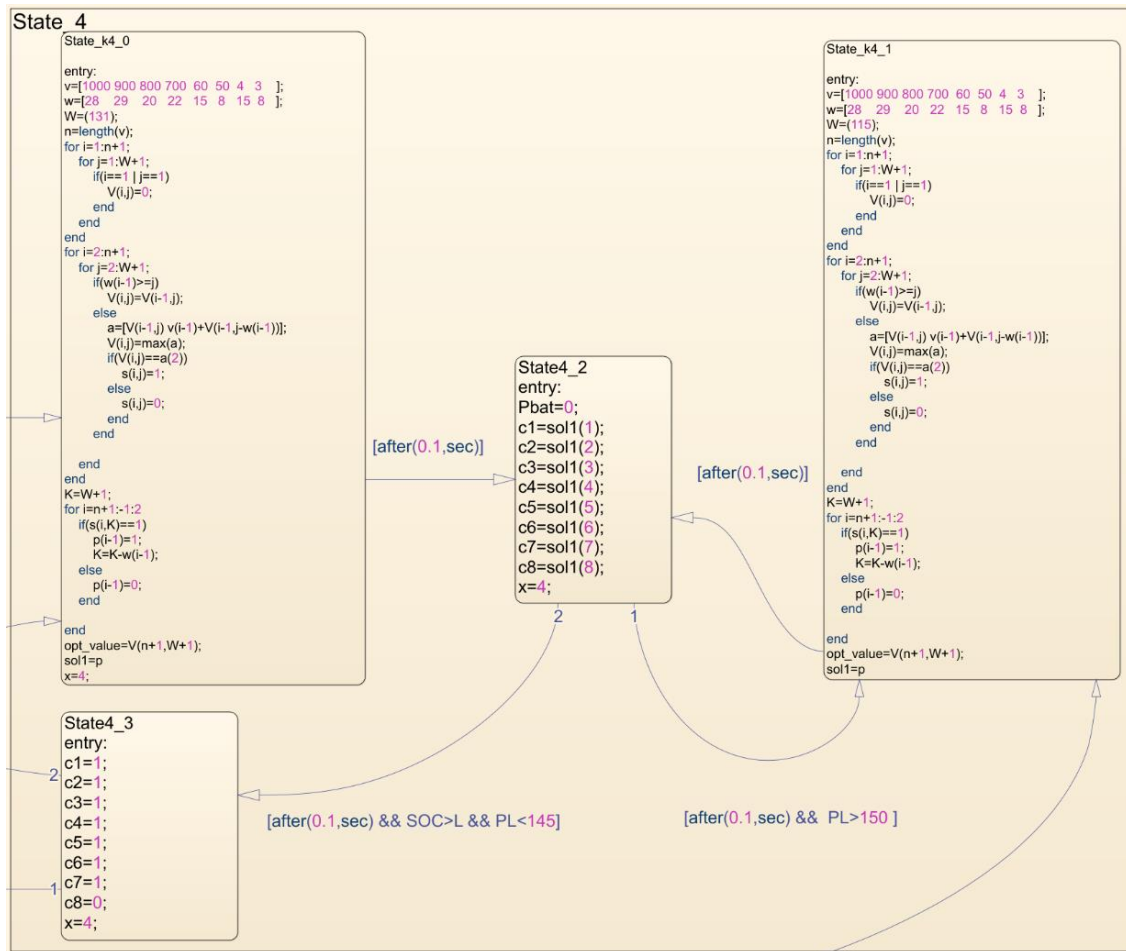


Fig. 8.21. STATE 4, overload scenario during low level of the SOC

If an overload occurs and the battery is discharged, the system goes into the STATE 4 where the charging operation is stopped, and the knapsack optimization (STATE K4.0 and STATE K4.1). The algorithm inside the states has been explained in the Chapter 5) and is applied in order to avoid the generator’s overload. If a second overload request occurs, the system will move in the STATE 4.2 to recalculate the distribution of the power and keep the de-icing system active. In the next section presented FSM will be tested through simulations.

## **8.4.2 Experimental results**

This section reports the experimental results for the described study case. It is divided in two different scenarios in order to show the operation with low SOC and with a high SOC with different power requests from the loads. In the first scenario the EPS is working at rated conditions with high level of the SOC. After 10s the system activates the ice-protection with a consequent increase of the requested power, in which, as already discussed in the Chapter 7, the worst-case scenario is represented from 6 minutes of ice-protection peak. Furthermore, a peak power request from the other loads occurs during the ice-protection peak operation, in order to test the SC operation during multiple events. Moreover, in this experiment, the system must also take into account the voltage drops due to the non-ideal resistance of the components (wire, switches, etc..), thus the power will be slightly smaller than the reference values.

### Scenario 1:

Fig. 8.22 shows the behaviour of the overall load power during the first scenario. For the first 10s the system is working at rated conditions (145W considering the losses), when the de-icing system starts to request the peak power the total load request rises from 145W to 159W, and the system moves to STATE6 (overload with high level of SOC). At the second 130 the system receives another extra power request from other loads (refer to TABLE 8.1); thus, the knapsack method is applied to reduce the power request from 174W to 159W by shedding 16W from the load 8 (Commercial load 2) and load 6 (Cabin equipment 2). Following the state diagram presented in Fig. 8.15, the SC has to enable the battery to provide the power to cope with the extra demanded power from the de-icing system. While, when another power request arrives, the SC must use the knapsack optimization for avoiding the overload, which is obtained by shedding 16W.

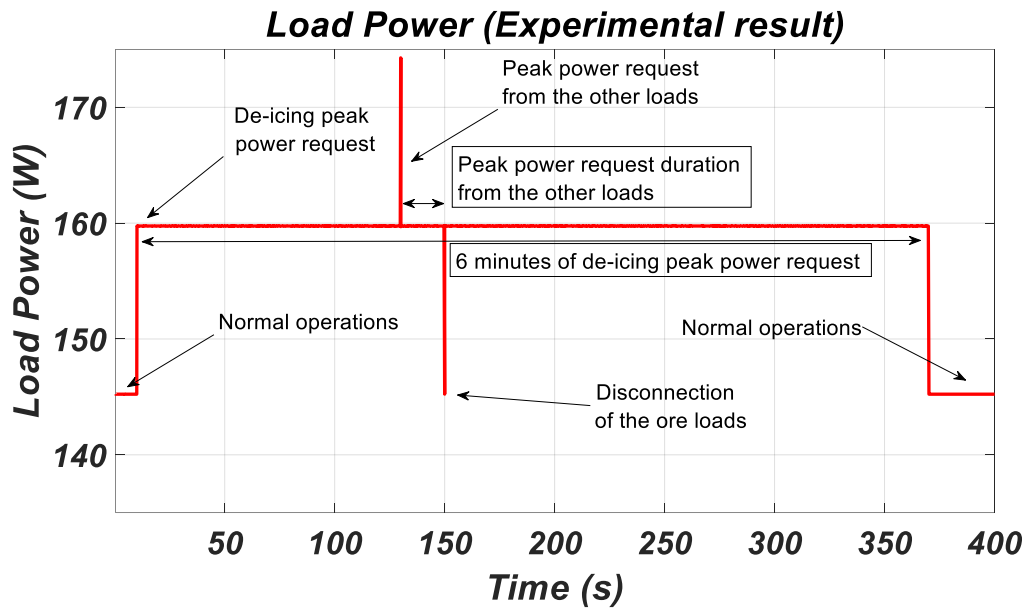


Fig. 8.22. Behaviour of the load power during different overload operations (scenario 1)

In Fig. 8.23 it's possible to see that at  $t=10s$  the system starts to use the battery in order to cope with the overload request. The drained power from the battery is calculated by the SC and it's around 16W (average value). From the plots of the load power and battery power, it's also possible to see the fast response of the SC in changing the system STATE. Even in the case of the application of the knapsack method, the SC is fast enough (few milliseconds) to find the right sequence of the loads that need to be disconnected for avoiding the overload.

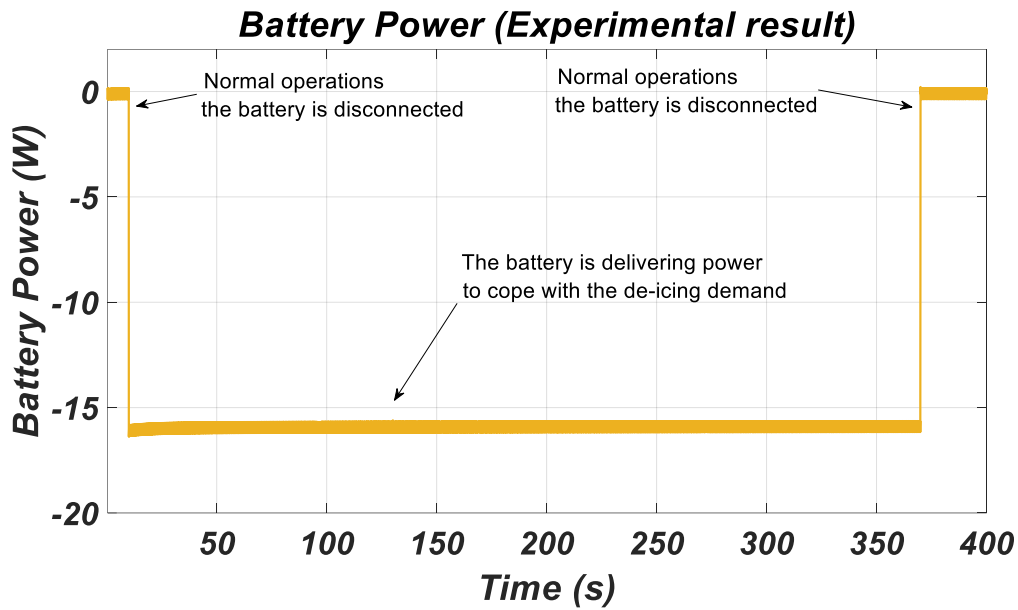


Fig. 8.23. Behaviour of the battery power during overload operation (scenario 1)

From sec 130 to 150, the system receives another overload request from the other loads, although, for these experimental tests, the battery is not able to provide more than 16W; thus, the delivered power is set to 16W and the knapsack optimization is applied in order to shed the additional 16W of power request. In Fig. 8.24 is shown the behaviour of the generator power, it can be remarked how the control system keeps the delivered power around 145W.

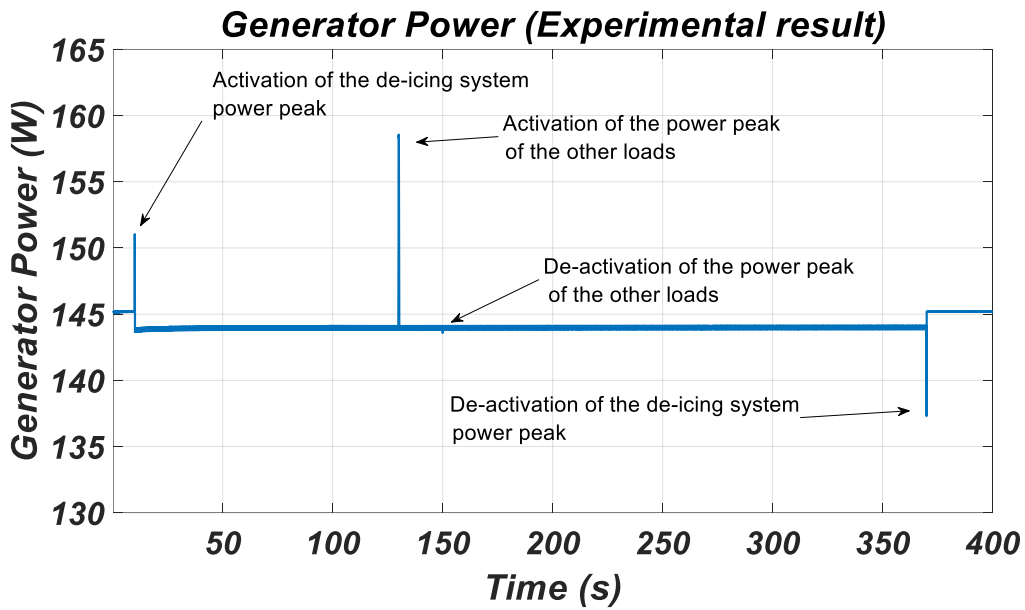


Fig. 8.24. Behaviour of the generator power during different loading conditions

The SOC of the battery is shown in Fig. 8.25, it shows how the battery is discharged during the overload scenario.

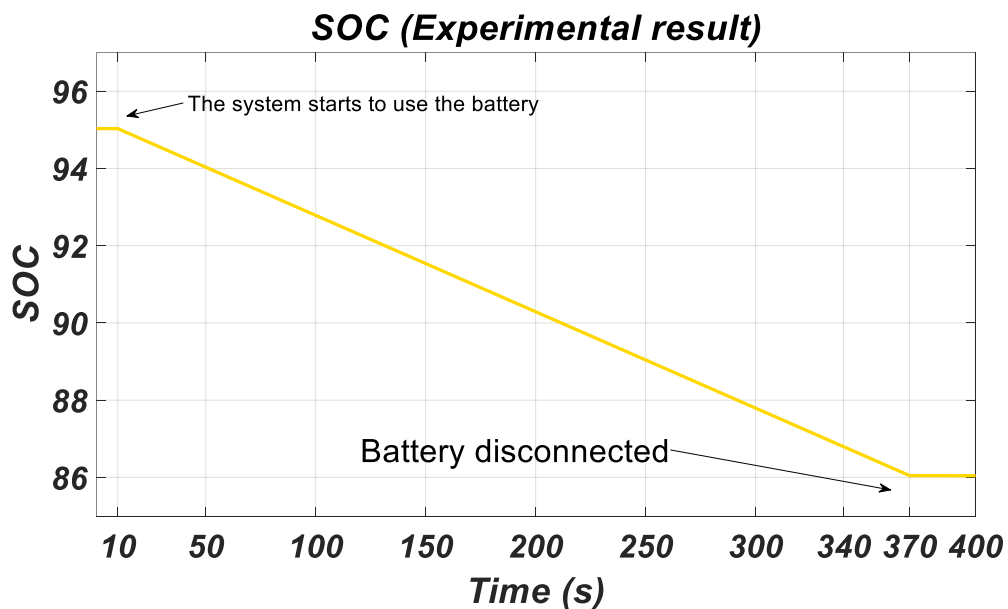


Fig. 8.25. Behaviour of the SOC during the scenario 1

In order to confirm the behaviour of the SC, Fig. 8.26 shows the system STATES during the scenario 1. Of note that the SC capabilities during the scenario, it can be observed how all the transitions from one STATE to another are processing with an almost no delay on the actions on the EPS.

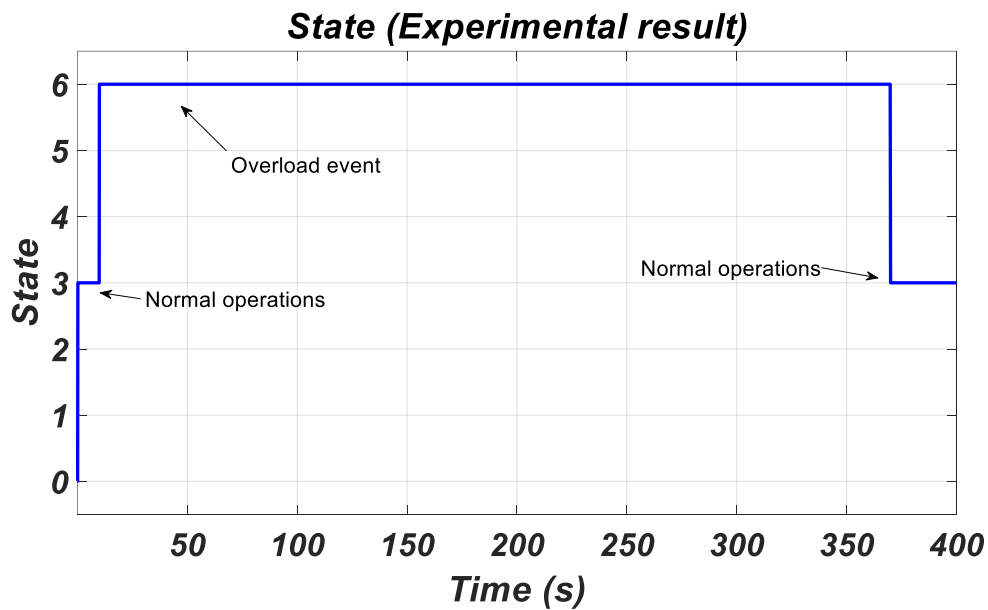


Fig. 8.26. STATE position of the system during the scenario 1

The first scenario presented a situation in which the EPS must deal with multiple overload requests. In this case, the SC must work by monitoring the EPS status in real-time and be able to change the system configuration by adapting the power levels and re-distributing the loads. From the presented plots the SC successfully covered scenario 1, following all the predicted steps of the FSM algorithm.



Scenario 2:

In Scenario 2, the system will receive the same overload request as the scenario 1, but the level of the SOC is low, thus the SC has the task to manage the variation of the loads without having help from the battery and try to charge the battery when the overloads are not present. In the Fig. 8.27 is shown the requested load power, initially the system is working at rated condition, but the level of the SOC is low, thus the SC sheds 8W of load (Load 8 - Commercial load 2) in order to start charging the battery. At the  $t=10s$  the system receives an overload request from the de-icing system (peak mode, 15W), the SC must stop the charging operation and apply the knapsack optimisation in order to avoid the overload of the generator.

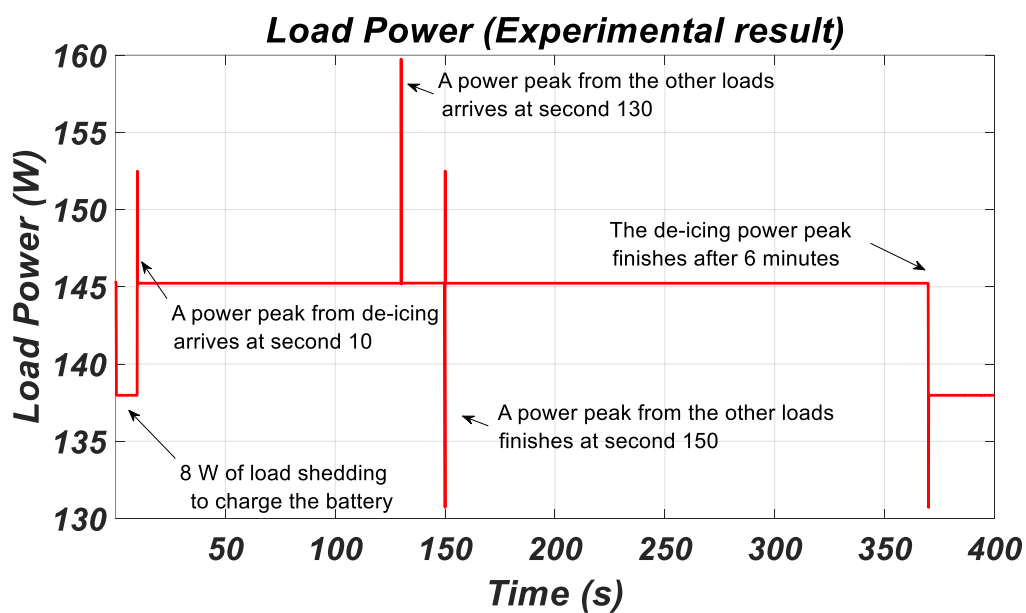


Fig. 8.27. Behaviour of the load power during the scenario

Referring to Fig. 8.27, a second overload request arrives at  $t=130s$ , in this case the SC must compute the optimisation algorithm again applying the knapsack and shedding more loads. Fig. 8.28 shows the battery power characteristic before the overload occurs, then when the battery is in charging operation at 8W, and when disconnected during the peak mode of the de-icing (after 6 mins, or at  $t=360s$ ).

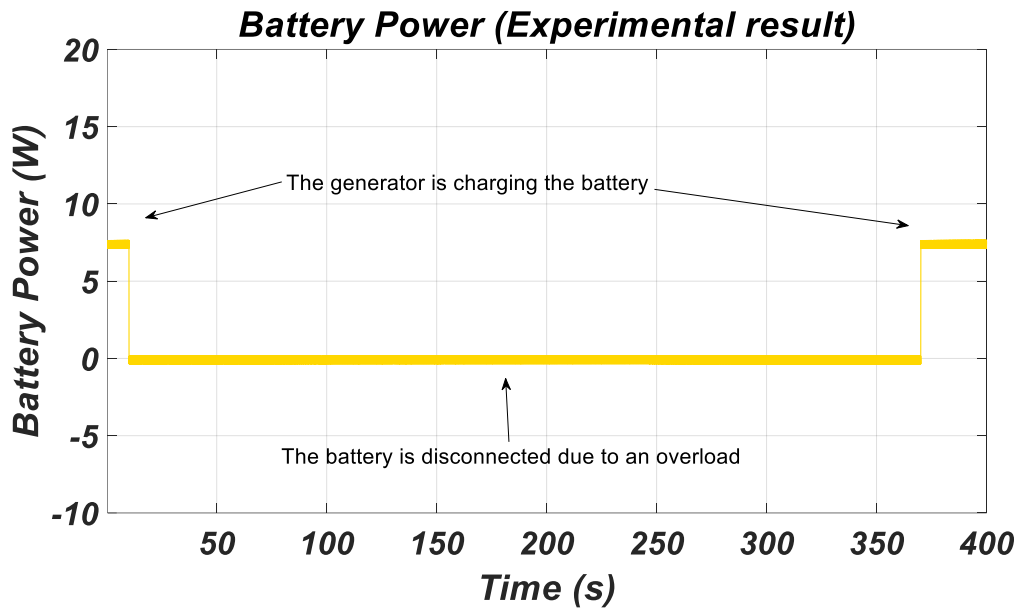


Fig. 8.28. Characteristic of the battery power

Fig. 8.29 reports the generator power during the scenario 2: similar to the scenario 1, the SC is able to keep the power within a range of 145W.

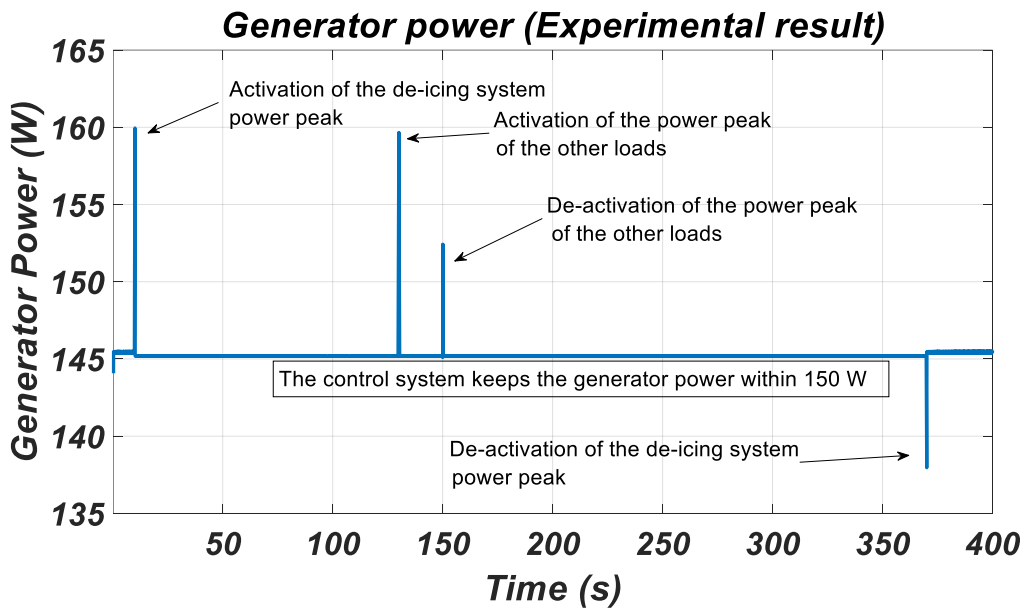


Fig. 8.29. Behaviour of the generator power during the scenario 2

It's possible to see the SOC level during the simulation time in Fig. 8.30, from which it is possible to see how the battery has been charged for a short period of time.

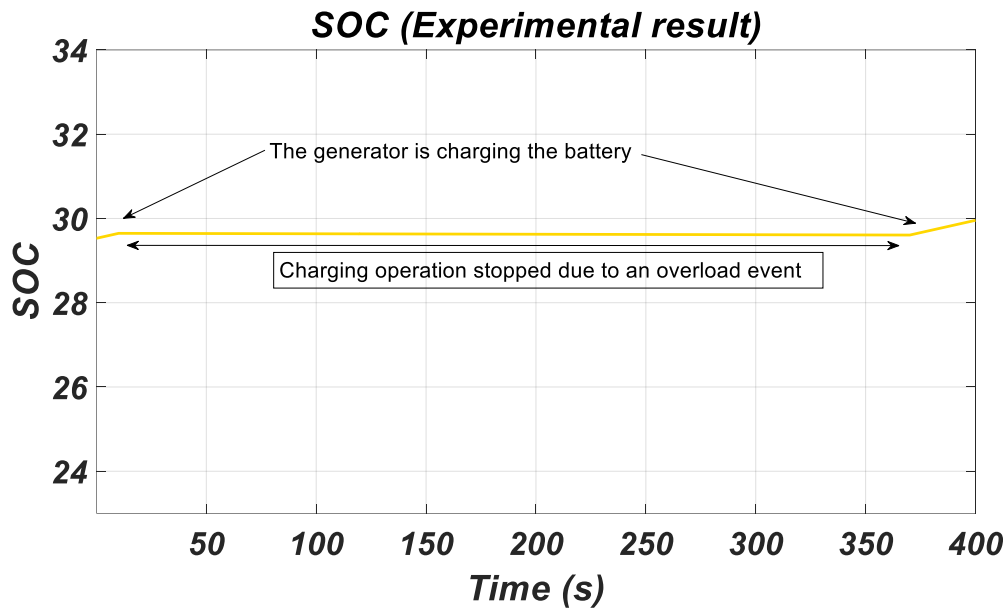


Fig. 8.30. SOC level during the charging and overload operations

Fig. 8.31 shows the operating STATES during all the simulation time.

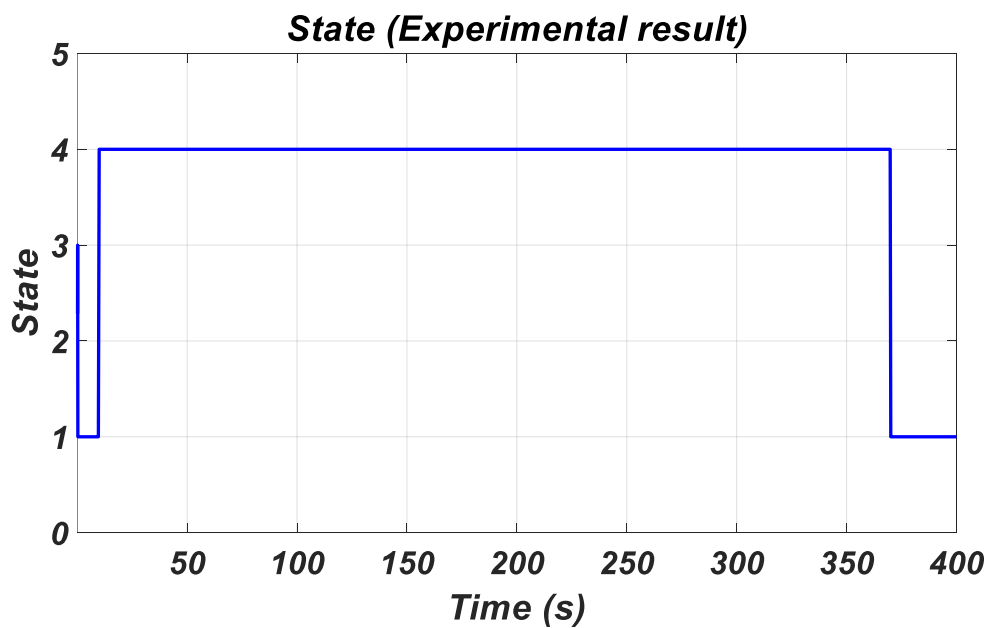


Fig. 8.31. STATE position of the system during the scenario 2

The second scenario presented a situation in which the EPS must deal with multiple overload requests in the particular case of low SOC level. In this case, the SC, which is monitoring the EPS in real-time, detects a low level of the SOC and starts to charge the battery by disconnecting load 8 (Commercial load 2) which is the lowest priority one. Once a second overload occurs, the SC must apply the knapsack method to avoid the overload of the generator, and stop the battery charging for all the overload duration. From the presented plots the SC successfully covered scenario 2, and once again following all the predicted steps of the FSM algorithm.

## **8.5 Conclusion**

This Chapter has presented the EPS emulator (test bench) for the verification of the developed in this work RCS and the LAP. Details the implementation are given, including the FSM code used for the applications of the algorithms. Through the tests on a scaled test bench, the SC was able to change the system configuration based on the power request or the status of the system components. The experimental test has been performed by applying a study case scenario, in which the RCS and the LAP have been applied for the managing of a predefined load set. The experimental tests have demonstrated how the SC has the capability to control the power flow across the EPS giving the following contributions:

- The SC can be easily applied to the MEA EPS using one single development tool to make the EPS more reliable and safer by controlling the EPS power flow.
- The set of algorithms identified, implemented, and tested are computationally inexpensive and practically applicable to MEA EPS. Thus, the SC has the capability to make the EPS more flexible by monitoring its status, and act to modify the EPS behaviours according with the operational requests
- The SC showed a fast response of the entire EPS, this enables an increased safety level since the system is instantaneously re-configured.

Moreover, the SC can give an important boost in the aircraft electrification. Since the laboratory experiments showed efficient and fast capabilities of the SC to take actions in the system re-configuration, the method can be easily translated in as an important help for the management of the electrical systems on-board. An optimised management of the EPS can improve the performance under several side aspects:

- Avoiding the overload of generators can lead lighter electrical machines to be installed on-board, since they do not need to be overrated
- Having a fast response of the SC can enable the installation of several electrical components, such as multiple converters that are used to re-distribute the power on the buses and also giving to the EPS additional redundancy
- The experimental test has demonstrated that the FSM can be used for developing complex algorithm, but in graphical language. This helps the developer to create

complex systems with reduced bugs. Moreover, a key component of the method is done by the modularity, thus more STATES can be added to the existing model in case of needed

The experimental test performed in this Chapter have never been demonstrated before, this is due to the fact that the previous methods, as explained in Chapter 2, were focused on the management of an isolated system in which each part of the EPS is controlled by a single board with an embedded code (i.e., real time C language). Thus, in this final experiment, the author has been demonstrating how a central unit has been used to control multiple devices, with a single tool that is composed by a graphical language, but capable to perform complex mathematical operations.

## **Chapter 9: Conclusion**

---

### **9.1 Introduction**

Flying being the fastest and one of the safest ways to travel over long distances has led to a sharp increase in air traffic. Before the covid-19 pandemic that affected the entire planet, more than one hundred thousand of flights per day were scheduled. However, looking at the increasing number of air vehicles, it is extremely important to address the key issues related with it, including constant increase of the carbon dioxide emissions with their significant environmental impact, and air traffic noise. To cope with high air traffic demand, and to improve the overall aircraft performances, the introduction of the aircraft electrification seems to be the viable option to move forward the next air transport generation, and lead to a substantial increase of the electrical power budgets required onboard. However, as the electrical power systems became more complex, there is the need to implement a control system, which aims to guarantee their optimal operations under all possible flight scenario. This work has proposed a SC to ensure that the electrical network of the aircraft works under safety conditions with a higher level of reliability, and automatic system management.

This has brought to achieve the following research objectives:

- Develop a methodology to design of a SC that is capable to manage the entire MEA EPS
  - Moving to the enhanced performance and efficiency of the EPS, while respecting safety constraints
- Automatization of the EPS reconfiguration during occurring or critical scenarios, with automatic switch of the power on the vital loads
- Identify, implement and test practical and computationally inexpensive algorithms and tools for the design of the SC
- Validate the selected approach, algorithms and tools through different study cases in simulation and in laboratory experiments

## **9.2 Research outcomes**

The research outcomes of this thesis are presented herein. The main contributions along with the implications of the study are emphasised.

### **9.2.1 Theoretical aspects**

Chapter 2 provided a comprehensive explanation of the methods that can be employed in the programming a SC. This is a key aspect, since this thesis work is focused on the electrical distribution system management, and how to apply a correct set of rules that allow all the correct system operations. Different type of algorithms and programming techniques are overviewed, and a final choice is justified. In the Chapter 3 a state-of-the-art of the aircraft electrical distribution systems has been presented, and potential candidates for the next generations of aircraft are reviewed.

In Chapter 4, the theoretical aspects presented in Chapter 2 have been applied to one of the electrical distribution systems proposed in Chapter 3. The SC showed the capability to control the power flow across the EPS, and bringing additional advantages over the previously used methods presented in Chapter 2:

- The SC can be easily applied to the MEA EPS using one single development tool
- The set of algorithms identified, implemented, and tested are computationally inexpensive and practically applicable to MEA EPS.
- The SC showed a fast response of the entire EPS, this enables an increased safety level since the system is instantaneously re-configured.
- The SC is built by using a graphical language leading to less bugs, so easier debugging
- The FSM used to develop the SC is composed by STATES. This method adds modularity to the code, which means a new STATE can be added without adding complexity to the FSM code

Moreover, in Chapter 5, the supervisor controller has been used to optimize the power distribution across the electrical buses. The method consisted in using a complex



mathematical optimization, called knapsack problem, to find a solution that guarantees that the power provided from the source is always used to supply the loads respect to their level of priority. This method is particularly useful in an environment as the aircraft EPS, since there is a presence of critical loads, in which their power request cannot be cut off. This method confirmed that the SC, coupled with the FSM, is able to solve a scenario in which complex mathematical optimization is needed, as a plus, it has also been performed in a fast computational time.

In Chapter 6, the management strategy has been applied to a realistic case study linked to ASPIRE project (see Chapter 6 for more details), demonstrating SC capabilities in managing the distribution of the power across the buses, and through the use of multiple converter cells. The outcome of the simulations confirmed the feasibility of implementing the SC to manage the entire EPS. In summary:

- An approach has been developed for designing a SC that can be easily applied to the MEA electrical systems using one single development tool to make it efficient and safer
- A set of algorithms and tools have been identified, implemented and tested as computationally inexpensive and practically applicable to MEA electrical system.

For all the simulations, the SC has been built into the Simulink® environment, together with the electrical model of the electrical distribution system.

### **9.2.1 Experimental aspects**

In order to validate the SC behaviour, a test bench has been developed, and the scenarios performed in the simulations have been replicated in the laboratory. In Chapter 7, it has been created a test case scenario, in which the following operations of a high voltage 270V bus have been simulated:

- Normal operations with the battery disconnected
- Overload operations with battery in discharging mode for helping the generator
- Overload operations with battery discharged
- Charging operations during a normal scenario

- Charging operations with a sudden overload
- Re-distribution of the power through the use of knapsack method during normal operations
- Re-distribution of the power through the use of Knapsack method during an overload scenario

The test case scenario is then replicated in the laboratory on a test bench (physical EPS emulator) scaled in power and voltage. Chapter 8 has presented all the components used to assemble the experimental platform, and the experimental results have been compared with the test case scenario performed in Chapter 7. The conclusions of the experimental test showed how the SC manages the aircraft's electrical power network, achieving the same behaviour in both the test case scenario and the experimental test.

Thus, the employment of the SC can give an important boost in aircraft electrification. Since the laboratory experiments showed efficient and fast capabilities of the SC to take actions in the system re-configuration, the method can easily be translated in as an important help for the management of the electrical systems on-board. An optimized management of the EPS can improve the performance under several side aspects:

- Avoiding the overload of the generators can lead lighter electrical machines to install on-board, since they do not need to be overrated
- Having a fast response of the SC can enable the installation of several electrical components, such as multiple converters that are used to re-distribute the power on the buses and also giving to the EPS additional redundancy

Even in the experimental test, it has been demonstrated that the FSM can be used for developing complex algorithms with a graphical language. This helps the developer to create complex systems with reduced bugs. Moreover, a key component of the method is done by modularity, thus more STATES can be added to the existing model in case of need.

In conclusion, in both simulation and experimental test, the SC has demonstrated the capability of managing the entire system, performing fast computational operations in modifying the EPS state when needed.

### **9.3 Future research**

This thesis has aimed to contribute towards the future of aircraft electrification, especially in the field of electrical power systems management. Two main areas can be further investigated amongst many others.

- The SC can be used to control the entire aircraft power network. This will enable new safety and reliability levels. In fact, the SC is capable to perform fast computational operations, and the EPS can be controlled also in the case of multiple buses. Indeed, one of the next steps could be consist of connecting multiple test benches on a single SC unit in order to test the behaviour and in more complex EPS architectures, thus, the electrical power system can be divided into multiple sub-systems and controlled by multiple SCs. This will give:
  - another level of redundancy to the entire network covering the possible failure of the SC units.

Another future investigation could consist in connecting multiple SCs and divide them into master and slave units. This solution can provide:

- additional redundancy to the control systems and give an optimization in terms of bus management.
- The slave units can be used to manage a single bus or a portion of the EPS, while the Master can be used to manage the slave units enabling more complex and faster operations since more units are employed.

## Appendix A – List of Simulink® Models

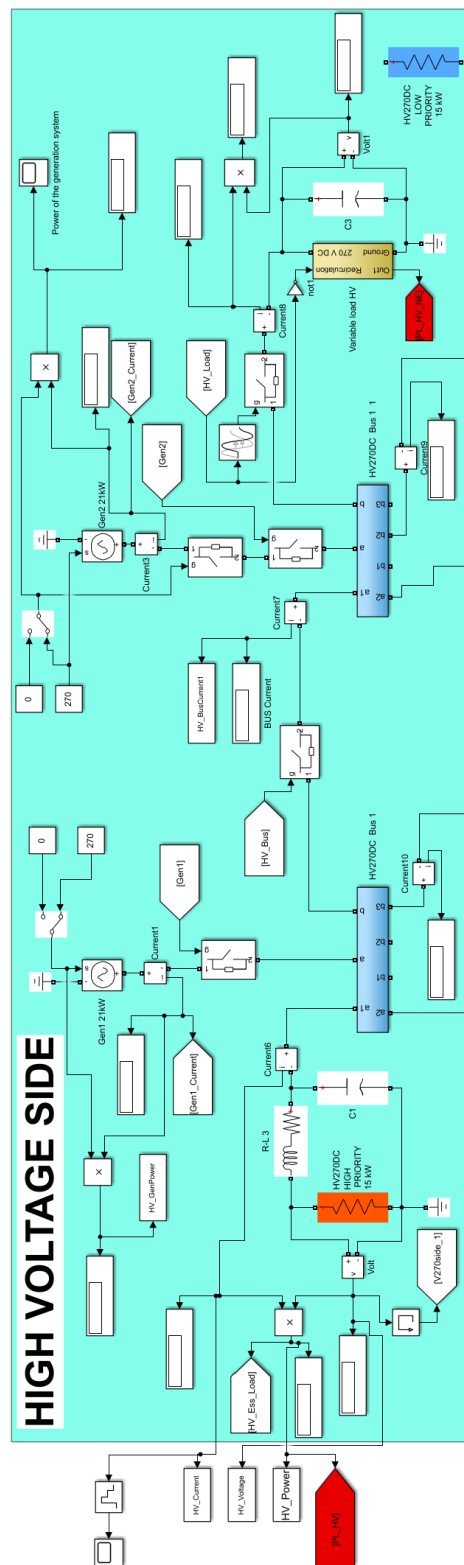


Fig. 1. Simulink® model of the high voltage part of the EPS used for the simulation in Chapters 4, and 6

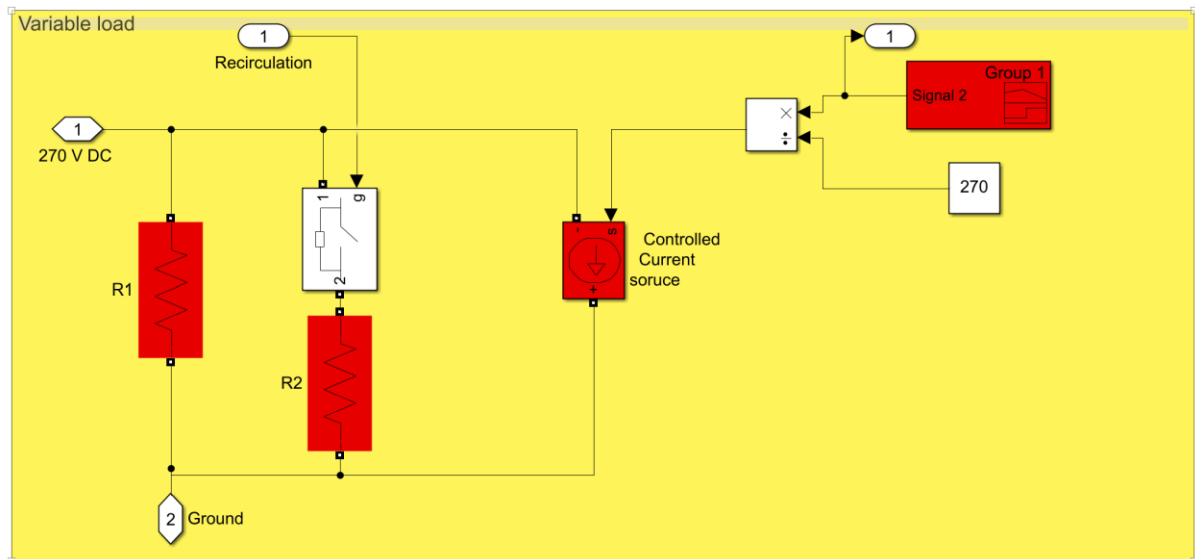


Fig. 2. Simulink® model of the High Voltage Variable load used for simulating the extra power request in chapters 4 and 6

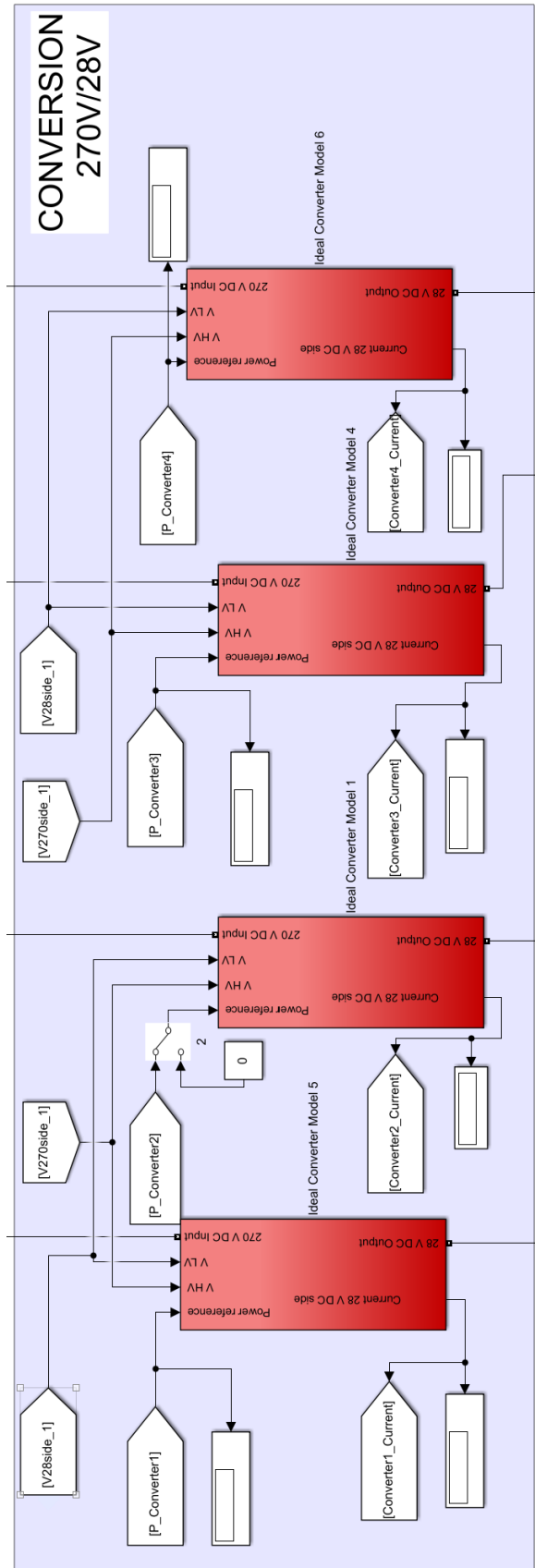


Fig. 3 Simulink® model of the conversion stage connection from 270V to 28V

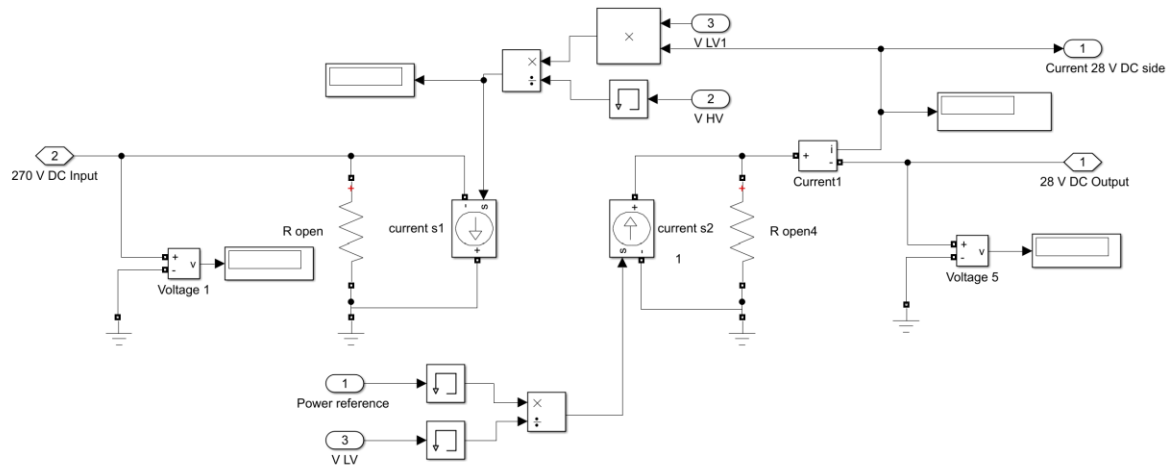


Fig. 4. Simulink® ideal model of the DC/DC converter (current-controlled) that connects the High voltage to Low voltage side

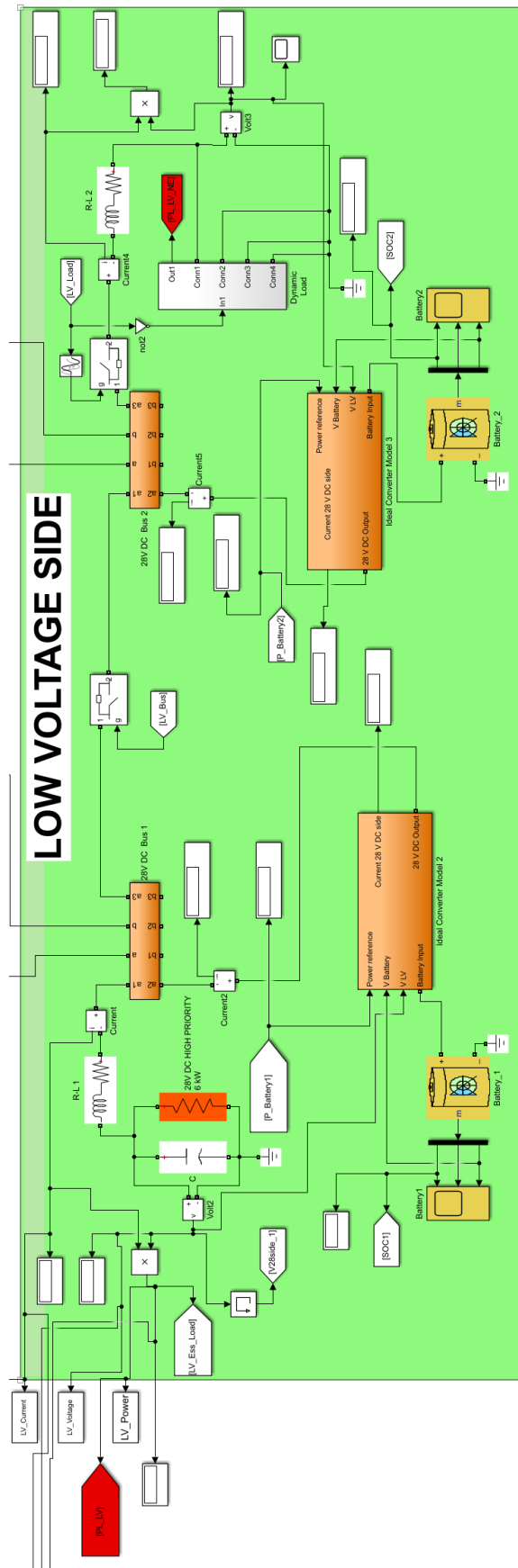


Fig. 5. Simulink® model of the Low voltage side



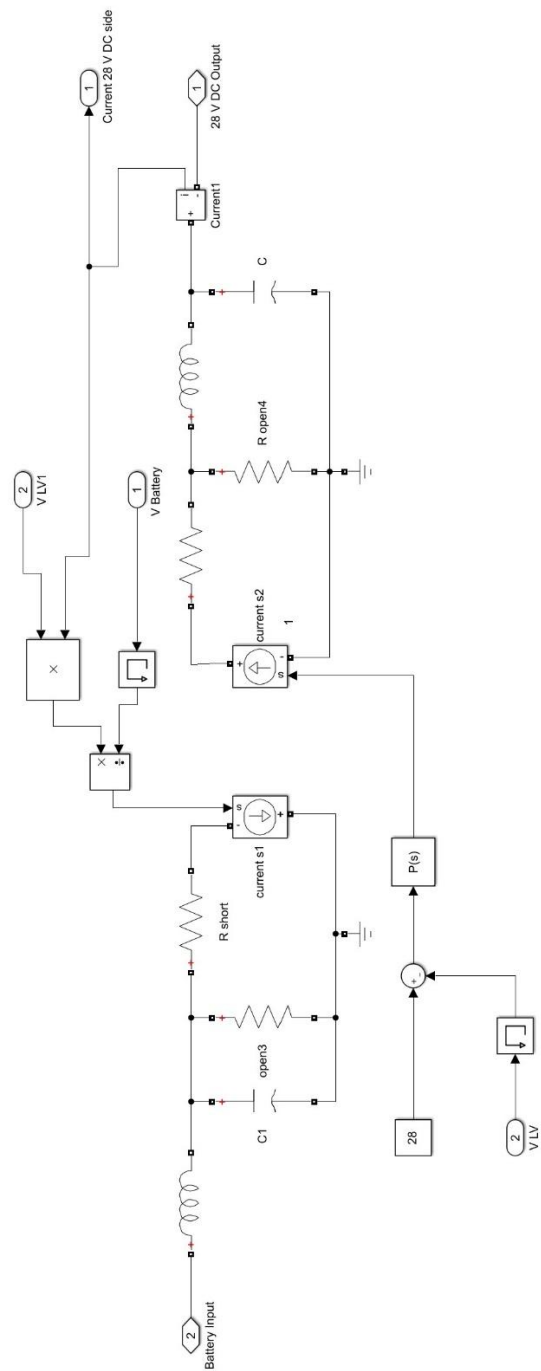
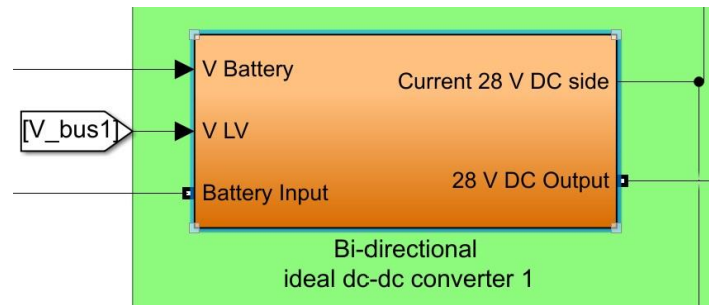


Fig. 6. Simulink® ideal model of the DC/DC converter (Voltage controlled) that connects the Battery to Low voltage side

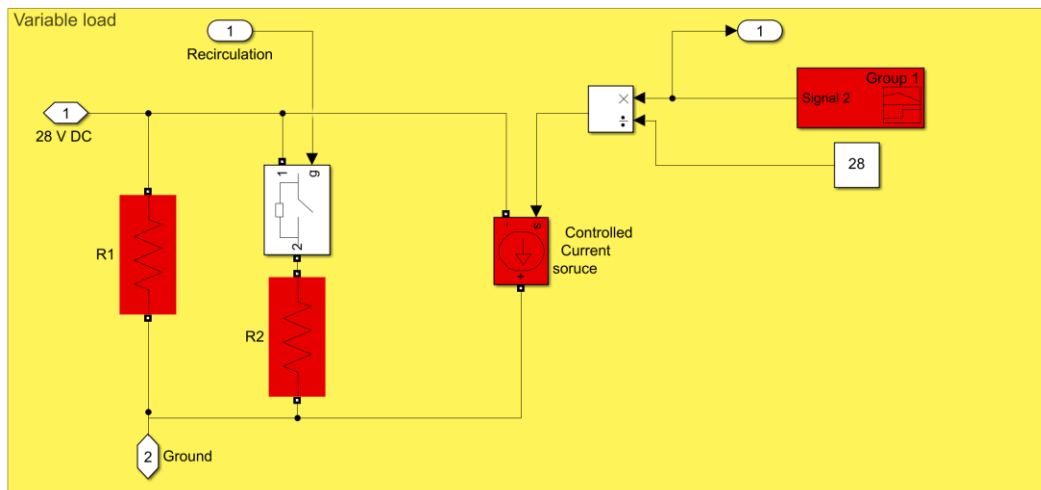
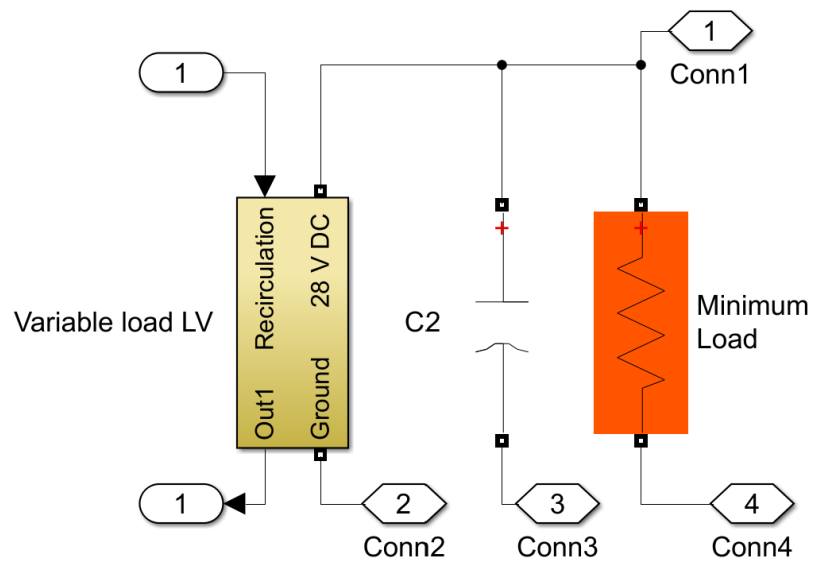


Fig. 7. Simulink® model of the Low Voltage Variable load used for simulating the extra power request in chapters 4, 6, and 7

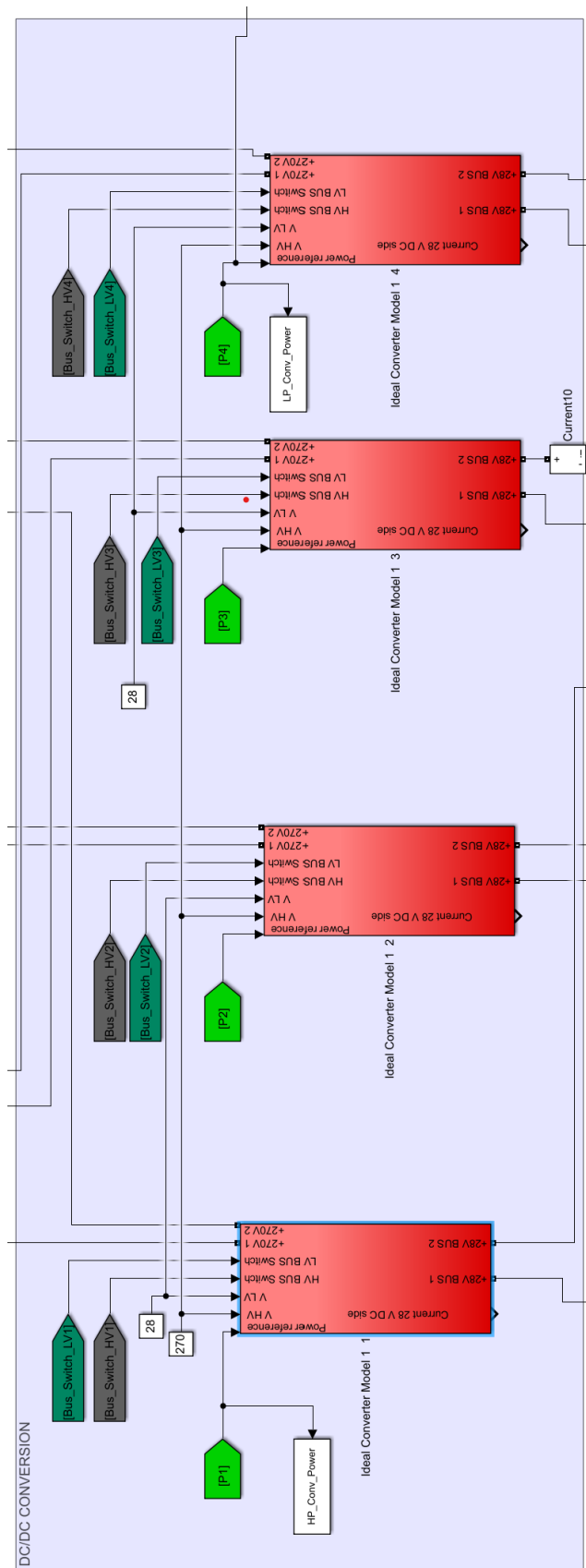


Fig. 8. Simulink® model of the conversion stage connection from 270V to 28V in ASPIRE project presented in

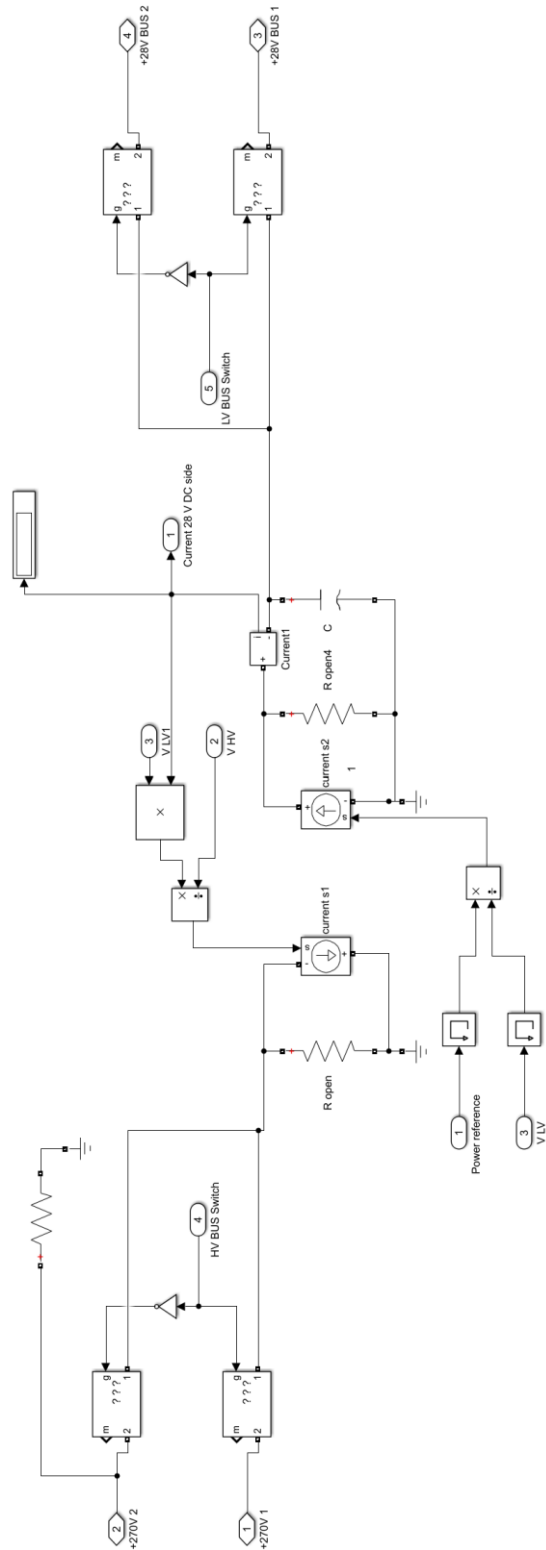


Fig. 9. Simulink® ideal model of the DC/DC converter (Current controlled) that connects the High voltage to Low voltage side with the bus switching capacity as described in the ASPIRE project in Chapter 7

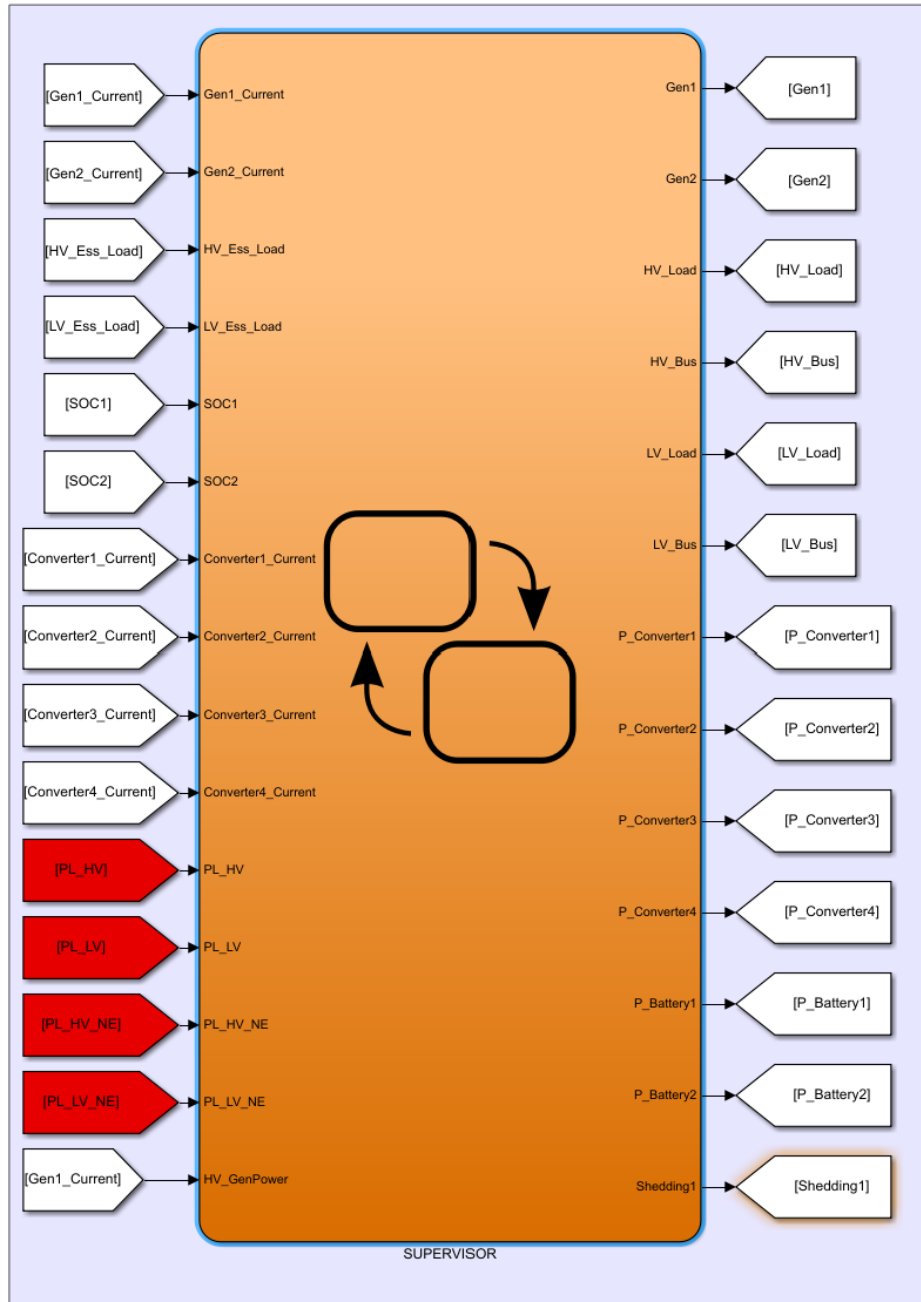


Fig. 10. Simulink® model of the Finite State Machine used in Chapters 4 and 6

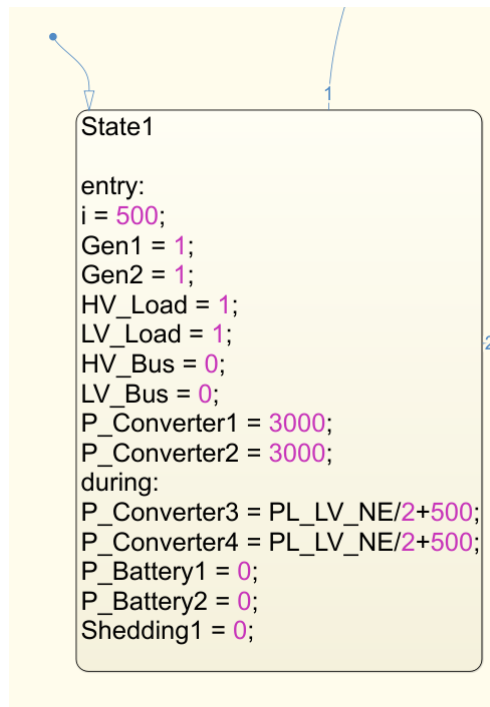


Fig. 11. Simulink® model of the FSM STATE1 used in Chapter 4 for the system initialization

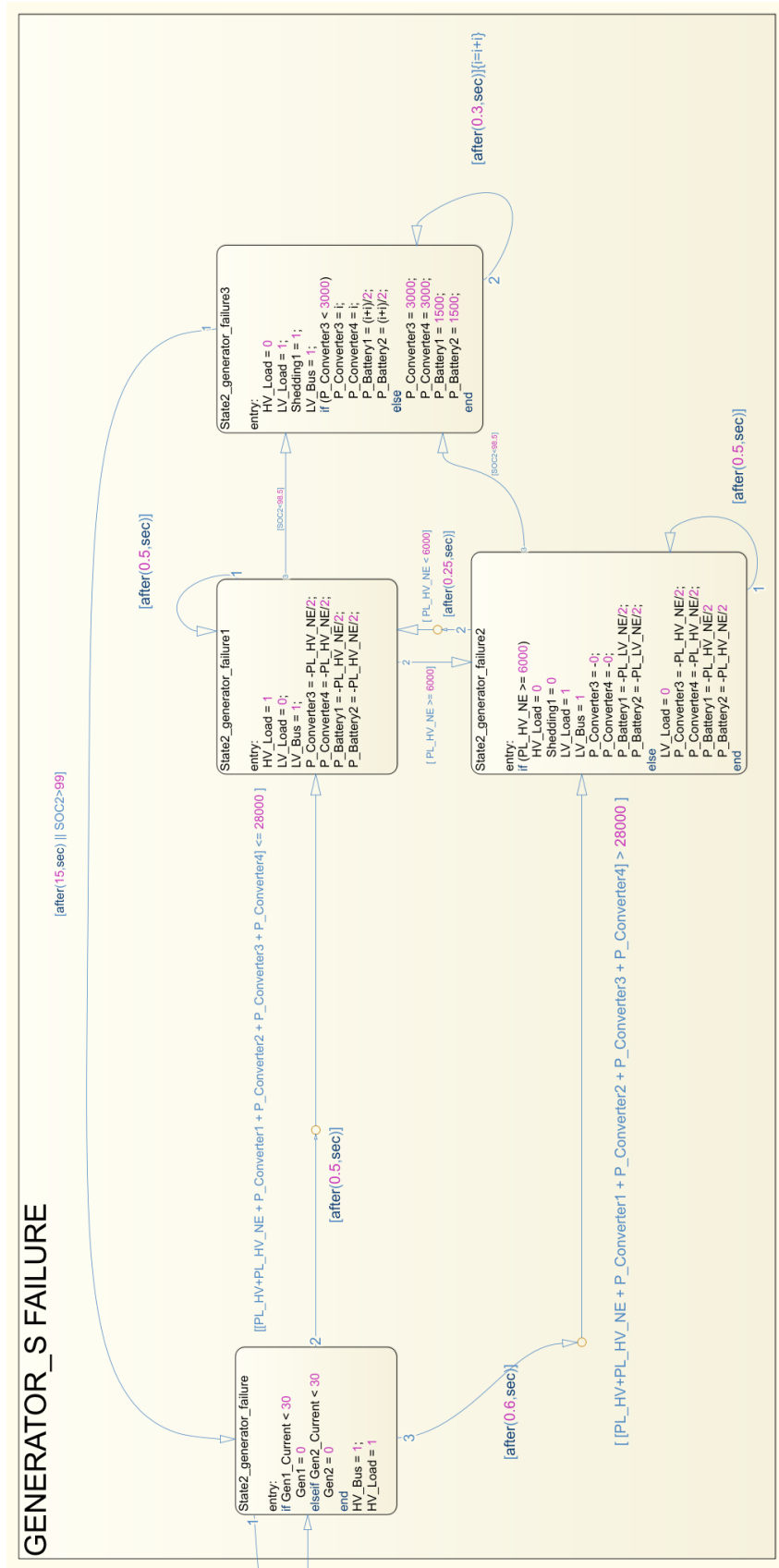


Fig. 12. Simulink® model of the FSM, Generator's failure event STATES used in Chapter 4

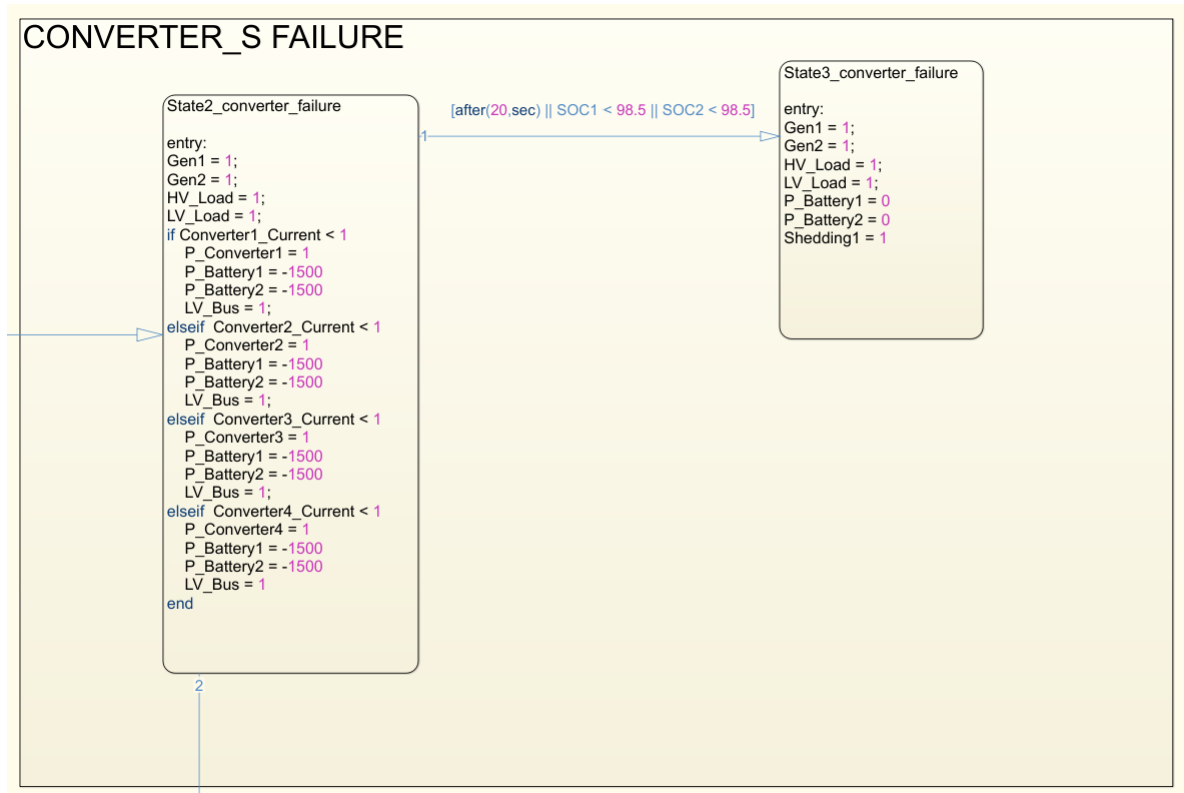


Fig. 13. Simulink® model of the FSM, Converter's failure event STATES used in Chapter 4





Fig. 14. Simulink® model of the FSM, Generator’s failure and Converter’s failure event STATES used in Chapter

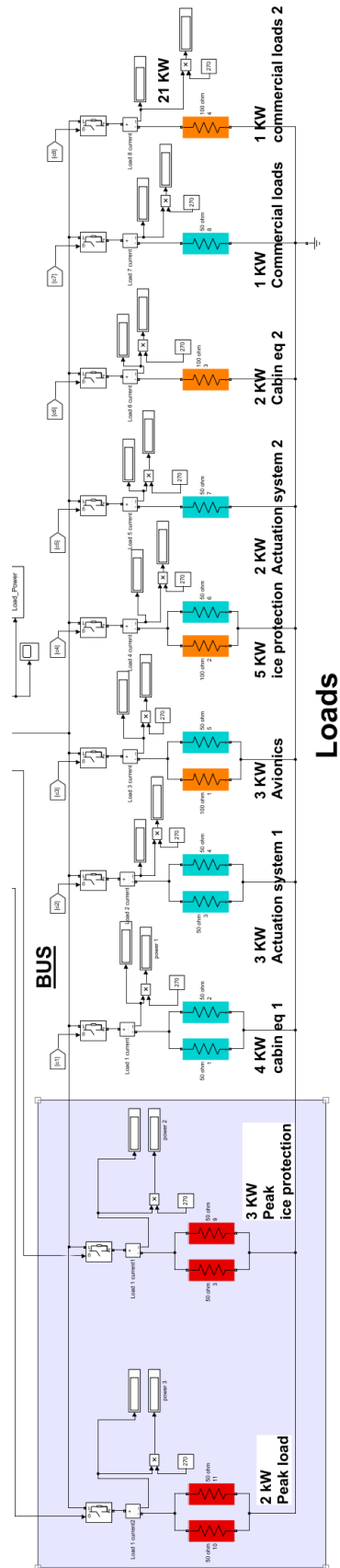


Fig. 15. Simulink® model of the Loads presented in chapter 7

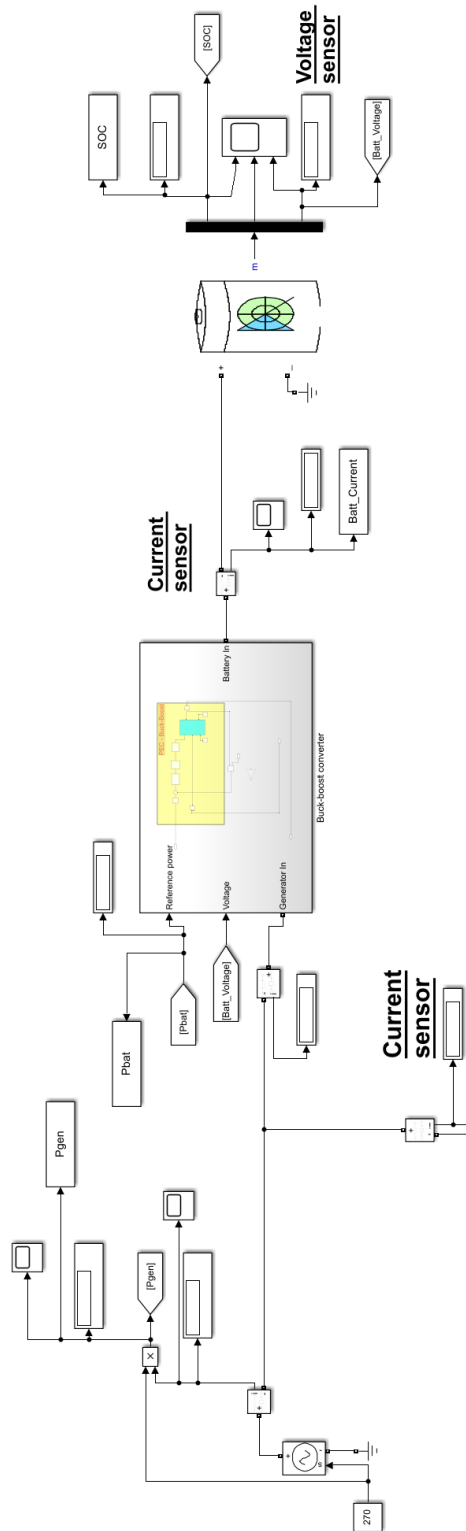


Fig. 16. Simulink® diagram of the battery and converter connections

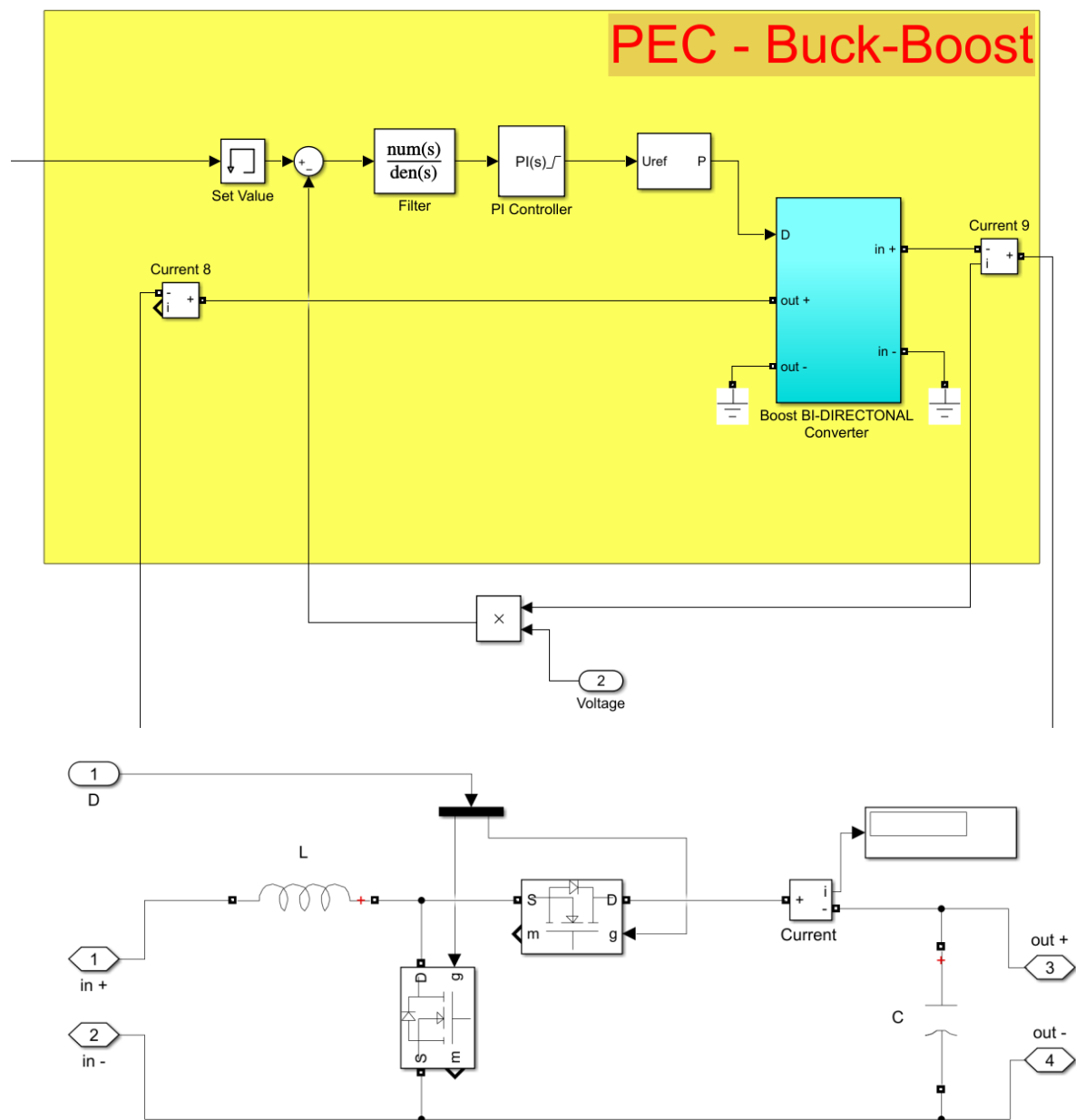


Fig. 17. Simulink® model of the ideal converter used in Chapter 7

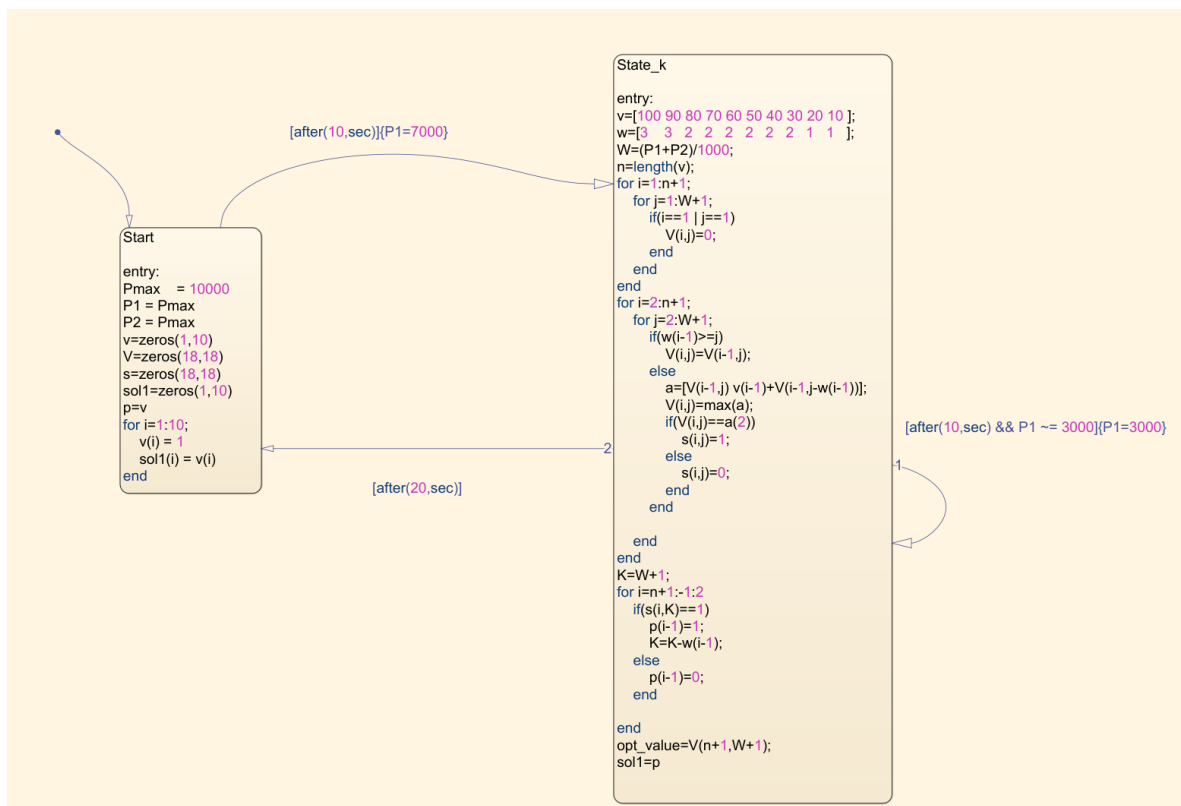
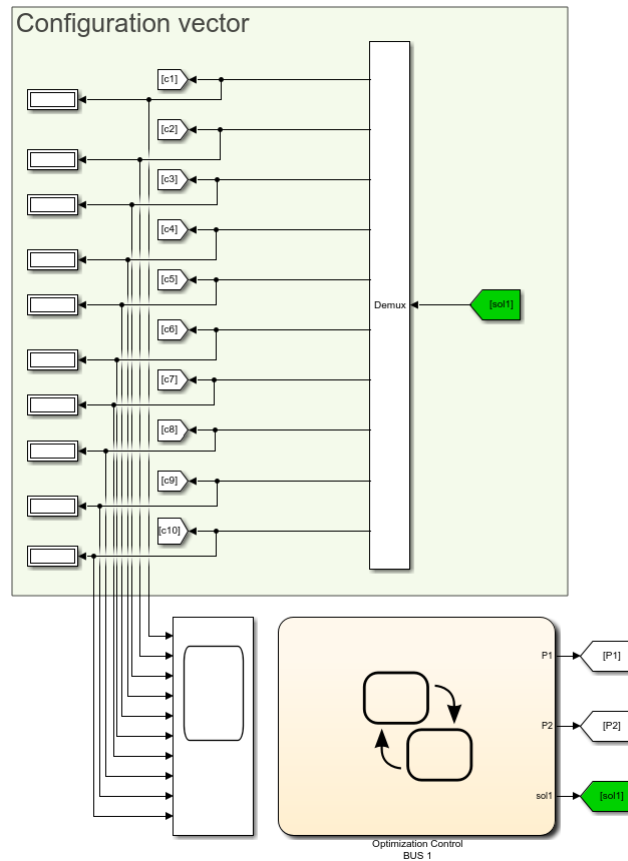


Fig. 18. Simulink® model of the FSM and Algorithm used for applying the Knapsack code of Chapter 5, 7, and 8



## List of References:

---

### References to Chapter 1

---

- [1]. *Flight Radar 24*. [cited 2019 01/07/2019]; Available from: <https://www.flightradar24.com/46.66,-43.1/3>.
- [2]. FederalAviationAdministration. [https://www.faa.gov/air\\_traffic/by\\_the\\_numbers/](https://www.faa.gov/air_traffic/by_the_numbers/).
- [3]. Chapman, L., *Transport and climate change: a review*. Journal of Transport Geography, 2007. **15**(5): p. 354-367.
- [4]. Chu, S. and A. Majumdar, *Opportunities and challenges for a sustainable energy future*. Nature, 2012. **488**: p. 294.
- [5]. Clarke, J.-P., *The role of advanced air traffic management in reducing the impact of aircraft noise and enabling aviation growth*. Journal of Air Transport Management, 2003. **9**(3): p. 161-165.
- [6]. Rosero, J., et al., *Moving towards a more electric aircraft*. IEEE Aerospace and Electronic Systems Magazine, 2007. **22**(3): p. 3-9.
- [7]. Ke, W., et al., *Assessing the future vehicle fleet electrification: the impacts on regional and urban air quality*. Environmental science & technology, 2017. **51**(2): p. 1007-1016.
- [8]. Alexander, R., D. Meyer, and J. Wang. *A Comparison of Electric Vehicle Power Systems to Predict Architectures, Voltage Levels, Power Requirements, and Load Characteristics of the Future All-Electric Aircraft*. in *2018 IEEE Transportation Electrification Conference and Expo (ITEC)*. 2018.
- [9]. Madonna, V., et al., *The Rebirth of the Current Source Inverter: Advantages for Aerospace Motor Design*. IEEE Industrial Electronics Magazine, 2019. **13**(4): p. 65-76.
- [10]. Sarlioglu, B. and C.T. Morris, *More electric aircraft: Review, challenges, and opportunities for commercial transport aircraft*. IEEE transactions on Transportation Electrification, 2015. **1**(1): p. 54-64.
- [11]. Galea, M., et al., *Reliability-Oriented Design of Electrical Machines: The Design Process for Machines' Insulation Systems MUST Evolve*. IEEE Industrial Electronics Magazine, 2020. **14**(1): p. 20-28.
- [12]. Madonna, V., et al., *Thermal overload and insulation aging of short duty cycle, aerospace motors*. IEEE Transactions on Industrial Electronics, 2019. **67**(4): p. 2618-2629.
- [13]. Jones, C.E., et al., *Electrical and Thermal Effects of Fault Currents in Aircraft Electrical Power Systems With Composite Aerostructures*. IEEE Transactions on Transportation Electrification, 2018. **4**(3): p. 660-670.
- [14]. Saleh, M., Y. Esa, and A.A. Mohamed, *Communication-based control for DC microgrids*. IEEE Transactions on Smart Grid, 2018. **10**(2): p. 2180-2195.
- [15]. Bozhko, S.V., et al. *More-electric aircraft electrical power system accelerated functional modeling*. in *Proceedings of 14th International Power Electronics and Motion Control Conference EPE-PEMC 2010*. 2010.
- [16]. Telford, R., S. Galloway, and G.M. Burt. *Evaluating the reliability & availability of more-electric aircraft power systems*. in *2012 47th International Universities Power Engineering Conference (UPEC)*. 2012. IEEE.
- [17]. Emadi, K. and M. Ehsani, *Aircraft power systems: technology, state of the art, and future trends*. IEEE Aerospace and Electronic Systems Magazine, 2000. **15**(1): p. 28-32.
- [18]. Zhao, X., J.M. Guerrero, and X. Wu. *Review of aircraft electric power systems and architectures*. in *2014 IEEE International Energy Conference (ENERGYCON)*. 2014. IEEE.
- [19]. Buticchi, G., et al., *On-Board Microgrids for the More Electric Aircraft—Technology Review*. IEEE Transactions on Industrial Electronics, 2019. **66**(7): p. 5588-5599.
- [20]. Fréville, A., *The multidimensional 0–1 knapsack problem: An overview*. European Journal of Operational Research, 2004. **155**(1): p. 1-21.

## References to Chapter 2

---

- [1] "Flight Radar 24." <https://www.flightradar24.com/46.66,-43.1/3>.
- [2] FederalAviationAdministration. "<https://www.faa.gov/air-traffic/by-the-numbers/>."
- [3] L. Chapman, "Transport and climate change: a review," *Journal of Transport Geography*, vol. 15, no. 5, pp. 354-367, 2007/09/01/ 2007, doi: <https://doi.org/10.1016/j.jtrangeo.2006.11.008>.
- [4] S. Chu and A. Majumdar, "Opportunities and challenges for a sustainable energy future," *Nature*, vol. 488, p. 294, 08/15/online 2012, doi: 10.1038/nature11475.
- [5] J.-P. Clarke, "The role of advanced air traffic management in reducing the impact of aircraft noise and enabling aviation growth," *Journal of Air Transport Management*, vol. 9, no. 3, pp. 161-165, 2003/05/01/ 2003, doi: [https://doi.org/10.1016/S0969-6997\(02\)00080-7](https://doi.org/10.1016/S0969-6997(02)00080-7).
- [6] J. Rosero, J. Ortega, E. Aldabas, and L. Romeral, "Moving towards a more electric aircraft," *IEEE Aerospace and Electronic Systems Magazine*, vol. 22, no. 3, pp. 3-9, 2007.
- [7] W. Ke, S. Zhang, Y. Wu, B. Zhao, S. Wang, and J. Hao, "Assessing the future vehicle fleet electrification: the impacts on regional and urban air quality," *Environmental science & technology*, vol. 51, no. 2, pp. 1007-1016, 2017.
- [8] R. Alexander, D. Meyer, and J. Wang, "A Comparison of Electric Vehicle Power Systems to Predict Architectures, Voltage Levels, Power Requirements, and Load Characteristics of the Future All-Electric Aircraft," in *2018 IEEE Transportation Electrification Conference and Expo (ITEC)*, 13-15 June 2018 2018, pp. 194-200, doi: 10.1109/ITEC.2018.8450240.
- [9] V. Madonna, G. Migliazza, P. Giangrande, E. Lorenzani, G. Buticchi, and M. Galea, "The Rebirth of the Current Source Inverter: Advantages for Aerospace Motor Design," *IEEE Industrial Electronics Magazine*, vol. 13, no. 4, pp. 65-76, 2019, doi: 10.1109/MIE.2019.2936319.
- [10] B. Sarlioglu and C. T. Morris, "More electric aircraft: Review, challenges, and opportunities for commercial transport aircraft," *IEEE transactions on Transportation Electrification*, vol. 1, no. 1, pp. 54-64, 2015.
- [11] M. Galea, P. Giangrande, V. Madonna, and G. Buticchi, "Reliability-Oriented Design of Electrical Machines: The Design Process for Machines' Insulation Systems MUST Evolve," *IEEE Industrial Electronics Magazine*, vol. 14, no. 1, pp. 20-28, 2020.
- [12] V. Madonna, P. Giangrande, L. Lusuardi, A. Cavallini, C. Gerada, and M. Galea, "Thermal overload and insulation aging of short duty cycle, aerospace motors," *IEEE Transactions on Industrial Electronics*, vol. 67, no. 4, pp. 2618-2629, 2019.
- [13] C. E. Jones *et al.*, "Electrical and Thermal Effects of Fault Currents in Aircraft Electrical Power Systems With Composite Aerostructures," *IEEE Transactions on Transportation Electrification*, vol. 4, no. 3, pp. 660-670, 2018, doi: 10.1109/TTE.2018.2833838.
- [14] M. Saleh, Y. Esa, and A. A. Mohamed, "Communication-based control for DC microgrids," *IEEE Transactions on Smart Grid*, vol. 10, no. 2, pp. 2180-2195, 2018.
- [15] S. V. Bozhko, T. Wu, Y. Tao, and G. M. Asher, "More-electric aircraft electrical power system accelerated functional modeling," in *Proceedings of 14th International Power Electronics and Motion Control Conference EPE-PEMC 2010*, 6-8 Sept. 2010 2010, pp. T9-7-T9-14, doi: 10.1109/EPEPEMC.2010.5606894.
- [16] R. Telford, S. Galloway, and G. M. Burt, "Evaluating the reliability & availability of more-electric aircraft power systems," in *2012 47th International Universities Power Engineering Conference (UPEC)*, 2012: IEEE, pp. 1-6.
- [17] K. Emadi and M. Ehsani, "Aircraft power systems: technology, state of the art, and future trends," *IEEE Aerospace and Electronic Systems Magazine*, vol. 15, no. 1, pp. 28-32, 2000.
- [18] X. Zhao, J. M. Guerrero, and X. Wu, "Review of aircraft electric power systems and architectures," in *2014 IEEE International Energy Conference (ENERGYCON)*, 2014: IEEE, pp. 949-953.
- [19] G. Buticchi, S. Bozhko, M. Liserre, P. Wheeler, and K. Al-Haddad, "On-Board Microgrids for the More Electric Aircraft—Technology Review," *IEEE Transactions on Industrial Electronics*, vol. 66, no. 7, pp. 5588-5599, 2019.
- [20] A. Fréville, "The multidimensional 0–1 knapsack problem: An overview," *European Journal of Operational Research*, vol. 155, no. 1, pp. 1-21, 2004.
- [21] X. Giraud, H. Piquet, M. Budinger, X. Roboam, M. Sartor, and S. Vial, "Knowledge-based system for aircraft electrical power system reconfiguration," in *2012 Electrical Systems for Aircraft, Railway and Ship Propulsion*, 2012: IEEE, pp. 1-6.



- [22] D. P. Bertsekas, D. P. Bertsekas, D. P. Bertsekas, and D. P. Bertsekas, *Dynamic programming and optimal control* (no. 2). Athena scientific Belmont, MA, 1995.
- [23] A. Pnueli, "The temporal logic of programs," in *18th Annual Symposium on Foundations of Computer Science (sfcs 1977)*, 1977: IEEE, pp. 46-57.
- [24] P. Nuzzo, J. B. Finn, A. Iannopolo, and A. L. Sangiovanni-Vincentelli, "Contract-based design of control protocols for safety-critical cyber-physical systems," in *2014 Design, Automation & Test in Europe Conference & Exhibition (DATE)*, 2014: IEEE, pp. 1-4.
- [25] S. J. Shue and J. J. Shillings, "Vehicle management system using finite state machines," ed: Google Patents, 2015.
- [26] J. García. "[https://ubidots.com/blog/advantages\\_and\\_disadvantages\\_of\\_finite\\_state\\_machines/](https://ubidots.com/blog/advantages_and_disadvantages_of_finite_state_machines/)." (accessed).
- [27] J. Reyes. "<https://code.tutsplus.com/tutorials/the-power-of-finite-state-machines-concept-and-creation--active-9566>." (accessed).
- [28] T. Wongpiromsarn, U. Topcu, N. Ozay, H. Xu, and R. M. Murray, "TuLiP: a software toolbox for receding horizon temporal logic planning," in *Proceedings of the 14th international conference on Hybrid systems: computation and control*, 2011, pp. 313-314.
- [29] I. Filippidis, S. Dathathri, S. C. Livingston, N. Ozay, and R. M. Murray, "Control design for hybrid systems with TuLiP: The temporal logic planning toolbox," in *2016 IEEE Conference on Control Applications (CCA)*, 2016: IEEE, pp. 1030-1041.
- [30] A. Cavallo, G. Canciello, and A. Russo, "Supervised energy management in advanced aircraft applications," in *2018 European Control Conference (ECC)*, 2018: IEEE, pp. 2769-2774.
- [31] A. Cavallo and B. Guida, "Sliding mode control for DC/DC converters," in *2012 IEEE 51st IEEE Conference on Decision and Control (CDC)*, 2012: IEEE, pp. 7088-7094.
- [32] L. Agnello, M. Cossentino, G. De Simone, and L. Sabatucci, "A Self-Adaptation Exemplar: the Shipboard Power System Reconfiguration Problem," in *WOA*, 2017, pp. 96-101.
- [33] W. M. Dahalan and H. Mokhlis, "Techniques of network reconfiguration for service restoration in shipboard power system: A review," *Australian Journal of Basic and Applied Sciences*, vol. 4, no. 11, pp. 5556-5563, 2010.
- [34] A. Barzegar *et al.*, "Intelligent power allocation and load management of more electric aircraft," in *2015 IEEE 11th International Conference on Power Electronics and Drive Systems*, 9-12 June 2015 2015, pp. 533-538, doi: 10.1109/PEDS.2015.7203445.
- [35] Y. Zhang, R. Su, C. Wen, M. Y. Lee, and C. Gajanayake, "Distributed power allocation and scheduling for electrical power system in more electric aircraft," in *IECON 2016 - 42nd Annual Conference of the IEEE Industrial Electronics Society*, 23-26 Oct. 2016 2016, pp. 102-107, doi: 10.1109/IECON.2016.7793600.
- [36] X. Giraud *et al.*, "Load allocation problem for optimal design of aircraft electrical power system," *International Journal of Applied Electromagnetics and Mechanics*, vol. 43, no. 1-2, pp. 37-49, 2013.
- [37] G. Rile. <http://www.clipsrules.net/> (accessed).
- [38] E. Novoseltseva. "<https://softjourn.com/blog/article/heuristic-programming>." (accessed).
- [39] Mike Wooldridge. "<https://www.cs.ox.ac.uk/people/michael.wooldridge/teaching/soft-eng/lect07.pdf>." (accessed).
- [40] Stanford. "[http://intrologic.stanford.edu/chapters/chapter\\_02.html](http://intrologic.stanford.edu/chapters/chapter_02.html)." (accessed).
- [41] P. Nuzzo, A. L. Sangiovanni-Vincentelli, D. Bresolin, L. Geretti, and T. Villa, "A platform-based design methodology with contracts and related tools for the design of cyber-physical systems," *Proceedings of the IEEE*, vol. 103, no. 11, pp. 2104-2132, 2015.
- [42] E. M. Clarke Jr, O. Grumberg, D. Kroening, D. Peled, and H. Veith, *Model checking*. MIT press, 2018.
- [43] H. Xu, "Design, specification, and synthesis of aircraft electric power systems control logic," California Institute of Technology, 2013.
- [44] H. Fairclough and M. Gilbert, "Layout optimization of simplified trusses using mixed integer linear programming with runtime generation of constraints," *Structural and Multidisciplinary Optimization*, pp. 1-23, 2020.
- [45] M. Y. Vardi, "An automata-theoretic approach to linear temporal logic," in *Logics for concurrency*: Springer, 1996, pp. 238-266.
- [46] M. Daniele, F. Giunchiglia, and M. Y. Vardi, "Improved automata generation for linear temporal logic," in *International Conference on Computer Aided Verification*, 1999: Springer, pp. 249-260.
- [47] A. Kumar and R. Kala, "Linear Temporal Logic-based Mission Planning," *IJIMAI*, vol. 3, no. 7, pp. 32-41, 2016.

- [48] M. Held and R. M. Karp, "A dynamic programming approach to sequencing problems," *Journal of the Society for Industrial and Applied mathematics*, vol. 10, no. 1, pp. 196-210, 1962.
- [49] P. Joshi, "<https://prateekvjoshi.com/2012/11/14/dynamic-programming/>." (accessed).
- [50] S. Sahni, "Approximate algorithms for the 0/1 knapsack problem," *Journal of the ACM (JACM)*, vol. 22, no. 1, pp. 115-124, 1975.
- [51] C. Chekuri and S. Khanna, "A polynomial time approximation scheme for the multiple knapsack problem," *SIAM Journal on Computing*, vol. 35, no. 3, pp. 713-728, 2005.
- [52] A. Cavallo, G. Canciello, and B. Guida, "Supervised control of buck-boost converters for aeronautical applications," *Automatica*, vol. 83, pp. 73-80, 2017.
- [53] G. Canciello, A. Russo, B. Guida, and A. Cavallo, "Supervisory control for energy storage system onboard aircraft," in *2018 IEEE International Conference on Environment and Electrical Engineering and 2018 IEEE Industrial and Commercial Power Systems Europe (EEEIC/I&CPS Europe)*, 2018: IEEE, pp. 1-6.
- [54] H. Hu, W. Shi, Y. Lu, and Y. Xing, "Design considerations for DSP-controlled 400 Hz shunt active power filter in an aircraft power system," *IEEE Transactions on Industrial Electronics*, vol. 59, no. 9, pp. 3624-3634, 2011.
- [55] A. Bogdanchikov, M. Zhaparov, and R. Suliyev, "Python to learn programming," *Journal of Physics: Conference Series*, vol. 423, p. 012027, 2013/04/10 2013, doi: 10.1088/1742-6596/423/1/012027.
- [56] K. J. Millman and M. Aivazis, "Python for Scientists and Engineers," *Computing in Science & Engineering*, vol. 13, no. 2, pp. 9-12, 2011, doi: 10.1109/MCSE.2011.36.
- [57] P. Nuzzo *et al.*, "A contract-based methodology for aircraft electric power system design," *IEEE Access*, vol. 2, pp. 1-25, 2013.
- [58] M. Maasoumy, P. Nuzzo, F. Iandola, M. Kamgarpour, A. Sangiovanni-Vincentelli, and C. Tomlin, "Optimal load management system for aircraft electric power distribution," in *52nd IEEE Conference on Decision and Control*, 2013: IEEE, pp. 2939-2945.
- [59] F. Bevilacqua, "<https://gamedevelopment.tutsplus.com/tutorials/finite-state-machines-theory-and-implementation--gamedev-11867>." (accessed).
- [60] J. E. Seem, G. M. Decious, C. Lomonaco, and A. Bernaden, "Hybrid finite state machine environmental system controller," ed: Google Patents, 2002.
- [61] J. Xu and L. Xie, "6 - Controllability and reachability," in *Control and Estimation of Piecewise Affine Systems*, J. Xu and L. Xie Eds.: Woodhead Publishing, 2014, pp. 101-121.
- [62] H. Liu, F. Yuan, J. Xie, and Y. Wang, "Research on EPS Control Strategy of Heavy Vehicle Based on Simulink," *Wireless Personal Communications*, vol. 103, no. 1, pp. 417-425, 2018/11/01 2018, doi: 10.1007/s11277-018-5451-9.
- [63] D. Harel and M. Politi, *Modeling reactive systems with statecharts: the STATEMATE approach*. McGraw-Hill, Inc., 1998.
- [64] E. Sekerinski, "Graphical design of reactive systems," in *International Conference of B Users*, 1998: Springer, pp. 182-197.
- [65] Mathworks, "<https://uk.mathworks.com/products/stateflow.html>." (accessed).
- [66] Texas-Instruments, "<http://www.ti.com/lit/ml/swrp161/swrp161.pdf?&ts=1590054752237>," ed.
- [67] V. Madonna, P. Giangrande, and M. Galea, "Electrical Power Generation in Aircraft: Review, Challenges, and Opportunities," *IEEE Transactions on Transportation Electrification*, vol. 4, no. 3, pp. 646-659, 2018, doi: 10.1109/TTE.2018.2834142.
- [68] J. Chen, C. Wang, and J. Chen, "Investigation on the selection of electric power system architecture for future more electric aircraft," *IEEE Transactions on Transportation Electrification*, vol. 4, no. 2, pp. 563-576, 2018.
- [69] J. Chen, C. Wang, and J. Chen, "Investigation on the selection of a more suitable power system architecture for future more electric aircraft from the prospective of system stability," in *2017 IEEE 26th International Symposium on Industrial Electronics (ISIE)*, 2017: IEEE, pp. 1861-1867.
- [70] T. Kostakis, P. J. Norman, and S. J. Galloway, "Assessing network architectures for the more electric engine and aircraft," in *2014 49th International Universities Power Engineering Conference (UPEC)*, 2014: IEEE, pp. 1-6.
- [71] Thales, "<https://sunjet-project.eu/sites/default/files/Thales%20AES%20-%20Thalin.pdf>." (accessed).
- [72] R. T. Naayagi, "A review of more electric aircraft technology," in *2013 International Conference on Energy Efficient Technologies for Sustainability*, 10-12 April 2013 2013, pp. 750-753, doi: 10.1109/ICEETS.2013.6533478.
- [73] M. Pagonis, "Electrical power aspects of distributed propulsion systems in turbo-electric powered aircraft," 2015.

- [74] M. E. Elbuluk and M. D. Kankam, "Potential starter/generator technologies for future aerospace applications," *IEEE Aerospace and Electronic Systems Magazine*, vol. 12, no. 5, pp. 24-31, 1997.
- [75] C. Avery, S. Burrow, and P. Mellor, "Electrical generation and distribution for the more electric aircraft," in *2007 42nd international universities power engineering conference*, 2007: IEEE, pp. 1007-1012.
- [76] X. Lang, T. Yang, H. B. Enalou, S. Bozhko, and P. Wheeler, "An Enhanced Power Generation Centre for More Electric Aircraft Applications," in *2018 IEEE International Conference on Electrical Systems for Aircraft, Railway, Ship Propulsion and Road Vehicles & International Transportation Electrification Conference (ESARS-ITEC)*, 7-9 Nov. 2018 2018, pp. 1-6, doi: 10.1109/ESARS-ITEC.2018.8607688.
- [77] X. Lang, T. Yang, C. Li, H. B. Enalou, S. Bozhko, and P. Wheeler, "A Dual-Channel-Enhanced Power Generation Architecture With Back-to-Back Converter for MEA Application," *IEEE Transactions on Industry Applications*, vol. 56, no. 3, pp. 3006-3019, 2020.
- [78] J. Brombach, A. Lücken, B. Nya, M. Johannsen, and D. Schulz, "Comparison of different electrical HVDC-architectures for aircraft application," in *2012 Electrical Systems for Aircraft, Railway and Ship Propulsion*, 2012: IEEE, pp. 1-6.
- [79] J. Brombach, T. Schröter, A. Lücken, and D. Schulz, "Optimized cabin power supply with a+/- 270 V DC grid on a modern aircraft," in *2011 7th International Conference-Workshop Compatibility and Power Electronics (CPE)*, 2011: IEEE, pp. 425-428.
- [80] C. A. Ferreira, S. R. Jones, W. S. Heglund, and W. D. Jones, "Detailed design of a 30-kW switched reluctance starter/generator system for a gas turbine engine application," *IEEE Transactions on Industry Applications*, vol. 31, no. 3, pp. 553-561, 1995.
- [81] L. Tarisciotti, A. Costabeber, C. Linglin, A. Walker, and M. Galea, "Evaluation of isolated DC/DC converter topologies for future HVDC aerospace microgrids," in *2017 IEEE Energy Conversion Congress and Exposition (ECCE)*, 2017: IEEE, pp. 2238-2245.
- [82] "More Open Electrical Technologies (MOET project)." <https://cordis.europa.eu/project/id/30861> (accessed).
- [83] I. Moir and A. Seabridge, *Aircraft systems: mechanical, electrical, and avionics subsystems integration*. John Wiley & Sons, 2011.
- [84] T. Wu, S. V. Bozhko, and G. M. Asher, "High speed modeling approach of aircraft electrical power systems under both normal and abnormal scenarios," in *2010 IEEE International Symposium on Industrial Electronics*, 4-7 July 2010 2010, pp. 870-877, doi: 10.1109/ISIE.2010.5637279.
- [85] L. Prisse, D. Ferer, H. Foch, and A. Lacoste, "New power centre and power electronics sharing in aircraft," in *2009 13th European Conference on Power Electronics and Applications*, 2009: IEEE, pp. 1-9.
- [86] N. Fritz, M. Rashed, S. Bozhko, F. Cuomo, and P. Wheeler, "Analytical modelling and power density optimisation of a single phase dual active bridge for aircraft application," *The Journal of Engineering*, vol. 2019, no. 17, pp. 3671-3676, 2019.
- [87] A. Barzkar and M. Ghassemi, "Electric power systems in more and all electric aircraft: A Review," *IEEE Access*, 2020.
- [88] T. Dragičević and Y. Li, "Chapter 18 - AC and DC Microgrid Control," in *Control of Power Electronic Converters and Systems*, F. Blaabjerg Ed.: Academic Press, 2018, pp. 167-200.
- [89] T. Dragičević, J. M. Guerrero, J. C. Vasquez, and D. Škrlec, "Supervisory Control of an Adaptive-Droop Regulated DC Microgrid With Battery Management Capability," *IEEE Transactions on Power Electronics*, vol. 29, no. 2, pp. 695-706, 2014, doi: 10.1109/TPEL.2013.2257857.
- [90] K. Kim, K. Park, G. Roh, and K. Chun, "DC-grid system for ships: a study of benefits and technical considerations," *Journal of International Maritime Safety, Environmental Affairs, and Shipping*, vol. 2, no. 1, pp. 1-12, 2018/11/14 2018, doi: 10.1080/25725084.2018.1490239.
- [91] K. Ni *et al.*, "Electrical and electronic technologies in more-electric aircraft: A review," *IEEE Access*, vol. 7, pp. 76145-76166, 2019.
- [92] F. Abdesselam, L. Boissy, A. Castellazzi, T. Wijekoon, P. Wheeler, and M. Johnson, "Preliminary study for the integrated design of an electro-mechanical wing de-icing system," in *2010 6th International Conference on Integrated Power Electronics Systems*, 16-18 March 2010 2010, pp. 1-6.
- [93] T. University of Dallas. "The Knapsack problem; <https://personal.utdallas.edu/~scniu/OPRE-6201/documents/DP3-Knapsack.pdf>." (accessed).
- [94] "<https://www.nottingham.ac.uk/aerospace/projects/cleansky/aspire-project.aspx>."
- [95] I. Munuswamy, P. W. Wheeler, B. G. Fernandes, and K. Chatterjee, "Electric AC WIPS: All Electric Aircraft," in *2019 Innovations in Power and Advanced Computing Technologies (i-PACT)*, 22-23 March 2019 2019, vol. 1, pp. 1-5, doi: 10.1109/i-PACT44901.2019.8960072.

## References to Chapter 3

---

- [1]. Sarlioglu, B. and C.T. Morris, *More electric aircraft: Review, challenges, and opportunities for commercial transport aircraft*. IEEE transactions on Transportation Electrification, 2015. **1**(1): p. 54-64.
- [2]. Madonna, V., P. Giangrande, and M. Galea, *Electrical Power Generation in Aircraft: Review, Challenges, and Opportunities*. IEEE Transactions on Transportation Electrification, 2018. **4**(3): p. 646-659.
- [3]. Chen, J., C. Wang, and J. Chen, *Investigation on the selection of electric power system architecture for future more electric aircraft*. IEEE Transactions on Transportation Electrification, 2018. **4**(2): p. 563-576.
- [4]. Zhao, X., J.M. Guerrero, and X. Wu. *Review of aircraft electric power systems and architectures*. in *2014 IEEE International Energy Conference (ENERGYCON)*. 2014. IEEE.
- [5]. Chen, J., C. Wang, and J. Chen. *Investigation on the selection of a more suitable power system architecture for future more electric aircraft from the prospective of system stability*. in *2017 IEEE 26th International Symposium on Industrial Electronics (ISIE)*. 2017. IEEE.
- [6]. Kostakis, T., P.J. Norman, and S.J. Galloway. *Assessing network architectures for the more electric engine and aircraft*. in *2014 49th International Universities Power Engineering Conference (UPEC)*. 2014. IEEE.
- [7]. Thales. <https://sunjet-project.eu/sites/default/files/Thales%20AES%20-%20Thalin.pdf>.
- [8]. Naayagi, R.T. *A review of more electric aircraft technology*. in *2013 International Conference on Energy Efficient Technologies for Sustainability*. 2013.
- [9]. Pagonis, M., *Electrical power aspects of distributed propulsion systems in turbo-electric powered aircraft*. 2015.
- [10]. Elbuluk, M.E. and M.D. Kankam, *Potential starter/generator technologies for future aerospace applications*. IEEE Aerospace and Electronic Systems Magazine, 1997. **12**(5): p. 24-31.
- [11]. Avery, C., S. Burrow, and P. Mellor. *Electrical generation and distribution for the more electric aircraft*. in *2007 42nd international universities power engineering conference*. 2007. IEEE.
- [12]. Lang, X., et al. *An Enhanced Power Generation Centre for More Electric Aircraft Applications*. in *2018 IEEE International Conference on Electrical Systems for Aircraft, Railway, Ship Propulsion and Road Vehicles & International Transportation Electrification Conference (ESARS-ITEC)*. 2018.
- [13]. Lang, X., et al., *A Dual-Channel-Enhanced Power Generation Architecture With Back-to-Back Converter for MEA Application*. IEEE Transactions on Industry Applications, 2020. **56**(3): p. 3006-3019.
- [14]. Brombach, J., et al. *Comparison of different electrical HVDC-architectures for aircraft application*. in *2012 Electrical Systems for Aircraft, Railway and Ship Propulsion*. 2012. IEEE.
- [15]. Emadi, K. and M. Ehsani, *Aircraft power systems: technology, state of the art, and future trends*. IEEE Aerospace and Electronic Systems Magazine, 2000. **15**(1): p. 28-32.
- [16]. Brombach, J., et al. *Optimized cabin power supply with a+/- 270 V DC grid on a modern aircraft*. in *2011 7th International Conference-Workshop Compatibility and Power Electronics (CPE)*. 2011. IEEE.
- [17]. Ferreira, C.A., et al., *Detailed design of a 30-kW switched reluctance starter/generator system for a gas turbine engine application*. IEEE Transactions on Industry Applications, 1995. **31**(3): p. 553-561.
- [18]. Tarisciotti, L., et al. *Evaluation of isolated DC/DC converter topologies for future HVDC aerospace microgrids*. in *2017 IEEE Energy Conversion Congress and Exposition (ECCE)*. 2017. IEEE.
- [19]. Buticchi, G., et al., *On-Board Microgrids for the More Electric Aircraft—Technology Review*. IEEE Transactions on Industrial Electronics, 2019. **66**(7): p. 5588-5599.
- [20]. *More Open Electrical Technologies (MOET project)*. Available from: <https://cordis.europa.eu/project/id/30861>.
- [21]. Moir, I. and A. Seabridge, *Aircraft systems: mechanical, electrical, and avionics subsystems integration*. Vol. 52. 2011: John Wiley & Sons.
- [22]. Wu, T., S.V. Bozhko, and G.M. Asher. *High speed modeling approach of aircraft electrical power systems under both normal and abnormal scenarios*. in *2010 IEEE International Symposium on Industrial Electronics*. 2010.
- [23]. Prisse, L., et al. *New power centre and power electronics sharing in aircraft*. in *2009 13th European Conference on Power Electronics and Applications*. 2009. IEEE.
- [24]. Fritz, N., et al., *Analytical modelling and power density optimisation of a single phase dual active bridge for aircraft application*. The Journal of Engineering, 2019. **2019**(17): p. 3671-3676.
- [25]. Barzkar, A. and M. Ghassemi, *Electric power systems in more and all electric aircraft: A Review*. IEEE Access, 2020.
- [26]. Dragičević, T. and Y. Li, *Chapter 18 - AC and DC Microgrid Control*, in *Control of Power Electronic Converters and Systems*, F. Blaabjerg, Editor. 2018, Academic Press. p. 167-200.

- [27]. Dragičević, T., et al., *Supervisory Control of an Adaptive-Droop Regulated DC Microgrid With Battery Management Capability*. IEEE Transactions on Power Electronics, 2014. **29**(2): p. 695-706.
- [28]. Kim, K., et al., *DC-grid system for ships: a study of benefits and technical considerations*. Journal of International Maritime Safety, Environmental Affairs, and Shipping, 2018. **2**(1): p. 1-12.
- [29]. Ni, K., et al., *Electrical and electronic technologies in more-electric aircraft: A review*. IEEE Access, 2019. **7**: p. 76145-76166.

## References to Chapter 4

---

- [1]. Abdesselam, F., et al. *Preliminary study for the integrated design of an electro-mechanical wing de-icing system*. in *2010 6th International Conference on Integrated Power Electronics Systems*. 2010.
- [2]. Meier, Oliver, and Dieter Scholz. "A handbook method for the estimation of power requirements for electrical de-icing systems." *DLRK, Hamburg* 31 (2010).
- [3]. Pourbagian, Mahdi, and Wagdi Habashi. "CFD-based optimization of electro-thermal wing ice protection systems in de-icing mode." *51st Aiaa Aerospace Sciences Meeting Including the New Horizons Forum and Aerospace Exposition*. 2013.

## References to Chapter 5

---

- [1]. Fréville, A., *The multidimensional 0–1 knapsack problem: An overview*. European Journal of Operational Research, 2004. **155**(1): p. 1-21.
- [2]. Sahni, S., *Approximate algorithms for the 0/1 knapsack problem*. Journal of the ACM (JACM), 1975. **22**(1): p. 115-124.
- [3]. Joshi, P. <https://prateekvjoshi.com/2012/11/14/dynamic-programming/>.
- [4]. Held, M. and R.M. Karp, *A dynamic programming approach to sequencing problems*. Journal of the Society for Industrial and Applied mathematics, 1962. **10**(1): p. 196-210.
- [5]. Bertsekas, D.P., et al., *Dynamic programming and optimal control*. Vol. 1. 1995: Athena scientific Belmont, MA.
- [6]. University of Dallas, T. *The Knapsack problem*; <https://personal.utdallas.edu/~scniu/OPRE-6201/documents/DP3-Knapsack.pdf>.

## References to Chapter 6

---

- 1 <https://www.nottingham.ac.uk/aerospace/projects/cleansky/aspire-project.aspx>.
- 2 ASPIRE project: [http://www.cordis.europa.eu/project/rcn/205649\\_en.htm](http://www.cordis.europa.eu/project/rcn/205649_en.htm)

## References to Chapter 7

---

- [1] I. Munuswamy, P. W. Wheeler, B. G. Fernandes, and K. Chatterjee, "Electric AC WIPS: All Electric Aircraft," in *2019 Innovations in Power and Advanced Computing Technologies (i-PACT)*, 22-23 March 2019 2019, vol. 1, pp. 1-5, doi: 10.1109/i-PACT44901.2019.8960072.